

See discussions, stats, and author profiles for this publication at: <https://www.researchgate.net/publication/239717437>

Cluster and Network Formation toward Percolation in the Microemulsion L₂ Phase Formed by an Amphiphilic Triblock Copolymer and Water in p Xylene

ARTICLE *in* LANGMUIR · FEBRUARY 1998

Impact Factor: 4.46 · DOI: 10.1021/la9711903

CITATIONS

14

READS

34

4 AUTHORS, INCLUDING:



Mats Almgren

Uppsala University

213 PUBLICATIONS 9,729 CITATIONS

[SEE PROFILE](#)

Letters

Cluster and Network Formation toward Percolation in the Microemulsion L₂ Phase Formed by an Amphiphilic Triblock Copolymer and Water in p-Xylene

Holger Mays,* Mats Almgren, and Wyn Brown

University of Uppsala, Department of Physical Chemistry, Box 532, S-751 21 Uppsala, Sweden

Paschalis Alexandridis

Department of Chemical Engineering, State University of New York at Buffalo,
Buffalo, New York 14260-4200

Received November 3, 1997. In Final Form: December 15, 1997

Evidence is presented for cluster formation in the L₂ phase of systems with the triblock copolymer Pluronic L64, water, and p-xylene. The static and dynamic properties have been investigated by time-resolved fluorescence quenching, rheology, conductometry, and dynamic light scattering as a function of the temperature and water content. A network of connected swollen reversed micelles forms a percolation cluster at temperatures below 20 °C. Droplet linking, present over the whole temperature range investigated, occurs via the two hydrophilic amphiphile moieties. Interdroplet connections are favored as the solvent quality for the hydrophobic copolymer moiety becomes worse on decreasing the temperature.

Amphiphilic triblock copolymers have attracted much interest in the past decade, due to theoretical questions concerning self-assembling polymers and their importance, e.g., in emulsification or in pharmaceutical applications.^{1–3} In ternary systems formed by mixing surfactant with water and a hydrocarbon, a rich variety of phases with different internal structures is found. However, only the isothermal phase behavior and static properties of mixtures with some Pluronics as the amphiphilic copolymer have been recently investigated in

detail.^{4,5} Not much information is available about the influence of the temperature on such systems, and nothing is known about the properties on the low-temperature side of the L₂-stability range. Interesting phenomena are expected to occur there if Pluronic triblock copolymers behave like the recently studied nonionic surfactants.^{6,7} Also, there is a lack of studies concerning the dynamics. The triblock copolymer EO₁₃PO₃₀EO₁₃ (EO, ethyleneoxide; PO, propyleneoxide), also known as Pluronic L64, is used in this work. The samples investigated are in the L₂ phase^{4,8} and are characterized by the polymer mass fraction $m'_p = 0.4$ in the mixture with the hydrocarbon

* To whom correspondence may be addressed: e-mail, Holger.Mays@fki.uu.se; fax, +46 (0)18 50 85 42.

(1) Almgren, M.; Brown, W.; Hvidt, S. *Colloid Polym. Sci.* **1995**, *273*,

2.

(2) Alexandridis, P. *Curr. Opin. Colloid Interface Sci.* **1996**, *1*, 490.

(3) Linse, P. In *Amphiphilic Block Copolymers: Self-Assembly and Application*; Alexandridis, P., Lindman, B. Eds.; Elsevier Science: Amsterdam, submitted.

(4) Alexandridis, P.; Olsson, U.; Lindman, B. *Macromolecules* **1995**, *28*, 7700.

(5) Alexandridis, P.; Olsson, U.; Lindman, B. *Langmuir* **1997**, *13*, 23.

(6) Strey, R. *Colloid Polym. Sci.* **1994**, *272*, 1005.

(7) Mays, H.; Pochert, J.; Ilgenfritz, G. *Langmuir* **1995**, *11*, 4347.

(8) Wu, G.; Chu, B. *Macromolecules* **1994**, *27*, 1766.

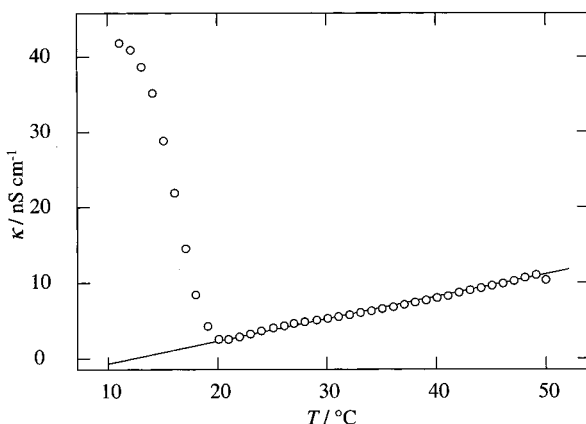


Figure 1. Electric conductivity κ of the microemulsion with *p*-xylene, water, and PEO₁₃PPO₃₀PEO₁₃ at $m'_p = 0.4$ and $m_w = 0.12$, as a function of temperature.

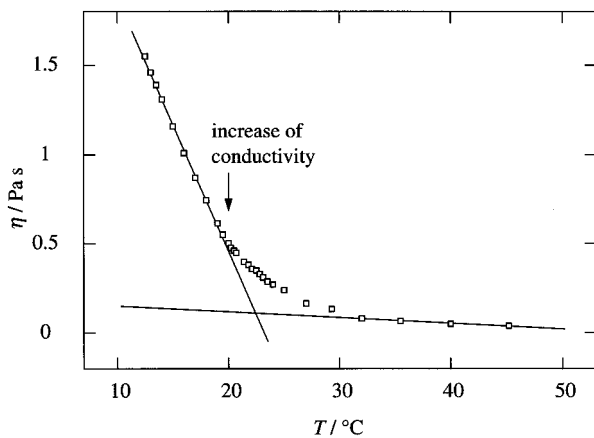


Figure 2. Temperature-dependent apparent viscosity η of the sample with $m'_p = 0.4$ and $m_w = 0.12$, measured at a low shear rate 24.2 s^{-1} .

p-xylene, and by the mass fraction of water in the final composition m_w . In focus here is the microemulsion at $m_w = 0.12$.

The electrical conductivity curve at $m_w = 0.12$ shown in Figure 1 was measured at the frequency 1 kHz with capacity compensation. To monitor the conductivity κ , the aqueous phase contained 0.1 mol dm⁻³ KCl (consistently also in the other experiments). Starting at high temperature, lowering T leads first to a decrease of the electric conductivity as a consequence of the increasing viscosity (cf. Figure 2). However, below 20 °C percolation occurs. The conductivity then increases from values less than 2.5 nS cm⁻¹ to more than 40 nS cm⁻¹ at 12.1 °C. This finding is typical for microemulsions with nonionic^{6,7} or ionic surfactant^{7,9–11} and is frequently discussed as a transition into a bicontinuous structure.¹² Another transition mechanism has been reported for particular ionic microemulsions occurring via extensive cluster formation.^{7,10,11,13–15} Percolation is surprising for systems with

the more complex triblock copolymer where it is not yet clear, whether the monolayer curvature concept applies.¹⁶

Rheological measurements were performed to further characterize the observed percolation phenomenon. Apparent viscosity data η obtained using a cone-plate viscometer (operated at the low shear rate $\dot{\gamma} = 24.2 \text{ s}^{-1}$) are shown in Figure 2. Again, the curve exhibits a clear change at the low-temperature side. However, the deviation from the trend at high temperatures commences at about 30 °C, rather than at 20 °C for conductivity. Additionally, the dependence of the apparent viscosity on the shear rate in the range between 24.2 and 1209 s⁻¹ was investigated. The shear stress in a log–log-plot is a linear function of the shear rate, yielding the pseudoplasticity constant s from the slope. Simple Newtonian flow is found at 40 °C and above, where s is unity. This constant then decreases slightly and linearly between 40 and 20.8 °C to 0.92 at 20.8 °C, followed by a drop to 0.82 over the narrow range to 17.2 °C in which κ also shows an increase. This finding differs basically from the work of Wu and Chu, where the apparent viscosity was independent of the shear rate.⁸

For the time-resolved fluorescence quenching experiments the probe molecule Ru(bpy)₃²⁺ ($\tau_0 \approx 600 \text{ ns}$) in combination with the quencher methyl viologen was employed. The decay curves obtained from picosecond laser equipment and single photon counting technique¹⁷ were analyzed on basis of the Infelta–Tachiya equation.^{18,19} All the systems studied were well described by this nonexponential decay function. Information about the micelle concentration C_m , the intradroplet quenching, and the interdroplet exchange rate constants k_{qm} and k_{ex} were obtained using the decay parameter interpretation suggested by Atik and Thomas.^{20,21} At high temperatures the predominant portion of excited probe molecules is quenched in droplets initially occupied by both excited probe and quencher in less than 300 ns. The final exponential decay, having almost the same decay constant as the unquenched curve, demonstrates a slow exchange process. The situation is clearly different at low temperatures, where quenching via exchange prevails at the expense of the intramolecular quenching reaction. The rate constant k_{qm} was found to decrease from values above $9 \times 10^6 \text{ s}^{-1}$ at $m_w = 0.08$ and 40 °C to less than half at $m_w = 0.12$ and 40 °C, and to $6.1 \times 10^6 \text{ s}^{-1}$ at $m_w = 0.08$ and $T = 25 \text{ }^\circ\text{C}$. Also, C_m decreases as a function of m_w and T . The average water core radii r_c given in Figure 3 were calculated directly from C_m assuming that all the water is confined in monodisperse, spherical droplets. The water pool radii and k_{qm} values reflect droplet swelling when T or m_w is increased. It is known that the amphiphilic PEO–PPO–PEO triblock copolymers are molecularly dissolved to a rather high amount on the oil-rich side of the phase diagram with a strong temperature dependence. From water uptake measurements it was concluded that the unimer concentration at the critical microemulsion concentration (c_{uc}) is 9% at 25 °C, increasing strongly to 16% at 40 °C.^{22,23} The temperature effect on aggregate swelling is readily understood since at high temperature the same

- (9) Laguës, M.; Ober, R.; Taupin, C. *J. Phys. (Paris), Lett.* **1978**, *39L*, 487.
- (10) Mays, H.; Ilgenfritz, G. *J. Chem. Soc., Faraday Trans.* **1996**, *92*, 3145.
- (11) Mays, H. *J. Phys. Chem. B* **1997**, *101*, 10271.
- (12) Lindman, B.; Olsson, U. *Ber. Bunsen-Ges. Phys. Chem.* **1996**, *100*, 344.
- (13) Chen, S. H.; Chang, S. L.; Strey, R. *J. Chem. Phys.* **1990**, *93*, 1907.
- (14) Almgren, M.; Johannsson, R. *J. Phys. IV* **1993**, *3*, 81.
- (15) Alexandridis, P.; Holzwarth, J. F.; Hatton, T. A. *J. Phys. Chem.* **1995**, *99*, 8222.

- (16) Chevalier, Y.; Zemb, T. *Rep. Prog. Phys.* **1990**, *53*, 279.
- (17) Almgren, M.; Alsins, J.; van Stam, J.; Mukhtar, E. *Prog. Colloid Polym. Sci.* **1988**, *76*, 68.
- (18) Infelta, P. P.; Grätzel, M.; Thomas, J. K. *J. Phys. Chem.* **1974**, *78*, 190.
- (19) Tachiya, M. *Chem. Phys. Lett.* **1975**, *33*, 289.
- (20) Atik, S. S.; Thomas, J. K. *J. Am. Chem. Soc.* **1981**, *103*, 3543.
- (21) Almgren, M.; Mays, H. In *Microemulsions: Fundamental and Applied Aspects*; Kumar, P., Mittal, M., Eds.; Marcel Dekker: New York, in press.
- (22) Alexandridis, P.; Andersson, K. *J. Phys. Chem.* **1997**, *101*, 8101.

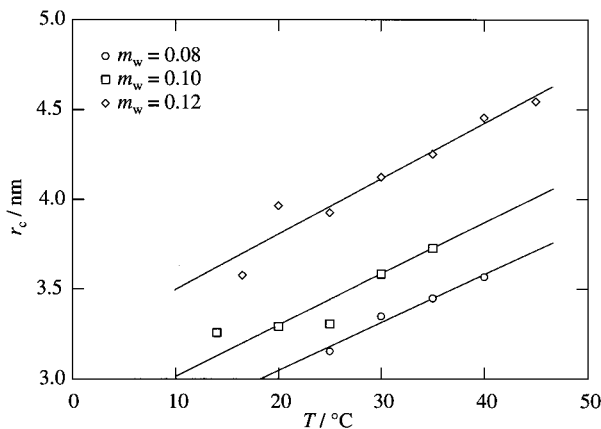


Figure 3. Water core radii, r_c , of microemulsion droplets, $m'_p = 0.4$, at various water contents determined by fluorescence quenching.

amount of water must be solubilized by less copolymer. Also the network formation and percolation can be explained by T -induced changes in the solvent quality of *p*-xylene. At lower temperatures aggregation of the hydrophilic copolymer moieties is favored, yielding a higher probability for droplet connections. The rate constant k_{ex} related to the transport of charge carriers through the microemulsion shows a strong increase on lowering the temperature. For $m_w = 0.12$ $k_{\text{ex}} = 2.86 \times 10^8 \text{ s}^{-1} \text{ dm}^3 \text{ mol}^{-1}$ at 40°C . The diffusion-controlled rate constant for reactions in this particular solvent is already exceeded at 30°C , and at 20°C k_{ex} reaches $2.1 \times 10^9 \text{ s}^{-1} \text{ dm}^3 \text{ mol}^{-1}$, showing that the model used for data analysis is no longer valid due to a dominating quenching contribution by exchange within a cluster.^{11,14,24}

Dynamic light scattering experiments were performed with the emission line at $\lambda = 488 \text{ nm}$ of an Ar⁺ laser. With the refractive index $n = 1.4672$ and 90° scattering angle, the scattering vector was $q^2 = 7.14 \times 10^{14} \text{ m}^{-2}$. The intensity correlation functions were analyzed using the REPES algorithm incorporated in the program package GENDIST,²⁵ yielding the relaxation time distribution function $\tau A(\tau)$ as a function of $\log \tau$. Three well-separated relaxation modes appear at all investigated temperatures. The linear dependence of the relaxation rate $G (=1/\tau)$ as a function of q^2 demonstrates the diffusive nature of all three relaxation processes. The fast mode diffusion coefficient D_1 of the order of $10^{-10} \text{ m}^2 \text{ s}^{-1}$ is attributed to the translational diffusion of the dissolved unimer. When

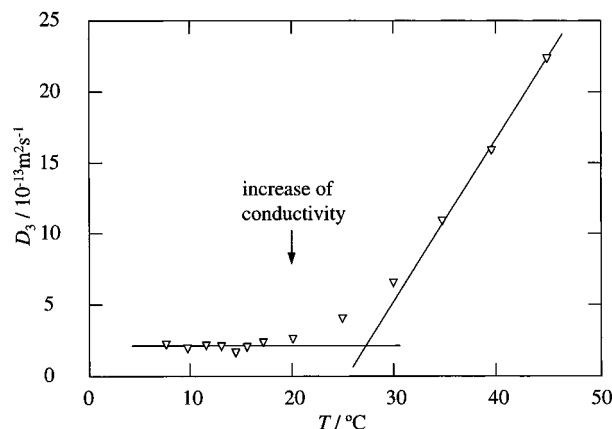


Figure 4. Diffusion coefficient D_3 of the slow cluster relaxation mode from dynamic light scattering as measured for the system *p*-xylene, water, and PEO₁₃PPO₃₀PEO₁₃ at $m'_p = 0.4$ and $m_w = 0.12$.

T is lowered D_1 decreases by a factor of 4. A similar temperature dependence is found for the droplet motion having $D_2 \approx 10^{-11} \text{ m}^2 \text{ s}^{-1}$. The slowest component D_3 shown in Figure 4 is attributed to the motion of large aggregates of connected droplets. D_3 starts to level out at 25°C and reaches a plateau at 20°C when the mobility of the network becomes slower than the motion of a time averaged cluster. The existence of the slow relaxation mode over the whole investigated temperature range means that clusters built up from more than one droplet are present even at high temperatures.

Summarizing, the amphiphilic triblock copolymer in the L₂ microemulsion phase behaves in many aspects like a typical nonionic surfactant. However, the results clearly show for the first time that a percolation phenomenon induced by clustering occurs in nonionic microemulsions without a transition to a bicontinuous structure. The transition in such systems is normally a consequence of a change in the spontaneous monolayer curvature toward a flat surfactant film on lowering the temperature.^{6,12,16} This finding is important for the understanding of the phase behavior of systems with such surfactants. More details about temperature-induced aggregation and structural changes will be considered in a following publication.

Acknowledgment. H.M. thanks the Deutsche Forschungsgemeinschaft (DFG) and Swedish Natural Science Research Council (NFR) for financial support of the postdoctoral fellowship. We thank Professor G. Ilgenfritz, University of Köln, for access to the conductometer, and G. Svensk, Uppsala, for help with the viscosity measurements.

LA9711903

(23) Alexandridis, P.; Andersson, K., *J. Colloid Interface Sci.* **1997**, *194*, 166.

(24) Almgren, M.; Johannsson, R. *J. Phys. Chem.* **1992**, *96*, 9512.

(25) Schillén, K.; Brown, W.; Johnsen, R. M. *Macromolecules* **1994**, *27*, 4825.

Colloidal Clusters of Microspheres from Water-in-Oil Emulsions

Young-Sang Cho,[†] Gi-Ra Yi,[‡] Shin-Hyun Kim,[†] David J. Pine,[§] and Seung-Man Yang^{*,†}

Department of Chemical and Biomolecular Engineering, Korea Advanced Institute of Science and Technology, 373-1 Guseong-dong, Yuseong-gu, Daejeon 305-701, Korea, Corporate R&D Center, LG Chem Research Park, 104-1 Moonji-dong, Yuseong-gu, Daejeon 305-380, Korea, and Department of Physics, New York University, 4 Washington Place, New York, New York 10003

Received May 27, 2005. Revised Manuscript Received August 4, 2005

We report a general method for small aggregates (or clusters) of water-borne colloids inside water-in-oil (W/O) emulsions. First, an aqueous suspension of monodisperse polystyrene or silica (SiO_2) microspheres was emulsified into polydisperse water droplets on micrometer scales in oil phase and colloidal aggregates were produced spontaneously during slow evaporation of water. Then, the colloidal clusters consolidated by complete removal of water were separated from the oil phase and re-dispersed in water for the subsequent fractionation according to the number (n) of the constituent spheres by a density gradient ultracentrifugation. Each cluster of n particles possessed a unique configuration except for a few particular cases of $n = 7, 8$, and 11 , in which we observed some isomeric structures, depending on their surface properties of colloidal microspheres. These isomers have not been reported in the preceding studies for colloidal clusters fabricated from the phase-inverted oil-in-water emulsions.

Introduction

Dense packings of identical spheres have been studied theoretically to elucidate the microscopic phenomena of crystallization of atoms or ions.^{1–3} Colloidal particles have been used for experimental demonstrations of such packing problems because their size and interparticle potentials could be controlled precisely. Similarly, small clusters of colloidal microspheres have been proposed as model systems for nanocrystals which are essentially aggregates of a few particles. Recently, encapsulation and shrinkage method of colloidal particles was reported in the literature, which showed that the packing structures were unique depending mainly on the number of the constituent particles.⁴ These clusters have attracted much attention due to their potential for exploring novel and new complex phenomena caused by nonisotropic shapes.^{4–6} More importantly, it is potentially possible to build up novel photonic crystals using dimeric or tetrahedral clusters as building blocks with further surface modification for directional assembly of diamond lattices.⁷ Also, the colloidal clusters can be used as photonic molecules for tight binding photon devices and sensors, and mirrorless microlasing.⁸

Several groups have also recently proposed other clever schemes for nonisotropic colloidal aggregates. Xia et al. have reported that a well-defined small number ($\sim 2–8$) of uniform colloidal particles could be organized into clusters by geometrical confinement in cylindrical holes patterned into a film of photoresist.⁹ In this case, the cluster structures could be controlled by varying the geometrical aspects of the cylindrical holes, but they were limited to those built up in a layer-by-layer fashion. Meanwhile, a few other groups have tried to seek out a chemical synthetic route and proposed that nonisotropic particles could be synthesized by controlled precipitation which produced dimers, tetramers, or daisy-like structures.¹⁰ However, their configurations were limited also and it is still challenging to control precisely the shape of clusters and the subsequent fractionations.

Aforementioned encapsulation and shrinkage approach was shown efficient to create clusters containing a small number of spheres ($n = \sim 2–15$) and was capable of producing a massively large number of clusters, approximately $10^8–10^{10}$ in lab-scale experiments.^{4,6} The process was based on emulsifying a dispersion of lightly cross-linked polystyrene (PS) microspheres in toluene into an aqueous surfactant solution. This yielded a toluene-in-water emulsion with the PS microspheres bound by surface tension to the droplet interfaces. When the toluene was removed by evaporation, the PS beads formed stable clusters of colloidal particles dispersed in water. Subsequently, clusters of different aggregation numbers were readily fractionated using a density gradient centrifugation. More recently, we expanded the oil-in-water emulsion-based process to a wide range of colloidal materials for the production of colloidal molecules with

* Corresponding author. E-mail: smyang@kaist.ac.kr.

[†] Korea Advanced Institute of Science and Technology.

[‡] LG Chem Research Park.

[§] New York University.

- (1) Maranas, C. D.; Floudas C. A. *J. Chem. Phys.* **1992**, 97, 7667.
- (2) Wille, L. T. *Nature* **1986**, 324, 46.
- (3) Zong, C. *Sphere Packings*; Springer: New York, 1999.
- (4) Manoharan, V. N.; Elsesser, M. T.; Pine D. J. *Science* **2003**, 301, 483.
- (5) Yi, G.-R.; Manoharan V. N.; Michel E.; Elsesser, M. T.; Yang, S.-M.; Pine, D.-J. *Adv. Mater.* **2004**, 16, 1205.
- (6) Manoharan, V. N.; Pine, D. J. *MRS Bull.* **2004**, 29, 91.
- (7) Lu, Y.; Yin, Y.; Xia, Y. *Adv. Mater.* **2001**, 13, 415.
- (8) Hara, Y.; Mukaiyama, T.; Takeda, K.; Kuwata-Gonokami, M. *Opt. Lett.* **2003**, 28 (24), 2437.

(9) Yin, Y.; Lu, Y.; Xia, Y. *J. Am. Chem. Soc.* **2001**, 123, 771.

(10) (a) Liddel, C. M.; Summers, C. J. *Adv. Mater.* **2004**, 15, 1715.

(b) Reculusa, S.; Mingotaud, C.; Bourgeat-Lami, E.; Duguet, E.; Ravaine, S. *Nano Lett.* **2004**, 4 (9), 1677.

various material properties.⁵ In our recent attempt, inorganic particles or polymer latexes, which generally were not stable in water but sterically stabilized in oil, were clustered and subsequently encapsulated by sol–gel reaction on the surface of the clusters.

Here, we described a simple and facile method for making colloidal clusters of PS or silica microspheres using *phase-inverted* water-in-oil (W/O) emulsions. Unlike the previous reports based on O/W emulsions that always required stable colloids in oil, the present method based on W/O emulsions is practically versatile since most of the commercially available colloids are suspended in aqueous media with much better phase stability. Obviously, when dispersed in aqueous phase, the PS or silica microspheres exhibit soft electrostatic repulsions due to the chargeable surface moieties in contact with water. In addition, the hydrophilic silica spheres in aqueous emulsion droplets tend to reside in the interior of the aqueous phase rather than migrating toward the interface between aqueous and oil phases. These situations are quite different from the oil-in-water emulsions, which have been considered by the previous studies.^{4–6} In this study, we thus investigated how the surface properties of the colloidal particles in water-in-oil emulsion droplets affected the cluster structures, which was in fact significant when the number of constituting particles in a cluster was greater than six. In particular, we observed some isomeric structures for a few cases of $n = 7, 8$, and 11 , depending on their surface properties of colloidal microspheres. These isomers have not been reported in the preceding studies for colloidal clusters fabricated from the phase inverted oil-in-water emulsions.

Experimental Section

Materials. Styrene (99%), potassium persulfate (initiator, 98%), and sodium hydrogen carbonate (buffer, 99%) were purchased from Kanto Chemicals and divinylbenzene monomer (80%) for seeded polymerization was obtained from Aldrich. Milli-Q water ($18.2\text{ M}\Omega\text{cm}^{-1}$) was used as the reaction medium for the polymerization. Tetraethyl orthosilicate (TEOS, 99.999%, Aldrich) and ammonia (28–30%, Junsei) were used as a sol–gel precursor and a catalyst, respectively. Ethanol (99.9%) and hexane (98%) were obtained from Merck and toluene (99.8%) and hexadecane (99%) from Sigma-Aldrich. Emulsifier, Span 80 (sorbitan monooleate), and Hypermer 2296 were obtained from Aldrich and Uniquema, respectively. Gradient maker, Ficoll 400, and glycerol (99%) were purchased from Sigma and Showa Chemicals, respectively.

Instrumentation. Optical microscopy was performed on a Nikon TE 2000 microscope and scanning electron microscopy was carried out on a field emission scanning electron microscope (FE-SEM, XL305FEG, Philips). Emulsification of the water in oil medium was performed by a homogenizer (DIAx 900, Heidolph). A vortex mixer was used to re-disperse PS and silica clusters in water (Maxi Mix II, Type 37600 mixer, Thermolyne).

Synthesis of Monodisperse Colloids. Cross-linked PS spheres of 230 nm in diameter were prepared by emulsifier-free emulsion polymerization following the procedures in the previous reports.¹¹ PS particles were cross-linked by copolymerization of styrene and divinylbenzene (DVB) at 70 °C with vigorous stirring for 10 h in which potassium persulfate was used as initiator. Since clusters of

the PS spheres were dispersed subsequently in an oil phase of toluene, the polymer particles were cross-linked by (DVB) to prevent the PS particles from being dissolved. PS particles of 830 nm in diameter were synthesized by the method of seeded growth using 230-nm particles as seed particles. Uniform silica particles with a mean diameter of 800 nm were prepared via controlled hydrolysis and condensation of TEOS in ethanol in the presence of water and ammonia following the modified seeded-growth method.¹² Detailed procedures were reported in our previous reports.⁵

Cluster Formation. Colloidal clusters of PS particles were prepared from W/O emulsion droplets. Three milliliters of aqueous PS suspension (0.9% w/w) was added to the mixture of 1% w/w Span 80 surfactant and 17 mL of toluene. To prepare water droplets in toluene, aqueous PS suspension was emulsified in toluene with a homogenizer for 60 s at 12000 rpm. Then, the PS particles were aggregated with slow evaporation of water from droplets at 100 °C for 1 h. During evaporation of water, a small amount of toluene was added to the vessel to keep toluene from being dried up. After being cooled to room temperature, clusters of the PS spheres were diluted with ethanol and solvent was replaced with water by centrifugation at 3000 rpm for 15 min and re-dispersion with a vortex mixer.

Colloidal clusters of 800-nm silica particles were formed by a similar process. Two milliliters of aqueous silica suspension (0.9% w/w) was added to 16 mL of hexadecane with 0.3% w/w. An amphiphilic block copolymer (Hypermer 2296: Uniquema) was used as a stabilizer. To obtain water droplets in hexadecane, the aqueous silica suspension was emulsified in hexadecane at 8000 rpm for 40 s and 9500 rpm for 20 s. By slow evaporation at 100 °C for 1 h, silica clusters were formed. Then, the sediment of colloidal clusters was collected with residual hexadecane, which was removed carefully from the sediment of clusters by washing with hexane and re-dispersion several times. Hexane was also evaporated from the sediments at room temperature and colloidal clusters were re-dispersed in water by gentle mixing.

Density Gradient Centrifugation. For colloidal clusters of PS microspheres of 830 nm in diameter, fractionation was performed by using a linear density gradient of polysaccharide (Ficoll 400). A two-jar type gradient forming device was used to make 3–9 wt % linear gradient inside a glass tube; 0.3 mL of the cluster suspension was carefully loaded on top of 11 mL of the gradient solution. Then, ultracentrifugation using a swing-bucket rotor at an acceleration of 3700g for 20 min fractionated the clusters into isolated bands, each of which contained clusters of an equal number of the constituent PS microspheres. The fractionated clusters were taken out from each band by a syringe in blunt needle. For fractionation of silica clusters, gentle centrifugation was performed using 24–85 wt % linear density gradient of glycerol, at 500g for 15 min. The clusters were also separated from the individual band with a syringe. These fractionated uniform clusters were washed by repeated centrifugation and redispersion several times to remove the gradient maker of polysaccharide or glycerol for clear SEM imaging without any contaminants.

Sample Characterization. PS and silica microspheres captured by water droplets in oil phase were observed by using an optical microscope. FE-SEM was performed to observe the configurations of PS and silica clusters. Before the SEM observation, the aqueous suspension of clusters was dried completely at room temperature and gold-coated to avoid electric charging.

(11) Zou, D.; Aklonis, L. J. J.; Salovey, R. *J. Polym. Sci., Part A* **1992**, *30*, 1463.

(12) Zhang, J. H.; Zhan, P.; Wang, Z. L.; Zhang, W. Y.; Ming, N. B. *J. Mater. Res.* **2003**, *18*, 649.

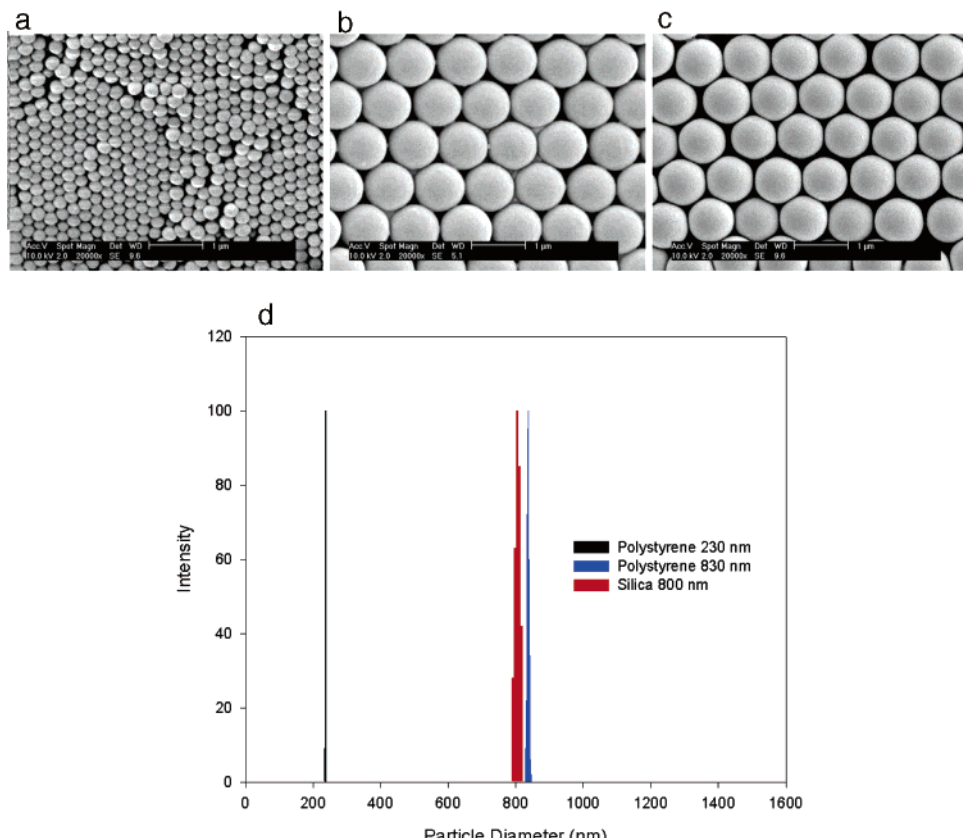


Figure 1. Scanning electron micrographs of monodisperse microspheres: (a) 230-nm PS, (b) 830-nm PS, and (c) 800-nm silica. (d) Particle size distribution measured by dynamic light scattering. Scale bars are 1 μm .

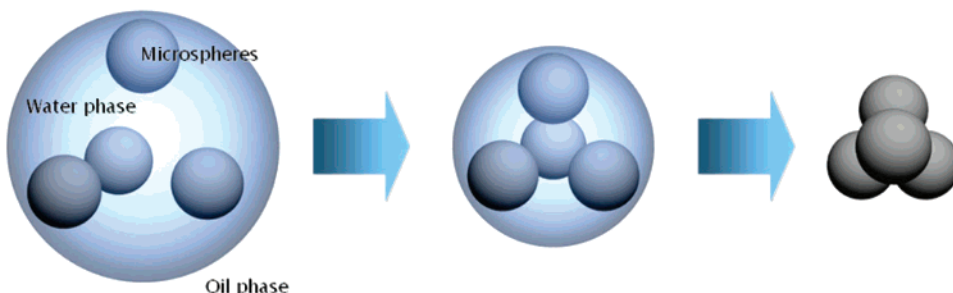


Figure 2. Schematic diagram for the fabrication of colloidal clusters of microspheres from water-in-oil emulsions.

Results and Discussion

Figure 1 shows the SEM images of PS or silica (SiO_2) microspheres, which were synthesized by emulsifier-free emulsion polymerization and modified Stöber method, respectively. As can be seen in the SEM images, monodisperse microspheres of PS and SiO_2 were successfully prepared and the size distributions of microspheres obtained from dynamic light scattering coincided well with the SEM observation.

The procedure for the fabrication of colloidal clusters from the W/O emulsion is described schematically in Figure 2. Monodisperse microspheres inside droplets were slowly aggregated as the aqueous droplet was shrunk with slow diffusion of water into the oil phase. To observe the behavior of PS microspheres in aqueous emulsion droplets in toluene through an optical microscope, we used rather large PS spheres of 830 nm in diameter. Preceding studies using a phase-inverted toluene-in-water emulsions revealed that

partially cross-linked PS microspheres resided near the interface of toluene and water.⁴ During evaporation of toluene, the PS microspheres on the interface approached each other and the adjacent microspheres began to contact, closely forming the so-called critical packings. Further evaporation of toluene induced the rearrangement and final dense packings of microspheres.¹³ Likewise, our PS particles in water-in-toluene emulsions were also positioned near the interfaces as shown in optical micrographs in Figure 3.

Our colloidal clusters from the W/O emulsions consisted of several types of regular polyhedral aggregates with various numbers (n) of the constituent PS microspheres. This is because the number of PS spheres captured in different water droplets were not uniform at all. Thus, polydisperse colloidal clusters were fractionated according to the number of constituent PS beads by density gradient centrifugation. To do this, we followed the procedure reported by Manoharan

(13) Lauga, E.; Brenner, M. P. *Phys. Rev. Lett.* **2004**, 93 (23), 238301.

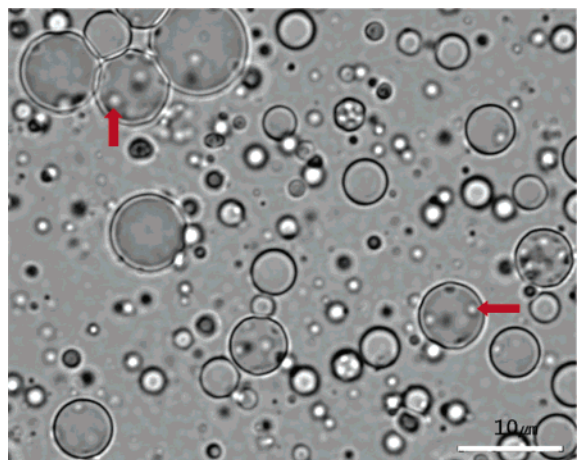


Figure 3. Optical microscope of 830-nm PS microspheres encapsulated in water droplets in toluene. Arrows indicate the PS microspheres near the interfaces of water-in-toluene emulsions.

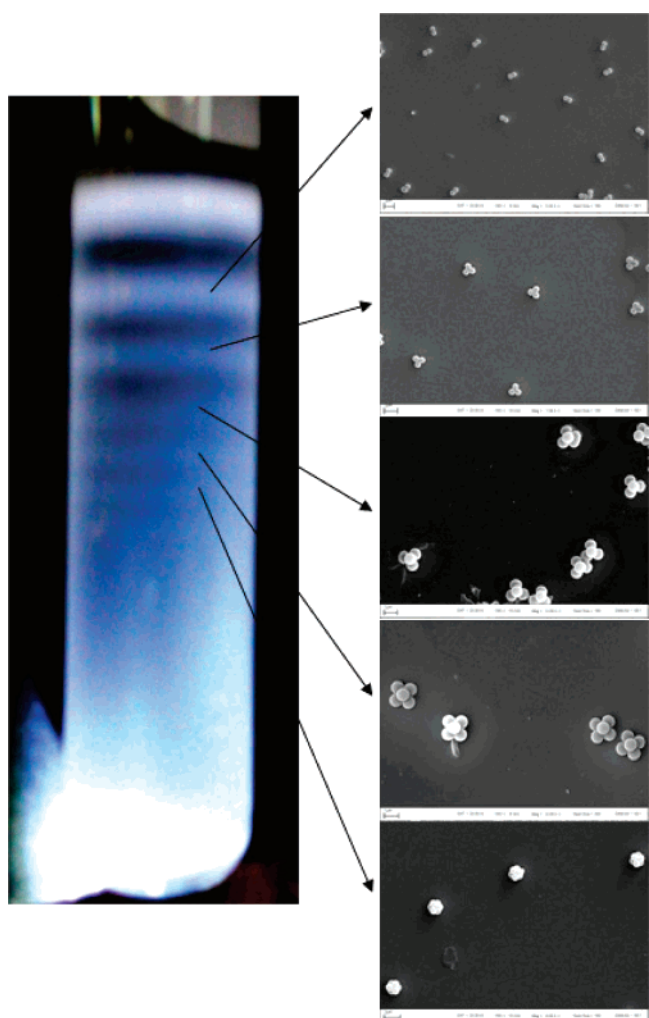


Figure 4. Test tube containing a cluster suspension of 830-nm PS microspheres separated by density gradient centrifugation and scanning electron micrograph image of colloidal clusters extracted from each band.

et al. Figure 4 shows that PS clusters redispersed in water were separated successfully into several isolated bands in linear density gradient of polysaccharide (Ficoll type 400) by centrifugation at 4000g for 30 min. From optical and SEM images, we observed that each band had all-identical clusters. The slight structural deviation of the fractionated $n = 5$

clusters from the original triangular dipyramid was caused by the repeated centrifugation and redispersion steps for the removal of density gradient maker, polysaccharide, to obtain clear SEM images without any contaminants.

Packings of microspheres were induced by capillary force acting on the particles. Since Kepler's conjecture on the optimal infinite packing of spheres, the theoretical studies on the sphere packings have been performed to predict the geometrical structure of clusters as a function of the number of constituent particles. Up to now, three typical optimal sphere packings or cluster structures have been proposed by optimizing their respective object functions, namely, Lennard-Jones (L-J) potential, second moment of the mass distribution, and Coulomb potential.^{1,2,14,15} First, the geometries of L-J clusters which minimize L-J potential between spheres were predicted using global optimization algorithm by Floudas. A few lower order L-J clusters are touching two particles for $n = 2$, triangles for $n = 3$, tetrahedrons for $n = 4$, triangular dipyramids for $n = 5$, octahedrons for $n = 6$, and pentagonal dipyramids for $n = 7$.¹ Second, the structures of clusters for the minimal second moment are the same as the L-J clusters for $n \leq 7$. However, for $n \geq 8$, the two model clusters do not have identical structures. For example, the second-moment clusters of snub disphenoids ($n = 8$), triaugmented triangular prisms ($n = 9$), and gyroelongated square dipyramids ($n = 10$) do not minimize the L-J potential. Third, the minimum Coulomb potential determines the configurations of repulsive point charges or so-called Coulomb clusters.^{2,15} Interestingly, the geometries of Coulomb clusters are also the same as L-J clusters for $n \leq 7$. For higher order clusters ($n \geq 8$), the structures are quite different from either L-J clusters or second-moment clusters. For instance, for $n = 8$, the Coulomb cluster is composed of two regular tetramers lying in parallel planes with one twisted relative to the other by 45° , forming a twisted-square structure. In the present study, we have investigated our PS and silica clusters obtained from the W/O emulsions and classified them according to the models outline above.

The SEM images of clusters of 230-nm PS microspheres formed inside aqueous emulsion droplets are reproduced in Figure 5. As noted, the configurations were unique depending on the number of constituent particles ($n = 2-13$). Their configurations for $n \leq 11$ corresponded to the theoretically predicted second-moment clusters except for $n = 8$. In this particular case, $n = 8$, we observed two isomers; one was a second-moment cluster of snub disphenoid and the other a Coulomb cluster of twisted squares.^{2,15} Twisted squares were less popular than snub disphenoids as observed through the scanning electron microscope. However, the fraction of twisted squares was high enough to be observed in every sample. We believe that electrostatic repulsion between the PS beads in water droplets caused formation of the Coulomb clusters for $n = 8$. In particular, Manoharan et al. prepared colloidal clusters of PS microspheres from phase-inverted toluene-in-water emulsions, and they could not observe the

(14) Sloane, N. J.; Hardin, R. H.; Duff, T. D. S.; Conway, J. H. *Discrete Comput. Geom.* **1995**, *14*, 237.

(15) Livshits, A. M.; Lozovik, Yu. E. *Chem. Phys. Lett.* **1999**, *314*, 577.

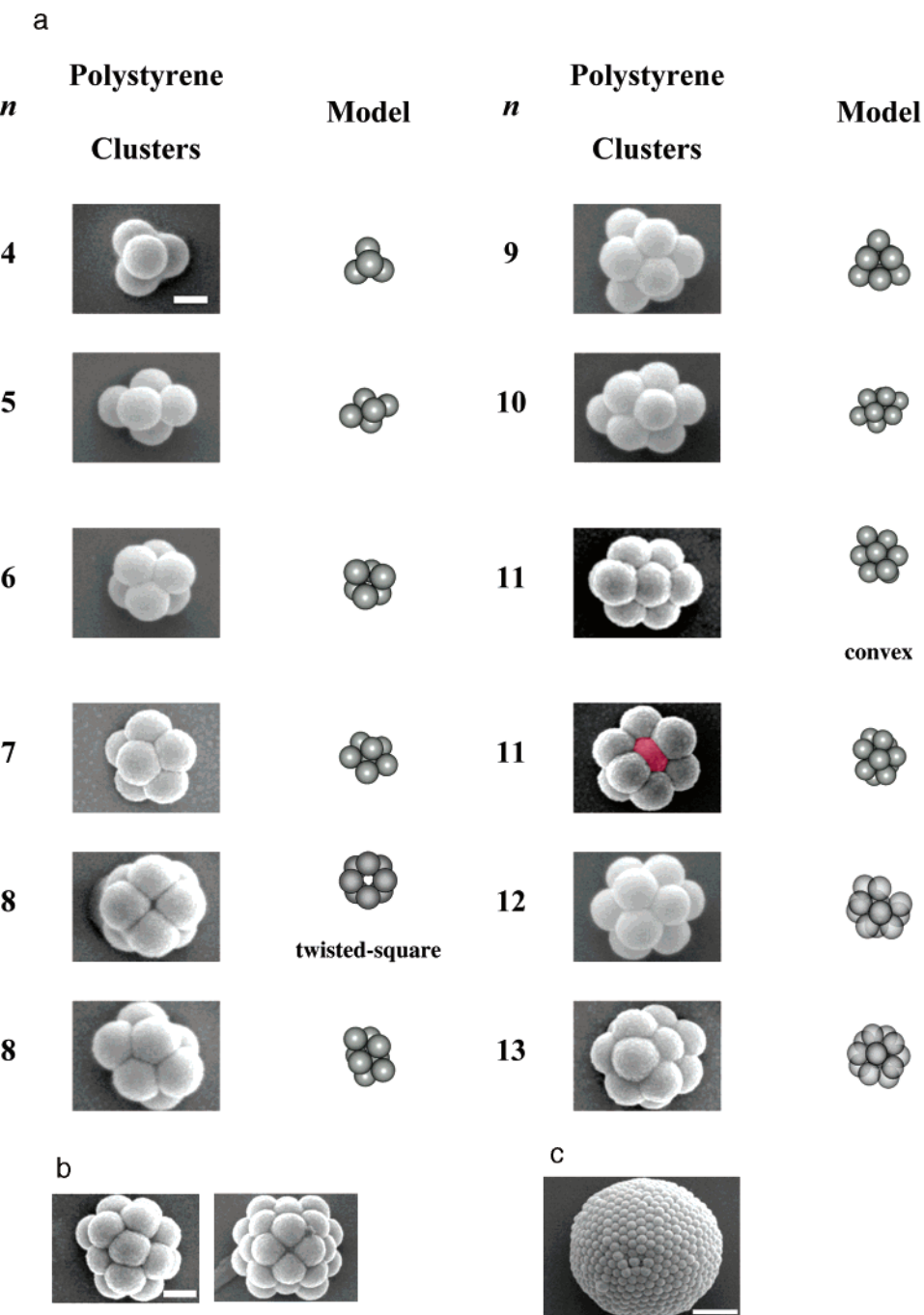


Figure 5. Scanning electron micrographs of (a) colloidal clusters of 230-nm PS for $n = 4-12$, (b) colloidal clusters of 230-nm PS for $n > 13$, in which the scale bar is 200 nm, and (c) supraballs: scale bar is 1 μm . All model clusters correspond to the minimal second-moment configurations except for the isomeric clusters of $n = 8$ (twisted-square) and 11 (convex).

Coulomb clusters for $n = 8$.⁴ This was because the PS microspheres in their case were dispersed in toluene, and consequently the electrostatic repulsion between the PS beads was negligibly small. Another isomeric structure was also found for $n = 11$. Both convex and nonconvex types of clusters were found together as shown in Figure 5. The nonconvex configuration corresponds to the eleventh order minimal second-moment cluster. In the eleventh order clusters of nonconvex shape, one sphere colored in red of the SEM image could not pop out in the rearrangement process. In their previous study, Manoharan et al. observed only a *nonconvex* structure for $n = 11$ colloidal clusters of PS microspheres prepared from toluene in water emulsions.⁴

Meanwhile, in our recent study, we found that *convex* clusters of poly(methyl methacrylate) (PMMA) microspheres were produced from hexane in water emulsions.⁵ In our case, the PMMA spheres were covered with a steric barrier of poly(dimethylsiloxane) (PDMS) and they had soft repulsive potentials. Therefore, the PMMA spheres in hexane behaved like soft spheres, which was responsible for the formation of convex structure. In the present case, the PS beads acted as soft spheres inside water droplets due to their negative surface charges, which possibly led to the formation of convex structure for the eleventh order clusters. Thus, we have observed isomeric clusters of order $n = 8$ and 11 when the constituting PS beads exhibited soft repulsive interactions.

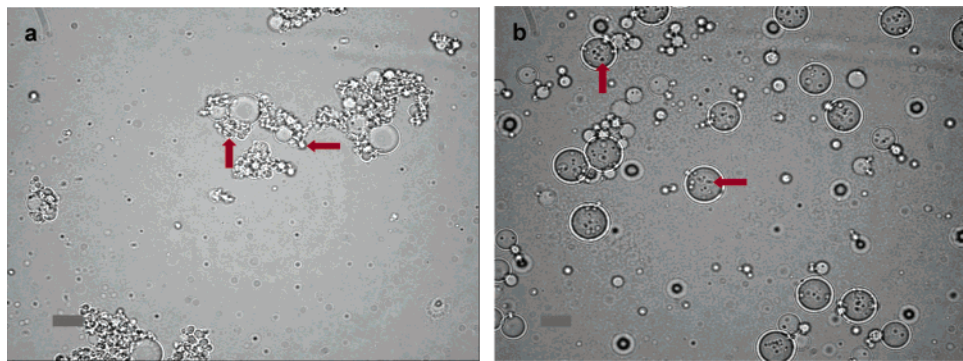


Figure 6. Optical micrographs of 800-nm silica microspheres encapsulated in water-in-oil emulsions: (a) water droplets in mineral oil stabilized with Span 80; (b) water droplets in hexadecane stabilized with Hypermer 2296. Scale bars are 5 μm . Arrows indicate the locations of silica microspheres.

Besides the cluster configurations, an interesting feature was observed in the morphology of the constituent PS particles. Since the evaporation of water droplets proceeded at 100 °C, which was around the glass transition temperature of PS, thermal annealing of touching microspheres could lead to the formation of polygonal interfaces between the PS particles after the formation of aggregates. In Figure 5, the interfacial facing area between particles turned out to be polygonal and in close contact with neighbors. Such morphological change was because of the viscoelastic deformation of PS microspheres which was similar to the space-filling shape of colloidal crystals by heating.^{16,17} Thermal annealing of the PS clusters and swelling in toluene resulted in such unusual morphologies as shown in Figure 5.

In general, the probability that a specific number (n) of spheres are captured in a single droplet is governed by Poisson distribution when the size of emulsion droplets is monodisperse.¹⁸ In our group, we reported a series of novel emulsification strategies which can generate monodisperse emulsion droplets using microfluidic devices,^{19a,19b} micropipet injection,^{20c} and electrospray.²¹ In these cases, therefore, the relative amount of clusters with an identical configuration will exhibit a Poisson distribution. For the present case, however, the situation is more complicated since the size distribution of emulsion droplets is polydisperse, and consequently the fluctuation in the number of microspheres encapsulated in a droplet is not exactly governed by Poisson distribution. In fact, a broad spectrum of small clusters for $n \leq 12$ was found as reproduced in Figure 5a. Nevertheless, we can adjust somehow the relative amount of clusters with an identical morphology type by changing the loadings of microspheres in colloidal suspension before emulsification or by changing the size of emulsion droplets under various shearing conditions.

- (16) Gates, B.; Park, S. H.; Xia, Y. *Adv. Mater.* **2000**, *12*, 653.
- (17) Pan, G.; Kesavamoorthy, R.; Asher, S. A. *J. Am. Chem. Soc.* **1998**, *120*, 6525.
- (18) Hinds, W. C. *Aerosol Technology*, 2nd ed.; John Wiley & Sons: New York, 1998.
- (19) (a) Yi, G.-R.; Thorsen, T.; Manoharan, V. N.; Hwang, M.-J.; Jeon, S.-J.; Pine, D. J.; Quake, S. R.; Yang, S.-M. *Adv. Mater.* **2003**, *15*, 1300. (b) Yi, G.-R.; Jeon, S.-J.; Thorsen, T.; Manoharan, V. N.; Pine, D. J.; Quake, S. R.; Yang, S.-M. *Synth. Met.* **2003**, *139*, 803.
- (20) Yi, G.-R.; Manoharan, V. N.; Klein, S.; Brzezinska, K. R.; Pine, D. J.; Lange, F. F.; Yang, S.-M. *Adv. Mater.* **2002**, *14*, 1137.
- (21) Moon, J. H.; Yi, G.-R.; Yang, S.-M.; Pine, D. J.; Park, S. B. *Adv. Mater.* **2004**, *16*, 605.

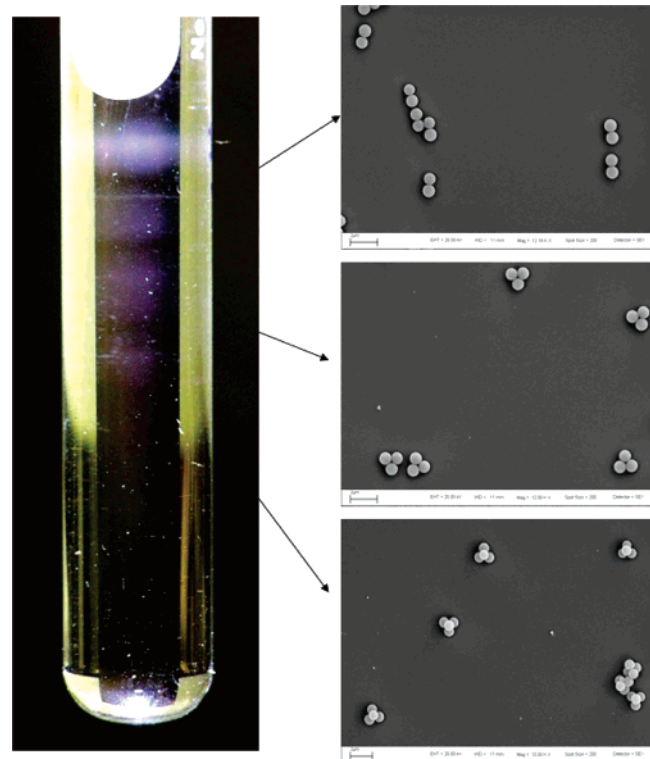


Figure 7. Test tube containing a cluster suspension of 800-nm silica microspheres separated by density gradient centrifugation and scanning electron micrograph of colloidal clusters extracted from each band.

It is noteworthy that the configurations of clusters belong to the subset of face-centered cubic (fcc) symmetry only for $n \leq 6$. We found also several types of higher order clusters ($n \geq 13$), but it was not easy to figure out their exact internal configurations from the SEM images in Figure 5b. Evidently, for large n , PS microspheres were hexagonally packed into a supraball of Figure 5c, as previously reported by Mauaziz et al.²² These supraballs have a face-centered cubic (fcc) symmetry in a finite spherical domain with a few inevitable defects as reported by Bausch et al.²³ As noted, the (111) direction of fcc packing was normal to the supraball surface. It is a simple matter to estimate the number of PS microspheres of radius r constituting a supraball of radius

- (22) Mauaziz, H.; Lacki, K.; Larsson, A.; Sherrington, D. C. *J. Mater. Chem.* **2004**, *14*, 2421.
- (23) Bausch, A. R.; Bowick, M. J.; Cacciuto, A.; Dinsmore, A. D.; Hsu, M. F.; Nelson, D. R.; Nikolaides, M. G.; Travesset, A.; Weitz, D. A. *Science* **2003**, *299*, 1716.

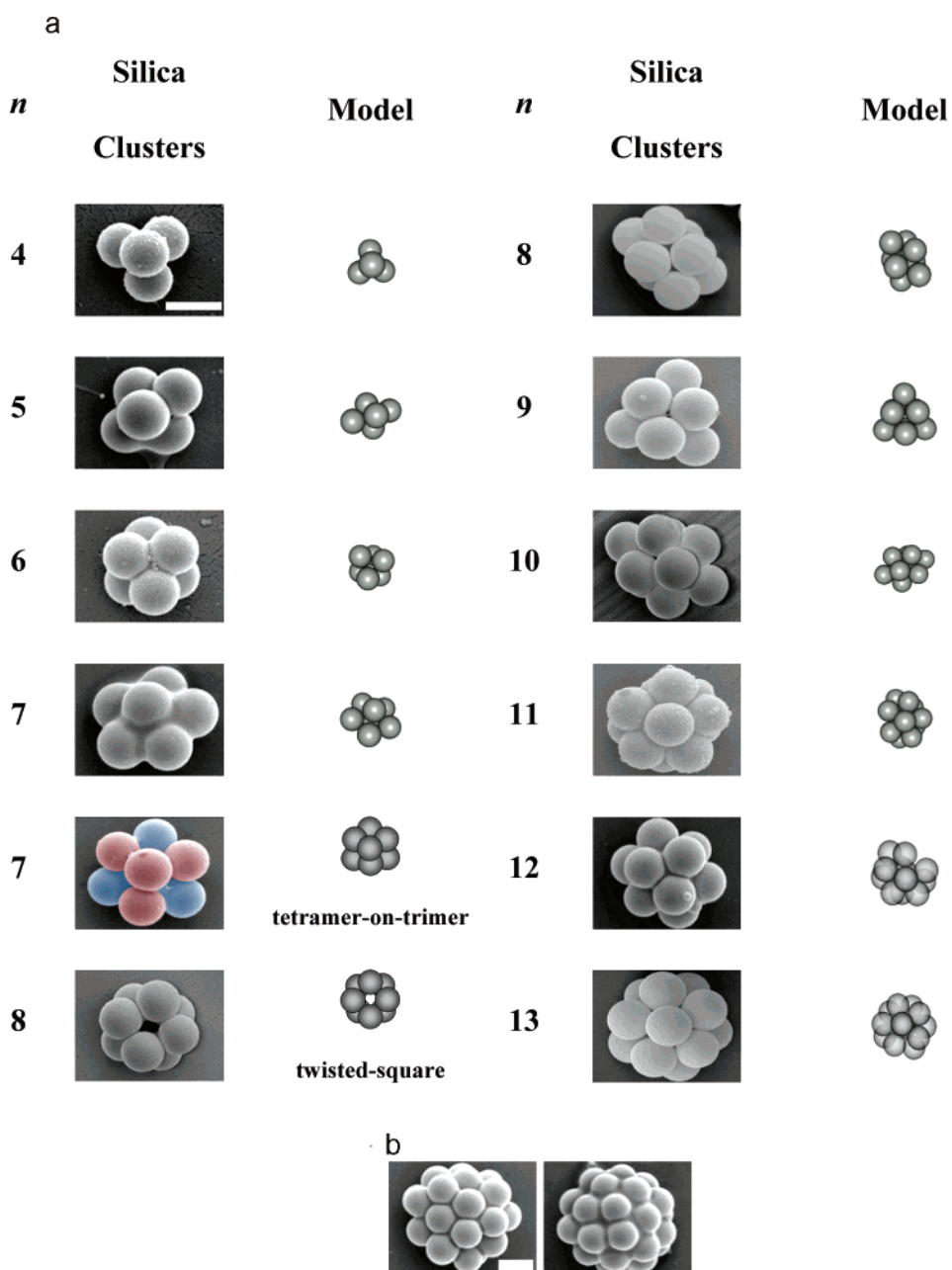


Figure 8. Scanning electron micrographs of (a) colloidal clusters for $n = 4\text{--}12$ and (b) higher order clusters of silica. Scale bars are $1 \mu\text{m}$. All model clusters correspond to the minimal second-moment configurations except for the isomeric clusters of $n = 7$ (tetramer-on-trimer) and 8 (twisted-square).

R from the simple relationship,

$$n = f \left(\frac{R}{r} \right)^3$$

in which f is the packing density of the fcc lattice. For the spherical aggregate of $3.2 \mu\text{m}$ in diameter as shown in Figure 5c, the number of 230-nm PS microspheres can be estimated as $n = 1993$, assuming that the inside of the supraball is completely packed in fcc symmetry.

Our strategy for the fabrication of colloidal clusters from W/O emulsions was not limited to the polymeric building blocks. With use of inorganic silica particles that were stable in water, small clusters could also be prepared with carefully selected oil and stabilizer for stable emulsions containing particles. In particular, when we used mineral oil as a continuous medium with nonionic surfactant of Span 80,

silica particles in aqueous emulsion drops escaped into the mineral oil phase as water evaporated. This can be clearly seen from the optical microscope image in Figure 6a. Such migration of the silica particles from water droplets to oil phase was due to the fact that the nonionic surfactant, Span 80, diffused into water droplets and adsorbed on the silica particles, which rendered them hydrophobic and stable in oil.¹⁹

To address this problem, we used hexadecane as the oil phase and nonionic polymeric surfactant (Hypermer 2296) which was insoluble in water. In addition, the mobility of the polymeric surfactant was negligibly small. The optical micrograph in Figure 6b shows that no migration of silica particles toward the oily hexadecane phases occurred in this particular case. In addition, unlike PS beads in aqueous emulsions in toluene, silica particles were not trapped at the

interface but resided inside the water droplets because of strong hydrophilicity of silica particles. After performing the same procedures as described previously, we obtained clusters of the silica microspheres. It is worth commenting that, for silica clusters, a glycerol–water mixture was used as a density gradient medium for the ultracentrifugal fractionation since silica spheres had a higher specific gravity than PS beads. As shown in Figure 7, the silica clusters were separated into about four bands inside a glass tube and each band has uniform clusters with the same size and configuration.

As noted from Figure 8, the configurations of silica clusters were almost the same as those observed in the PS clusters in Figure 5. For $n = 7$, we observed an isomeric structure of “tetramer-on-trimer” configuration, which was different from the minimal second moment cluster of the pentagonal dipyramid. However, even though the majority of the seventh order clusters was the minimal second moment, it was not that difficult to find out the former type cluster under a scanning electron microscope. As noted previously, the silica spheres resided in the interior of the water droplets rather than gathering near the interface. Under this situation, the silica spheres were able to form this compact isomeric cluster for $n = 7$ by the compressive capillary forces. As before, the silica clusters for $n = 8$ have two isomeric structures, namely, minimal second moment and Coulomb clusters. This is again due to the fact that the silica microspheres were highly negatively charged due to the hydroxyl group, which induced Coulombic twisted-square clusters. When the number of silica microspheres encapsulated inside aqueous emulsion droplets in hexadecane were large enough, higher order clusters were also obtained as shown in Figure 8b.

Conclusions

A simple and facile method for small colloidal clusters of microspheres was proposed based on evaporation-induced

assembly of water-borne colloids in water-in-oil (W/O) emulsions. With use of an aqueous suspension of mono-disperse cross-linked PS microspheres, colloidal clusters were produced from slow evaporation of water droplets in toluene and fractionated according to the number of constituent particles in each cluster by density gradient centrifugation. The clusters that we produced were unique configurations, but we have observed some isomeric clusters for $n = 8$ and 11 depending on the electro-kinetic surface properties of the colloidal particles. The same procedures have been applied to aqueous silica suspension droplets in hexadecane with nonionic polymeric stabilizer and also produced some isomeric structures. The isomers of PS and silica spheres formed in our water-in-oil emulsions have not been reported in the preceding studies for colloidal clusters fabricated from the phase-inverted oil-in-water emulsions. The colloidal clusters have diverse applications including photonic crystals with novel and promising structures, photonic molecules, additives for latex paints, and so forth.²⁴ In particular, dimeric ($n = 2$) or tetragonal ($n = 4$) clusters can be used as building blocks of diamond lattices which possess complete, full photonic band gaps.

Acknowledgment. We would like to thank Vinothan N. Manoharan for useful discussions. We are also thankful for financial support from the Korea-USA Joint Research Project and partial support from the BK21 Program, CUPS-ERC, National R&D Project of Nano Science and Technology of Korea, and Center for Nanoscale Mechatronics & Manufacturing of the 21st Century Frontier Research Program (M102KN010001-02K1401-00212). SEM images were taken in the Korea Basic Science Institute.

CM051123R

(24) Chou, C.-S.; Kowalski, A.; Rokowski, J. M.; Schaller, E. J. *J. Coating Technol.* **1987**, *59* (755), 93.

Synthesis and Structure of a Water-Soluble Hexanuclear Silver(I) Nicotinate Cluster Comprised of a “Cyclohexane-Chair”-Type of Framework, Showing Effective Antibacterial and Antifungal Activities: Use of “Sparse Matrix” Techniques for Growing Crystals of Water-Soluble Inorganic Complexes

Irina Tsyba, Becky Bun-kit Mui, Robert Bau,* Ryusuke Noguchi, and Kenji Nomiya*

Department of Chemistry, University of Southern California, Los Angeles, California 90089, and the Department of Materials Science, Kanagawa University, Hiratsuka 259-1293, Japan

Received May 6, 2003

The synthesis of a water-soluble anionic silver 2-mercaptopicotinate complex having effective antibacterial and antifungal properties is described. Its structure has been confirmed to be a hexameric cluster by an X-ray diffraction analysis of a mixed $\text{Na}^+/\text{Tris}^+$ salt (Tris^+ = tris(hydroxymethyl)methylammonium cation). The $[\text{Ag}(\text{mna})]_6^{6-}$ cluster has a Ag_6S_6 core and an overall shape of twisted hexagonal cylinder with six sulfur atoms and six silver atoms alternating on a puckered drum-like surface. Each Ag atom is trigonally coordinated by one N and two S ligands. The overall $[\text{Ag}(\text{mna})]_6^{6-} \cdot 4\text{Na}^+ \cdot 2[(\text{HOCH}_2)_3\text{CNH}_3]^+ \cdot 10\text{H}_2\text{O}$ complex has a layered appearance in the crystal packing diagram, with a $[\text{Ag}(\text{mna})]_6^{6-}$ cluster layer alternating with a solvent layer consisting of sodium atoms, Tris buffer cations, and water molecules. The structure is almost identical to that of a neutral $[\text{Ag}(\text{Hmna})]_6$ complex reported earlier. The neutral and charged complexes are both known to possess antimicrobial activities, and some biological properties of these and related compounds are briefly discussed in this paper.

Introduction

There is considerable interest in the coordination chemistry of silver(I) and gold(I) complexes with biological and pharmacological activity. Studies of gold(I) complexes have focused mostly on their antiarthritic applications^{1,2} and antimicrobial activities,^{3,4} while studies of silver(I) complexes have been mainly related to their antimicrobial and antifungal properties.^{4,5} However, compared to the number of gold(I) complexes, far fewer Ag(I) complexes have been investigated in this connection. The molecular design of such silver(I)

and gold(I) complexes are an intriguing aspect of the bioinorganic chemistry of metal-based drugs. One of the problems in the study of pharmacologically active silver(I) and gold(I) compounds is the fact that, in some cases, their three-dimensional structures are not well-established. Many metal complexes of thiol and nitrogen-containing heterocyclic ligands (especially those of gold) are hard to crystallize and some are believed to be polymeric.^{2,6,7}

In the past decade, the antimicrobial activities of Ag(I) and Au(I) complexes have been actively studied.^{3–5,7} The main aims of that research are the synthesis of compounds with Ag(I)–N, Ag(I)–S, Ag(I)–O, and Ag(I)–P bonds and the establishment of structural relationship of such complexes with antimicrobial activities. It was suggested^{5,8} that one of the key factors determining the antimicrobial effects of silver complexes is the nature of the atom coordinated to Ag and

- * Author to whom correspondence should be addressed. E-mail: bau@chem1.usc.edu.
- (1) (a) Kaim, W.; Schwederski, B. *Bioinorganic Chemistry: Inorganic Elements in the Chemistry of Life*; John Wiley: New York, 1994; p 373. (b) Brown, D. H.; Smith, W. E. *Chem. Soc. Rev.* **1979**, 9, 217.
- (c) Shaw, C. F., III. *Chem. Rev.* **1999**, 99, 2589. (d) Dash, K. C.; Schmidbaur, H. In *Metal Ions in Biological Systems*; Sigel, H., ed.; Marcel Dekker: New York, 1982; Vol. 14, p 179. (e) Sutton, B. M. *ACS Symp. Ser.* **1983**, 209, 355.
- (2) Bau, R. *J. Am. Chem. Soc.* **1998**, 120, 9380–9381.
- (3) (a) Nomiya, K.; Tsuda, K.; Kasuga, N. C. *J. Chem. Soc., Dalton Trans.* **1998**, 1653. (b) Nomiya, K.; Noguchi, R.; Ohsawa, K.; Tsuda, K.; Oda, M. *J. Inorg. Biochem.* **2000**, 78, 363. (c) Nomiya, K.; Noguchi, R.; Oda, M. *Inorg. Chim. Acta* **2000**, 298, 24–32.
- (4) Nomiya, K.; Takahashi, S.; Noguchi, R. *J. Chem. Soc., Dalton Trans.* **2000**, 2091–2097.

- (5) (a) Nomiya, K.; Takahashi, S.; Noguchi, R.; Nemoto, S.; Takayama, T.; Oda, M. *Inorg. Chem.* **2000**, 39, 3301–3311. (b) Nomiya, K.; Tsuda, K.; Sudoh, T.; Oda, M. *J. Inorg. Biochem.* **1997**, 68, 39–44.
- (6) Elder, R. C.; Eidsness, M. K. *Chem. Rev.* **1987**, 87, 1027.
- (7) Nomiya, K.; Kondoh, Y.; Kasuga, N. C.; Nagano, H.; Oda, M.; Sudoh, T.; Sakuma, S. *J. Inorg. Biochem.* **1995**, 58, 255–267.
- (8) Nomiya, K.; Yokoyama, H. *J. Chem. Soc., Dalton Trans.* **2002**, 2483–2490.

its bonding properties, rather than the solubility, charge, chirality, or degree of polymerization of the complexes. For example, it has been speculated that the weak Ag(I)–N⁵ and Ag(I)–O⁸ bond strengths might play an important role in exhibiting a wider spectrum of antimicrobial and antifungal activities and that the potential target sites for the inhibition of bacterial and yeast growth by Ag(I)–N complexes might be the sulfur-containing residues of proteins.⁴ In general, Ag(I)–S complexes have been shown to have a narrower spectrum of antimicrobial activity than Ag(I)–N complexes, but no antifungal activity.^{5b} In contrast, almost all compounds with Ag(I)–P bonds investigated thus far have shown no activity against bacteria, yeast, or molds.^{5,7}

Recently, several silver complexes of 2-mercaptoponicotinic acid ($H_2mna = 2\text{-HS(C}_5\text{H}_3\text{N)COOH}$) have been prepared and investigated for their antimicrobial properties.⁴ Under acidic conditions, the neutral species $[\text{Ag(Hmna)}]_6$ could be synthesized, and its hexameric nature was confirmed by X-ray analysis. In contrast, under alkaline conditions a water-soluble charged species, $\{\text{Na}[\text{Ag(mna)}]\}_n$, was formed and this compound was also believed to be hexameric, but a full structural analysis could not be completed because of crystallographic difficulties.^{4,13}

Our group had been successful earlier in using systematic crystallization procedures⁹ that have been used widely for the crystallization of macromolecules to obtain crystals of various water-soluble compounds that had never been crystallized before.^{2,10,11} The idea behind these procedures is to change various crystallization parameters (concentration of sample, concentration of precipitants, nature of solvents, ionic strength, pH, etc.) in a systematic way until optimum conditions for the formation of high-quality crystals are obtained.^{9b} In this paper, we describe the application of this approach to the water-soluble anionic Ag/mna complex and have confirmed the hexameric nature of this cluster, $[\text{Ag(mna)}]_6^{6-}$, by X-ray structural analysis.

Experimental Section

Synthesis. (1) **Sodium Salt of Silver 2-Mercaptomicotinate, $\{\text{Na}[\text{Ag(mna)}]\}_6 \cdot n\text{H}_2\text{O}$.** This compound was obtained according to the previously reported method⁴ in 90.0% yield (0.90-g scale) by a reaction in an aqueous solution of $\text{Ag}_2\text{O}\text{:H}_2\text{mna}\text{:NaOH} = 1\text{:}2\text{:}4$ molar ratio, followed by crystallization by vapor diffusion of a water/acetone system and identified with CHNS analysis and TG/DTA, FTIR, and ¹H, ¹³C, and ¹⁰⁹Ag NMR spectroscopy.

(2) **Potassium and Cesium Salts of Silver 2-Mercaptomicotinate, $\{\text{K}[\text{Ag(mna)}]\}_6 \cdot n\text{H}_2\text{O}$, and $\{\text{Cs}[\text{Ag(mna)}]\}_6 \cdot n\text{H}_2\text{O}$.** These compounds were obtained in a fashion analogous to the sodium salt, with slightly different yields: 98.4% for the potassium salt and 76.8% yield for the cesium salt.

- (9) (a) Jancarik, J.; Kim, S.-H. *J. Appl. Crystallogr.* **1991**, *24*, 409–411.
 (b) Ducruix, A.; Giege, R. *Crystallization of Nucleic Acids and Proteins*, 2nd ed.; Oxford University Press: Oxford, 1999; p 435.
- (10) Bau, R.; Tsypa, I. *Tetrahedron* **1999**, *55*, 14839–14846.
- (11) Bau, R.; Jin, K. K. *J. Chem. Soc., Perkin Trans. 2000*, *1*, 2079–2082.
- (12) Silica Hydrogel, from Hampton Research, Inc.
- (13) Nomiyama, K., and co-workers, unpublished results. In the earlier X-ray analysis of $\text{Na}_6[\text{Ag(mna)}]_6$, the structural details are as follows: space group $P\bar{6}_3/m$ (hexagonal), $a = b = 12.880\text{\AA}$, $c = 26.566\text{\AA}$. The structural analysis was complicated by disorder of the carbonyl groups of the (mna) ligands, and the structural refinement could not be completed satisfactorily.

Initial Structural Analysis of the Na^+ Salt of $[\text{Ag}_6(\text{mna})]^{6-}$.

The sample of $[\text{Ag}_6(\text{mna})]_6\text{Na}_6$ used was prepared as described above. Commercially available crystallization kits (Crystal screens I and II, from Hampton Research) were used to determine the preliminary crystallization conditions for a 0.2 M solution of $[\text{Ag}_6(\text{mna})]_6\text{Na}_6$ with the vapor diffusion hanging drop technique.⁹ After numerous trials, it was found that this compound could be successfully crystallized using the following precipitation conditions: 1.5 M ammonium sulfate, 0.1 M Tris buffer (pH 8.5), and 12% glycerol. We also found that crystal size and appearance could be significantly improved by carrying out the crystallization in a gel,¹² which has the effect of slowing down the crystal growth process.⁹

The sodium salt of silver mercaptomicotinate crystallizes¹³ as a hexameric complex in the triclinic space group $P\bar{1}$ with the unit cell dimensions $a = 12.590(6)\text{\AA}$, $b = 12.908(5)\text{\AA}$, and $c = 13.892(5)\text{\AA}$ with $\alpha = 62.75(1)^\circ$, $\beta = 65.12(2)^\circ$, $\gamma = 61.48(3)^\circ$, and $V = 1303.5(19)\text{\AA}^3$. Data were collected on a Siemens P4 X-ray diffractometer at $-100\text{ }^\circ\text{C}$. The structure was solved by direct methods and refined to an agreement factor of $R = 0.080$. A centrosymmetric $[\text{Ag}_6(\text{mna})]^{6-}$ cluster was found together with two Na^+ ions and numerous water molecules, and the basic structure of the $[\text{Ag}_6(\text{mna})]^{6-}$ cluster is similar to the neutral $\text{Ag}_6(\text{Hmna})_6$ molecule reported earlier.⁴ However, the final stoichiometry of the anionic complex could not be definitively established because the presence of the other four expected Na^+ cations could not be determined unambiguously from the X-ray data (in other words, it was difficult to distinguish potential Na^+ ions from the oxygen atoms of water molecules in the electron density maps). The application of silica hydrogel did slow the crystallization process and improve the crystal quality, but even so the results did not lead to an unambiguous structure for the sodium salt of $[\text{Ag}_6(\text{mna})]^{6-}$.

Structural Analyses of the K^+ and Cs^+ Salts of $[\text{Ag}_6(\text{mna})]^{6-}$.

In an attempt to resolve the ambiguity of the number of cations in the structure of the alkali salts of $[\text{Ag}_6(\text{mna})]^{6-}$, the structures of the K^+ and Cs^+ salts of this cluster were also studied.¹⁴ The hope was that the larger sizes of the K^+ and Cs^+ ions would make them more easily distinguishable from the O atoms of the water molecules and that this would lead to an unambiguous count of the number of alkali metal cations.

Clear chunky crystals of the potassium salt of $[\text{Ag}_6(\text{mna})]^{6-}$ could be grown from a precipitating solution consisting of 35% v/v MPD (2-methyl-pentane-2,4-diol), 0.1 M K–HEPES pH 7.5 (*N*-2-hydroxyethylpiperazine-*N*-2-ethanesulfonate buffer), and 0.4 M ammonium sulfate. It crystallizes as a hexameric complex in the triclinic space group $P\bar{1}$. Data were collected at 183(2) K and the unit cell dimensions are $a = 12.837(4)\text{\AA}$, $b = 12.595(5)\text{\AA}$, $c = 13.725(4)\text{\AA}$, $\alpha = 64.67(2)^\circ$, $\beta = 63.26(2)^\circ$, $\gamma = 61.55(2)^\circ$, $V = 1676.8(10)\text{\AA}^3$, and $Z = 2$; structure refined down to $R = 7.6\%$ for 5583 reflections. In the case of the Cs^+ salt, crystals were grown from very similar conditions (35% MPD, 0.1 M HEPES–Cs pH 7.5, and 0.4 M ammonium sulfate), and the unit cell also had very similar dimensions: space group $P\bar{1}$, $a = 12.665(3)\text{\AA}$, $b = 12.898(4)\text{\AA}$, $c = 14.014(3)\text{\AA}$, $\alpha = 62.72(1)^\circ$, $\beta = 65.449(9)^\circ$, $\gamma = 61.15(1)^\circ$, $V = 1725.8(12)\text{\AA}^3$, and $Z = 2$; structure refined to $R = 4.3\%$ for 5876 reflections.

Unfortunately, even in those cases the “solvent regions” were still disordered and could not be resolved completely, despite the fact that the structures appeared to have been refined satisfactorily in both cases. Thus, the use of heavier cations could not resolve

(14) Mui, B. K. M.S. Thesis, University of Southern California, 2001.

the ambiguity of the charge of the central $[\text{Ag}_6(\text{mna})_6]^{n-}$ cluster: the solvent regions were still intractably disordered, and cations could not be distinguished from H_2O molecules.

Structural Analysis of the Mixed Na^+ /Tris⁺ Salt of $[\text{Ag}_6(\text{mna})_6]^{6-}$. At this stage, we noticed that a crystallization tray that we had set up earlier with the original Na^+ salt of $[\text{Ag}_6(\text{mna})_6]^{n-}$ had produced excellent crystals. In this tray we had used the water-soluble polymer PEG (poly(ethylene glycol)) as the main precipitant instead of ammonium sulfate, and the conditions were as follows: 30% PEG 4000 (mol. wt. 4000), 0.1 M Tris HCl buffer [$(\text{HOCH}_2)_3\text{C}-\text{NH}_3^+\text{Cl}^-$, pH 8.5], and 0.2 M sodium acetate. This crystallization tray had been neglected for a long period of time because initially (after the first 2–3 weeks) the only thing visible in that drop was a small amount of precipitation. However, over a period of a few months, the microcrystalline precipitate had gradually transformed itself into a crop of excellent diffraction-quality crystals, subsequently found to be that of a mixed Na^+ /Tris⁺ salt (vide infra). Poly(ethylene glycol) is a high-viscosity precipitant, and crystallization trials using PEG 4000 as a dehydrating agent usually proceed slowly.

Diffraction data for the mixed Na^+ /Tris⁺ salt of $[\text{Ag}_6(\text{mna})_6]^{n-}$ were collected at low temperature [$T = 85(2)$ K] on a Bruker SMART/APEX CCD diffractometer with graphite monochromated Mo K α radiation ($\lambda = 0.71073$ Å). The cell parameters were initially obtained from the least-squares refinement of the spots from three sets of 20 frames, collected at different regions of reciprocal space, and later improved using spots from the full set of collected data. A hemisphere of data was collected up to a resolution of 0.75 Å, and the intensity data were processed using the SAINT-PLUS program [$R(\text{int}) = 0.015$]. All calculations for the subsequent structure determination were carried out using the SHELXTL package (version 5.1),¹⁵ and absorption corrections were applied using SADABS.¹⁶ The initial atomic positions of the Ag atoms were located by direct methods, and the structure was expanded using standard heavy-atom techniques. The structure was refined by least-squares methods using data within the θ range from 1.8° to 28.2° (completeness of the highest shell = 88%). Calculated hydrogen positions were input and refined in a riding manner along with the attached carbons. All non-hydrogen atoms were refined anisotropically to yield a final R factor of 3.26% for 6936 independent reflections. A summary of the refinement details and the resulting factors are given in Table 1.

Results and Discussion

Molecular Structure of $[\text{Ag}(\text{mna})_6]^{6-}\cdot 4\text{Na}^+\cdot 2[\text{C}_4\text{O}_3\text{H}_{12}\text{N}]^+\cdot 10\text{H}_2\text{O}$. The mixed Tris/sodium salt of silver(I) mercaptocanticotinate crystallizes as a hexameric complex in the triclinic space group $P\bar{1}$. There are three independent $[\text{Ag}(\text{mna})]^-$ units in the asymmetric unit, forming the centrosymmetric Ag_6S_6 cluster through crystallographic inversion center (Figure 1). In addition, two sodium atoms and one protonated Tris cation, $(\text{HOCH}_2)_3\text{C}-\text{NH}_3^+$, were found in the asymmetric unit, which corresponds to an overall stoichiometry of $[\text{Ag}(\text{mna})]^{6-}\cdot 4\text{Na}^+\cdot 2[\text{C}_4\text{O}_3\text{H}_{12}\text{N}]^+$ and confirms that the Ag_6S_6 cluster has a charge of -6 under the conditions of crystallization (pH 8.5). The Ag_6S_6 core has an overall shape of a twisted hexagonal cylinder consisting of two connected Ag_3S_3 units, with six sulfur

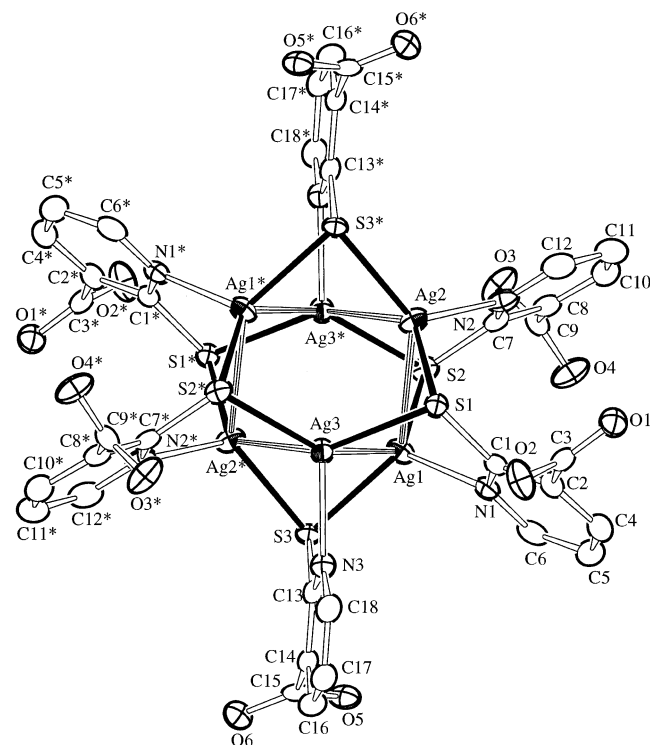


Figure 1. A view of the $[\text{Ag}_6(\text{mna})_6]^{6-}$ cluster, with an overall shape of a twisted hexagonal cylinder. The cylinder consists of two Ag_3S_3 connected units, with six sulfur atoms and six silver atoms alternating on the puckered drumlike surface.

Table 1. Crystal and Refinement Data for $[\text{Ag}(\text{mna})_6]^{6-}\cdot 4\text{Na}^+\cdot 2[\text{C}_4\text{O}_3\text{H}_{12}\text{N}]^+\cdot 10\text{H}_2\text{O}$

empirical formula	$\text{C44 H42 Ag6 N8 Na4 O28 S6}$
fw	2060.3
temp	85(2) K
wavelength	0.71073 Å
cryst syst	triclinic
space group	$P\bar{1}$ (#2)
unit cell dimensions	$a = 12.1119(15)$ Å; $\alpha = 62.874(2)$ ° $b = 12.5555(15)$ Å; $\beta = 70.151(2)$ ° $c = 12.6565(15)$ Å; $\gamma = 84.075(2)$ °
vol	1608.2(3) Å ³
Z	1
θ range for data collection	1.79–28.19°
independent reflns	6936 [$R(\text{int}) = 0.0153$]
completeness to $\theta = 28.19$ °	87.9%
final R indices [$I > 2\sigma(I)$]	$R = 0.0326$, $wR2 = 0.0763$
R indices (all data)	$R = 0.0347$, $wR2 = 0.0775$
transm factors	min/max ratio: 0.869

atoms and six silver atoms alternating on a puckered drumlike surface (Figure 1). The Ag_3S_3 units are distinctly crown-shaped, having chairlike conformations, and are staggered with respect to each other. They are attached to each other by two sets of $\text{Ag}\cdots\text{Ag}\cdots\text{Ag}$ triangular interactions, also shown in Figure 1. The Ag–Ag distances in the present complex are slightly elongated compared to those in the neutral $[\text{Ag}(\text{Hmna})_6]$ compound previously analyzed⁴ (Table 2) and those in $\text{Ag}_6[\text{SC}_6\text{H}_3\text{SiH}_2\text{C}_4\text{H}_9]_6$.¹⁷ The Ag...Ag separations, which are slightly longer than those in metallic silver (2.88 Å)¹⁸ and less than the expected van der Waals radius for silver atoms (3.44 Å),¹⁹ indicate the existence of weak metal–metal interactions.^{4,20}

(15) Sheldrick, G. M. *SHELXTL*, version 5.1; Bruker Analytical X-ray System, Inc.: Madison, WI, 1997.

(16) Blessing, R. H. *Acta Crystallogr.* **1995**, A51, 33.

(17) Perez-Lourido, P. A.; Garcia-Vazquez, J. A.; Romero, J.; Louro M. S.; Sousa, A.; Chen, Q.; Chang, Y.; Zubietta, J. *J. Chem. Soc., Dalton Trans.* **1996**, 2047–2054.

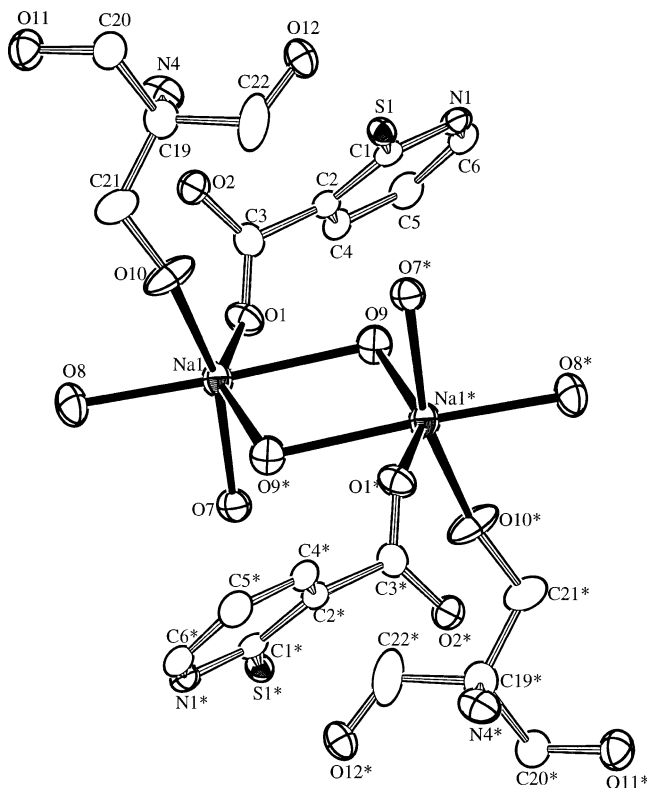


Figure 2. The region around one of the Na^+ ions, showing the distorted octahedral coordination. Each Na^+ ion is coordinated to one of the oxygen atoms of the Tris^+ cation, $[(\text{HOCH}_2)_3\text{CNH}_3]^+$, an oxygen atom from one of the $(\text{mna})^{2-}$ ligands of the cluster, and four water molecules. A crystallographic center of symmetry is situated at the center of this plot.

Table 2. Comparison of Selected Bond Distances (\AA) and Angles (deg) between the Anionic $[\text{Ag}(\text{mna})_6]^{6-}$ and Neutral $[\text{Ag}(\text{Hmna})_6]$ Clusters (Ref 4)

$[\text{Ag}(\text{mna})_6]^{6-}$ cluster (this work)		neutral $[\text{Ag}(\text{Hmna})_6]$ cluster ⁴	
$\text{Ag1}-\text{Ag2}'$	2.9373(4)	$\text{Ag1}\cdots\text{Ag2}$	2.911(1)
$\text{Ag1}-\text{Ag3}'$	2.9884(5)	$\text{Ag1}\cdots\text{Ag3}'$	2.924(1)
$\text{Ag2}-\text{Ag3}$	3.3485(5)	$\text{Ag2}\cdots\text{Ag3}'$	3.1129(8)
$\text{Ag1}'-\text{Ag3}-\text{Ag2}$	54.874(9)	$\text{Ag1}-\text{Ag3}'-\text{Ag2}$	57.54(2)
$\text{Ag1}'-\text{Ag2}-\text{Ag3}$	56.316(10)	$\text{Ag1}-\text{Ag2}-\text{Ag3}'$	57.97(3)
$\text{Ag3}'-\text{Ag1}-\text{Ag2}'$	68.810(12)	$\text{Ag2}-\text{Ag1}-\text{Ag3}'$	64.48(3)
$\text{Ag3}-\text{N3}$	2.292(3)	$\text{Ag1}-\text{N1a}$	2.273(5)
$\text{Ag1}-\text{N1}'$	2.293(3)	$\text{Ag2}-\text{N1}$	2.317(5)
$\text{Ag2}-\text{N2}$	2.298(3)	$\text{Ag3}-\text{N1b}$	2.294(5)
$\text{Ag1}-\text{S2}$	2.4682(9)	$\text{Ag1}-\text{S1}$	2.490(2)
$\text{Ag1}-\text{S3}$	2.4773(9)	$\text{Ag1}-\text{S3}'$	2.490(2)
$\text{Ag2}-\text{S3}$	2.4742(9)	$\text{Ag2}-\text{S2}$	2.465(2)
$\text{Ag2}-\text{S1}$	2.5175(9)	$\text{Ag2}-\text{S3}$	2.497(2)
$\text{Ag3}-\text{S2}$	2.4795(9)	$\text{Ag3}-\text{S1}$	2.505(2)
$\text{Ag3}-\text{S1}$	2.5180(9)	$\text{Ag3}-\text{S2}'$	2.459(2)
$\text{C3}-\text{O1}$	1.246(4)		
$\text{C3}-\text{O2}$	1.266(4)		
$\text{C9}-\text{O3}$	1.239(4)		
$\text{C9}-\text{O4}$	1.266(4)		
$\text{C15}-\text{O5}$	1.255(4)		
$\text{C15}-\text{O6}$	1.255(4)		

The coordination environments around each silver atom in the salt and neutral Ag_6S_6 clusters are identical: two weak silver(I)–silver(I) interactions, two sulfur atoms, and one monodentate nitrogen atom from each mna^{2-} ligand.⁴ The

observed Ag–N bond distances, which connect the six carboxyl–pyridine rings to the Ag_6S_6 cluster, are almost identical [2.292(3), 2.298(3), and 2.292(3) \AA] and are very similar to the Ag–N distances found in the other hexanuclear complexes of silver(I) with derivatives of pyridine-2-thione [2.273(5)–2.345(2) \AA].^{4,17,21} All observed Ag–S bond distances are within the range of 2.4682(9)–2.5180(9) \AA and in agreement with the Ag–S bond distances found in similar complexes.^{4,17,21}

Cation and Solvent Region. There are, unambiguously, three cations present in the asymmetric unit and five water molecules. The cations consist of two Na^+ and one $[\text{C}_4\text{H}_{12}\text{O}_3\text{N}]^+$ cation (a protonated Tris buffer molecule), which confirms that the total complex is neutral (one $[\text{Ag}(\text{mna})_6]^{6-}$, four Na^+ , and two Tris^+ ions). Both Na^+ ions have a distorted octahedral coordination, and one of them is shown in Figure 2 coordinated to an oxygen atom from a Tris^+ cation. The packing structure of the full complex is quite interesting. It packs as layers in the crystal, with the $[\text{Ag}(\text{mna})_6]^{6-}$ clusters forming a layer which is followed by a layer of solvent, then another layer of $[\text{Ag}(\text{mna})_6]^{6-}$ ions, and so on. It appears that the interstitial space between the layers cannot be efficiently filled just by a combination of alkali metal ions and water molecules. This leads to a disordered solvent region in the previous structure analyses of the Na^+ , K^+ , and Cs^+ salts of $[\text{Ag}(\text{mna})_6]^{6-}$ (vide supra) and prevented the determination of the exact number of alkali metal cations in those cases. In the present structural analysis, the key feature is that two Tris^+ buffer cations help to efficiently fill the available space in the solvent region, leading to a very smooth refinement of the overall structure, $[\text{Ag}(\text{mna})_6]^{6-}\cdot 4\text{Na}^+\cdot 2[\text{C}_4\text{O}_3\text{H}_{12}\text{N}]^+\cdot 10\text{H}_2\text{O}$, to a final R factor of 3.3%.

Antimicrobial Activities of the Neutral and Anionic $\text{Ag}_6(\text{mna})_6$ Complexes. Silver(I) and gold(I) complexes have shown a variety of noteworthy antimicrobial activities, although mode of action and mechanism of their antimicrobial activities have not been clarified. Generally speaking, the antimicrobial activities by metal complexes strongly depend on the metal centers. Moreover, it has been found that most silver(I) complexes having the same or similar core structures consisting of the same coordinating donor atoms have shown a very similar spectrum of the antimicrobial activities (Supporting Information).

For example, silver(I) complexes with the dimeric Ag_2O_4 -core molecular structure, such as $\{[\text{Ag}(\text{S-Hpyrrld})_2]\}_n$ ($\text{H}_2\text{pyrrld} = 2\text{-pyrrolidone-5-carboxylic acid}$), $\{[\text{Ag}(\text{R-Hpyrrld})_2]\}_n$,²² $\{[\text{Ag}_2(\text{R-Hpyrrld})(\text{S-Hpyrrld})]\}_n$,²² $\{[\text{Ag}(\text{S-othf})_2]\}_n$,²³ ($\text{Hothf} = 5\text{-oxo-2-tetrahydrofuran carboxylic acid}$), $\{[\text{Ag}(\text{R-othf})_2]\}_n$,²³ $\{[\text{Ag}_2(\text{R-othf})(\text{S-othf})]\}_n$,²³ $[\text{Ag}_2(\text{D-Hasp})(\text{L-Hasp})]_n$,⁸ ($\text{Hasp} = \text{aspartic acid}$), and $[\text{Ag}(\text{hino})_2]$,²⁴ ($\text{Hhino} = \text{hinokitiol}$ or $4\text{-isopropyltropolone}$), have shown a very

(21) (a) Block, E.; Geron, M.; Kang, H.; Zubieta, J. *Angew. Chem., Int. Ed.* **1988**, 27, 1342–1344. (b) Block, E.; Mecherone, D.; Shaikh, S. N.; Zubieta, J. *Polyhedron* **1990**, 9, 1429.

(22) Nomiya, K.; Takahashi, S.; Noguchi, R. *J. Chem. Soc., Dalton Trans.* **2000**, 4369–4373.

(23) Nomiya, K.; Takahashi, S.; Noguchi, R. *J. Chem. Soc., Dalton Trans.* **2000**, 1343–1348.

- (18) Wells, A. F., *Structural Inorganic Chemistry*, 4th ed.; Oxford University Press: Oxford, 1975; p 1075.
 (19) (a) Bondi, A. *J. Phys. Chem.* **1964**, 68, 441. (b) Shannon, R. D.; Prewitt, C. T. *Acta Crystallogr., Sect. B* **1969**, 25, 925.
 (20) Pykkö, P. *Chem. Rev.* **1997**, 97, 597.

similar and wide spectrum of antimicrobial activities against selected bacteria, yeasts, and molds. On the other hand, phosphine gold(I) complexes with a linear two-coordinate AuNP-core structure, such as $[\text{Au(im)}(\text{PPh}_3)]^{25}$ (Him = imidazole), $[\text{Au(py)}(\text{PPh}_3)]^{25}$ (Hpy = pyrazole), $[\text{Au}(1,2,3\text{-triz})(\text{PPh}_3)]^{25}$ (Htriz = triazole), $[\text{Au}(1,2,4\text{-triz})(\text{PPh}_3)]^{25}$ and $[\text{Au(tetz})(\text{PPh}_3)]^{3c,25}$ (Htetz = tetrazole), have shown a very similar spectrum of selective activities against Gram-positive bacteria. Such a spectrum of antimicrobial activities has also been found in phosphine gold(I) complexes with a linear two-coordinate AuSP-core structure, such as $[\text{Au}(2\text{-Hmpa})(\text{PPh}_3)]$ (H_2mpa = mercaptopropionic acid) and $[\text{Au}(\text{D-Hpen})(\text{PPh}_3)]$ (H_2pen = penicillamine).²⁶ These silver(I) and gold(I) complexes show that their antimicrobial activities are related to their molecular structures. For metal complexes with the same or similar core structures, we have proposed that the magnitudes of their antimicrobial properties are related to the ease with which they participate in ligand-exchange reactions.^{24,26}

In this work, we have found that the anionic complex $[\text{Ag(mna)}]_6^{6-}$ with mna²⁻ ligand has almost the same hexanuclear core structure as that of the previously reported, neutral complex $[\text{Ag(Hmna)}]_6$. Surprisingly, these two silver(I) complexes have shown a different spectrum of antimicrobial activities: the neutral complex has shown activity against both Gram-negative and -positive bacteria, while the anionic complex has shown activity against only Gram-negative bacteria.⁴ The most remarkable difference is found with the Gram-positive bacteria *B. subtilis* and *S. aureus*; the neutral complex is active, while the salt complex is not.⁴

- (24) Nomiya, K.; Yoshizawa, A.; Tsukagoshi, K.; Kasuga, N. C.; Hirakawa, S.; Watanabe, J., submitted.
- (25) Nomiya, K.; Noguchi, R.; Ohsawa, K.; Tsuda, K.; Oda, M. *J. Inorg. Biochem.* **2000**, *78*, 363–370.
- (26) Nomiya, K.; Yamamoto, S.; Noguchi, R.; Yokoyama, H.; Kasuga, N. C.; Ohyama, K.; Kato, C. *J. Inorg. Biochem.* **2003**, *95*, 208–220.
- (27) Vaara, M. *Microbiol. Rev.* **1992**, *56*, 395–411.
- (28) Nomiya, K.; Noguchi, R.; Shigeta, T.; Kondoh, Y.; Tsuda, K.; Ohsawa, K.; Kasuga, N. C.; Oda, M. *Bull. Chem. Soc. Jpn.* **2000**, *73*, 1143–1152.

Because both complexes are active against the Gram-negative bacteria *E. coli* and *P. aeruginosa*, the permeability²⁷ of the outer membrane of the Gram-negative bacteria cannot be a factor. The results would suggest a mechanism for the antimicrobial function, which is determined not only by the structure of the anion and its conjugate acid but also by solubility and transport phenomena and by ligand exchange equilibria.

In relation to the present work, we know in fact that the neutral complex can be changed by reaction with PPh_3 in solution, to the monomeric three-coordinate $\text{Ag}-(\text{S}, \text{P})$ -bonding complex, $[\text{Ag(mna)}(\text{PPh}_3)_2]$.²⁸ It is conceivable that ligand replacement from the $\text{Ag}-(\text{N}, \text{S})$ -core cluster to a new $\text{Ag}-\text{S}(\text{biological ligand})$ complex could occur in the presence of sulfur-containing biological molecules. Thus, we suggest that, rather than the geometries of the silver(I) clusters, other factors may account for observed differences in antimicrobial activity: factors such as the hydrophobicity or hydrophilicity of the clusters or the ease of ligand exchange between $\text{Ag}-(\text{N}, \text{S})$ cores and $\text{Ag}-\text{S}$ (biological ligand) bonds.

Acknowledgment. R.B. and I.T. acknowledge support from the U.S. National Science Foundation (Grant No. CHE-98-16294). K.N. acknowledges financial support from a Grant-in-Aid for Scientific Research (C) No. 13640566 from the Ministry of Education, Culture, Sports, Science and Technology, Japan, as well as a “High-Tech Research Center Project” Grant from the Ministry of Education, Culture, Sports, Science and Technology, Japan.

Supporting Information Available: Summary of the antimicrobial activities of selected silver(I) and gold(I) complexes studied in the Nomiya laboratory; details of crystallographic analysis of $[\text{Ag(mna)}]_6^{6-} \cdot 4\text{Na}^+ \cdot 2[\text{C}_4\text{O}_3\text{H}_{12}\text{N}]^+ \cdot 10\text{H}_2\text{O}$. This material is available free of charge via the Internet at <http://pubs.acs.org>.

IC030149M

Coexistence of Water Dimer and Hexamer Clusters in 3D Metal–Organic Framework Structures of Ce(III) and Pr(III) with Pyridine-2,6-dicarboxylic Acid

Sujit K. Ghosh and Parimal K. Bharadwaj*

Chemistry Department, Indian Institute of Technology Kanpur, 208016, India

Received August 16, 2003

Ce(NO₃)₃·6H₂O or Pr(NO₃)₃·6H₂O and pyridine-2,6-dicarboxylic acid form a linear coordination polymeric structure under hydrothermal conditions. Hexameric water clusters join these linear chains through bonding to the metal ions. Other coordinated water and the carboxylate oxygen form an intricate array of hydrogen bonding resulting in a 3D network where each metal ion shows 9-coordination with an approximate D_3 symmetry. Dimeric water clusters are also located in the void spaces. In the structure containing Pr(III), the water dimers are hydrogen-bonded to the hexamers, whereas in the Ce(III) structure, the dimers and the hexamers are far apart.

Introduction

Characterization of small hydrogen bonded water clusters are important as they not only help in understanding bulk water¹ but also provide clues to understand better how such aggregates influence the overall structure of their surroundings.² Hydrogen-bonding involving water molecules along with other noncovalent interactions is capable of guiding the self-assembly processes in chemical systems.³ In biology, self-assembly depends on many noncovalent interactions where water can play an important role by stabilizing the native conformation of the biomolecules. Thus, studies of small water clusters in crystal hydrates have the ultimate goal(s) of understanding the role(s) played by small water clusters in the stabilization and functioning of biomolecules⁴ as well as in designing of new materials.⁵ Moreover, hydrogen-bonding interactions and their fluctuations determine the properties of bulk water although correct evaluation of these interactions has been the major impediment in our understanding of the “anomalous” behavior of water. For this, there have been attempts^{6–13} to simulate water crystallization in restricted environments such as organic and

inorganic host lattices. In these studies, small water clusters, (H₂O)_n where $n = 2–10$, have been reported. Among these clusters, the hexamer is particularly interesting as this cluster can exhibit¹⁴ some of the properties of bulk water. Theoretical calculations¹⁵ have predicted several different isomers for this cluster of which the five low energy ones, viz., “cage”, “prism”, “book”, “boat”, and “cyclic”, are almost isoenergetic (i.e. within ~ 0.7 kcal mol⁻¹). The “cage” structure, predicted to be the most stable conformation at very low temperature, has been observed¹⁶ by vibration–rotation tunneling spectroscopy while a higher energy quasi-planar cyclic hexamer could be detected¹⁷ in a helium droplet. The lattice of a

- (6) (a) Atwood, J. L.; Barbour, L. J.; Ness, T. J.; Raston, C. L.; Raston, P. L. *J. Am. Chem. Soc.* **2001**, *123*, 7192. (b) MacGillivray, L. R.; Atwood, J. L. *J. Am. Chem. Soc.* **1997**, *119*, 2592.
- (7) Infantes, L.; Motherwell, S. *CrystEngComm* **2002**, *4*, 454.
- (8) Blanton, W. B.; Gordon-Wylie, S. W.; Clark, G. R.; Jordan, K. D.; Wood, J. T.; Geiser, U.; Collins, T. J. *J. Am. Chem. Soc.* **1999**, *121*, 3551.
- (9) Keutsch, F. N.; Cruzan, J. D.; Saykally, R. J. *Chem. Rev.* **2003**, *103*, 2533.
- (10) Pal, S.; Sankaran, N. B.; Samanta, A. *Angew. Chem., Int. Ed.* **2003**, *42*, 1741.
- (11) Supriya, S.; Manikumari, S.; Raghavaiah, P.; Das, S. K. *New J. Chem.* **2003**, *27*, 218.
- (12) Müller, A.; Krickemeyer, E.; Bögge, H.; Schmidtmann, M.; Botar, B.; Talismanova, M. O. *Angew. Chem., Int. Ed.* **2003**, *42*, 2085.
- (13) Raghuraman, K.; Katti, K. K.; Barbour, L. J.; Pillarssetty, N.; Barnes, C. L.; Katti, K. V. *J. Am. Chem. Soc.* **2003**, *125*, 6955.
- (14) Gregory, J. K.; Clary, D. C.; Liu, K.; Brown, M. G.; Saykally, R. J. *Science* **1997**, *275*, 814.
- (15) (a) Tsai, C. J.; Jordan, K. D. *Chem. Phys. Lett.* **1993**, *213*, 181. (b) Kim, K.; Jordan, K. D.; Zwier, T. S. *J. Am. Chem. Soc.* **1994**, *116*, 11568.
- (16) Liu, K.; Brown, M. G.; Carter, C.; Saykally, R. J.; Gregory, J. K.; Clary, D. C. *Nature* **1996**, *381*, 501.

* Author to whom correspondence should be addressed. E-mail: pkb@iitk.ac.in.

- (1) (a) Ludwig, R. *Angew. Chem., Int. Ed.* **2000**, *40*, 1808. (b) Matsumoto, M.; Saito, S.; Ohmine, I. *Nature* **2002**, *416*, 409.
- (2) (a) Liu, K.; Cruzan, J. D.; Saykally, R. J. *Science* **1996**, *271*, 929. (b) Keutsch, F. N.; Saykally, R. J. *Proc. Natl. Acad. Sci. U.S.A.* **2001**, *98*, 10533.
- (3) Barbour, L. J.; Orr, G. W.; Atwood, J. L. *Nature* **1998**, *393*, 671.
- (4) ten Wolde, P. R.; Frankel, D. *Science* **1997**, *277*, 1975.
- (5) Joannopoulos, J. D. *Nature* **2001**, *414*, 257.

crystal host may offer an environment for stabilizing a higher energy hexamer with a particular topology. Thus far, chair,¹⁸ boat,¹⁹ and planar²⁰ cyclic hexamers have been characterized in host lattices. Water dimers are the simplest water cluster and have been the focus of attention^{21–23} by several groups.

Metal–organic framework (MOF) structures with suitable organic ligands can provide void spaces where discrete water clusters can exist. Metal ions in such structures can act as anchors for holding the water clusters. Precise structural data of such hydrogen-bonded water clusters hold the key to unravel the properties of bulk water. Moreover, the structure of enclathrated water can be an important parameter in understanding the mechanism⁵ of formation of different MOFs. Crystal engineering of MOFs has attracted a lot of interest due to potential applications and unusual topologies of these materials. Much of the work has so far been focused on the coordination polymers containing transition elements. However, recent years have seen^{24–27} an upsurge in the use of lanthanide elements for constructing MOFs. Due to their high coordination number along with special magnetic and luminescence properties, the MOFs containing lanthanides are likely to provide new materials with desirable properties. We have initiated research in building MOFs with lanthanide elements and different multidentate ligands. We have used pyridine-2,6-dicarboxylate (pdc^{2-}) as a chelating ligand which has limited steric hindrance combined with weak stacking interactions offering possibilities to form homoleptic coordination polymers with concomitant scopes for bridging metal ions through carboxylate groups to propagate the coordination chain. Herein, we describe the presence of both cyclic chairlike hexamer and dimer water clusters in metal–organic frameworks (MOFs) constructed from Ce(III) or Pr(III) and pyridine-2,6-dicarboxylic acid. This is one of the rare examples where two different types of water clusters coexist in the same host lattice. The presence of cyclic hexamers and octamers has been reported²⁸ recently in an MOF structure built from Er(III) and fumaric acid. An MOF

structure of Ce(III) similar to ours has been reported recently²⁹ although it is silent about the presence of water clusters.

Experimental Section

Materials. $\text{Pr}(\text{NO}_3)_3 \cdot 6\text{H}_2\text{O}$, $\text{Ce}(\text{NO}_3)_3 \cdot 6\text{H}_2\text{O}$, and pyridine-2,6-dicarboxylic acid were acquired from Aldrich and used as received.

Synthesis of 1. Standard hydrothermal conditions used for the synthesis of **1** afforded solids not suitable for X-ray crystallography. We adopted a different approach where 1 mmol of $\text{Pr}(\text{NO}_3)_3 \cdot 6\text{H}_2\text{O}$ and 2 mmol of pyridine-2,6-dicarboxylic acid (pdcH_2) were taken in 5 mL of water in a Teflon-lined autoclave. The autoclave was heated under autogenous pressure to 180° C for 3 days and then left to cool to room temperature (RT). On allowing the filtrate from the reaction to evaporate at RT, pale green rectangular parallelepipeds of $[\text{Pr}(\text{pdc})(\text{pdcH})_2\text{H}_2\text{O}] \cdot 4\text{H}_2\text{O}$ (**1**) could be isolated in ~65% yield. Anal. Calcd for $\text{C}_{14}\text{H}_{19}\text{N}_2\text{O}_{14}\text{Pr}$: C, 28.98; H, 3.30; N, 4.83%. Found: C, 29.06; H, 3.38; N, 4.76%.

Synthesis of 2. Compound **2** $[\text{Ce}(\text{pdc})(\text{pdcH})_2\text{H}_2\text{O}] \cdot 4\text{H}_2\text{O}$ was isolated as pale yellow prismatic crystals following the above procedure using $\text{Ce}(\text{NO}_3)_3 \cdot 6\text{H}_2\text{O}$ in place of $\text{Pr}(\text{NO}_3)_3 \cdot 6\text{H}_2\text{O}$. Yield: ~62%. Anal. Calcd for $\text{C}_{14}\text{H}_{19}\text{N}_2\text{O}_{14}\text{Ce}$: C, 29.02; H, 3.30; N, 4.83%. Found: C, 28.95; H, 3.41; N, 4.78%.

Measurements. Spectroscopic data were collected as follows: IR (KBr disk, 400–4000 cm^{-1}) Perkin-Elmer model 1320, X-ray powder pattern (Cu K α radiation at a scan rate of 3 °/min, 293 K) Sievert ISODEBYEFLEX-2002 X-ray generator, thermogravimetric analysis (heating rate of 20° C/min) Perkin-Elmer Pyris 6. Microanalyses were obtained either from IIT Kanpur or from CDRI, Lucknow.

X-ray Structural Studies. Single-crystal X-ray data on **1** and **2** were collected at room temperature on an Enraf-Nonius CAD4 Mach2 X-ray diffractometer using graphite monochromated Mo K α radiation ($\lambda = 0.71073 \text{ \AA}$). The cell parameters in each case were determined by least-squares refinement of the diffractometer setting angles from 25 centered reflections that were in the range $18^\circ \leq 2\theta \leq 22^\circ$. Three standard reflections were measured every hour to monitor instrument and crystal stability. The linear absorption coefficients, scattering factors for the atoms, and the anomalous dispersion corrections were taken from *International Tables for X-ray Crystallography*.³⁰ The structures were solved by the direct method using SIR92³¹ and refined on F^2 by full-matrix least-squares techniques using the SHELXL-97³² program package. The H atom positions or thermal parameters were not refined but included in the structure factor calculations. The crystal data for the two structures are collected in Table 1.

Results and Discussion

Both the compounds are stable in air and soluble in water but insoluble in common organic solvents. The structure of each MOF consists of linear chains of M(III) ions where each metal ion shows 9-coordination binding two pdc^{2-} ligands, one bridging carboxylate O atom from a neighbor, and two water molecules (Ow1,Ow2). The asymmetric unit

- (17) Nauta, K.; Miller, R. E. *Science* **2000**, 287, 293.
- (18) (a) Cuscean, R.; Afloraei, C.; Vlassa, M.; Polverejan, M. *Angew. Chem., Int. Ed.* **2000**, 39, 3094. (b) Foces-Foses, C.; Cano, F. H.; Martinez-Ripoli, M.; Faure, R.; Roussel, C.; Claramunt, R. M.; Lopez, C.; Sanz, D.; Elguero, J. *Tetrahedron: Asymmetry* **1990**, 1, 65.
- (19) Park, K. M.; Kuroda, R.; Iwamoto, T. *Angew. Chem., Int. Ed. Engl.* **1993**, 32, 884.
- (20) Moorthy, J. N.; Natarajan, R.; Venugopalan, P. *Angew. Chem., Int. Ed.* **2002**, 41, 3417.
- (21) Manikumari, S.; Shivaiah, V.; Das, S. K. *Inorg. Chem.* **2002**, 41, 6953.
- (22) Fellers, R. S.; Leforestier, C.; Braly, L. B.; Brown, M. G.; Saykally, R. J. *Science* **1999**, 284, 945.
- (23) (a) Grootenhuis, P. D. J.; Uiterwijk, J. W. H. M.; Reinoudt, D. N.; van Staveren, C. J.; Sudhölder, E. J. R.; Bos, M.; van Eerden, J.; Klooster, W. T.; Kruise, L.; Harkema, S. *J. Am. Chem. Soc.* **1986**, 108, 780. (b) Chand, D. K.; Bharadwaj, P. K. *Inorg. Chem.* **1998**, 37, 5050. (c) Newkome, G. R.; Fronczek, F. R.; Kohli, D. K. *Acta Crystallogr.* **1981**, B37, 2114.
- (24) Pan, L.; Adams, K. M.; Hernandez, H. E.; Wang, X.; Zheng, C.; Hattori, Y.; Kaneko, K. *J. Am. Chem. Soc.* **2003**, 125, 3062.
- (25) Filipe, A.; Paz, A.; Klinowski, J. *Chem. Commun.* **2003**, 1484.
- (26) Bünzli, J.-C. G.; Piguet, C. *Chem. Rev.* **2002**, 102, 1897.
- (27) Wu, C.-De.; Lu, C.- Zhong.; Zhuang, H.-Hui.; Huang, J.-Shun. *J. Am. Chem. Soc.* **2002**, 124, 3836.
- (28) Michaelides, A.; Skoulika, S.; Bakalbassis, E. G.; Mrozinski, J. *J. Cryst. Growth Des.* **2003**, 4, 487.

- (29) Nobuo, O.; Hasuyo, K.; Ayumi, F. *Acta Crystallogr. E* **2002**, E58, m354.
- (30) *International Tables for X-ray Crystallography*; Kynoch Press: Birmingham, England, 1974; Vol. IV.
- (31) Altomare, A.; Cascarano, G.; Giacovazzo, C.; Gualandi, A. *J. Appl. Crystallogr.* **1993**, 26, 343.
- (32) Sheldrick, G. M. *SHELXL-97: Program for Crystal Structure Refinement*; University of Göttingen: Göttingen, Germany, 1997.

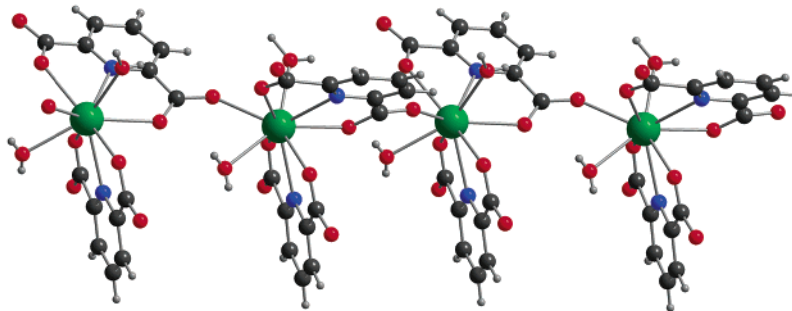


Figure 1. A view of the linear coordination polymeric chain along the crystallographic *a* axis. Carbon: black. Hydrogen: gray. Nitrogen: blue. Oxygen: red. Praseodymium: green.

Table 1. Crystal Data and Structure Refinement for **1** and **2**

	1	2
empirical formula	C ₁₄ H ₁₉ N ₂ O ₁₄ Pr	C ₁₄ H ₁₉ N ₂ O ₁₄ Ce
fw	580.21	579.43
temp	293(2) K	293(2) K
radiation, wavelength	Mo K α , 0.71073 Å	Mo K α , 0.71073 Å
crystal system	monoclinic	monoclinic
space group	P2 ₁ / <i>a</i>	P2 ₁ / <i>a</i>
<i>a</i> , Å	12.893(3)	12.953 (2)
<i>b</i> , Å	11.200(3)	11.237 (2)
<i>c</i> , Å	14.060(2)	14.007 (3)
β (deg)	102.04(5)	101.86 (5)
<i>V</i> , Å ³	1985.6(9)	1995.3(8)
<i>Z</i>	4	4
ρ_{calc} Mg/m ³	1.94	1.93
μ , mm ⁻¹	2.53	2.36
<i>F</i> (000)	1152	1148
reflns collected	2586	2598
indep reflns	2289	1752
refinement meth	full-matrix least-squares on F^2	full-matrix least-squares on F^2
GOF	1.04	1.03
final <i>R</i> indices		
[<i>I</i> > 2 σ (<i>I</i>)]	R1 = 0.044	R1 = 0.044
all data	wR2 = 0.112	wR2 = 0.102
<i>R</i> indices		
(all data)	R1 = 0.052	R1 = 0.109
	wR2 = 0.117	wR2 = 0.119

contains one M(III) ion and two ligands besides six H₂O molecules. For charge neutralization, it is suggested that one of the ligands is not deprotonated completely but exists as (pdch)⁻. However, we were unable to detect this hydrogen in the difference map. The bridging carboxylate propagates the polymeric chain approximately (Figure 1) along the crystallographic *b* axis. The coordination symmetry around the metal ion is deviated significantly from *D*₃ symmetry as expected. Bond distances and bond angles involving the metal ion are closely similar to those observed in several related species.^{33–35}

The atom Ow1 is hydrogen bonded to two carboxylate O atoms of two other chains while Ow2 is H-bonded to two more water molecules (Ow3, Ow4) forming a hexameric water cluster with three other water molecules related by a center of symmetry and belonging to a different polymeric chain. In addition, two more water molecules, Ow5 and Ow6, are also present in the lattice. In **1**, these two water molecules

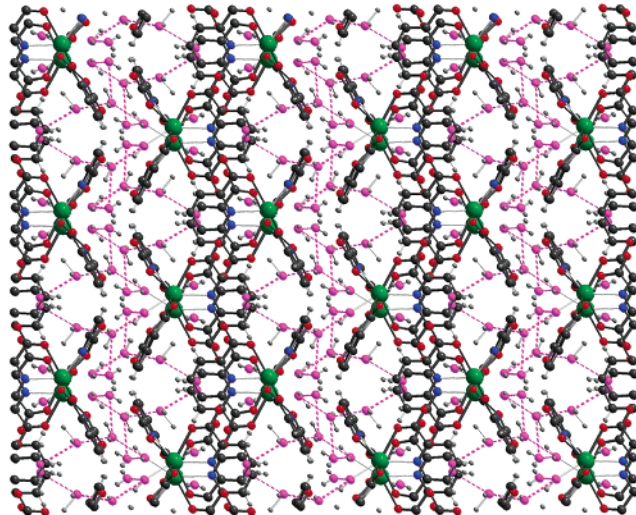


Figure 2. The MOF structure of **1** viewed in the *bc* plane. The dimeric and hexameric water clusters are shown in purple.

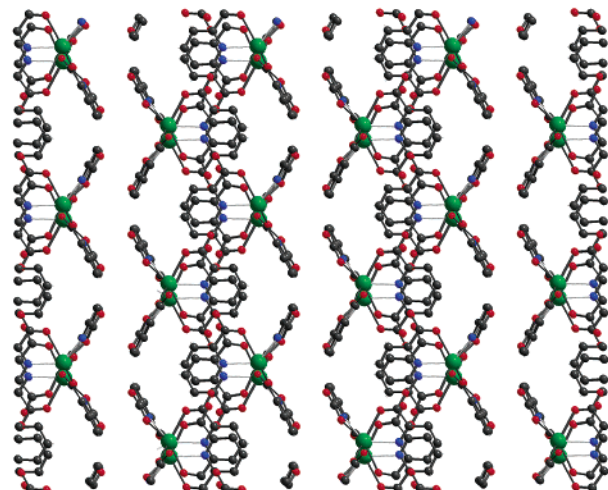


Figure 3. The MOF structure of **1** viewed in the *bc* plane. The water clusters have been omitted to show the zigzag channel along the *b* axis.

form a dimer, whereas in **2**, each of Ow5 and Ow6 forms a dimer with an O atom related by a center of symmetry. The water molecules of the dimeric and hexameric clusters are hydrogen bonded to carboxylate O atoms of different polymeric chains resulting in an overall 3D network structure—the water clusters occupying the 3D channels (Figure 2). Once the water molecules are deleted from the packing diagram, zigzag channels can be seen (Figure 3).

(33) Yu, J.; Zhang, H.; Fu, L.; Deng, R.; Zhou, L.; Li, H.; Liu, F.; Fu, H. *Inorg. Chem. Commun.* **2003**, *6*, 852.

(34) Bower, J. F.; Cotton, S. A.; Fawcett, J.; Hughes, R. S.; Russel, D. R. *Polyhedron* **2003**, *22*, 347.

(35) Pan, L.; Huang, X.; Li, J.; Wu, Y.; Zheng, N. *Angew. Chem., Int. Ed.* **2000**, *39*, 527.

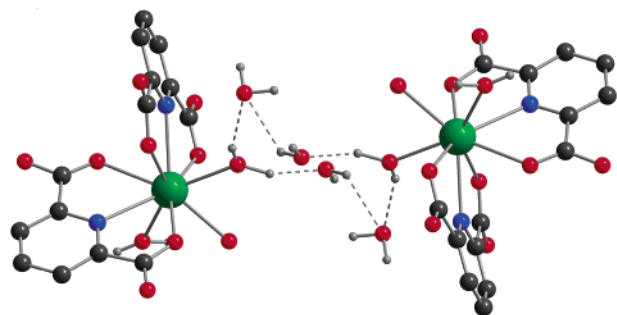


Figure 4. A perspective view of the hexameric water cluster connecting two Pr(III) ions. Each metal ion is showing 9-coordination. Color codes of atoms are same as in Figure 1.

Table 2. Geometrical Parameters of Hydrogen Bonds (Å, deg) for the Water Dimer and the Hexamer and Its Association with the Host in **1** and **2**

		1					
Ow2...	Ow3	2.743	Ow2...	Ow3...	Ow4'		
Ow3...	Ow4'	2.877	Ow3...	Ow4'...	Ow2'		
Ow5...	Ow6	2.829	Ow3...	Ow2...	Ow4		
Ow2...	Ow4	2.702	Pr–Ow2...	Ow3	124.70		
Ow4...	Ow5	3.021	Pr–Ow2...	Ow4	144.70		
Ow2...		Ow4...		Ow5...			
Ow2...		Ow4...		Ow6			
Ow2...		Ow3...		Ow5'			
Ow2–H		1.018	H–Ow4	1.729	Ow2–H...	Ow4	159.68
Ow2–H		0.778	H–Ow3	2.149	Ow2–H...	Ow3	155.20
Ow4'–H		0.942	H–Ow3	2.189	Ow4'–H...	Ow3	130.84
Ow6–H		0.773	H–Ow5	2.223	Ow6–H...	Ow5	139.15
		2					
Ow2...	Ow3	2.728	Ow2...	Ow3...	Ow4'		
Ow3...	Ow4'	2.886	Ow3...	Ow4'...	Ow2'		
Ow2...	Ow4	2.700	Ow3...	Ow2...	Ow4		
Ow5...	Ow5'	2.779	Ce–Ow2...	Ow3	124.95		
Ow6...	Ow6'	2.782	Ce–Ow2...	Ow4	142.48		

The geometrical parameters of the water clusters are collected in Table 2. In the case of **1**, all hydrogen atoms (except one bound to Ow5) bound to water oxygens could be located in the difference maps, which was not the case for **2** apparently because of inferior quality of crystals. The O...O distance in the dimer in **1** is 2.830 Å while this distance³⁶ in regular ice, in liquid water, and in the vapor phase is respectively 2.74, 2.85, and 2.98 Å. In **2**, the dimeric clusters are present in two different types of surroundings showing the O...O distances of 2.779(4) and 2.782(6) Å. Shorter O...O dimer distances in **2** result from the overall compactness of the MOF compared to that of **1**. Thus, the water clusters are sufficiently flexible to respond to small changes in the environment. Recently, the O...O distance of water dimers present in an MOF structure was found²¹ to be 2.84 Å where the O–H–O angle was nearly linear (~170°). In **1**, the O–H–O angle is deviated significantly from linearity (139.15°).

In both the MOFs, the hexameric clusters form an ice-like chair conformation (Figure 4) connecting two M(III) ions in the 1,4-position. The atoms Ow2, Ow3, and Ow4 are connected to the atoms Ow2', Ow3', and Ow4', which are related by the center of symmetry forming the hexamer

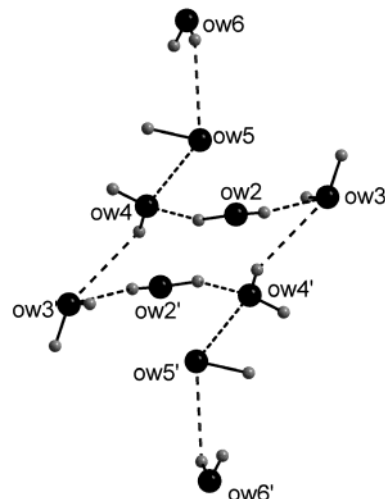


Figure 5. A perspective view of the association of dimeric and hexameric water clusters in **1**. The dimers and hexamers are far apart in **2**.

(Figure 5). These clusters can be regarded as the simplest supramolecular analogue of cyclohexane. As H atoms bound to the O atoms could be located only for **1**, the coordination properties of water O atoms are discussed for this compound. The water molecule Ow2 behaves as H donors, Ow3 as H acceptors, while Ow4 behaves as an acceptor as well as a donor in the hydrogen-bonding scheme. Thus, Ow3 and Ow4 show tetracoordination, and Ow2 which is coordinated to Pr(III) shows tricoordination. The average O...O distances are 2.783 and 2.771 Å in **1** and **2**, respectively. The corresponding value³⁶ is 2.759 Å in ice *I*_h at –90 °C. The bond angles in the hexamer vary widely with the average angle being 98.36° and 98.41° in **1** and **2**, respectively, which deviates considerably from the corresponding value of 109.3° in hexagonal ice. The conformational variation from that of ice with the *I*_h symmetry is due to the constrained environment these clusters are in. Theoretical calculations for the hexamer have revealed the existence of several conformations with energies within 0.7 kcal mol^{–1} of each other. This nearly isoenergetic nature of the different clusters of water hexamers suggests that the conformation that will be detected depends strongly on the chemical environment the cluster is in. The possible effect of the presence of water dimers on the conformation of the hexamer would be minimum in the present structures. This is because the hexamer is weakly hydrogen bonded (Figure 5) to one of the dimers at a O...O distance of 3.024 Å only in structure **1**. In structure **2**, however, none of the dimers are hydrogen bonded to the hexamer, although in both structures, the hexamer forms the same chair conformation.

The 3D structure is largely a consequence of hydrogen bonding interactions among water molecules themselves and the MOF. This association is quite strong as thermal gravimetric analysis of **1** with a 8.75 mg sample in air shows that weight loss occurs in stages beginning at 60 °C and the loss 12.8% corresponding to all of the water (calculated 12.1%) takes place above 140 °C. Similarly, thermal gravimetric analysis of **2** performed in N₂ atmosphere with 10.34 mg of sample shows that the compound begins to lose weight

(36) Eisenberg, D.; Kauzmann, W. *The Structure and Properties of Water*; Oxford University Press: Oxford, 1969.

above 50 °C. Water removal continues in several steps giving a total loss of 12.9% at ~130 °C corresponding to loss of all water molecules (calculated value, 12.2%). The complete decomposition of the compounds is achieved above ~280 °C. The FTIR spectra of **1** and **2** show a broad band centered around 3400 cm⁻¹ attributable²⁰ to the O–H stretching frequency of the water cluster. This broad band vanishes on heating the compounds under vacuum (0.1 mm) at 140 °C for 2 h, suggesting escape of the water clusters from the lattice. Deliberate exposure to water vapor for 3 days does not lead to reabsorption of water into the lattice as monitored by FTIR spectroscopy. Powder X-ray diffraction patterns of the compounds before and after water expulsion show major changes in peak positions as well as their intensities, suggesting complete breakdown of the host lattice due to the exclusion of water.

Conclusion

Thus, we have shown that pyridine-2,6-dicarboxylic acid is a suitable ligand to form linear coordination polymers with lanthanide ions under hydrothermal conditions. Here, the metal ion shows 9-coordination with a distorted D_3 sym-

metry. The 3D structure is largely a consequence of hydrogen bonding interactions among water molecules, and upon removal of water from the lattice, the structures break down. Besides, this is the first set of examples showing the presence of dimeric and hexameric water clusters in the lattice of an MOF. Hydrogen-bonded water clusters can play important roles in stabilizing supramolecular structures quickly without incurring any defects. We are presently probing this aspect of supramolecular chemistry.

Acknowledgment. We gratefully acknowledge the financial support received from the Council of Scientific and Industrial Research, New Delhi, India (Grant No.1638/EMR II) and a JRF to S.G. We thank Prof. V. Chandrasekhar for the TGA data.

Supporting Information Available: X-ray crystallographic files in CIF format for the structure determination of compound **1** and **2**. Table of selected bond distances and angles for **1** and **2**. IR spectra and X-ray powder diffraction patterns. This material is available free of charge via the Internet at <http://pubs.acs.org>.

IC034976Z

Structure of a Discrete Hexadecameric Water Cluster in a Metal–Organic Framework Structure

Sujit K. Ghosh and Parimal K. Bharadwaj*

Department of Chemistry, Indian Institute of Technology, Kanpur 208016, India

Received July 7, 2004

Pyrazine-2,3,5,6-tetracarboxylic acid (pytcH₄) reacts with Cu(NO₃)₂·6H₂O in 1:2 molar ratio in the presence of pyridine (py) vapor to form blue crystals of a coordination polymer with the empirical formula {Cu_{2.5}(pytc)(py)₈(NO₃)⁻·10H₂O}_n (**1**). Four such polymeric chains gather around a hexadecameric water cluster to form an overall 3D metal–organic framework structure. Once the water molecules are removed, the 3D structure breaks down. It presents a new mode of association of water molecules not predicted theoretically or found experimentally.

Diversity of hydrogen bonding interactions among water molecules is responsible for the anomalous behavior of bulk water, cloud and ice formation, as well as structure and function of biomolecules.¹ The energetic optimization of mutual hydrogen-bonded networks involving enzyme, water, and substrate is an intrinsic part of the molecular recognition process in these biological macromolecules. In the abiological world, the degree of structuring of the water cluster that can be imposed by its environment and vice versa can be of importance in the design of new metal–organic framework structures. Recent years have witnessed both theoretical^{2–5} and experimental^{6–14} scrutiny of a number of small water clusters in different surroundings to investigate the develop-

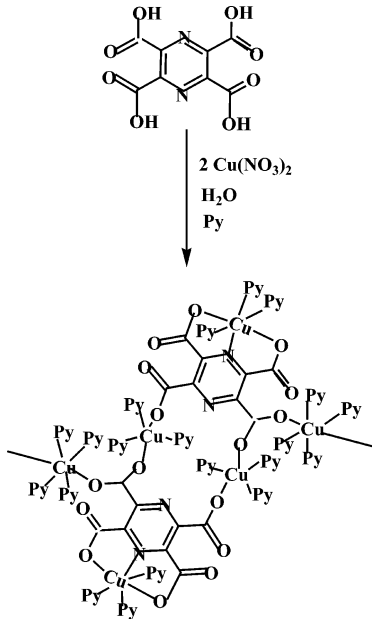
ment of properties of the condensed phase in a stepwise manner. We report here the structure of a novel hexadecameric water cluster present in the cavity of a supramolecularly built metal–organic framework. These water clusters assemble coordination polymeric chains to form the overall 3D metal–organic framework (MOF) structure.

Construction of MOFs via crystal engineering principles uses metal ions, multidentate ligands, and dative bonding to drive and direct the self-assembly processes. Syntheses of these coordination polymers with designer structures are pursued^{15,16} in several laboratories with the ultimate goal(s) of having new materials with a range of applications. Success in producing such structures depends on the understanding and controlling the topological and geometric relationships between molecular modules along with the coordination characteristics of the metal ions. Water clusters can influence the final overall MOF structure via hydrogen bonding interactions with the coordination polymeric units.

The compound {Cu_{2.5}(pytc)(py)₈(NO₃)⁻·10H₂O}_n (**1**) was synthesized¹⁷ by allowing a solution of Cu(NO₃)₂ with pyrazine-2,3,5,6-tetracarboxylic acid (pytcH₄) in aqueous pyridine to evaporate slowly. The compound once formed is insoluble in most solvents including water. In the solid

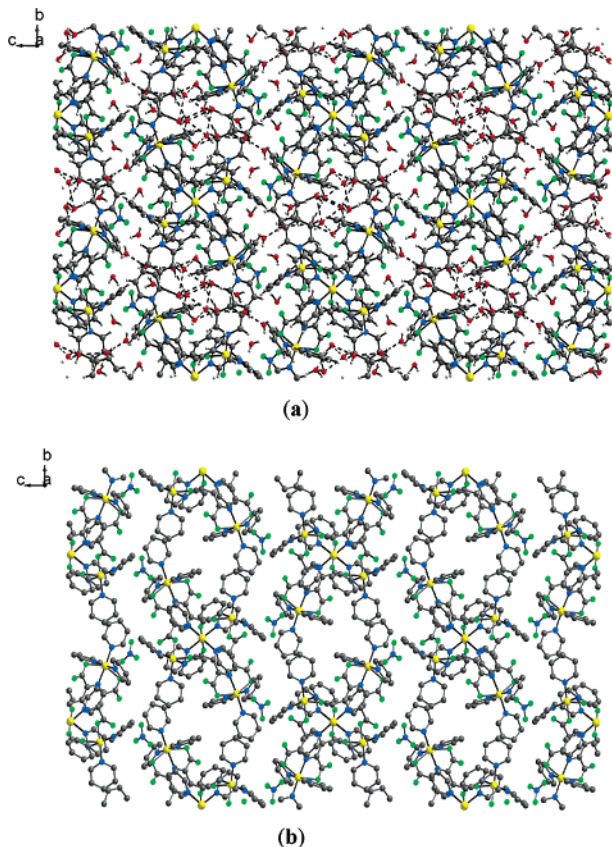
- * To whom correspondence should be addressed. E-mail: pkb@iitk.ac.in.
- (1) (a) Ludwig, R. *Angew. Chem., Int. Ed.* **2001**, *40*, 1808. (b) Keutsch, F. N.; Saykally, R. J. *Proc. Natl. Acad. Sci. U.S.A.* **2001**, *98*, 10533.
- (c) Ball, P. *H₂O: A Biography of Water*; Weidenfeld & Nicolson: London, 1999. (d) *Water and Biological Macromolecules*; Westhoff, E., Ed.; CRC Press: Boca Raton, FL, 1993. (e) Eisenberg, D.; Kauzmann, W. *The Structure and Properties of Water*; Oxford University Press: Oxford, 1969.
- (2) (a) Head-Gordon, T.; Hura, G. *Chem. Rev.* **2002**, *102*, 2651. (b) G. Chaplin, M. F. *Biophys. Chem.* **1999**, *83*, 211.
- (3) (a) Keutsch, F. N.; Cruzan, J. D.; Saykally, R. J. *Chem. Rev.* **2003**, *103*, 2533. (b) Mas, E. M.; Bukowski, R.; Szalewicz, K. *J. Chem. Phys.* **2003**, *118*, 4386.
- (4) Matsumoto, M.; Saito, S.; Ohmine, I. *Nature* **2002**, *416*, 409.
- (5) (a) Jordan, K. D.; Tsai, C. J. *J. Phys. Chem.* **1993**, *97*, 5208. (b) Maheshwary, S.; Patel, N.; Sathyamurthy, N.; Kulkarni, A. D.; Gadre, S. R. *J. Phys. Chem. A* **2001**, *105*, 10525.
- (6) (a) Ma, B.-Q.; Sun, H.-L.; Gao, S. *Angew. Chem., Int. Ed.* **2004**, *43*, 1374. (b) Pal, S.; Sankaran, N. B.; Samanta, A. *Angew. Chem., Int. Ed.* **2003**, *42*, 1741.
- (7) (a) Ghosh, S. K.; Bharadwaj, P. K. *Angew. Chem., Int. Ed.* **2004**, *43*, 3577. (b) Neogi, S.; Savitha, G.; Bharadwaj, P. K. *Inorg. Chem.* **2004**, *43*, 3771. (c) Ghosh, S. K.; Bharadwaj, P. K. *Inorg. Chem.* **2003**, *42*, 8250. (d) Ghosh, S. K.; Bharadwaj, P. K. *Inorg. Chem.* **2004**, *43*, 5180.
- (8) Zhao, B.; Cheng, P.; Chen, X.; Cheng, C.; Shi, W.; Liao, D.; Yan, S.; Jiang, Z. *J. Am. Chem. Soc.* **2004**, *126*, 3012.

- (9) Cheruzel, L. E.; Pometun, M. S.; Cecil, M. R.; Mashuta, M. S.; Wittebort, R. J.; Buchanan, R. M. *Angew. Chem., Int. Ed.* **2003**, *42*, 5452.
- (10) (a) Mukherjee, A.; Saha, K. M.; Nethaji, M.; Chakravarty, A. K. *Chem. Commun.* **2004**, 716. (b) Wakahara, A.; Ishida, T. *Chem. Lett.* **2004**, *33*, 354. (c) Manikumari, S.; Shivaiah, V.; Das, S. K. *Inorg. Chem.* **2002**, *41*, 6953. (d) Supriya, S.; Das, S. K. *New J. Chem.* **2003**, *27*, 1568. (e) Supriya, S.; Das, S. K. *J. Cluster Sci.* **2003**, *14*, 337.
- (11) (a) Raghuraman, K.; Katti, K. K.; Barbour, L. J.; Pillarsetty, N.; Barnes, C. L.; Katti, K. V. *J. Am. Chem. Soc.* **2003**, *125*, 6955. (b) Michaelides, A.; Skoulika, S.; Bakalbassis, E. G.; Mrozniki, J. *Cryst. Growth Des.* **2003**, *3*, 487.
- (12) (a) Barbour, L. J.; Orr, G. W.; Atwood, J. L. *Nature* **1998**, *393*, 671. (b) Barbour, L. J.; Orr, G. W.; Atwood, J. L. *Chem. Commun.* **2002**, *859*.
- (13) Doedens, R. J.; Yohannes, E.; Khan, M. I. *Chem. Commun.* **2002**, 62.
- (14) Custelcean, R.; Afloreaei, C.; Vlassa, M.; Polverejan, M. *Angew. Chem., Int. Ed.* **2000**, *39*, 3094.
- (15) Yaghi, O. M.; O'Keeffe, M.; Ockwig, N. W.; Chae, H. K.; Eddaoudi, M.; Kim, J. *Nature* **2003**, *423*, 705.
- (16) Roesky, H. W.; Andruth, M. *Coord. Chem. Rev.* **2003**, *236*, 91.
- (17) Synthesis of **1**: reaction of Cu(NO₃)₂·2.5H₂O (0.64 g; 2 mmol) and pyrazine-2,3,5,6-tetracarboxylic acid (0.26 g; 1 mmol) dissolved in 25 mL of aqueous pyridine (1: 1 v/v) produces a dark blue solution. This is allowed to evaporate at room temperature whereupon blue crystals of **1** appeared after 6 days in the form of rectangular parallelopipeds in 42% yield. Anal. Calcd for C₄₈H₆₀Cu_{2.5}N₁₁O₂₁: C, 44.84; H, 4.70; N, 11.98%. Found: C, 44.67; H, 4.62; N, 12.04%.

Scheme 1. Schematic Diagram Showing the Bonding Modes of the Ligand with Cu(II)

state, it exhibits a broad absorption band centered at 515 nm. The effective magnetic moment value is found to be $2.01 \mu_B$ at 300 K which is normal for Cu(II) complexes.¹⁸ The compound displays an EPR signal (X-band, Bruker 300E) with $g_{\perp} = 2.22$ and $g_{\parallel} = 2.07$ at 300 K consistent¹⁹ with the d_2^2 ground state of the metal ion. The signal sharpens somewhat as the temperature is lowered to 120 K without revealing any detail indicative of its stereochemistry.

The structure of the compound²⁰ can be described as a 2D coordination polymer of hexa- and pentacoordinated Cu(II) with coordination from pyrazine tetracarboxylate and pyridine. Both the carboxylate groups and the ring N on one side of the ligand bind one Cu(II) showing NO_2 coordination leaving one O atom on each carboxylate free. Three pyridine molecules bind this Cu(II) ion to complete hexacoordination. Two such metal–ligand ensembles axially coordinate two Cu(II) ions through carboxylate O atoms on the other side of the ligand where the equatorial sites on the metals are occupied by three rather than four pyridine molecules to avoid steric crowding leading to trigonal bipyramidal coordination geometry. Two more Cu(II) ions are axially bonded to this tetranuclear unit sideways via carboxylate oxygens propagating the coordination polymeric chain along the crystallographic a axis. These Cu(II) ions achieve hexacoordination with equatorial binding of four pyridine molecules. A view of the binding mode of the ligands to Cu(II)

**Figure 1.** (a) The MOF structure of **1** viewed in the bc plane. The water molecules are shown in red. (b) The MOF structure of **1** viewed in the bc plane. The water molecules have been omitted to show the cavities.

is illustrated in Scheme 1. The bond distances and bond angles involving the metal ions are similar to those found in other Cu(II) complexes^{7d} while bond distances and bond angles in the ligand moieties are within normal statistical errors. The NO_3^- anions are not bonded to any of the metal ions. Out of the 10 water molecules present in the asymmetric unit, the group of eight forms a $(\text{H}_2\text{O})_{16}$ cluster with a centrosymmetrically related group. Four coordination polymeric chains gather around these $(\text{H}_2\text{O})_{16}$ clusters via hydrogen bonding to the free carboxylate O atoms and the nitrate anions leading to the 3D network structure (Figure 1a). Once the water molecules are deleted from the packing diagram, the cavities can be seen (Figure 1b).

Theoretical calculations⁵ present a rich structural landscape for the $(\text{H}_2\text{O})_{16}$ cluster showing a number of local minima. The structures associated with these minima include fused cubes derived from the D_{2d} and S_4 forms of $(\text{H}_2\text{O})_8$ as well as structures containing various numbers of five-membered rings, two of which also contain one six-membered ring. The structures derived from fused cubes are more stable than the rest by ~ 1.2 kcal/mol of energy. A closer view of the $(\text{H}_2\text{O})_{16}$ cluster in **1** (Figure 2) illustrates a new mode of supramolecular association of the water molecules that has not been predicted theoretically. Important bond distances and angles related to the $(\text{H}_2\text{O})_{16}$ cluster collected in Table 1 also illustrate this point. A wide variation in the $\text{O}\cdots\text{O}$ nonbonding distances is found. These distances span the range 2.848–2.441 Å, compared^{1a} to 2.759 Å in ice I_h or 2.85 Å in liquid

(18) Cotton, F. A.; Wilkinson, G. *Advanced Inorganic Chemistry*, 5th ed; Wiley: New York, 1988; p 768.

(19) Hathaway, B. J.; Billing, D. E. *Coord. Chem. Rev.* **1970**, *5*, 143.

(20) Crystal data for **1**: crystal dimensions $0.14 \times 0.11 \times 0.09$ mm³, formula $\text{C}_{48}\text{H}_{60}\text{Cu}_{2.5}\text{N}_{11}\text{O}_{21}$, fw 1285.92, monoclinic, space group $P2_1/c$, $a = 12.6380(6)$ Å, $b = 16.7017(8)$ Å, $c = 26.4479(13)$ Å, $\beta = 94.0080(10)^\circ$, $U = 5568.9(5)$ Å³, $Z = 4$, $\rho_{\text{calcd}} = 1.534$ g cm⁻³, $T = 100$ K, $\mu = 1.037$ mm⁻¹, $R1 = 0.0350$ ($I > 2\sigma(I)$), $wR2 = 0.0944$, $S = 1.081$. All non-hydrogen atoms were refined anisotropically. Hydrogen atoms were located in successive difference Fourier maps, and they were treated as riding atoms using SHELXL default parameters.

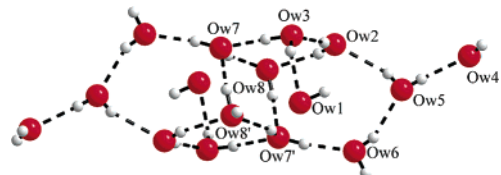


Figure 2. A perspective view of the $(\text{H}_2\text{O})_{16}$ cluster illustrating the hydrogen bonding scheme. No connection between Ow1 and Ow7 is shown as one of the H atoms of Ow1 could not be located in the map.

Table 1. Bond Lengths and Angles for the Hexadecameric Water Cluster^a

length (Å)		angle (deg)	
OW4…OW5	2.769(6)	OW4…H–OW5	177.6(2)
OW5…OW6	2.716(6)	OW5…H–OW6	153.9(2)
OW6…OW7	2.681(5)	OW6…H–OW7	169.0(1)
OW7…OW8	2.835(4)	OW8…H–OW7	155.4(2)
OW8…OW7'	2.757(6)	OW7'…H–OW8	159.6(1)
OW8…OW1	2.557(3)		
OW7…OW1	2.827(4)		
OW1…OW3	2.441(5)		
OW3…OW2	2.711(6)	OW3…H–OW2	177.3(1)
OW2…OW5	2.819(3)	OW2…H–OW5	148.1(2)
OW7'…OW3	2.848(5)	OW7'…H–OW3	161.2(2)
OW2…OW8'	2.824(6)	OW8…H–OW2	170.5(1)

^a One H atom attached to OW1 could not be located in the difference Fourier map.

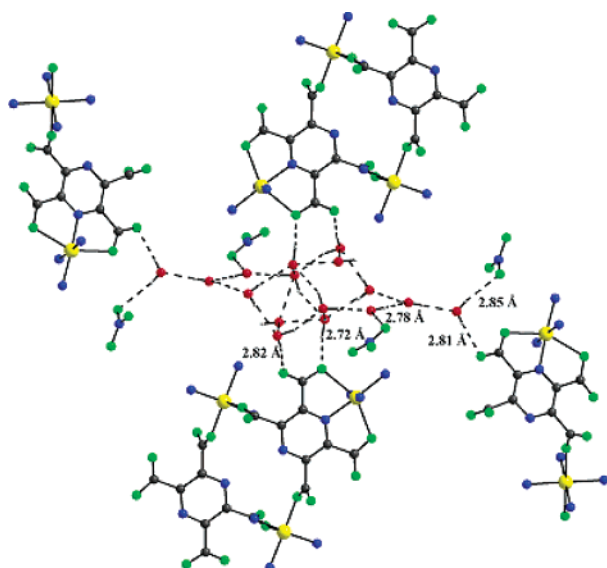


Figure 3. A view showing how water molecules are bound to the MOF. The lone blue spheres are pyridine N atoms. The entire pyridine molecule is not shown for clarity.

water. The O…O…O angles also vary widely (range 151–81°) with an average of 117° deviating considerably from the corresponding value of 109.3° in hexagonal ice. Not every O atom in the cluster shows four-coordination just like water molecules²¹ at the surface of ice or liquid water. However, a majority of the nonbonding hydrogen atoms of the cluster are hydrogen-bonded to the available O atoms of the carboxylate and nitrate groups that are present nearby (Figure 3). As can be seen from Figure 1a,b, the shape of the cavity in the MOF closely follows the shape of the water cluster to maximize the strength as well as number of interactions with the MOF. This indicates a complementary relationship between the cluster and its surroundings in terms of occupy-

ing the voids, underlining the importance of water molecules in establishing hydrogen-bonding contributions to the total lattice energy and not just filling the voids in the 3D structure.

Thermal gravimetric analysis on a 9.85 mg sample of **1** shows onset of water loss at 30° C. Water removal takes place without showing any distinct plateau in the curve giving a total loss of 28.1% at ~130 °C corresponding to loss of all water molecules (calculated value, 27.6%). The complete decomposition of the compound is achieved above 150° C. The FTIR spectrum of **1** shows a broad band centered around 3405 cm⁻¹ which vanishes on heating the compound under vacuum (0.1 mm) at 120° C for 2 h due to escape of water from the lattice. Deliberate exposure to water vapor for 3 days does not lead to reabsorption of water into the lattice as monitored by FTIR spectroscopy. The O–H stretching vibrations of small water clusters (H_2O)_n ($n = 2–10$) in the gaseous state have been investigated²² using infrared depletion and fragment spectroscopy. The stretching vibrations are found to be size specific spreading over a wide range from 3720 to 2935 cm⁻¹ with the higher nuclearity clusters showing the vibration below 3400 cm⁻¹. In comparison, the O–H stretching vibration in ice appears^{1e} at 3220 cm⁻¹ while in liquid it shifts^{1e} to 3280 and 3490 cm⁻¹. Therefore, the O–H stretching frequency of the water cluster in **1** is more like liquid water with a slight variation attributable to its surroundings. Powder X-ray diffraction patterns of **1** before (simulated) and after water expulsion show a complete change in the pattern, suggesting breakdown of the host lattice due to the exclusion of water. This result is expected, as the water cluster acts as a “glue” to assemble the coordination polymeric chains around it leading to the 3D structure.

In conclusion, we have identified a novel discrete hexadecameric water cluster in an MOF structure. This new mode of association of water molecules has not been predicted theoretically. The water clusters here take the role of a “glue” in forming the 3D supramolecular network. The cluster exhibits wide variation in the hydrogen-bonding interactions and adopts a structure necessary for optimal attractive forces with the MOF. However, the degree of structuring of the water cluster that can be imposed by its environment and vice versa can be commented upon once a large number of similar water clusters in different environments are available. Water clusters of different sizes and shapes in diverse environments are presently being investigated in our laboratory.

Acknowledgment. We gratefully acknowledge the financial support received from the Council of Scientific and Industrial Research, New Delhi, India (grant No.1638/EMR II), and an SRF to S.K.G.

Supporting Information Available: Crystallographic data (CIF) and figures depicting the binding mode of ligand with Cu(II), binding mode of waters, IR, thermal analysis, and X-ray powder diffraction patterns for **1** (PDF). This material is available free of charge via the Internet at <http://pubs.acs.org>.

IC049111F

(21) Gruenloh, C. J.; Carney, J. R.; Arrington, C. A.; Zwier, T. S.; Fredericks, S. Y.; Jordan, K. D. *Science* **1997**, 276, 1678.

(22) Buck, U.; Huisken, F. *Chem. Rev.* **2000**, 100, 3863.

Puckered-Boat Conformation Hexameric Water Clusters Stabilized in a 2D Metal–Organic Framework Structure Built from Cu(II) and 1,2,4,5-Benzenetetracarboxylic Acid

Sujit K. Ghosh and Parimal K. Bharadwaj*

Chemistry Department, Indian Institute of Technology Kanpur, 208016 India

Received February 29, 2004

1,2,4,5-Benzenetetracarboxylic acid (btcH_4) reacts with $\text{Cu}(\text{NO}_3)_2 \cdot 6\text{H}_2\text{O}$ to form 2D coordination polymeric structure $\{[\text{Cu}_2(\text{btc})(\text{Py})_4] \cdot 2\text{H}_2\text{O}\} \cdot 4\text{H}_2\text{O}\}_n$, **1**, in the presence of pyridine from water at room temperature. Puckered-boat-shaped hexameric water clusters resulting from four free water molecules and two water molecules coordinating to metal ions join these sheets to make a 3D network. These water clusters behave as pillars to join those sheets which is the key factor stabilizing the 3D network. Thermal analysis, X-ray powder diffraction, and X-ray structure analysis have been used to characterize this compound. Crystal data for **1** follow: triclinic space group $P\bar{1}$, $a = 8.905(3)$ Å, $b = 11.137(4)$ Å, $c = 17.484(2)$ Å, $\alpha = 82.342(6)^\circ$, $\beta = 81.312(3)^\circ$, $\gamma = 82.361(4)^\circ$, $V = 1687.5(1)$ Å³, $Z = 2$, $R1 = 0.0331$, $wR2 = 0.0886$, $S = 1.066$.

Hydrogen bonding interactions, their fluctuations, and their rearrangement dynamics determine the properties of liquid water, some of which are considered anomalous. A major obstacle¹ to fully comprehend its behavior is a correct description of the cooperative nature of hydrogen bonding interactions among a collection of water molecules. This diversity of hydrogen bonding interactions is very important in the biological world as it can enforce a delicate balance² among several possible conformations of enzymes essential for their functions. The key to testing and calibrating theoretical studies to understand this liquid is having precise structural data of hydrogen bonded small water clusters in diverse environments. The advantage of clusters is the possibility to simply vary the size and to investigate the development of properties of the condensed phase in a step by step manner. This realization has led to the upsurge^{3–10}

in studying small water clusters in different environments. An understanding of the properties of water is important from the perspectives of protein crystallization,¹¹ stabilization and functioning of biomolecules,¹² cloud and ice formation, solution chemistry, and so on. Moreover, the degree of structuring of the water cluster that can be imposed by its environment, and vice versa, can be of importance in the design of new metal–organic framework (MOF) structures.¹³ Here, both water–MOF and water–water interactions can be important for the stability of the overall structure. Among the small water clusters, the hexamer is subjected to a number of experimental and theoretical studies as this cluster is the building block of ice¹⁴ and also exhibits¹⁵ some of the properties of bulk water. Theoretical calculations¹⁶ have predicted five low energy isomers for this cluster that are isoenergetic. While chair,¹⁷ boat,¹⁸ and planar cyclic¹⁹ forms of hexamers have been identified in crystal hydrates, the

- (5) Raghuraman, K.; Katti, K. K.; Barbour, L. J.; Pillarssetty, N.; Barnes, C. L.; Katti, K. V. *J. Am. Chem. Soc.* **2003**, *125*, 6955.
- (6) Mukherjee, A.; Saha, K. M.; Nethaji, M.; Chakravarty, A. K. *Chem. Commun.* **2004**, 716.
- (7) Wakahara, A.; Ishida, T. *Chem. Lett.* **2004**, 33, 354.
- (8) Ma, B.-Q.; Sun, H.-L.; Gao, S. *Angew. Chem., Int. Ed.* **2004**, *43*, 1374.
- (9) Cheruzel, L. E.; Pometun, M. S.; Cecil, M. R.; Mashuta, M. S.; Wittebort, R. J.; Buchanan, R. M. *Angew. Chem., Int. Ed.* **2003**, *42*, 5452.
- (10) Zhao, B.; Cheng, P.; Chen, X.; Cheng, C.; Shi, W.; Liao, D.; Yan, S.; Jiang, Z. *J. Am. Chem. Soc.* **2004**, *126*, 3012.
- (11) Quiocho, F. A.; Wilson, D. K.; Vyas, N. K. *Nature* **1989**, *340*, 404.
- (12) ten Wolde, P. R.; Frenkel, D. *Science* **1997**, *277*, 1975.
- (13) Michaelides, A.; Skoulika, S.; Bakalassis, E. G.; Mroznik, J. *Cryst. Growth Des.* **2003**, *3*, 487.
- (14) (a) Matsumoto, M.; Saito, S.; Ohmine, I. *Nature* **2002**, *416*, 409. (c) Fletcher, N. H. *The Chemical Physics of Ice*; Cambridge University Press: Cambridge, 1970.
- (15) (a) Gregory, J. K.; Clary, D. C.; Liu, K.; Brown, M. G.; Saykally, R. J. *Science* **1997**, *275*, 814. (b) Eisenberg, D.; Kauzmann, W. *The Structure and Properties of Water*; Oxford University Press: Oxford, 1969. (c) Jeffrey, G. A. *An Introduction to Hydrogen Bonding*; Oxford University Press: Oxford, 1997.
- (16) (a) Kim, K.; Jordan, K. D.; Zwier, T. S. *J. Am. Chem. Soc.* **1994**, *116*, 11568. (b) Tsai, C. J.; Jordan, K. D. *Chem. Phys. Lett.* **1993**, *213*, 181.
- (17) (a) Custecean, R.; Afloreaei, C.; Vlassa, M.; Polverejan, M. *Angew. Chem., Int. Ed.* **2000**, *39*, 3094. (b) Ghosh, S. K.; Bharadwaj, P. K. *Inorg. Chem.* **2003**, *42*, 8250.
- (18) (a) Park, K. M.; Kuroda, R.; Iwamoto, T. *Angew. Chem., Int. Ed. Engl.* **1993**, *32*, 884. (b) Ren, Y.-P.; Long, L.-S.; Mao, B.-W.; Yuan, Y.-Z.; Huang, R.-B.; Zheng, L.-S. *Angew. Chem., Int. Ed.* **2003**, *42*, 532.

* To whom correspondence should be addressed. E-mail: pkb@iitk.ac.in.

- (1) Keutsch, N. K.; Saykally, R. J. *Proc. Natl. Acad. Sci. U.S.A.* **2001**, *98*, 10533.
- (2) Ben-Naim, A. *Biophys. Chem.* **2002**, *101*, 309.
- (3) (a) Atwood, J. L.; Barbour, L. J.; Ness, T. J.; Raston, C. L.; Raston, P. L. *J. Am. Chem. Soc.* **2001**, *123*, 7192. (b) MacGillivray, L. R.; Atwood, J. L. *J. Am. Chem. Soc.* **1997**, *119*, 2592. (c) Barbour, L. J.; Orr, G. W.; Atwood, J. L. *Nature* **1998**, *393*, 671. (d) Barbour, L. J.; Orr, G. W.; Atwood, J. L. *Chem. Commun.* **2000**, 859.
- (4) Pal, S.; Sankaran, N. B.; Samanta, A. *Angew. Chem., Int. Ed.* **2003**, *42*, 1741.

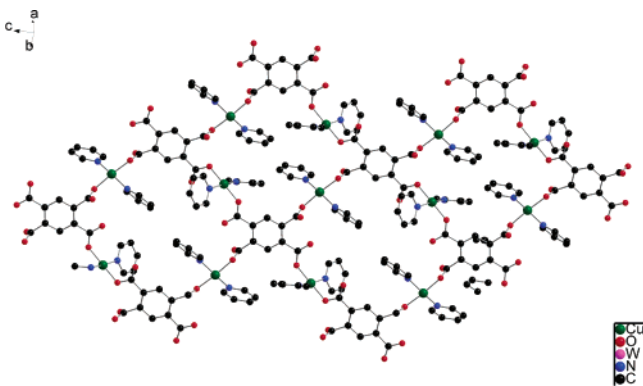


Figure 1. Perspective view of the planar sheet structure of **1**. Hydrogen atoms are omitted for clarity.

“cage” conformer predicted to be the most stable at very low temperature has been observed²⁰ by vibration–rotation tunneling spectroscopy. A quasiplanar cyclic hexamer had been detected²¹ in a helium droplet. Herein, we describe discrete hexameric water clusters with puckered-boat conformation acting as pillars between 2D metal coordination polymers to form a stable 3D MOF.

Compound **1** was prepared²² by evaporating at room temperature an aqueous solution containing 1,2,4,5-benzene-tetracarboxylic acid (btc), $\text{Cu}(\text{NO}_3)_2 \cdot 6\text{H}_2\text{O}$, and pyridine. Blue crystals of **1**, which grew over a period of 14 days, were characterized by X-ray crystallography,²³ elemental analysis, vibrational spectroscopy, X-ray powder diffraction, and thermal analysis.

The asymmetric unit of **1** contains one btc^{4-} , two Cu^{2+} , four pyridines, and six water molecules. The MOF consists of two-dimensional sheets (Figure 1) formed by interconnecting ring structures made from four btc^{4-} units, four Cu^{2+} ions, and eight pyridines. Each metal ion is five-coordinate, having square-pyramidal geometry with equatorial coordination from two carboxylate oxygens from two different btc^{4-} units and two nitrogens from two pyridines. The axial site is occupied by a water oxygen. Two coordinated water molecules in adjacent Cu(II) ions are hydrogen-bonded to

Table 1. Geometrical Parameters of Hydrogen Bonds (Å, deg) for the Water Hexamer^a

Ow1…Ow2	2.735	Ow1…Ow2…Ow3	99.77
Ow2…Ow3	2.923	Ow2…Ow3…Ow4	93.25
Ow3…Ow4	2.797	Ow3…Ow4…Ow5	97.20
Ow4…Ow5	2.893	Ow5…Ow6…Ow1	77.71
Ow5…Ow6	2.819	Ow6…Ow1…Ow2	107.29
Ow6…Ow1	2.906		
Ow1…O1a	2.66	Ow1—H…O1a	163.53
Ow2…O7b	2.78	Ow2—H…O7b	172.11
Ow3…O3a	2.73	Ow3—H…O3a	179.10
Ow3…O5b	2.72	Ow3—H…O5b	163.21
Ow4…O1a	2.79	Ow4—H…O1a	164.18
Ow5…O7b	2.70	Ow5—H…O7b	178.51
Cu1…Ow6	2.27		
Cu2…Ow1	2.29		
Ow1—H…Ow2	170.50	Ow2—H…Ow3	166.50
Ow4—H…Ow3	173.57	Ow5—H…Ow4	177.90
Ow6—H…Ow5	169.67	Ow6—H…Ow1	157.78

^a Please refer to Figure 3 for atom designation.

each other while another water molecule is hydrogen-bonded to an available carboxylate O atom of the same sheet. The remaining three water molecules are hydrogen-bonded to free carboxylate O atoms of another sheet leading to an overall 3D structure. Thus, the hexameric water clusters act as pillars separating two layers of coordination polymers (Figure 2). An approximate distance of 6.962 Å between the layers is maintained by these pillars.

The geometrical parameters of the water clusters are collected in Table 1. Both Ow1 and Ow6 are coordinated to adjacent Cu(II) ions from the same 2D sheet. Atom Ow1 acts as a double hydrogen bond donor while Ow4 acts as a double hydrogen bond acceptor. The remaining water molecules act as hydrogen bond donors as well as acceptors. So, every oxygen atom in the cluster does not show four-coordination. Such hydrogen bond deficient water molecules are present²⁴ at the surface of ice while recent X-ray absorption spectroscopy and Raman scattering studies of liquid water also point to the fact that significant numbers of O atoms show less than four-coordination in liquid water.²⁵ The cluster takes the shape of a puckered boat (Figure 3). The interconnected boat conformation was found¹⁴ in hexagonal ice (I_h) and also identified¹⁸ between the layers of an inorganic polymer constructed from $\text{CdNi}(\text{CN})_4$ units. However, the boats are not interconnected in **1** due to the particular orientation of the btc^{4-} moieties in the structure (Figure 3). In the hexamer, the average O…O distance is found to be 2.845 Å which compares well with the distance¹⁵ in liquid water. The bulk water exhibits a short-range O…O order in the X-ray diffraction radial distribution curve at 2.85 Å, while for the gas phase, this value is ~0.1 Å longer.^{15c} On the other hand, in I_h the average O…O distance is less at 2.74 Å. Also, the O…O…O angles in the present structure span a wide range (93.2(4)–113.2(2)°) deviating considerably from the corresponding value in ice.¹⁴ In a recent

- (19) Moorthy, J. N.; Natarajan, R.; Venugopalan, P. *Angew. Chem., Int. Ed.* **2002**, *41*, 3417.
- (20) Liu, K.; Brown, M. G.; Carter, C.; Saykally, R. J.; Gregory, J. K.; Clary, D. C. *Nature* **1996**, *381*, 501.
- (21) Nauta, K.; Miller, R. E. *Science* **2000**, *287*, 293.
- (22) To an aqueous solution containing btcH_4 (1 mmol) and $\text{Cu}(\text{NO}_3)_2 \cdot 6\text{H}_2\text{O}$ (2 mmol) was added pyridine (5 mmol), and the resulting dark blue solution was allowed to slowly evaporate at room temperature. After two weeks, large blue crystals in the form of rectangular parallelopipeds were collected by filtration. Crystals are stable at room temperature. Yield 40%. Anal. Calcd for $\text{C}_{30}\text{H}_{34}\text{N}_4\text{O}_{14}\text{Cu}_2$: C, 44.93; H, 4.27; N, 6.99%. Found: C, 46.12; H, 4.11, N, 6.78%.
- (23) Crystal data for **1** follow: $M = 801.69 \text{ g mol}^{-1}$, triclinic, space group $P\bar{1}$, $a = 8.905(5)$ Å, $b = 11.137(5)$ Å, $c = 17.484(5)$ Å, $\alpha = 82.342(5)^\circ$, $\beta = 81.312(5)^\circ$, $\gamma = 82.361(5)^\circ$, $U = 1687.5(13)$ Å³, $T = 100$ K, $Z = 4$, $D_c = 1.578 \text{ g cm}^{-3}$, $\mu = 1.334 \text{ mm}^{-1}$, $F(000) = 824$, crystal size = $0.18 \times 0.15 \times 0.13$ mm³. A total of 11333 reflections up to $\theta = 28.30^\circ$ were collected of which 8033 unique reflections were used. The structure was solved using SHELXS-97 and refined using SHELXL-97 to $R_1 = 0.0331$, $wR_2 = 0.0886$, $GOF = 1.067$, final residual peak = +0.796 and hole = -0.462 e Å⁻³ for 7182 reflections with $I > 2\sigma(I)$ and data/parameter ratio of 14.4. All non-hydrogen atoms were refined anisotropically. Hydrogen atoms were located in successive difference Fourier maps, and they were treated as riding atoms using SHELXL default parameters.

- (24) Gruenloh, C. J.; Carney, J. R.; Arrington, C. A.; Zwier, T. S.; Fredericks, S. Y.; Jordan, K. D. *Science* **1997**, *276*, 1678.
- (25) Warnet, Ph.; Nordlund, D.; Bergmann, U.; Cavalleri, M.; Odelius, M.; Ogasawara, H.; Näslund, L. A.; Hirsch, T. K.; Ojamäe, L.; Glatzel, P.; Pettersson, L. G. M.; Nilsson, A. *Science* **2004**, *304*, 995.

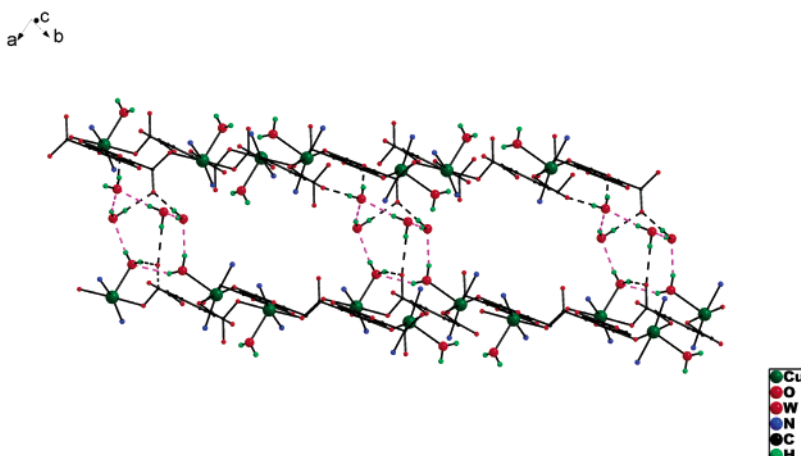


Figure 2. View of the puckered-boat-shaped hexameric water clusters between two sheets of MOF.

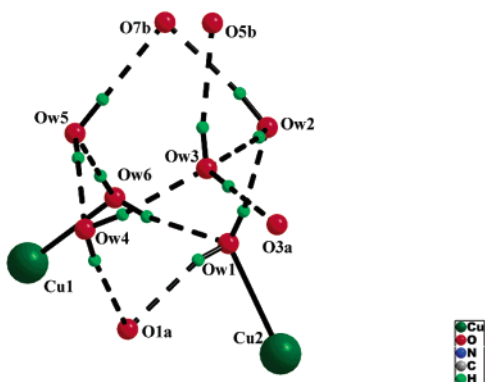


Figure 3. Perspective view of the hexameric water cluster showing hydrogen bonding interactions.

theoretical study²⁶ on the structure of water, an icosahedral 3D network of 280 hydrogen-bonded water molecules with an O···O distance of 2.84 Å has been proposed. This structure is based on the regular arrangement of 20 slightly flattened tetrahedral (H_2O)₁₄ units. Within these units, boat forms of hexamers are predicted to be present along with pentamers, and this proposed structure allows an explanation of several anomalous properties of water. Supramolecular association of water molecules to form a chair conformation and self-assembly into a 1D tape had been identified¹⁷ in an organic host constructed from 2,4-dimethyl-5-aminobenzo-[*b*]-1,8-naphthyridine. A discrete chair conformer has recently been found²⁷ in the zigzag voids of an MOF constructed from pyridine-2,6-dicarboxylic acid and Ce(III) or Pr(III). The puckered-boat conformation of water molecules in **1** is enforced by the quasiplanar metal-ligand sheetlike structure. The interaction between the MOF and the water cluster is moderately strong as thermal gravimetric analysis with an 8.75 mg sample in air shows that weight

loss occurs in stages beginning at 60° C and the loss of 16.24% corresponding to all of the water (calculated 16.78%) takes place above 140° C. The complete decomposition of the compound is achieved above 300 °C. The FTIR spectrum of **1** shows a broad band centered at 3415 cm⁻¹ attributable to the O-H stretching frequency of the water cluster. This broad band vanishes on heating the compound under vacuum (0.1 mm) at 140° C for 2 h suggesting escape of the water molecules from the lattice. The IR spectrum of ice^{15b} shows the O-H stretching at 3220 cm⁻¹ while this stretching vibration in liquid water^{15b} appears at 3490 and 3280 cm⁻¹. This suggests that the water cluster in **1** shows an O-H stretching vibration similar to that of liquid water. Deliberate exposure to water vapor for 3 days does not lead to reabsorption of water into the lattice as monitored by FTIR spectroscopy. Powder X-ray diffraction patterns of the compounds before and after water expulsion show major changes in peak positions as well as their intensities suggesting breakdown of the host lattice once the water molecules are expelled.

In conclusion, we have identified, for the first time, a discrete water hexamer with significantly puckered-boat conformation as suggested to be present in bulk water. These clusters act as pillars between 2D sheets of MOFs. The extent of puckering is commensurate with the MOF structure.

Acknowledgment. We gratefully acknowledge the financial support received from the Council of Scientific and Industrial Research, New Delhi, India (Grant No.1638/EMR II), and an SRF to S.G.

Supporting Information Available: X-ray crystallographic files in CIF format for the structure determination of compound **1**. Structural figures, IR spectra, and X-ray powder diffraction patterns. This material is available free of charge via the Internet at <http://pubs.acs.org>.

IC049739Q

(26) (a) Chaplin, M. F. *Biophys. Chem.* **1999**, *83*, 211. (b) Ludwig, R. *Angew. Chem., Int. Ed.* **2000**, *40*, 1808.

(27) Ghosh, S. K.; Bharadwaj, P. K. *Inorg. Chem.* **2003**, *42*, 8250.

Mn(II) Staircase Structures Stitched by Water Clusters to a 3D Metal-Organic Open Framework: X-ray Structural and Magnetic Studies

Sujit K. Ghosh,[†] Joan Ribas,^{*‡} M. Salah El Fallah,[‡] and Parimal K. Bharadwaj^{*†}

Chemistry Department, Indian Institute of Technology Kanpur, Kanpur 208016, India, and Departament de Química Inorgànica, Universitat de Barcelona, Martí i Franquès, 1-11, 08028-Barcelona, Spain

Received January 22, 2005

4-Hydroxypyridine-2,6-dicarboxylic acid (chelidamic acid, cdaH₂) reacts with Mn(OAc)₂·4H₂O to form a 1D staircase structure with dimeric Mn(II) units connected by water clusters to form a 3D framework, {[Mn₂(cda)₂·4H₂O]_n}, 1, in aqueous pyridine at room temperature. The compound crystallizes in the triclinic space group *P*̄1 with *a* = 9.495(3), *b* = 10.733(5), *c* = 11.065(4) Å, α = 87.42(5), β = 74.14(5), γ = 80.07(2)°, *U* = 1068.5(9) Å³, *Z* = 2, ρ_{calcd} = 1.915 g cm⁻³, *T* = 100 K, μ = 1.28 mm⁻¹, *R*₁ = 0.0453 (*I* > 2*σ*(*I*)), *wR*₂ = 0.1046, GOOF = 1.282. Upon removal of the water molecules by heating, the 3D structure breaks down. Thermogravimetric analysis, infrared, X-ray powder diffraction studies, and X-ray crystallography were performed to characterize this compound. Since the coordination polymer has diaqua-bridged Mn(II) centers, it was subjected to variable-temperature magnetic studies.

Bulk water exhibits¹ a fascinating array of properties, some of which are considered anomalous. A large number of efforts have been made to develop model force fields in the quest to achieve an accurate description of liquid water capable of explaining its properties besides getting an insight into the study of solvation, cloud and ice formation, biological processes, and so forth. It is recognized that hydrogen-bonding interactions, their fluctuations, and rearrangement dynamics determine the properties of bulk water. But, none of the existing models can explain all of the properties of water, even with considerable interpretation. A major obstacle² to fully comprehending its behavior is that of correctly describing the cooperative nature of hydrogen-bonding interactions among a collection of water molecules; the key to tackling this will be the exploration of structural and binding properties of small water clusters in different surroundings. This realization has led to an upsurge^{3–9} in the

characterization of water clusters of different nuclearity in crystal hydrates. The advantage of clusters is the possibility to simply vary the size and to investigate the development of properties of the condensed phase in a step-by-step manner. Moreover, the degree of structuring of a water cluster that can be imposed by its environment and vice versa can be of importance in designing new metal-organic framework (MOF) structures.¹⁰

* To whom correspondence should be addressed. E-mail: pkb@iitk.ac.in (P.K.B.), joan.ribas@qi.ub.es (J.R.).

[†] Indian Institute of Technology Kanpur.

[‡] Universitat de Barcelona.

- (1) (a) Ludwig, R. *Angew. Chem., Int. Ed.* **2001**, *40*, 1808. (b) Eisenberg, D.; Kauzmann, W. *The Structure and Properties of Water*; Oxford University Press: Oxford, 1969.
- (2) (a) Keutsch, F. N.; Saykally, R. J. *Proc. Natl. Acad. Sci. U.S.A.* **2001**, *98*, 10533. (b) Chaplin, M. F. *Biophys. Chem.* **1999**, *83*, 211.
- (3) (a) Sreenivasulu, B.; Vittal, J. J. *Angew. Chem., Int. Ed.* **2004**, *43*, 5769. (b) Ng, M. T.; Deivaraj, T. C.; Klooster, W. T.; McIntyre, G. J.; Vittal, J. J. *Chem. Eur. J.* **2004**, *10*, 5853.

- (4) Yoshizawa, M.; Kusukawa, T.; Kawano, M.; Ohhara, T.; Tanaka, I.; Kurihara, K.; Nimura, N.; Fujita, M. *J. Am. Chem. Soc.* **2005**, *127*, 2798.
- (5) (a) Liu, Q.-Y.; Xu, L. *CrystEngComm* **2005**, *7*, 87. (b) Ma, B. Q.; Sun, H. L.; Gao, S. *Angew. Chem., Int. Ed.* **2004**, *43*, 1374. (c) Müller, A.; Krickemeyer, E.; Böggie, H.; Schmidtmann, M.; Botar, B.; Talismanova, M. O. *Angew. Chem., Int. Ed.* **2003**, *42*, 2085.
- (6) (a) Ghosh, S. K.; Bharadwaj, P. K.; *Angew. Chem., Int. Ed.* **2004**, *43*, 3577. (b) Neogi, S.; Savitha, G.; Bharadwaj, P. K. *Inorg. Chem.* **2004**, *43*, 3771.
- (7) (a) Cuamatzi, P. R.; Diaz, G. V.; Hopfl, H. *Angew. Chem., Int. Ed.* **2004**, *43*, 3041. (b) Raguraman, K.; Katti, K. K.; Barbour, L. J.; Pillarsetty, N.; Barnes, C. L.; Katti, K. V. *J. Am. Chem. Soc.* **2003**, *125*, 6955. (c) Pal, S.; Sankaran, N. B.; Samanta, A. *Angew. Chem., Int. Ed.* **2003**, *42*, 1741.
- (8) (a) Barbour, L. J.; Orr, G. W.; Atwood, J. L. *Chem. Commun.* **2002**, 859. (b) Atwood, J. L.; Barbour, L. J.; Ness, T. J.; Raston, C. L.; Raston, P. L. *J. Am. Chem. Soc.* **2001**, *123*, 7192. (c) Barbour, L. J.; Orr, G. W.; Atwood, J. L. *Nature* **1998**, *393*, 671.
- (9) (a) Infantes, L.; Motherwell, S. *CrystEngComm* **2002**, *4*, 454. (b) Infantes, L.; Chisholm, J.; Motherwell, S. *CrystEngComm* **2003**, *5*, 480.
- (10) (a) Ghosh, S. K.; Bharadwaj, P. K. *Inorg. Chem.* **2004**, *43*, 5180. (b) Ghosh, S. K.; Bharadwaj, P. K. *Inorg. Chem.* **2004**, *43*, 6887.

Synthesis of MOFs with multidentate ligands may provide voids to accommodate water clusters where both water–MOF and water–water interactions determine the overall structure. Any such exercise has the ultimate aim(s) of having novel materials with useful applications. Metal-organic hybrid structures of paramagnetic metal ions are particularly interesting as these may give rise to a series of novel framework structures with potential applications in the fields of molecular magnetism¹¹ and material chemistry.¹² A commonly used strategy in building such extended network structures is to employ bridging ligands capable of transmitting magnetic interactions in addition to propagate the network. We report here an MOF, built from 4-hydroxypyridine-2,6-dicarboxylic acid (chelidamic acid, cdaH₂) and Mn(II)-acetate salt. Earlier, we¹³ and others¹⁴ had used closely related pyridine-2,6-dicarboxylic acid for generating novel MOFs with transition- as well as lanthanide-metal ions. To probe the effect of the hydroxyl group at the 4-position, cdaH₂ was used here to afford a stairlikelike coordination polymer built through carboxylate- and aquo-bridging. Discrete tetradecameric water clusters assemble these staircases via an intricate array of hydrogen bonding into an overall 3D MOF. The water cluster takes the shape of a hexameric chair buttressed on two sides by acyclic tetramers. While no experimental report is available identifying a tetradecameric water cluster either in inorganic or in organic crystal hosts, theoretical calculations on (H₂O)₁₄ have revealed¹⁵ four energy minima corresponding to four structures arising from extensions of cuboids, pentagonoids, and their combinations. The present contribution reports the synthesis, crystal structure, thermal stability, and variable-temperature magnetic susceptibility of the compound.

Experimental Section

Materials. The metal salt and 4-hydroxypyridine-2,6-dicarboxylic acid (chelidamic acid) were acquired from Aldrich and used as received.

Physical Measurements. Spectroscopic data were collected as follows: IR (KBr disk, 400–4000 cm⁻¹) Perkin-Elmer model 1320; X-ray powder pattern (Cu K α radiation at a scan rate of 3°/min, 293 K) Sievert ISODEBYEFLEX-2002 X-ray generator; thermogravimetric analysis (heating rate of 5 °C/min) Mettler Toledo Star System. Magnetic susceptibility measurements were carried out on

the polycrystalline sample at the Servei de Magnetoquímica of the Universitat de Barcelona, with a Quantum Design SQUID MPMS-XL susceptometer apparatus working in the range 2–300 K under a magnetic field of approximately 500 G (2–30 K) and 1000 G (35–300 K). Diamagnetic corrections were estimated from Pascal Tables. The EPR spectra have been recorded on a X-band Bruker Spectrometer (ESR 300E), working with an oxford liquid helium cryostat for variable temperature. Microanalysis data for the compound were obtained from CDRI, Lucknow.

Syntheses

{[Mn₂(cda)₂·4H₂O]·4H₂O}n, 1. A solution containing Mn(OAc)₂·4H₂O (0.25 g; 1 mmol) and chelidamic acid (0.18 g; 1 mmol) dissolved in 25 mL of aqueous pyridine (1:1 v/v) on slow evaporation at room temperature, affords light purple crystals of **1** after 14 days in the form of a rectangular parallelepiped in 55% yield. Anal. Calcd for C₁₄H₂₂N₂O₁₈Mn₂: C, 27.28; H, 3.56; N, 4.54%. Found: C, 27.15; H, 3.62; N, 4.37%.

X-ray Structural Studies. Single-crystal X-ray data on **1** were collected at 100 K on a Bruker SMART APEX CCD diffractometer using graphite-monochromated Mo K α radiation ($\lambda = 0.71073 \text{ \AA}$). The linear absorption coefficients, scattering factors for the atoms, and the anomalous dispersion corrections were taken from International Tables for X-ray Crystallography. The data integration and reduction were processed with SAINT¹⁶ software. An empirical absorption correction was applied to the collected reflections with SADABS¹⁷ using XPREP.¹⁸ The structure was solved by the direct method using SHELXTL¹⁹ and was refined on F² by full-matrix least-squares technique using the SHELXL-97²⁰ program package. Non-hydrogen atoms were refined anisotropically. All hydrogen atoms were located in successive difference Fourier maps, and they were treated as riding atoms using SHELXL default parameters. The crystal and refinement data are collected in Table 1.

Results and Discussion

The compound is air-stable and, once formed, is insoluble in most solvents including water. The asymmetric unit of **1** contains two cda²⁻, two Mn(II), and eight water molecules. Each Mn(II) ion exhibits heptacoordination with a distorted pentagonal bipyramidal geometry where equatorial coordination comes from the ring N and the carboxylates of a cda²⁻ ligand, one water, and one carboxylate from the neighboring cda²⁻ ligand (NO₄ donor set). Two water molecules occupy the axial positions. The hydroxyl group at the 4-position of cda²⁻ does not take part in metal coordination; it is involved in hydrogen-bonding interactions with neighboring carboxylate O atoms. The lone equatorial and one of the axial water molecules are involved in bridging another Mn(II) ion, thus

- (11) (a) Kahn, O. *Molecular Magnetism*; Wiley-VCH: New York, 1993. (b) Miller, J. S.; Epstein, A. J. *Angew. Chem., Int. Ed. Engl.* **1994**, *33*, 385. (c) Ohba, M.; Okawa, H. *Coord. Chem. Rev.* **2000**, *198*, 313. (d) Tasiopoulos, A. J.; Vinslava, A.; Wernsdorfer, W.; Abboud, K. A.; Christou, G. *Angew. Chem., Int. Ed.* **2004**, *43*, 2117.
- (12) (a) Venkataraman, D.; Gardner, G. B.; Lee, S.; Moore, J. S. *J. Am. Chem. Soc.* **1995**, *117*, 11600. (b) Yaghi, O. M.; Li, G.; Li, H. *Nature* **1995**, *378*, 703. (c) Kepert, C. J.; Rosseinsky, M. J. *Chem. Commun.* **1999**, 375.
- (13) (a) Ghosh, S. K.; Bharadwaj, P. K. *Inorg. Chem.* **2003**, *42*, 8250. (b) Ghosh, S. K.; Bharadwaj, P. K. *Inorg. Chem.* **2004**, *43*, 2293. (c) Ghosh, S. K.; Savita, G.; Bharadwaj, P. K. *Inorg. Chem.* **2004**, *43*, 5495. (d) Ghosh, S. K.; Ribas, J.; Bharadwaj, P. K. *CrystEngComm* **2004**, *45*, 250. (e) Ghosh, S. K.; Ribas, J.; Bharadwaj, P. K. *Cryst. Growth Des.* **2005**, *5*, 623.
- (14) (a) Nobuo, O.; Hasuyo, K.; Ayumi, F. *Acta Crystallogr. E* **2002**, *E58*, m354. (b) Zhao, B.; Yi, D.; Chen, X.-Y.; Cheng, P.; Liao, D.-Z.; Yan, S.-P.; Jiang, Z.-H. *Inorg. Chem.*, in press.
- (15) Maheswary, S.; Patel, N.; Sathyamurthy, N.; Kulkarni, A. D.; Gadre, S. R. *J. Phys. Chem. A* **2001**, *105*, 10525.

(16) SAINT+, 6.02 ed.; Bruker AXS: Madison, WI, 1999.

(17) Sheldrick, G. M. SADABS, *Empirical Absorption Correction Program*; University of Göttingen: Göttingen, Germany, 1997.

(18) XPREP, 5.1 ed.; Siemens Industrial Automation Inc.: Madison, WI, 1995.

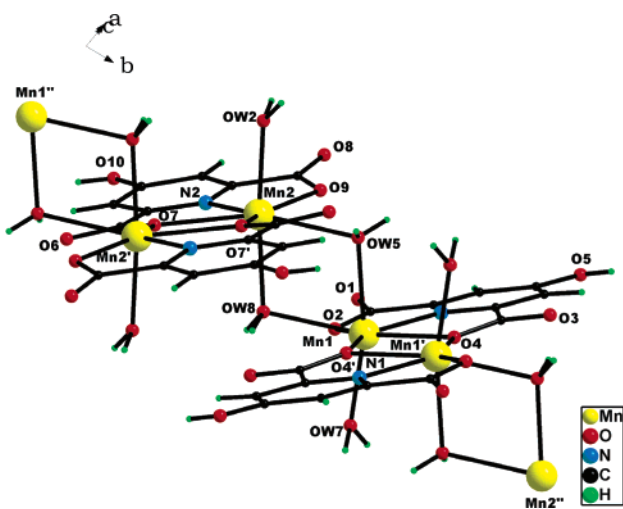
(19) Sheldrick, G. M. *SHELXTL, Reference Manual*: version 5.1: Bruker AXS; Madison, WI, 1997.

(20) Sheldrick, G. M. *SHELXL-97: Program for Crystal Structure Refinement*; University of Göttingen: Göttingen, Germany, 1997.

Table 1. Crystal and Structure Refinement Data for **1**

empirical formula	C ₁₄ H ₂₂ N ₂ O ₁₈ Mn ₂
formula weight	616.22
temperature	100 K
radiation, wavelength	Mo K α , 0.71073 Å
crystal system	triclinic
space group	P-1
a, Å	9.495(3)
b, Å	10.733(5)
c, Å	11.065(4)
α (°)	87.425(5)
β (°)	74.143(5)
γ (°)	80.076(2)
U, Å ³	1068.5(9)
Z	2
ρ_{calc} , Mg/m ³	1.915
μ , mm ⁻¹	1.280
F(000)	628
refl. collected	5096
independent refl.	4949
refinement method	full-matrix least-squares on F^2
GOOF	1.282
final R indices	$R_1 = 0.0453$
[$I > 2\sigma(I)$]	$wR_2 = 0.1046$
R indices	$R_1 = 0.0464$
(all data)	$wR_2 = 0.1052$

propagating the coordination polymeric chain along the crystallographic *b*-axis. Each Mn(II) in the chain is further involved in making double carboxylate bridging with another Mn(II) forming a dimeric unit that forms a step in the stairlike coordination polymeric chain (Figure 1). All Mn–O and Mn–N bond distances (Table 2) are somewhat longer

**Figure 1.** A view of the carboxylate-bridged Mn(II) dimeric units further joined by diaquo bridging to form a stairlike structure.

compared²¹ to those found in several related species. The bond angles involving a metal center are all different and deviate from an ideal pentagonal bipyramidal coordination geometry.

One bridging and two nonbridging axial water molecules belong to a staircase unit and are connected to a similar set of water molecules belonging to another staircase through eight other intervening water molecules forming an overall

(21) (a) Tynan, E.; Jensen, P.; Kruger, P. E.; Lees, A. C. *Chem. Commun.* **2004**, 23, 2660. (b) Marioni, P.-A.; Marty, W.; Stoeckli-Evans, H.; Whitaker, C. *Inorg. Chem. Acta* **1994**, 219, 161.

Table 2. Selected Bond Distances (Å) and Bond Angles (°) in **1**

	Bond Distances (Å)		
Mn1–Ow7	2.157(3)	Mn1–Ow5	2.215(2)
Mn1–O4	2.234(2)	Mn1–N1	2.234(2)
Mn1–O2	2.330(2)	Mn1–Ow8	2.413(2)
Mn1–O4'	2.432(2)	Mn2–Ow2	2.123(2)
Mn2–N2	2.216(2)	Mn2–O7	2.232(2)
Mn2–O9	2.285(2)	Mn2–Ow8	2.308(2)
Mn2–Ow5	2.351(2)	Mn2–O7'	2.420(2)
	Bond Angles (°)		
Ow7–Mn1–Ow5	171.03(10)	Ow7–Mn1–O4	89.44(9)
Ow5–Mn1–O4	84.49(8)	Ow7–Mn1–N1	91.18(11)
Ow5–Mn1–N1	97.77(9)	O4–Mn1–N1	136.95(8)
Ow7–Mn1–O2	80.77(9)	Ow5–Mn1–O2	101.60(8)
O4–Mn1–O2	151.78(7)	N1–Mn1–O2	70.11(8)
Ow7–Mn1–Ow8	97.50(10)	Ow5–Mn1–Ow8	75.18(8)
O4–Mn1–Ow8	82.33(7)	N1–Mn1–Ow8	140.01(8)
O2–Mn1–Ow8	72.91(7)	Ow7–Mn1–O4'	96.90(10)
Ow5–Mn1–O4'	87.03(8)	O4–Mn1–O4	68.55(8)
N1–Mn1–O4'	68.65(8)	O2–Mn1–O4'	138.64(7)
Mn1–O4–Mn1	111.45(8)	Ow8–Mn1–O4'	147.24(7)
Ow2–Mn2–N2	104.52(9)	Ow2–Mn2–O7	85.61(8)
N2–Mn2–O7	137.59(8)	Ow2–Mn2–O9	82.46(9)
N2–Mn2–O9	70.96(8)	O7–Mn2–O9	151.28(7)
Ow2–Mn2–Ow8	165.23(8)	Mn2–Ow8–Mn1	100.40(8)
N2–Mn2–Ow8	90.24(8)	O7'–Mn2–Ow8	83.78(7)
O9–Mn2–Ow8	102.25(8)	Ow2–Mn2–Ow5	93.80(9)
N2–Mn2–Ow5	135.68(8)	O7–Mn2–Ow5	82.89(7)
O9–Mn2–Ow5	72.00(7)	OW8–Mn2–OW5	74.73(8)
OW2–Mn2–O7	100.09(9)	N2–Mn2–O7	69.01(8)
O7–Mn2–O7	68.68(8)	O9–Mn2–O7'	139.20(7)
OW8–Mn2–O7	85.56(8)	OW5–Mn2–O7'	147.02(7)
Mn2–O7–Mn2	111.32(8)	Mn1–Ow5–Mn2	105.22(9)

tetradecameric cluster. Atom Ow6 or Ow6', present at either end of this cluster (Figure 2), is within a hydrogen-bonding distance (2.702 Å) from the terminal atom of the next cluster. However, they are related by a center of symmetry, and so their corresponding H-atoms are oriented either face to face (that is, angle, O–H···H 177°) or away from each other and are not considered hydrogen-bonded. The H···H separation of 1.144 Å is, however, shorter compared to the shortest intermolecular H···H separation (1.949 Å) found in the polymorph A of 1,2,3,5-tetra-*O*-acetyl- β -D-ribofuranose.²² The repulsive interaction associated with this short distance is compensated by strong nonbonding water–MOF interactions. Also, atoms Ow5 and Ow8 show a distance of 2.827 Å, although their H-atoms are pointing away from each other leaving the two O atoms face to face and so are not considered as hydrogen-bonded. Therefore, the group of 14 water molecules are regarded as a discrete water cluster. These water clusters assemble the staircases along the crystallographic *a*-axis (Figure 3) while other (H_2O)₁₄ clusters extend the polymeric chain in the crystallographic *c*-axis to form an overall 3D structure (Figure 4). An approximate distance of 9.50 Å is maintained between the staircases by these clusters acting as pillars.

Various nonbonding distances and angles relevant to the water cluster are collected in Table 3. Its structure can be described as an ice-like (I_h) hexameric chair with two acyclic tetramers dangling from two opposite ends (Figure 2). The hexameric part shows a wide variation in the O···O nonbonding distances (Table 3) that range from 2.669 to 2.938

(22) Bombicz, P.; Czugler, M.; Tellgren, R.; Kálmán, A. *Angew. Chem., Int. Ed.* **2003**, 42, 1957.

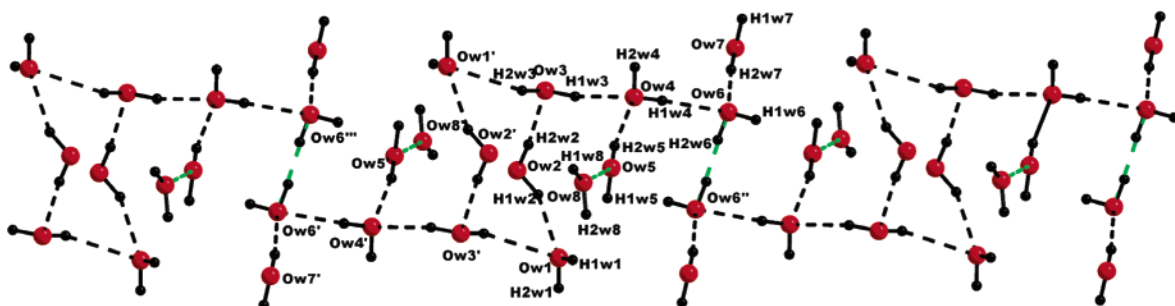


Figure 2. A perspective view of the $(\text{H}_2\text{O})_{14}$ cluster illustrating the hydrogen bonding scheme. The O atoms connected by blue-colored bonds are related by center of symmetry and even though their distances lie within normal hydrogen-bonding distances, they are considered nonbonded as the H-atoms are not pointing in the right directions.

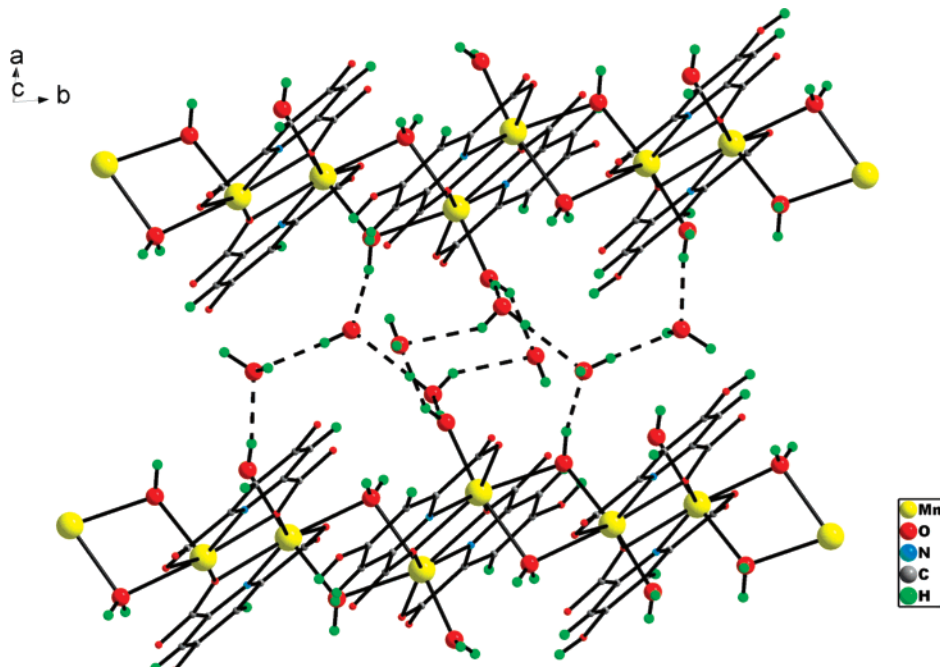


Figure 3. A view showing a tetradecameric water cluster connecting two staircases.

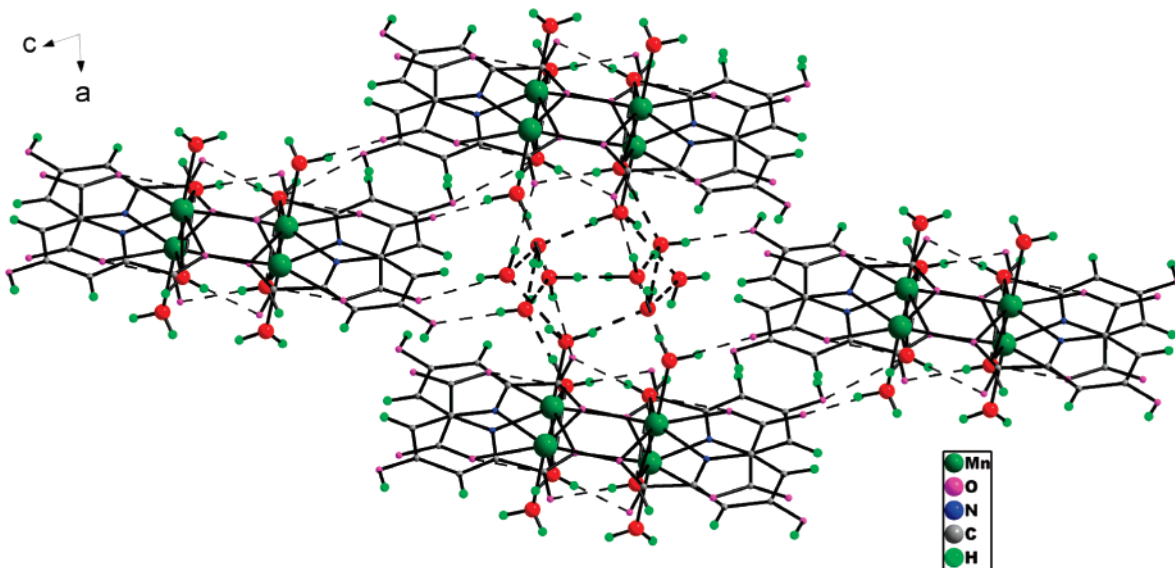


Figure 4. A perspective view showing how the water clusters form the overall 3D MOF.

\AA compared²³ to 2.759 \AA in ice I_h at -90°C or 2.85 \AA in liquid water. The $\text{O}\cdots\text{O}\cdots\text{O}$ angles in the hexamer also vary

widely with an average of 93.57° that is considerably different from the corresponding value of 109.3° in hexagonal

Table 3. Nonbonding Distances (\AA) and Angles ($^\circ$) Pertaining to the Tetradecameric Cluster

Nonbonding Distances (\AA)			
Ow1...Ow2	2.777(6)	H1w1...Ow1	0.826(4)
Ow2...Ow3	2.669(4)	H2w1...Ow1	0.826(3)
Ow3...Ow1	2.938(4)	H1w2...Ow2	0.834(4)
Ow3...Ow4	2.812(6)	H2w2...Ow2	0.849(2)
Ow4...Ow5	2.696(6)	H1w3...Ow3	0.855(1)
Ow4...Ow6	2.810(6)	H2w3...Ow3	0.844(4)
Ow6...Ow7	2.699(6)	H1w4...Ow4	0.841(2)
Ow1...O6	2.840(4)	H2w4...Ow4	0.828(3)
Ow1...O8	2.727(6)	H1w5...Ow5	0.888(4)
Ow4...O5	2.770(3)	H2w5...Ow5	0.841(1)
Ow6...O3	2.811(4)	H2w6...Ow6	0.821(3)
Ow7...O1	2.687(4)	H2w7...Ow7	0.841(4)
Angles ($^\circ$)			
Ow1...H...Ow2	151.2(2)	Ow3...H...Ow2	173.1(1)
Ow3...H...Ow1	150.7(2)	Ow4...H...Ow3	163.3(2)
Ow4...H...Ow5	169.4(2)	Ow6...H...Ow4	177.0(2)
Ow6...H...Ow7	172.2(2)	Ow1-H...O6	159.9(1)
Ow1-H...O8	161.9(2)	Ow4-H...O5	174.6(2)
Ow6-H...O3	145.5(1)	Ow7-H...O1	167.1(2)
Ow1...Ow2...Ow3	104.1(2)	Ow2...Ow3...Ow1'	102.5(1)
Ow3'...Ow1...Ow2	73.9 (3)	Ow3...Ow4...Ow5	106.5(2)
Ow3...Ow4...Ow6	113.6(2)	Ow4...Ow6...Ow7	111.7(3)

ice. Theoretical calculations on the water hexamer revealed²⁴ the existence of several “cage”, “prism”, “book”, “boat”, and “cyclic” conformers which are almost isoenergetic to within ~ 0.7 kcal mol⁻¹. The “cage” conformer is the most stable one at very low temperature and has been observed²⁵ by vibration–rotation tunneling spectroscopy, while a quasi-planar cyclic hexamer was detected²⁶ in a helium droplet. However, the lattice of a crystal host offers an environment where a higher-energy conformer can be stabilized via water–water and water–host interactions, and chair,^{7a,13a,27} boat,²⁸ and planar²⁹ conformers have been characterized crystal hosts.

Supramolecular association of water molecules to form a chair conformation and their self-assembly into a 1D tape

- (23) (a) Buck, U.; Huisken, F. *Chem. Rev.* **2000**, *100*, 3863. (b) Eisenberg, D.; Kauzmann, W. *The Structure and Properties of Water*; Oxford University Press: Oxford, 1969.
- (24) (a) Tsai, C. J.; Jordan, K. D. *Chem. Phys. Lett.* **1993**, *213*, 181. (b) Kim, K.; Jordan, K. D.; Zwier, T. S. *J. Am. Chem. Soc.* **1994**, *116*, 11568.
- (25) Liu, K.; Brown, M. G.; Carter, C.; Saykally, R. J.; Gregory, J. K.; Clary, D. C. *Nature* **1996**, *381*, 501.
- (26) Nauta, K.; Miller, R. E. *Science* **2000**, *287*, 293.
- (27) (a) Foces-Foses, C.; Cano, F. H.; Martinez-Ripoli, M.; Faure, R.; Roussel, C.; Claramunt, R. M.; Lopez, C.; Sanz, D.; Elguero, J. *Tetrahedron: Asymmetry* **1990**, *1*, 65. (b) Michaelides, A.; Skoulika, S.; Bakalbassis, E. G.; Mrozninski, J. *Cryst. Growth Des.* **2003**, *3*, 487.
- (28) Ren, Y.-P.; Long, L.-S.; Mao, B.-W.; Yuan, Y.-Z.; Huang, R.-B.; Zheng, L.-S. *Angew. Chem., Int. Ed.* **2003**, *42*, 532.
- (29) Moorthy, J. N.; Natarajan, R.; Venugopalan, P. *Angew. Chem., Int. Ed.* **2002**, *41*, 3417.

had been identified³⁰ in an organic host constructed from 2,4-dimethyl-5-aminobenzo[*b*]-1,8-naphthyridine. A discrete chair conformer has recently been found^{13a} in the zigzag voids of an MOF constructed from pyridine-2,6-dicarboxylic acid and Ce(III) or Pr(III), while 1D chains consisting of chair conformers connected by Zn(II) or Co(II) have been found³¹ in the complexes, $[\text{M}(\text{H}_2\text{biim})_2(\text{OH}_2)_2](\text{ina})_2 \cdot 4\text{H}_2\text{O}$ [$\text{M} = \text{Zn(II)}$ or Co(II) , $\text{H}_2\text{biim} = 2,2'\text{-biimidazole}$, $\text{ina} = \text{isoniconate}$]. In the present structure, the chair conformation is slightly different from the reported structures with respect to the O...O distances or O...O...O angles, and the hydrogen-bonding interactions are strong and highly directional (Table 3) commensurate with the environment the cluster is in. Each acyclic tetramer is bound to the hexameric unit quite strongly (Ow3...Ow4, 2.812 \AA), while the O...O distances in the tetrameric part span a wide range (2.696–2.810 \AA). It follows, therefore, that the structure of the cluster is sufficiently flexible to be accommodated in the voids between the polymeric chains and at the same time maximizing the interactions among water molecules themselves and between water and carboxylate or hydroxyl O of the coordination polymeric chains (Figure 3). Every O atom in the cluster does not show four coordination just like water molecules³² at the surface of ice or liquid water. Theoretical calculations¹⁵ for the $(\text{H}_2\text{O})_{14}$ cluster have revealed the existence of four energy minima in the potential energy surface corresponding to four different structures arising from extensions of cuboids, pentagonoids, and their combinations. The minimum energy structure is suggested to result from a cube with two parallel pentamers sharing two edges of the cube, while higher-energy structures include extended cuboid, two edge-sharing cuboids, and two parallel fused pentamers attached to a cyclic tetramer on one side (Figure 5). The structure of the cluster described herein is very different from these predicted ones due to the chemical environment.

Thermal gravimetric analysis of **1** further corroborates the existence of strong hydrogen-bonding interactions between the MOF and the water cluster. Weight loss in air due to exclusion of water begins³³ only after 140 °C, and the loss of 23.1% corresponding to all of the water (calculated 23.4%) takes place above 300 °C. Complete decomposition of the compound is achieved above 450 °C. The FTIR spectrum of **1** shows a broad band centered around 3405 cm^{-1} without showing any resolution. This band is not seen in the spectrum taken after heating the compound under vacuum (0.1 mm) at 300 °C for 4 h due to escape of water from the lattice. Deliberate exposure to water vapor for 3 days does not lead to reabsorption of water into the lattice as monitored by FTIR spectroscopy. The powder X-ray diffraction pattern of **1** simulated from the single-crystal data shows several prominent peaks which match with the diffraction peaks on the powdered sample before heating.³³ However, after water

(30) Custecean, R.; Afonsoei, C.; Vlassa, M.; Polverejan, M. *Angew. Chem., Int. Ed.* **2000**, *39*, 3094.

(31) Ye, B.-H.; Ding, B.-B.; Weng, Y.-Q.; Chen, X.-M. *Inorg. Chem.* **2004**, *43*, 6866.

(32) Gruenloh, C. J.; Carney, J. R.; Arrington, C. A.; Zwier, T. S.; Fredericks, S. Y.; Jordan, K. D. *Science* **1997**, *276*, 1678.

(33) See Supporting Information.

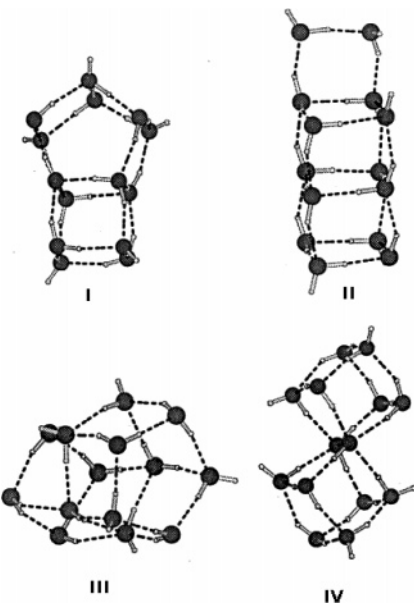


Figure 5. Schematic representation of theoretically calculated low-energy structures of $(\text{H}_2\text{O})_{14}$ cluster.

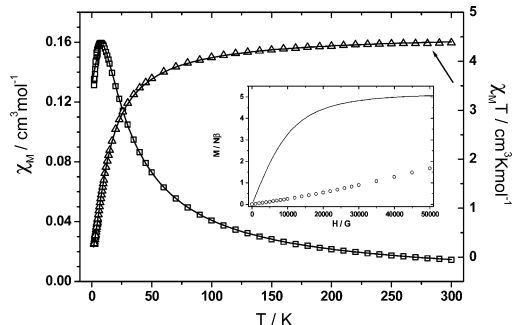


Figure 6. Plot of the $\chi_M T$ vs T for complex **1**. The open points are the experimental ones, and the solid lines correspond to the best fit obtained. Inset: Plot of the magnetization in 2S units measured at 2 K (open circles). Continuous line corresponds to the Brillouin function for an isolated $S = 5/2$.

expulsion by heating, a total change in the pattern is observed, suggesting complete breakdown of the host lattice. This is expected, as the water cluster acts as a “glue” to assemble the overall structure.

Magnetic Properties

The existence of diaquo-bridged Mn(II) centers in the structure prompted us to carry out variable-temperature magnetic studies. The magnetic susceptibility measurements were carried out from 300 to 2 K. Diamagnetic corrections were estimated³⁴ from Pascal’s Table. The magnetic behavior of **1** is illustrated in Figure 6 by means of a plot of $\chi_M T$ vs the temperature. At room temperature, $\chi_M T$ gives a value of $4.37 \text{ cm}^3 \text{ K mol}^{-1}$ which is as expected for one Mn(II) ion ($4.375 \text{ cm}^3 \text{ mol}^{-1} \text{ K}$ per Mn(II) with $g = 2.0$). When the sample is cooled, the $\chi_M T$ decreases slowly; below approximately 100 K, it decreases more quickly and reaches $0.271 \text{ cm}^3 \text{ K mol}^{-1}$ at 2 K. The χ_M value increases continuously on cooling to reach a maximum of $0.1595 \text{ cm}^3 \text{ mol}^{-1}$ at 7.5 K and decreases to a value of $0.1354 \text{ cm}^3 \text{ mol}^{-1}$

(34) Kahn, O. *Molecular Magnetism*; VCH: Weinheim, 1993.

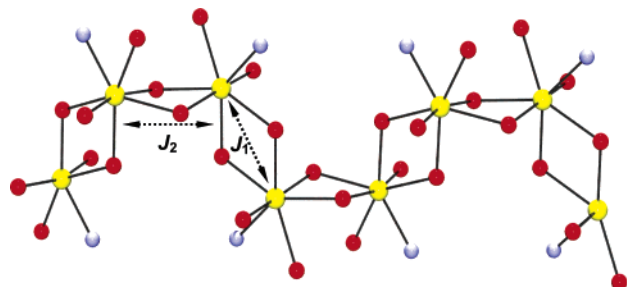


Figure 7. Schematic exchange interactions within **1**.

at 2 K. As shown in the Figure 1, the structure consists of Mn(II) ions linked by two 4-hydroxy-2,6-pyridynedicarboxylate groups and two asymmetric diaqua bridge alternatively to give an alternating 1D system. Thus, two coupling parameter J_1 and J_2 must be considered to interpret the two possible magnetic interactions in this complex (Figure 7). In the first approach and taking into account the above consideration, the experimental magnetic data have been fitted using the Drillon’s equation³⁵ based upon the spin Hamiltonian $H = -J_1\sum(S_{2i}S_{2i+1}) - J_2\sum(S_{2i+1}S_{2i+2})$, where the Mn(II) ion and the J_1 and J_2 values are isotropic.

$$\chi = [Ng^2\beta^2/3kT][S(S+1)][(1+u_1+u_2+u_1u_2)/(1-u_1u_2)] \quad (1)$$

Here, $u_1 = \coth[J_1[S(S+1)]/kT] - kT/J_1[S(S+1)]$ and $u_2 = \coth[J_2[S(S+1)]/kT] - kT/J_2[S(S+1)]$.

The J_1 and J_2 are obtained by minimizing the function $R = \sum[(\chi_M)_{\text{exp}} - (\chi_M)_{\text{calc}}]^2/\sum(\chi_M)_{\text{exp}}^2$. The best-fit parameters from 300 down to 2 K are found as follows: $J_1 = -1.57 \text{ cm}^{-1}$, $J_2 = -1.17 \text{ cm}^{-1}$, and $g = 2.05$ with an error $R = 2.3 \times 10^{-5}$. The bridging angles involving carboxylate and water lie in the range $105\text{--}110^\circ$, leading to small antiferromagnetic coupling. On the other hand, the diaqua bridging that gives nonplanarity favors ferromagnetic coupling.³⁶ Taking these two factors together, we can attribute the greater value $J_1 = -1.57 \text{ cm}^{-1}$ to the double 4-hydroxy-2,6-pyridynedicarboxylate bridging with the large angle, $\text{Mn1-O4-Mn2} = 111.44(8)^\circ$ and the lower value $J_2 = -1.17 \text{ cm}^{-1}$ to the asymmetric diaqua angle, $\text{Mn1-Ow2-Mn2} = 100.44(8)^\circ$ and $\text{Mn1-Ow4-Mn2} = 105.26(9)^\circ$. On the other hand, considering that the two J_1 and J_2 values are weak and are close in value, we have also interpreted the experimental data to the reduced classical uniform chain, taking $u_1 = u_2$, and following the Fisher’s equation³⁷

$$c = [Ng^2b^2/3kT][S(S+1)][(1+u)/(1-u)] \quad (2)$$

with $u = \coth[J[S(S+1)]/kT] - kT/J[S(S+1)]$ and $J_1 = J_2 = J$. The new fitting leads to the following values: $J = -1.38 \text{ cm}^{-1}$, $g = 2.05$, and $R = 7.1 \times 10^{-5}$.

The weak, yet nonnegligible, antiferromagnetic interaction between the Mn(II) centers is confirmed by magnetization measurements at 2 K up to an external field of 5 T. At higher

(35) Drillon, M. *Inorg. Chem.* **1997**, *36*, 677.

(36) Ruiz, E.; Alemany, P.; Alvarez, S.; Cano, J. *J. Am. Chem. Soc.* **1997**, *119*, 1297 and references therein.

(37) Fisher, A. *J. Phys.* **1964**, *32*, 343.

field, the magnetization corresponds to a nonsaturated $S = \frac{5}{2}$ system (Figure 4, inset). Comparison of the overall shape of the plot with the Brillouin plot for a fully isolated $S = \frac{5}{2}$ system indicates slower magnetization, consistent with a weak antiferromagnetic interaction. The solid-state EPR spectrum of **1** at room temperature exhibits an isotropic signal without revealing any fine structure indicative of the coordination geometry. The g_{av} is found to be 2.02 with a peak-to-peak line width of 357 G.³³

In conclusion, we have shown that supramolecular association of water molecules joins stairlike coordination polymers into an overall 3D MOF. The association of water molecules is best described as a discrete tetradecameric cluster in the form of a chair conformer with two acyclic tetramers dangling at two opposite ends. A wide variation in the hydrogen-bonding distances and angles are found commensurate with the MOF. The resulting material exhibits weak antiferromagnetic coupling between Mn(II) centers. Water clusters of different sizes and shapes in diverse

environments are presently being investigated in our laboratory with the ultimate aim to know how the degree of structuring of a cluster can be imposed by its environment and vice versa besides facilitating our understanding the properties of liquid water in a stepwise manner.

Acknowledgment. We gratefully acknowledge the financial support received from the Council of Scientific and Industrial Research, New Delhi, India (Grant No.1638/EMR II) and a SRF to S.G. Authors from Barcelona acknowledge the financial support from Ministerio de Educación y Ciencia (Programa Ramón y Cajal, Grant No. BQU2003/ 00539).

Supporting Information Available: Crystallographic data (CIF), binding mode of ligand with Mn(II), binding mode of waters, thermogram and X-ray powder diffraction patterns for **1** (PDF). This material is available free of charge via the Internet at <http://pubs.acs.org>.

IC050102W

Theoretical Study of Small Water Clusters: Low-Energy Fused Cubic Structures for $(H_2O)_n$, $n = 8, 12, 16$, and 20

C. J. Tsai and K. D. Jordan*

Department of Chemistry, University of Pittsburgh, Pittsburgh, Pennsylvania 15260

Received: January 29, 1993; In Final Form: March 30, 1993

Force field calculations employing the TIP4P potential are used to optimize several structures of the $(H_2O)_n$, $n = 8, 12, 16$, and 20 clusters. $(H_2O)_8$ is found to have, in agreement with previous studies, low-energy cubic structures of D_{2d} and S_4 symmetry. The lowest-energy forms of the larger clusters are found to have fused cubic structures rather than cagelike or networklike structures. The stability of the fused cubic structures of $(H_2O)_{12}$ is confirmed by means of MP2 calculations.

The most stable form of ice, ice Ih, has a hexagonal structure with each oxygen atom surrounded by a tetrahedron of other oxygen atoms.¹ This structure attains the maximal degree of hydrogen bonding while being relatively free of strain. On the other hand, in finite water clusters, the maximization of the number of hydrogen bonds comes at the expense of forming rings containing three, four, or five oxygen atoms (and the associated hydrogen atoms), introducing some strain. Thus, it is not clear that the most stable structures for small water clusters will be those that maximize the number of hydrogen bonds. It is of considerable interest, therefore, that $(H_2O)_8$ in its energetically most stable form has a cubiclike structure,^{2–6} which maximizes the number of hydrogen bonds. The cubic structure reported in the theoretical studies of Brink and Glaser² and Kim and co-workers³ has D_{2d} symmetry. Recently, we have shown that there is a second cubic structure of S_4 symmetry which is nearly isoenergetic with the D_{2d} structure.⁵ Figure 1 shows “ball and stick” models for these two forms of $(H_2O)_8$. Calculations using the TIP3P potential⁷ indicate that these two cubic forms of $(H_2O)_8$ are over 2 kcal/mol more stable than other structures.⁵

The stability of the D_{2d} and S_4 forms of $(H_2O)_8$ leads us to raise the question as to whether the most stable forms of $(H_2O)_{12}$, $(H_2O)_{16}$, and $(H_2O)_{20}$ might consist of “fused” cubic structures, rather than cagelike or networklike structures containing one or more five- or six-membered oxygen rings. (In this paper ring sizes are specified by the number of oxygen atoms.) To address this question, we have optimized the geometries of several forms of the $(H_2O)_8$, $(H_2O)_{12}$, $(H_2O)_{16}$, and $(H_2O)_{20}$ clusters. The optimizations were done with the TIP4P potential⁷ rather than the TIP3P potential because the former more closely reproduces the relative energies found in ab initio calculations. Initial structures, built graphically, were minimized either by means of the Monte Carlo simulated annealing procedure⁸ with sampling done using the jump-walking method^{9,10} or by means of an eigenmode following surface walking algorithm.¹⁰ MP2 calculations^{11,12} were carried out for selected TIP4P optimized structures of $(H_2O)_8$ and $(H_2O)_{12}$. These calculations employed the augmented correlation-consistent valence double-zeta + polarization (aug-ccpVDZ*) basis set.¹³ (This basis set is contracted to 4s3p2d on the oxygen atoms and to 3s1p on the hydrogen atoms.¹⁴) The suitability of the aug-ccpVDZ* and related basis sets for describing hydrogen-bonded systems has been demonstrated in ref 15.

For the $(H_2O)_8$ cluster, we have found over 100 distinct potential energy minima, in contrast to earlier studies^{2,3} which located eight or fewer minima. Figure 1 depicts, in addition to the previously discussed D_{2d} and S_4 structures, the next six lowest-energy structures (in the TIP4P model), all of which are cubic, as well as one of the lowest-energy noncubic structures, designated

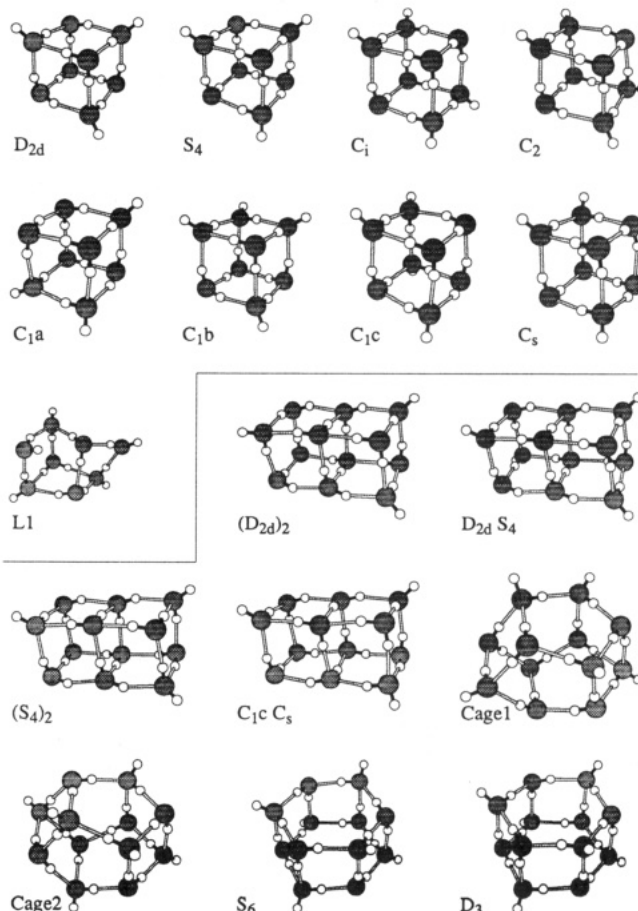


Figure 1. Low-energy structures of $(H_2O)_8$ and $(H_2O)_{12}$ obtained using the TIP4P potential.

L1. Structures with symmetry are labeled according to their symmetry point group. The TIP4P energies of these nine structures for $(H_2O)_8$ and for selected low-energy forms of the $(H_2O)_{12}$, $(H_2O)_{16}$, and $(H_2O)_{20}$ clusters are summarized in Tables I and II. Table I also reports MP2 energies for five of the $(H_2O)_8$ structures and for three of the $(H_2O)_{12}$ structures.

With the TIP4P potential, the S_4 structure of $(H_2O)_8$ is only 0.03 kcal/mol more stable than the D_{2d} structure but over 1.8 kcal/mol more stable than any of the other cubic structures. The MP2 calculations place the D_{2d} structure 0.2 kcal/mol below the S_4 structure and 3.9 kcal/mol below the next most stable (C_2) cubic structure. These energy separations are relatively unchanged upon inclusion of correction for basis set superposition error (BSSE).¹⁶ The energy separation between the S_4 and $L1$

TABLE I: TIP4P and MP2/aug-ccp VDZ* Energies of $(\text{H}_2\text{O})_8$ and $(\text{H}_2\text{O})_{12}$

cluster	TIP4P (kcal/mol)	MP2 (hartrees) ^a
($\text{H}_2\text{O})_8$		
D_{2d}	-73.027 25	-609.701 17 (-609.686 81) ^b
S_4	-73.053 00	-609.700 89 (-609.686 51)
C_i	-71.205 82	-609.694 31 (-609.680 02)
C_2	-71.178 62	-609.694 66 (-609.680 41)
C_1a	-70.664 42	-609.691 99 (-609.677 67)
C_1b	-70.632 40	
C_1c	-70.559 10	
C_s	-70.344 60	
L1	-69.354 68	-609.691 99 (-609.677 91)
($\text{H}_2\text{O})_{12}$		
$(D_{2d})_2$	-117.852 87	-914.565 48 (-914.544 09)
$(D_{2d})(S_4)$	-117.856 13	
$(S_4)_2$	-117.859 82	
$(C_1c)(C_s)$	-117.070 15	
cage1	-114.609 80	-914.564 07 (-914.543 04)
cage2	-114.518 34	
S_6	-114.205 41	
D_3	-114.202 64	-914.562 79 (-914.542 25)

^a The MP2 calculations were carried out at TIP4P optimized geometries and excluded excitations from the 16 lowest-energy MO's of $(\text{H}_2\text{O})_8$ and 24 lowest-energy orbitals of $(\text{H}_2\text{O})_{12}$. Justification for this restriction was provided by MP2 calculations on $(\text{H}_2\text{O})_8$ which showed that the relative energies of the various structures are nearly the same (agreeing on the average to 0.1 kcal/mol) when only the lowest eight MO's are frozen and when the lowest 16 MO's are frozen. ^b The results in parentheses include corrections for basis set superposition error.¹⁸

TABLE II: TIP4P Energies (kcal/mol) of $(\text{H}_2\text{O})_{16}$ and $(\text{H}_2\text{O})_{20}$

($\text{H}_2\text{O})_{16}$		($\text{H}_2\text{O})_{20}$	
cluster	energy	cluster	energy
$(D_{2d})_3$	-162.861 78	$(D_{2d})_4$	-207.874 18
$(S_4)(D_{2d})(S_4)$	-162.880 50	$(D_{2d}S_4)_2$	-207.786 30
$(D_{2d})(D_{2d})(S_4)$	-162.871 83	$(S_4)_4$	-207.700 31
$(D_{2d})(S_4)(D_{2d})$	-162.770 36	ring5a	-207.350 94
$(D_{2d})(S_4)(S_4)$	-162.777 42	ring5b	-207.241 49
$(S_4)_3$	-162.785 84	C_i	-206.503 95
C_i	-161.683 54	network	-204.516 02
C_1a	-159.369 12	cage	-196.789 25
C_1b	-158.876 63		
network1	-159.059 79		
network2	-159.165 05		

structures is 3.7, 5.8, and 5.6 kcal/mol in the TIP4P, MP2, and MP2(BSSE-corrected) approximations, respectively.

Eight low-energy structures for $(\text{H}_2\text{O})_{12}$ are also shown in Figure 1, and their energies are reported in Table II. The three lowest-energy structures are of the fused cubic variety and are designated as $(D_{2d})_2$, $D_{2d}S_4$, and $(S_4)_2$, indicating their parentage in terms of the D_{2d} and S_4 forms of $(\text{H}_2\text{O})_8$. With the TIP4P potential, these three structures lie within 0.07 kcal/mol of one another, with the $(S_4)_2$ structure being most stable. There are several other fused cubic structures of $(\text{H}_2\text{O})_{12}$, one of which is included in Figure 1. As described by the TIP4P potential, these alternative fused cubic structures are less stable than the $(D_{2d})_2$, $D_{2d}S_4$, and $(S_4)_2$ structures by over 0.7 kcal/mol. The remaining low-energy structures include two cage-like structures with four five-membered rings and nine four-membered rings and two high symmetry structures with two six-membered rings and six four-membered rings. With the TIP4P potential, these four structures are between 3.2 and 3.6 kcal/mol less stable than the lowest-energy fused cubic structure. HF and MP2 calculations with the aug-ccpVDZ* basis set were carried out for the $(D_{2d})_2$ fused cubic structure (with overall S_4 symmetry), the cage1 structure, and the D_3 structure. The relative energies from these and the TIP4P calculations are shown in Figure 2. The MP2/aug-ccpVDZ* calculations place the S_4 structure lowest in energy, with the cage1 and D_3 structures lying respectively 0.9 and 1.7 kcal/mol above the S_4 structure. The cage1 and D_3 structures

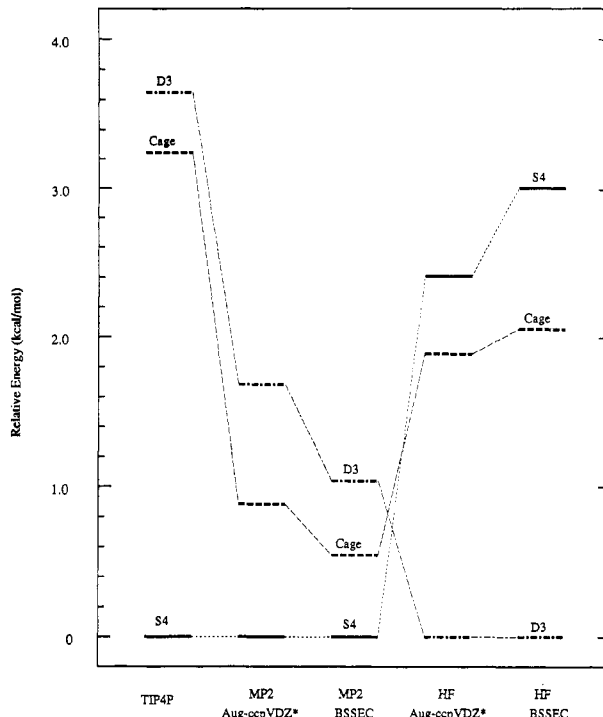


Figure 2. Relative energies of the S_4 , D_3 , and cage1 forms of $(\text{H}_2\text{O})_{12}$ calculated in the TIP4P model and by means of the HF and MP2 procedures using the aug-ccpVDZ* basis set and the TIP4P geometries. Ab initio results are presented with and without corrections for basis set superposition error.

are further stabilized, relative to the S_4 structure, by 0.2 and 0.5 kcal/mol, respectively, upon inclusion of the correction for BSSE.

Both the MP2 and TIP4P procedures predict the S_4 structure to be the most stable and the D_3 structure the least stable of the three structures considered. However, the energy separations between the S_4 structure and the D_3 and cage1 structures are appreciably smaller in the MP2 approximation, indicating a deficiency in the TIP4P potential. The cage1 and D_3 species containing the five- and six-membered rings have two fewer hydrogen bonds than does the S_4 fused cubic species. Thus, it appears that the "driving" force to maximize the number of hydrogen bonds more than compensates for the ring strain in the fused cubic forms of $(\text{H}_2\text{O})_{12}$. The HF procedure is inappropriate for predicting the relative stabilities of the various structures, as evidenced by the fact that it gives the opposite energy ordering for the S_4 , Cage1, and D_3 structures than does the MP2 approximation.

Figure 3 displays for $(\text{H}_2\text{O})_{16}$ one of the six fused cubic structures that can be derived from the D_{2d} and S_4 forms of $(\text{H}_2\text{O})_8$ as well as five structures containing various numbers of five-membered rings. Two of these, the so-called network structures, also contain one six-membered ring. The TIP4P calculations indicate that the six fused cubic structures are close in energy and also appreciably more stable than the structures containing less strained rings (but also fewer hydrogen bonds), with the energy separation between the most stable fused cubic structure and the most stable structure containing five-membered rings being about 1.2 kcal/mol.

Selected optimized structures for $(\text{H}_2\text{O})_{20}$ are also shown in Figure 3. These include the $(D_{2d})_4$ fused cubic structures, two "ring" structures, a structure with C_i symmetry, and so-called network and cage structures. The cage structure consists entirely of five-membered rings and has ten hydrogen atoms not involved in hydrogen bonding. The network structure has eight hydrogen atoms not involved in hydrogen bonding, whereas the fused-cubic, ring and C_i structures have respectively four, five, and six hydrogen atoms not involved in hydrogen bonding. With the TIP4P potential the $(D_{2d})_4$, $(D_{2d}S_4)_2$, and $(S_4)_4$ fused cubic structures

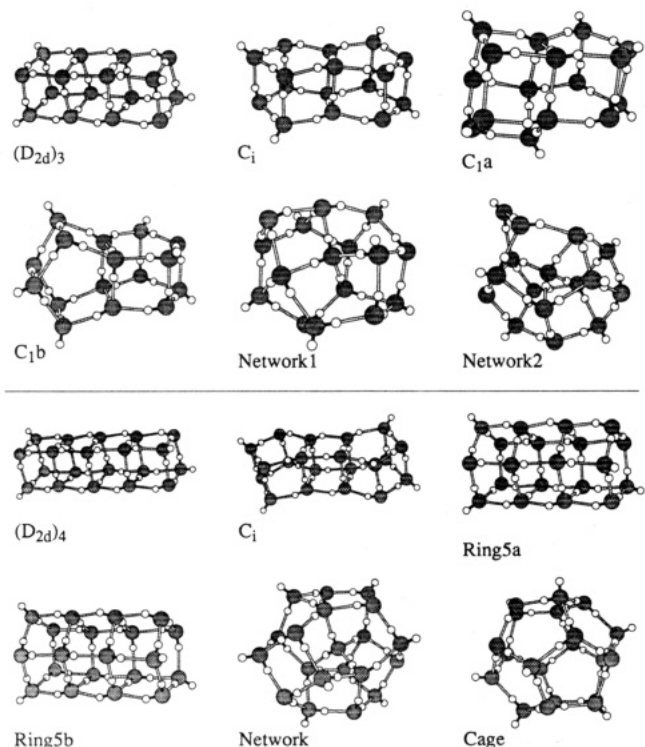


Figure 3. Low-energy structures of $(\text{H}_2\text{O})_{16}$ and $(\text{H}_2\text{O})_{20}$ obtained using the TIP4P potential.

are more stable than any of the other structures considered. The so-called network structure lies above the most stable fused cubic structure by 3.4 kcal/mol, and the cage structure is even less stable. The structures labeled by ring5a, ring5b, and C_i are respectively 0.5, 0.6, and 1.4 kcal/mol less stable than the $(\text{D}_{2d})_4$ cluster.

Our MP2/aug-ccpVDZ* calculations on $(\text{H}_2\text{O})_{12}$ indicate that the TIP4P model exaggerates the stability of the fused cubic species relative to structures containing five- and six-membered rings. It seems likely that MP2/aug-ccpVDZ* calculations on $(\text{H}_2\text{O})_{16}$ and $(\text{H}_2\text{O})_{20}$ at their TIP4P geometries would locate structures with five- and six-membered rings energetically below the fused cubic structures. On the other hand, the use of MP2-optimized geometries, rather than TIP4P geometries, is expected to favor the more strained fused cubic structures. Thus, although fused cubic structures may not correspond to the most stable class of structures for $(\text{H}_2\text{O})_{16}$ and $(\text{H}_2\text{O})_{20}$, they are expected to be relatively low lying in energy.

We have also explored the utility of the simulated annealing method⁸ for locating the fused cubic forms of the water clusters, starting from arbitrary structures and using the TIP4P potential. For $(\text{H}_2\text{O})_8$ and $(\text{H}_2\text{O})_{12}$ the simulated annealing method proved successful in locating the fused cubic structures.¹⁷ However, this was not the case for $(\text{H}_2\text{O})_{16}$ and $(\text{H}_2\text{O})_{20}$, presumably because the fused cubic forms are highly disfavored on entropic grounds and, thus, were not sampled in the Monte Carlo calculations at higher temperatures.

Acknowledgment. This research was carried out with support of a grant from the National Science Foundation. The calculations were carried out on Cray YMP and Cray C90 computers at the Pittsburgh Supercomputing Center and on a large memory Cray YMP at Cray Research. We thank Carlos Sosa for carrying out the calculations on the latter system.

References and Notes

- (1) Kamb, B. In *Structural Chemistry and Molecular Biology*; Rich, A., Davidson, N., Eds.; W. H. Freeman and Company: San Francisco, 1968; p 507.
- (2) Brink, G.; Glasser, L. *J. Phys. Chem.* **1984**, *88*, 3412.
- (3) Kim, K. S.; Dupuis, M.; Lie, G. C.; Clementi, E. *Chem. Phys. Lett.* **1986**, *131*, 7766.
- (4) Dykstra, C. E. *J. Chem. Phys.* **1989**, *91*, 6472.
- (5) Tsai, C. J.; Jordan, K. D. *J. Chem. Phys.* **1991**, *95*, 3850.
- (6) Knochenmuss, R.; Leutwyler, S. *J. Chem. Phys.* **1992**, *96*, 5233.
- (7) Jorgensen, W. L.; Tirado-Rivers, J. *J. Am. Chem. Soc.* **1988**, *110*, 1657.
- (8) Kirkpatrick, S.; Gelatt, C. D., Jr.; Vecchi, M. P. *Science* **1983**, *220*, 671.
- (9) Frantz, D. D.; Freeman, D. L.; Doll, J. D. *J. Chem. Phys.* **1990**, *93*, 2769.
- (10) Tsai, C. J.; Jordan, K. D. Manuscript in preparation.
- (11) Møller, C.; Plesset, M. S. *Phys. Rev.* **1934**, *46*, 618.
- (12) Gaussian 92: Frisch, M. F.; Head-Gordon, M.; Trucks, G. W.; Foresman, J. B.; Schlegel, H. B.; Raghavachari, K.; Robb, M. A.; Binkley, J. S.; Gonzalez, C.; Defrees, D. J.; Fox, D. J.; Whiteside, R. A.; Seeger, R.; Melius, C. F.; Baker, J.; Martin, R. L.; Kahn, L. R.; Stewart, J. J. P.; Topiol, S.; Pople, J. A. Gaussian Inc., Pittsburgh, PA, 1991.
- (13) Kendall, R. A.; Dunning, T. H.; Harrison, R. J. *J. Chem. Phys.* **1992**, *96*, 6796.
- (14) The diffuse p hydrogen function has been deleted from the aug-ccpVDZ* basis set, since calculations on the water dimer showed that it was relatively unimportant for the binding.
- (15) del Bene, J. *Int. J. Quantum Chem., Quantum Chem. Symp.* **1992**, *26*, 527.
- (16) Boys, S. F.; Bernardi, F. *Mol. Phys.* **1970**, *19*, 553; **1970**, *26*, 527.
- (17) Tsai, C. J.; Jordan, K. D. Manuscript in preparation.
- (18) For example, in estimating the BSSE for the various $(\text{H}_2\text{O})_x$ clusters, MP2 calculations were carried on each symmetry-unique monomer in a specific cluster both in the presence of and in the absence of the basis functions from the other centers. The BSSE for a specific water monomer is given by the difference in energies of the isolated monomer and the monomer in the presence of the basis functions on the other centers, and the total BSSE is given by the sum of the BSSE corrections for the individual monomers in the cluster.

Chemistry in Nanodroplets: Studies of Protonation Sites of Substituted Anilines in Water Clusters Using FT-ICR

Sang-Won Lee,[†] Heather Cox, William A. Goddard, III, and J. L. Beauchamp*

Contribution from the Beckman Institute, California Institute of Technology, Pasadena, California 91125

Received March 20, 2000

Abstract: Water clusters of protonated substituted anilines generated by an electrospray ion source have been investigated using a Fourier Transform ion cyclotron resonance mass spectrometer. It is observed that evaporation kinetics and cluster distributions are highly dependent on sites of protonation in the substituted anilines. Based on the examination of the water cluster distributions of protonated aniline derivatives, the site of protonation is postulated to be the amine group for aniline, *p*-anisidine, *p*-thiomethylaniline, *p*-ethylaniline, and *m*-ethylaniline. The water cluster distributions of these compounds display magic number clusters ($[M + nH_2O]^+$) for $n = 20, 27, 50$, and 52 . However, there is no indication of clusters with special stability for *m*-anisidine and *m*-thiomethylaniline, suggesting that these compounds protonate on the ring. DFT calculations have been performed to obtain proton affinities for the different sites of protonation in the substituted anilines and are in good agreement with experimental observation.

Introduction

Solvated ions in the gas phase are frequently referred to as model systems that provide a bridge between the gas-phase chemistry and structure of an isolated ion and its chemistry and structure in solution. This has led to wide-ranging investigations of the solvation of small ions in the gas phase and the effect of solvent on reactivity using various techniques, including high-pressure mass spectrometry,¹ flow tubes,² guided ion beam instruments,³ and Fourier transform ion cyclotron resonance (FT-ICR) mass spectrometry.^{4,5} Direct structural information on small solvated ions has been obtained by infrared predissociation spectroscopy⁶ and by theoretical ab initio calculations.⁷

Sites of protonation and proton affinities of gas-phase aromatic compounds have attracted considerable interest. Information on the role of solvation in determining the site of protonation has been obtained through the comparison of gas-phase proton affinities with solution-phase basicities. Various aromatic compounds have exhibited linear correlations between gas-phase proton affinity and solution-phase basicity; failure to do so occurs when the site of protonation in the gas phase differs from that in solution.

[†] Current address: Battelle-Pacific Northwest National Laboratories, P.O. Box 999 (K8-98), Richland, WA 99352.

(1) (a) Kebarle, P.; Tang, L. *Anal. Chem.* 1993, 65, 972A–986A. (b) Meot-Ner, M.; Speller, C. V. *J. Phys. Chem.* 1986, 90, 6616–6624.

(2) (a) Viggiani, A. A.; Dale, F.; Paulson, J. F. *J. Chem. Phys.* 1988, 88, 2469–2477. (b) Castleman, A. W., Jr.; Bowen, K. H., Jr. *J. Phys. Chem.* 1996, 100, 12911–12944.

(3) (a) Honma, K.; Sunderlin, L. S.; Armentrout, P. B. *Int. J. Mass Spectrom. Ion Processes* 1992, 117, 237–259. (b) Armentrout, P. B.; Baer, T. *J. Phys. Chem.* 1996, 100, 12866–12877.

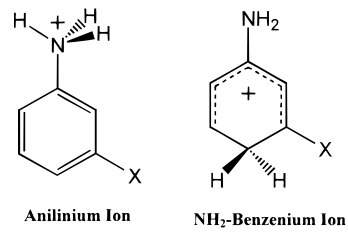
(4) Kofel, P.; McMahon, T. B. *Int. J. Mass Spectrom. Ion Processes* 1990, 98, 1–24.

(5) (a) Schindler, T.; Berg, C.; Niedner-Schatteburg, G.; Bondybey, V. E. *Chem. Phys. Lett.* 1994, 229, 57–64. (b) Schindler, T.; Berg, C.; Niedner-Schatteburg, G.; Bondybey, V. E. *J. Chem. Phys.* 1996, 104, 3998–4004.

(6) (a) Yeh, L. I.; Okumura, M.; Myer, J. D.; Price, J. M.; Lee, Y. T. *J. Chem. Phys.* 1989, 91, 7319–7330. (b) Cao, Y.; Choi, J.-H.; Haas, B.-M.; Johnson, M. S.; Okumura, M. *J. Chem. Phys.* 1993, 99, 9307–9309.

(7) (a) Xantheas, S. S. *J. Phys. Chem.* 1996, 100, 9703–9713. (b) Wei, D.; Salahub, D. R. *J. Chem. Phys.* 1997, 106, 6086–6094.

In the case of substituted anilines, a comparison of the proton affinity of ammonia (853.5 kJ/mol) with that of benzene (750.2 kJ/mol) would suggest that substituted anilines would preferentially protonate on the amine group. However, some substituted anilines, such as *m*-anisidine, *m*-thiomethylaniline, and *m*-ethylaniline, have been observed to protonate on the benzene ring in the gas phase due to the increased electron density (relative to aniline) on the benzene ring.⁸ In aqueous solution all of these substituted anilines are amine protonated. Highly localized charge in the protonated amine group of an anilinium ion (**1**) can be more effectively solvated by water molecules than can the extensively delocalized charge of a benzenium ion (**2**). These substituted anilines have different protonation sites



1

2

in the gas phase than they do in the solution phase, so it is of interest to determine both their protonation sites in water clusters and the number of water molecules required for proton transfer to occur.

Recently, it has been shown that a carefully optimized electrospray source can be used to produce extensively hydrated molecular ions. The water clusters in this study can contain hundreds of molecules, and so the clusters are nanometer size droplets containing ions of interest. Here we report studies of slow evaporation of the “nanodroplets” containing protonated substituted anilines and their utilization in unambiguous determination of protonation sites in the water cluster. These results

(8) Lau, Y. K.; Tse, N. A.; Brown, R. S.; Kebarle, P. *J. Am. Chem. Soc.* 1981, 103, 6291–6295.

are used to interpret chemistry observed in water clusters, distinct from the chemistry in both the solution phase and the gas phase.

Experimental Section

All experiments were performed in an external ion source 7T FTICR mass spectrometer that has been described in detail elsewhere.⁹ Briefly, the instrument is equipped with a radio frequency-only octopole ion guide, which transfers the ions from the atmospheric pressure ion source into the ICR cell. An electromechanical shutter that is located between the ESI source and the octopole was opened for 2 s to allow ions continuously being generated by the ESI source to enter the octopole ion guide. The radio frequency-field of the octopole was turned on only during this period of time. Argon collision gas (2–5 ms pulse, 10^{-6} Torr) was introduced to moderate the ion kinetic energy while ions were travelling through the octopole ion guide and being trapped in the ICR cell. For production of hydrated substituted anilines a modified version of a commercially available electrospray ion source (Analytica of Branford, Branford, CT) was used that has been described elsewhere.¹⁰ The anilines were dissolved in pure deionized water containing 0.01% acetic acid at concentrations around 100 μM . A syringe pump (Harvard Apparatus, Model PHD 2000, South Natick, MA) injects electrospray solution through a hypodermic stainless steel capillary (63 μm i.d.) at a flow rate of 80–150 nL/min. No nebulizer or counterflowing drying gas was used and the desolvation capillary is operated at room temperature. All substituted anilines were purchased from Aldrich Chemical Co. (Milwaukee, WI) and used without further purification.

DFT calculations have been performed to obtain proton affinities at different sites of protonation of various anilines, including aniline, *m*-/*p*-anisidine, *m*-/*p*-thiomethylaniline, and *m*-/*p*-toluidine.¹¹ Full geometry optimizations of each compound have been performed at the B3LYP/631G** level with the Jaguar software package¹² running on Origin2000 (Silicon Graphics Inc.). More refined energies for the optimized structures were obtained at the B3LYP/6311G**++ level. Zero-point energy corrections and enthalpy corrections at 298 K were obtained at the B3LYP/6311G** level. It was observed that the DFT calculations (B3LYP/6311G**++//B3LYP/631G**) used in this study overestimate proton affinity of benzene by 4.4 kcal/mol ($\text{PA}_{\text{calc}} = 183.7$ kcal/mol, $\text{PA}_{\text{exp}} = 179.3$ kcal/mol). The proton affinities for ring protonation of substituted anilines presented here are corrected accordingly.

Results and Discussion

In a previous study from our laboratory,¹⁰ we have shown that water cluster distributions of protonated primary alkylamines display characteristic magic numbers of 20, 27, 50, 52, and 54 (Figure 1a). On the basis of experiments using several amines with different hydrocarbon groups, we proposed structure **3** for the 20-mer water cluster of protonated 1-adamantylamine, where the protonated amine group replaces one of the water molecules in the clathrate structure and an extra neutral water molecule is encapsulated in the cavity. For clusters with fewer than 100 water molecules, solvation is dominated entirely by the protonated amine functional group and not by the hydrophobic hydrocarbon portion of the molecule. We note that it requires three hydrogens from the protonated primary alkylamine to form the proposed structure.

(9) Rodgers, M. T.; Campbell, S.; Marzluff, E. M.; Beauchamp, J. L. *Int. J. Mass Spectrom. Ion Processes* **1994**, *137*, 121–149.

(10) Lee, S.-W.; Freivogel, P.; Schindler, T.; Beauchamp, J. L. *J. Am. Chem. Soc.* **1998**, *120*, 11758–11765.

(11) To avoid the complication in calculations from the different orientation of the ethyl group in ethylanilines, proton affinities of *m*-/*p*-toluidine were calculated in this study instead of *m*-/*p*-ethylaniline. It is expected that the substituent effects of methyl and ethyl groups are similar. Calculation results from *m*-/*p*-toluidine are accordingly used to explain and compare with experimental results of *m*-/*p*-ethylaniline.

(12) Jaguar 3.5, Schrödinger, Inc.: Portland, OR, 1998.

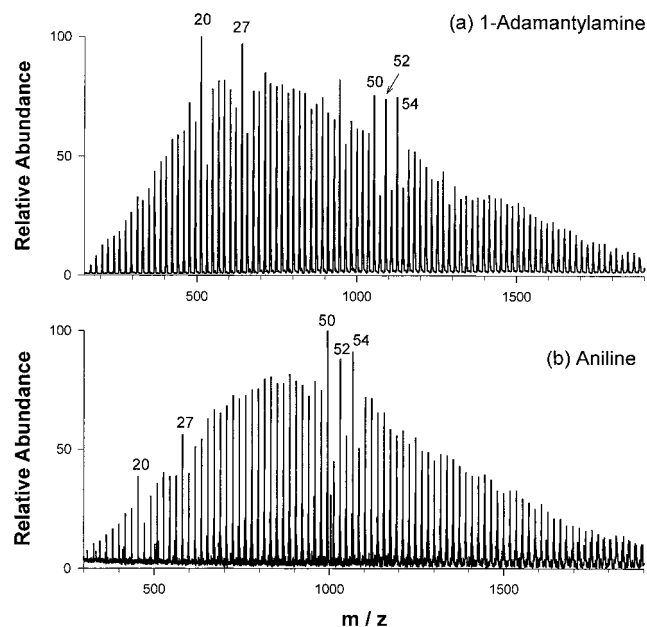
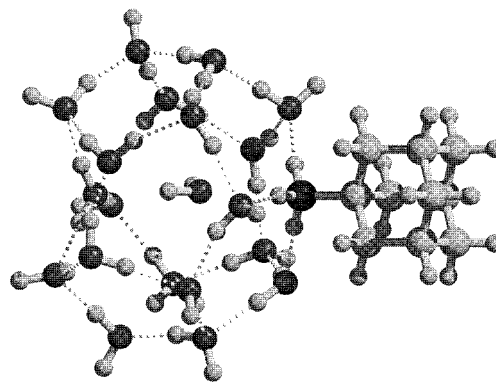


Figure 1. Water clusters of (a) protonated 1-adamantylamine (13 s) and (b) protonated aniline (18 s). Sample concentrations are approximately 100 μM in 0.01% acetic acid solution. Both are amine protonated in water clusters.



3

A spectrum of solvated protonated aniline is shown in Figure 1b. The question of the preferred site of protonation of substituted aromatics in the gas phase has been the subject of numerous publications.^{9,13} Using a combination of STO-3G calculated energy changes for isodesmic proton-transfer reactions and experimentally determined proton affinities of substituted anilines, Hehre, Taft, and co-workers reported that protonation on the aromatic ring of aniline (para position to the amine group, NH₂-benzenium ion, **2**) is only 4–12 kJ/mol less favorable than protonation on the amine nitrogen (anilinium ion, **1**).¹⁴ The water cluster distribution of protonated aniline (Figure 1b) clearly displays magic numbers characteristic of protonated primary alkylamines.

Figure 2 shows the relative intensity ratios of the 20-mer, 27-mer, and 30-mer peaks as a function of time, where the relative intensity ratio is defined as the intensity of the *N*-mer

(13) (a) Freiser, B. S.; Woodin, R. L.; Beauchamp, J. L. *J. Am. Chem. Soc.* **1975**, *97*, 6893–6894. (b) Martinsen, D. P.; Buttrill, S. E. *Org. Mass Spectrom.* **1976**, *11*, 762–772. (c) Dookeran, N. N.; Harrison, A. G. *J. Am. Soc. Mass Spectrom.* **1995**, *6*, 19–26. (d) Chiavarino, B.; Crestoni, M. E.; Rienzo, B. D.; Fornarini, S. *J. Am. Chem. Soc.* **1998**, *120*, 10856–10862.

(14) Pollack, S. K.; Devlin, J. L., III; Summerhays, K. D.; Taft, R. W.; Hehre, W. J. *J. Am. Chem. Soc.* **1977**, *99*, 4583–4584.

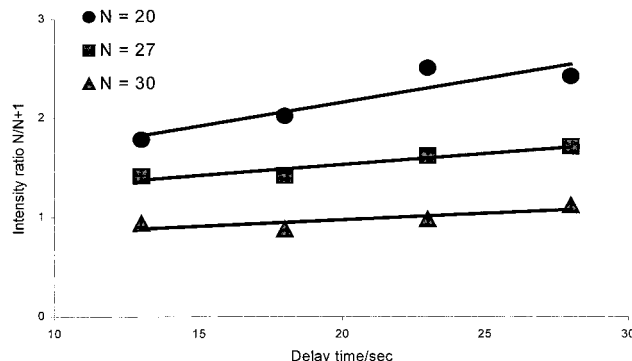


Figure 2. Anilinium ion intensity ratios of three different sets of peaks: 20/21 (circles), 27/28 (squares), and 30/31 (triangles). Intensity ratios are defined as the intensity of the N -mer peak over that of the $(N + 1)$ -mer peak. The 20-mer and 27-mer are especially stable structures, as indicated by the high-intensity ratio. The 30-mer exhibits no special stability.

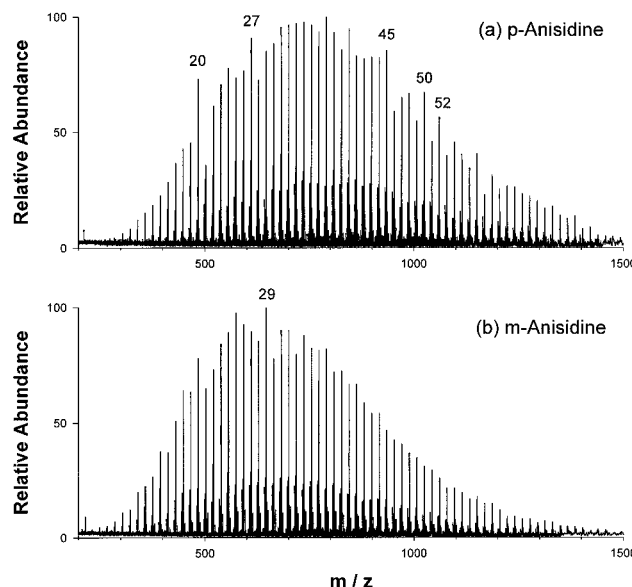


Figure 3. Water clusters of (a) protonated *p*-anisidine and (b) protonated *m*-anisidine detected 23 s after ion accumulation. Sample concentrations are approximately $100 \mu\text{M}$ in 0.01% acetic acid solution. While *p*-anisidine is observed to be amine protonated, reduction in the intensity of clusters indicative of specific solvation of a protonated amine suggests that protonation occurs on the aromatic ring of *m*-anisidine in water clusters.

peak over the intensity of the $(N + 1)$ -mer peak. All clusters show an increase in the relative intensity ratio as a function of time, because the maximum in the distribution of water clusters shifts to lower m/z values as evaporation proceeds. However, at all times the 20-mer and 27-mer exhibit special stability compared to the 30-mer (and other nonmagic water clusters). This is a strong indication that protonation occurs on the amine group of aniline. The ring-protonated aniline (NH_2 -benzenium ion, **2**) does not have a convenient hydrogen bonding site to incorporate into the pentagonal dodecahedron structure of 20-mer water clusters such as shown in structure **3**. It is accordingly expected that ring-protonated aniline would have substantially different cluster distributions from those of primary alkylamines.

Cluster distributions for protonated *p*- and *m*-anisidine ($X = -\text{OCH}_3$) are compared in Figure 3. While the cluster distribution of protonated *p*-anisidine exhibits the characteristic magic numbers suggesting amine protonation, protonated *m*-anisidine

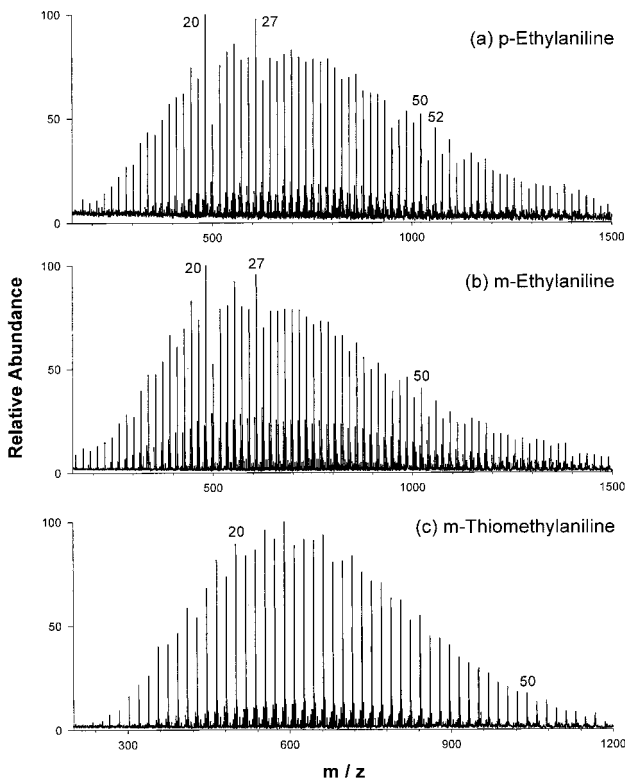


Figure 4. Water clusters of (a) protonated *p*-ethylaniline (18 s), (b) protonated *m*-ethylaniline (18 s), and (c) protonated *m*-thiomethylaniline (28 s). Sample concentrations are approximately $100 \mu\text{M}$ in 0.01% acetic acid solution. Both *p*- and *m*-ethylaniline are amine protonated; *m*-thiomethylaniline is ring protonated.

has a markedly different water cluster distribution, showing no specific solvation.¹⁶ This is an indication that protonation occurs on the aromatic ring of *m*-anisidine in water clusters. Clearly, even with a large number of water molecules, the gas-phase behavior of the naked ion is still observed.

Figure 4 shows water cluster distributions observed for protonated *p*-ethylaniline, methylaniline, and *m*-thiomethylaniline.¹⁵ The mass spectrum (Figure 4a) of hydrated *p*-ethylaniline again shows the magic number clusters characteristic of protonated amines, suggesting amine protonation. Interestingly, methylaniline also exhibits the same magic number clusters, indicative of amine protonation (Figure 4b). This indicates a shift in the favored site of protonation to the amine nitrogen from the ring, the preferred site of protonation in the naked ion. The water cluster distribution of protonated *m*-thiomethylaniline (Figure 4c) is quite smooth with no indication of specific solvation. This suggests that protonation occurs on the ring in water clusters.

Density functional calculations have been performed to obtain proton affinities at specific sites on each substituted aniline (Figure 5). The proton affinities obtained with B3LYP/

(15) We were not able to measure water clusters of *p*-thiomethylaniline, since the mass spectrum of *p*-thiomethylaniline contains a strong impurity peak, which is not assigned, and overlaps with water cluster peaks of protonated *p*-thiomethylaniline, affecting the relative abundance of cluster peaks.

(16) There is a slight indication of a magic number at $n = 20$ for *m*-anisidine (the average intensity ratio for *m*-anisidine is 1.01 with a standard deviation of 0.15, and the intensity ratio at $n = 20$ is 1.26). However, the intensity ratio at $n = 20$ for *p*-anisidine is 2.02 (average = 1.02, standard deviation = 0.26). It is unclear whether the slight increase in intensity ratio at $n = 20$ for *m*-anisidine is due to a small sub-population of amine-protonated species, a stable isomer at $n = 20$ which does not resemble the clathrate structures proposed here, or whether it simply occurs as a statistical fluctuation in the data.

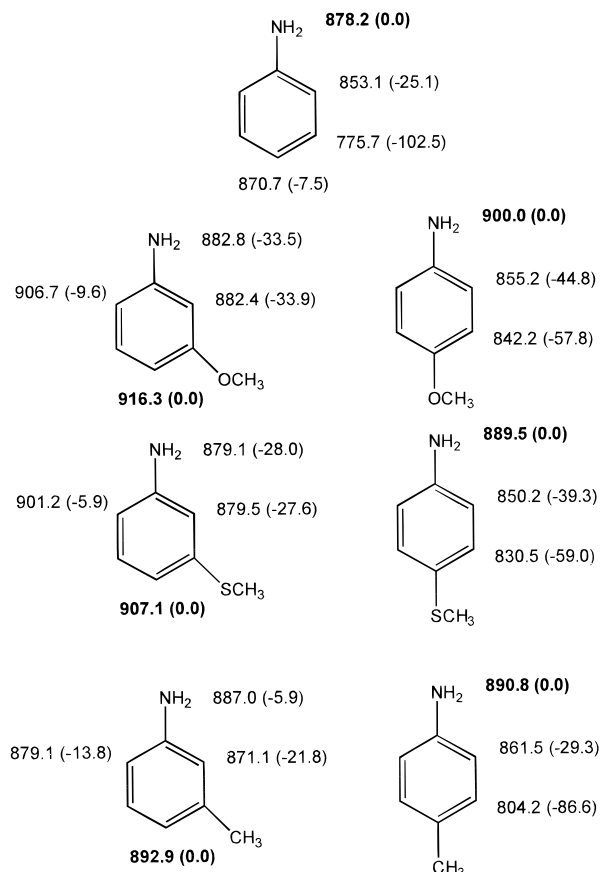


Figure 5. Theoretical site-specific proton affinities (in kJ/mol). Proton affinities were calculated at B3LYP/6311G**++//B3LYP/631G** + ZPE(B3LYP/6311G**). The highest proton affinities are in bold. The proton affinity differences between the specific site of protonation and the site of highest proton affinity are in parentheses. Experimental proton affinities are aniline (882.4), *m*-anisidine (912.9), *p*-anisidine (900.4), *m*-thiomethylaniline (902.1), *p*-thiomethylaniline (N/A), *m*-toluidine (895.8), and *p*-toluidine (896.6).

6311G**++//B3LYP/631G** + ZPE(B3LYP/6311G**) calculations are in good agreement with experimental values. For aniline, ring protonation is calculated to be 7.5 kJ/mol (1.8 kcal/mol) less favorable than amine protonation, which agrees well with the results of Hehr, Taft and co-workers. For all para-substituted anilines used in this study, amine protonation is favored over ring protonation. However, ring protonation is favored over amine protonation for all meta-substituted anilines.

We note that the proton affinity difference ($\Delta PA = PA_{\text{ring}} - PA_{\text{amine}}$) between the ring protonation and amine protonation for meta-substituted anilines decreases as the substituent's electron donating abilities decrease. For example, the ΔPA 's of *m*-anisidine ($X = -\text{OCH}_3$) and *m*-thiomethylaniline ($X = -\text{SCH}_3$) are 33.5 and 28.0 kJ/mol (8.0 and 6.7 kcal/mol), respectively, while the ΔPA of *m*-toluidine ($X = -\text{CH}_3$) is only 5.9 kJ/mol (1.4 kcal/mol). Figure 6 compares the intensity ratios of the 20-mer water clusters of the meta-substituted anilinium ions, plotted against ΔPA . When ring protonation is highly preferred to amine protonation, the 20-mer cluster is not favored. As ΔPA decreases, we observe an increase in intensity ratio, corresponding to increased stability of the 20-mer water cluster and indicating amine protonation.

Kebarle and co-workers measured monohydration equilibria in the gas phase for several substituted anilines.⁸ From the measured hydration energy of the first water, they predicted that proton transfer from ring to amino group occurred for

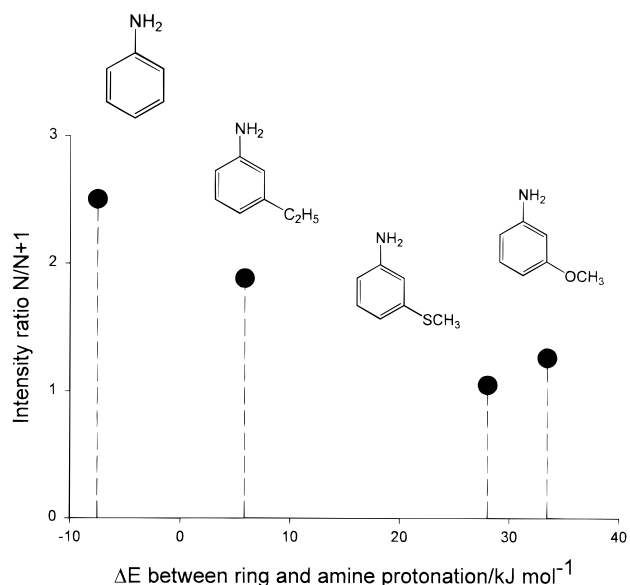


Figure 6. Variation in the ratios of the 20-mer to 21-mer water cluster intensities with the change in proton affinity between ring and amine protonation for aniline, *m*-ethylaniline, *m*-anisidine, and *m*-thiomethylaniline. When ring protonation is highly preferred to amine protonation, the intensity ratio is low. As the difference in energy between the protonation sites decreases, an increase in intensity ratio characteristic of amine protonation is observed.

m-thiomethylaniline, *m*-hydroxyaniline, and methylaniline with one water molecule attached while *m*-anisidine and 1,3-diaminobenzene remained ring protonated. Our results for *m*-ethylaniline indicate that a significant amount of amine protonation occurs with a large number of water molecules. However, contrary to Kebarle's conclusions, we observe a preference for ring protonation in small water clusters of *m*-thiomethylaniline. This difference appears because we calculate the proton affinity difference between ring and amine protonation as 28 kJ/mol, while Kebarle estimated the same difference to be 15 kJ/mol by correlating experimental nitrogen 1s core electron ionization energies with free energies of proton transfer to aniline. We believe that the calculated values are more accurate for species such as *m*-thiomethylaniline, for which the amine protonation and ring protonation differ in energy by less than 50 kJ/mol.

Conclusion

Slow evaporation of water clusters containing 10–100 water molecules ("nanodroplets") of substituted anilines formed by an electrospray ion source has been studied using a FT-ICR mass spectrometer. The generation of hydrated substituted anilines in the gas phase provides a unique possibility for studying the interface between gas phase and solution chemistry in water clusters. Water cluster distributions of substituted anilines are observed to be heavily dependent on their site of protonation in water clusters. While protonated aniline, *p*-anisidine, *p*-ethylaniline, and *m*-ethylaniline exhibit characteristic magic numbers of protonated primary amines, none are observed for *m*-anisidine and *m*-thiomethylaniline. These observations lead to the conclusion that the favored site of protonation in nanodroplets can be readily correlated (as shown in Figure 6) with energetic differences of protonation at different positions in a molecule, as calculated for the unsolvated species. Nanodroplets thus represent a unique environment for studies of solvated ions, since bulk phase behavior is not always observed.

Acknowledgment. The authors are grateful to Dr. Yun Hee Chang for helpful discussions. This work was supported in part by the National Science Foundation under Grant CHE-9727566. Funds for instrument development have been provided by ARPA and the DOD-URI program (ONR-N0014-92-J-1901). H.C. gratefully acknowledges the support of a National Science Foundation graduate research fellowship. We are also

indebted to the Beckman Foundation and Institute for the initial funding and continuing support of the research facilities. Computing resources were generously provided by the Material and Process Simulation Center (MSC), also part of the Beckman Institute.

JA0009875

Detection of Localized Water Clusters in a Charged Peptidyl Resin

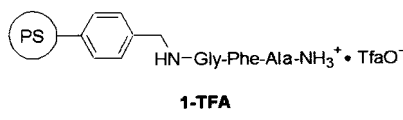
Gianni Chessari, Jean-Michel Wieruszewski, and Guy Lippens*

CNRS UMR 8525, Institut de Biologie de Lille
Institut Pasteur de Lille
1 rue du Professeur Calmette, 59019 Lille, France

Received May 30, 2001

The understanding of local solvent structure and especially that of water in the proximity of ions represents a challenging area of research due to its importance in many chemical and biological processes¹. Very recently, the isolated dynamics of water molecules in the solvation shell of an ion in bulk aqueous solution was obtained using femto-second mid-infrared nonlinear spectroscopy,² but the distinction of the water molecules in the solvation shells from those in the bulk solvent, because of the unfavorable population ratio and the rapid exchange between both components, remains a enormous challenge. Therefore, most of the information regarding the physicochemical properties of water-solvated species originates from gas-phase experiments,^{3,4} where microclusters composed of an ion or a neutral species surrounded by a few water molecules are studied, or from theoretical calculations^{5,6} on similar clusters. The extension of those clusters to macroscopic systems, however, including possible interactions with higher solvation shells, remains an open question. Here, we report the presence of a distinct water component around the ion pair formed by the terminal ammonium group of a resin-anchored peptide and its counterion and study its localization and dynamic behavior in atomic detail by high-resolution magic angle spinning (HR MAS) NMR.

Our experimental system, a model peptide (Ala-Phe-Gly) in the charged form synthesized on a *p*-aminomethyl polystyrene (PS) support swollen in deuterated dimethylformamide (DMF), corresponds to the status of the peptidyl resin after the last Boc deprotection step with trifluoroacetic acid concentrate (TFA). After extensive washing of the resin with dichloromethane and drying under vacuum conditions, all excess acid was removed, leaving the peptide on the resin as an ammonium salt with trifluoroacetate as counterion.



HR MAS NMR, which is emerging as a powerful analytical tool for the study of heterogeneous systems,⁷ was used to characterize this supramolecular system. After total ¹H NMR assignments of the proton resonances corresponding to the peptide at 10 °C using TOCSY and NOESY spectra, and confirmation of the full assignment of the peptide by the carbon resonance assignment from a ¹H-¹³C HSQC experiment, two well-separated

(1) Robinson, G. W.; Zhu, S.-B.; Singh, S.; Evans, M. W. *Water in Biology, Chemistry and Physics: Experimental Overviews and Computational Methodologies*; World Scientific: Singapore, 1996.

(2) Kropman, M. F.; Bakker, H. J. *Science* **2001**, 291, 2118–2120.

(3) Weber, J. M.; Kelley, J. A.; Nielsen, S. B.; Ayotte, P.; Johnson, M. A. *Science* **2000**, 287, 2461–2463.

(4) Keutsch, F. N.; Saykally, R. J. *Proc. Natl. Acad. Sci. U.S.A.* **2001**, 98, 10533–10540.

(5) Dang, L. X.; Rice, J. E.; Caldwell, J.; Kollman, P. A. *J. Am. Chem. Soc.* **1991**, 113, 2481.

(6) Smith, D. E.; Dang, L. X. *J. Chem. Phys.* **1994**, 100, 3757.

(7) (a) Fitch, W. L.; Detre, G.; Holmes, C. P.; Shoorely, J. N.; Keifer, P. A. *J. Org. Chem.* **1994**, 59, 7955–7956. (b) Anderson, R. C.; Stokes, J. P.; Shapiro, M. J. *Tetrahedron Lett.* **1995**, 36, 5311–5314.

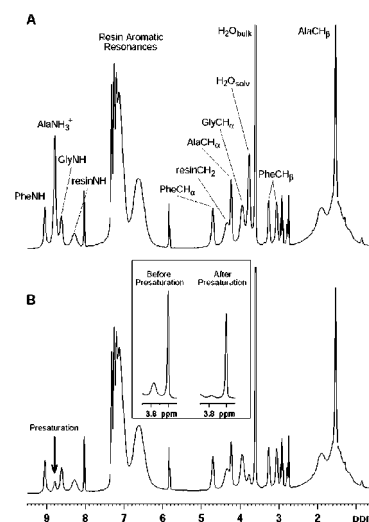


Figure 1. HR MAS ¹H NMR 1D spectra at 600 MHz of 1-TFA. Spectra were recorded at 283 K, spinning rate 6 kHz, in a 4 mm rotor with 10 mg of resin swollen in 100 μL of DMF-d₇: (A) single pulse sequence; (B) 1D proton spectra with presaturation on the AlaNH₃⁺ resonance. The boxed insert shows the water resonances before and after presaturation of the ammonium protons.

resonances remained unassigned in the ¹H NMR spectra (Figure 1A). The signal at 3.60 ppm has the same chemical shift of water in DMF at 10 °C, and displayed a narrow line width (12 Hz at half-maximum). Both arguments identify it as residual water in the resin, that might have come with the DMF solution or just captured from air moisture. We will further denote it as H₂O_{bulk}. The other resonance at 3.77 ppm was characterized by a larger line width of 46 Hz, even larger than that of the peptide resonances (36 and 39 Hz for the Phe amide or H_α protons).

Saturation NMR experiments gave a first indication of the chemical nature of the resonance at 3.77 ppm. The presaturation of H₂O_{bulk} during 1 s led to small decrease in intensity of both this resonance and the NH₃⁺ ammonium signal, whereas the rest of the peptide resonances were basically unaffected. On the other hand, presaturation of the peak at 3.77 ppm not only induced the expected symmetrical small intensity decrease of the H₂O_{bulk} resonance but also generated an almost complete loss of the intensity of the NH₃⁺ resonance, but not of the other amide protons. This contrasts to earlier TOCSY studies where the water stripe showed correlations to many exchangeable protons on a peptide.⁸ More importantly, the presaturation of the ammonium protons' resonance induced a considerable intensity loss for the resonance at 3.77 ppm and a small loss of the H₂O_{bulk} line, whereas all of the other resonances were unaffected (Figure 1B). The good chemical shift correlation and complete coupling by chemical exchange of the ammonium protons and those corresponding to the signal at 3.77 ppm not only identified the latter as water molecules (that we will further indicate as H₂O_{solv}) but also allowed us to localize them in the immediate vicinity of the N terminus of the charged peptide moiety.

The underlying process of chemical exchange between the Ala NH₃⁺ and the water protons of H₂O_{solv} was subsequently confirmed by the presence of a strong exchange cross-peak between both species with the same sign of the diagonal peak in a ROESY⁹ 2D experiment. Two-dimensional EXSY experiments¹⁰

(8) (a) Nakashima, T. T.; McClung, R. E. D.; and Kotovych, G. *J. Magn. Res.* **1998**, 133, 222. (b) McClung, R. E. D.; Nakashima, T. T.; Yamamoto, H.; and Kotovych, G. *Can. J. Chem.* **1999**, 77, 1728–1733.

(9) Bothner-By, A. A.; Stephens, R. L.; Lee, J.-M.; Warren, C. D.; Jeanloz, R. W. *J. Am. Chem. Soc.* **1984**, 106, 811–813.

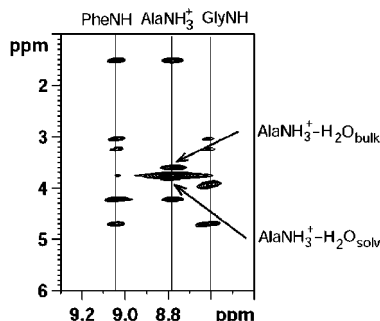


Figure 2. EXSY spectrum at 600 MHz of 1-TFA showing the exchange between the ammonium protons and the two water components.

with increasing mixing times yielded an exchange rate $k_{\text{ex}} = (48 \text{ ms})^{-1}$ for the ammonium protons and H₂O_{solv}. In this spectrum, we equally noted an exchange peak between H₂O_{bulk} and the protons of H₂O_{solv} (and thus indirectly with the ammonium protons), but the reduced intensity of their exchange peak indicated a slower time scale for this exchange process with a $k_{\text{ex}} = (1183 \text{ ms})^{-1}$ (Figure 2). The exchange process between H₂O_{bulk} and the AlaNH₃⁺ protons was on a similar time scale as the latter process, with a value for $k_{\text{ex}} = (967 \text{ ms})^{-1}$.

Whereas the chemical exchange between the protons of the ammonium moiety and the H₂O_{solv} signal probably contributes to the line width of both, the time scale is too slow compared to their chemical shift separation to explain the important line width of the latter. A valid alternative is the quasi-permanent attachment of these water molecules to the N-terminal moiety of the anchored peptide chains, leading to similar processes of line broadening as for the tethered peptide chains. Because this should lead to a loss in translational mobility, we used the LED diffusion pulse sequence¹¹ to probe the degree of anchoring of both water species to the resin. The diffusion experiments confirmed the absence of diffusion for the peptide resonances but equally showed that H₂O_{solv} corresponds to a very slowly diffusing species, with a diffusion coefficient $D_c = 2.2 \times 10^{-10} \text{ m}^2/\text{s}$, hence 55 times lower compared to that of water in DMF ($D_c = 1.2 \times 10^{-8} \text{ m}^2/\text{s}$ at 10 °C). The other water component of the system (H₂O_{bulk}) diffused only twice more slowly, with a value for $D_c = 6.8 \times 10^{-9} \text{ m}^2/\text{s}$.

Both observations of fast exchange with the ammonium protons and very slow diffusion suggest that the protons corresponding to the H₂O_{solv} resonance are associated with water molecules that reside with an important lifetime in direct contact with the N-terminal ion pair. Interestingly, integration of the signal yielded a value of two to three water molecules in the first hydration shell of every N-terminal ion pair, which should be compared with the five water molecules that were found in the first solvation shell of the free ammonium ion.¹² The second water signal corresponds to twice this amount of molecules and might be putatively assigned to a second hydration shell. Significantly, even at the longest mixing times, no exchange peak was seen with the Gly or Phe amide protons, confirming the localized character of even this more mobile water component. Whereas the use of Cl⁻ as a counterion equally led to the observation of two distinct water components, the absolute necessity of a stable ion pair became

(10) Jeener, J.; Meier, B. H.; Bachmann, P.; Ernst, R. R. *J. Chem. Phys.* **1979**, *71*, 4546.

(11) Gibbs, S. J.; Johnson, C. S. *J. Magn. Res.* **1991**, *93*, 395–402.

(12) Brugé, F.; Bernasconi, M.; Parrinello, M. *J. Am. Chem. Soc.* **1999**, *121*, 10883–10888.

clear when we used a weaker acid such as acetic acid. This led to the disappearance of not only the distinct water signals, but also of the proton signals of the ammonium moiety, probably due to rapid exchange with the unique water signal at 3.58 ppm. A similar behavior was previously noticed upon neutralization of the peptide amino group by washing with a base, where the signal of the NH₂ terminal disappeared from the spectrum¹³ and only one water signal could be observed in the HR MAS ¹H NMR spectra. Presaturation of this unique water resonance resulted in an intensity decrease of the Phe amide proton,¹⁴ indicating a more diffuse character for the water molecules in the absence of a stable ion pair at its N terminus.

At 10 °C, the two water resonances were best resolved, which was the primary reason for the temperature choice of our experiments. However, varying the temperature yielded some interesting results as well. For temperatures below 50 °C, both resonances could be distinguished individually, and a linear relationship with temperature coefficient of 7 ppb/K was observed for both line positions. Upon raising the temperature from 10 to 20 °C, the exchange rate between H₂O_{solv} and the NH₃⁺ protons increased from (48 ms)⁻¹ to (15 ms)⁻¹, whereas the exchange processes implying protons of the other water component did not show any change in dynamics. Above 50 °C, both the NH₃⁺ and H₂O_{solv} signals became severely broadened, probably because the exchange rate approaches their chemical shift separation.

To study the dynamical behavior of both water components, we carried out T_1 relaxation experiments at 10 °C. We cannot exclude completely that the measurement is hampered by radiation damping,¹⁵ but if so, the effect should be more pronounced for the most intense H₂O_{bulk} water component. The experimental results, however, were quite the opposite: the T_1 value of H₂O_{bulk} was found to be 956 ms, nearly double the T_1 value of H₂O_{solv} at 565 ms. Whereas molecular dynamics simulations probably will be necessary to separate the intra- from intermolecular contributions to those relaxation rates,¹⁶ the results point to a reduced rotational freedom for the water molecules that are in the direct vicinity of the anchored ammonium moiety.

Similar to the case of an aggregating peptide,¹⁷ the solid-phase resin offers the possibility of dilution of the peptide chains on the resin, to further isolate the water clusters. We thus believe that the present demonstration of two distinct water components in commonly used peptidyl resins opens up prospects for new theoretical and experimental work related to the study of solvation and applicable to solid-phase chemistry.

Acknowledgment. G.C. acknowledges Hoechst Marion Roussel (Romainville) for a postdoctoral fellowship. The 600 MHz facility used in this study was funded by the Région Nord-Pas de Calais (France), the CNRS, and the Institut Pasteur de Lille. We thank Professor A. Tartar for stimulating this research.

Supporting Information Available: HR-MAS diffusion experiment on 1-TFA (PDF). This material is available free of charge via the Internet at <http://pubs.acs.org>.

JA011311S

(13) Dhalluin, C.; Boutillon, C.; Tartar, A.; Lippens, G. *J. Am. Chem. Soc.* **1997**, *119*, 10494–10500.

(14) Warrass, R.; Lippens, G. In *Combinatorial Chemistry*; Jung, G., Ed.; Wiley: Germany, 2000; pp 533–542.

(15) Bloembergen, N.; Pound, R. V. *Phys. Rev.* **1954**, *95*, 8–12.

(16) Lippens, G.; Van Belle, D.; Wodak, S. J.; Jeener, J. *J. Mol. Phys.* **1993**, *80*, 1469–1484.

(17) Warrass, R.; Wieruszewski, J.-M.; Boutillon, C.; Lippens, G. *J. Am. Chem. Soc.* **2000**, *122*, 1789–1795.

Single-Molecule Precipitation of Transition Metal(I) Chlorides in Water Clusters

Brigitte S. Fox, O. Petru Balaj, Iulia Balteanu, Martin K. Beyer,* and Vladimir E. Bondybey*

Institut für Physikalische und Theoretische Chemie, Technische Universität München, Lichtenbergstrasse 4, 85747 Garching, Germany

Received September 25, 2001

Aqueous chemistry of uncomplexed transition metals in oxidation state +I is virtually unknown, since the singly charged metal ions are unstable in bulk aqueous media.¹ Their instability is in part due to the much higher hydration energy of the M²⁺ ions, which for instance in copper is known to lead to a rapid disproportionation $2\text{Cu}^{\text{I}} \leftrightarrow \text{Cu}^{\text{II}} + \text{Cu}(\text{s})$.¹ In some cases the +I state can be stabilized by complexation, and in fact the Cu^{II}/Cu^I couple is believed to be important in a number of electron-transfer processes in enzymes and proteins.² We demonstrate, however, that clusters with typically 20–50 water molecules containing the uncomplexed, singly charged metal ion can be stabilized for at least several seconds in ultrahigh vacuum, and their chemistry in collisions with single reactant molecules can be investigated.

We have previously established that reactions in such clusters proceed comparably to those in bulk aqueous solutions,^{3–5} and macroscopic concepts such as pH⁵ or solubility⁴ can be transferred to the single-ion level. Precipitation reactions serve as the first application of water clusters in the study of aqueous transition metal(I) chemistry.

Hydrated metal cations of the type M(H₂O)_n⁺, $n \leq 50$, are generated by laser vaporization of the metal followed by a supersonic expansion of the hot plasma in a helium/water mixture.⁶ The species produced are trapped in ultrahigh vacuum in a Fourier transform ion cyclotron resonance (FT-ICR) mass spectrometer, where their temperature is controlled by competition between evaporative cooling and heating by blackbody radiation^{7–11} and collisions. Neutral reactants are introduced into the ICR cell at pressures corresponding to about five collisions between the ionic cluster and the neutral gas molecule per second.

Figure 1 illustrates how the reaction of hydrated ions with HCl proceeds over a time span of typically 50 s. The HCl molecules collide with the ionic clusters, and about 10% of the collisions are reactive, with the hydrochloric acid being taken up and ionically dissolved in the cluster.^{4,12} The enthalpy of this reaction is released and heats the cluster, which in turn leads to evaporative cooling by loss of two to three water molecules. Depending on the number of available water ligands, additional HCl molecules may be absorbed into the water cluster. Conversely, as the solvent molecules are continuously removed from the clusters due to collisional and radiative heating, ultimately the ionic solution becomes destabilized, and an HCl molecule may evaporate from the cluster.

Once the HCl molecule is dissolved in the water cluster, solution-phase chemical reactions can take place. For instance, the proton may oxidize the metal ion, with (a) atomic or (b) molecular hydrogen being released, as we previously observed for hydrated Mg⁺ or Al⁺ ions,^{13,14} respectively. An alternative possibility is the precipitation of a single molecule of the metal chloride in the solution (c), which does not leave an immediate signature in the

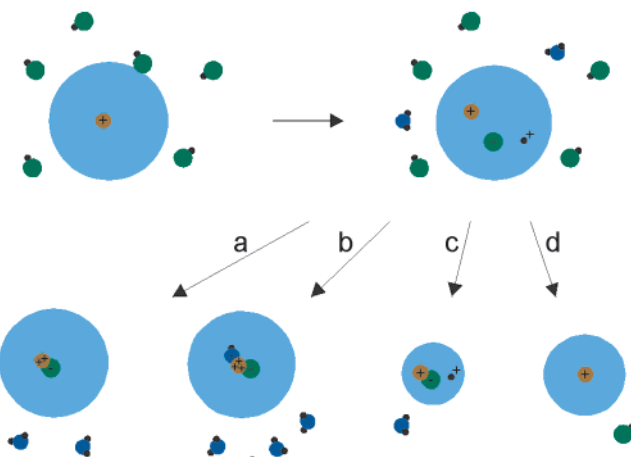


Figure 1. Possible reaction pathways of hydrated metal(I) cations with HCl. In a reactive collision with HCl, the molecule is ionically dissolved in the cluster, and typically two water molecules are released due to the reaction enthalpy. (a) The metal ion is oxidized to +II, thereby reducing the proton to atomic hydrogen, which is eliminated together with typically two water molecules. (b) If the preferred oxidation state of the metal is +III, the proton and a hydrogen atom in a water molecule are both reduced, releasing molecular hydrogen and typically three water molecules from the cluster. (c) No redox reaction takes place when a single molecule of M(I)-Cl precipitates in the strongly acidic water cluster with pH ≤ 0. Water molecules are gradually lost until the cluster becomes very small. (d) If no precipitation or redox reaction takes place, three individual ions need to be solvated by water. Solvation breaks down at fairly large sizes of the cluster, and a molecule of HCl is released.

mass spectrum. By monitoring the subsequent reactions and the ligand evaporation as a function of time, however, one can unmistakably diagnose if the salt remains ionized, or forms a single molecule “precipitate”.⁴

In a cluster containing a metal cation, which forms a highly soluble chloride such as sodium, three ions, that is, Na⁺, H⁺, and Cl⁻, have to be individually solvated. Similarly, in a protonated water cluster containing dissolved HCl, three ions, 2H⁺ and Cl⁻, are present. As the cluster is gradually heated and desolvated, eventually the H⁺ and Cl⁻ recombine to form HCl, and the covalent hydrogen chloride evaporates from the M(HCl)(H₂O)_n⁺ cluster (d). This occurs around $n = 12$.⁴ A quite different situation was found for Ag⁺, which forms an insoluble chloride. In this case the last HCl is lost when only four molecules of water are left, $n = 4$, surely too little solvent to hydrate the three separate ions.⁴ One can conclude from this observation that only a single H⁺ ion is present and that the covalent AgCl molecule formed as a precipitate in the solution. Thus, the number of water molecules n at which HCl is eliminated from the M(HCl)(H₂O)_n⁺ cluster in the desolvation process can be viewed as a measure of solubility of the

Table 1. Precipitate, Number of Water Molecules n_{\min} When Last HCl Is Eliminated, Ionization Potential of the Metal, and, If Known, the Solubility Product in Bulk Solution

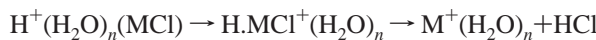
precipitate	n_{\min}	I. P. [eV]	solubility product
CrCl	4	6.77	
MnCl	≤ 3	7.43	
FeCl	3	7.90	
CoCl	6	7.88	
NiCl	7	7.63	
CuCl	5	7.73	$1.7 \times 10^{-7}^c$
NaCl	12^a	5.14	$\sim 3.7 \times 10^1^d$
AgCl	4^a	7.58	$1.8 \times 10^{-10}^c$
AgBr	3^b	7.58	$5.4 \times 10^{-13}^c$
HCl	11	13.60	

^a Reference 4. ^b Reference 18. ^c Reference 15. ^d Reference 17.

corresponding chloride. The observations correlate nicely with solubility products known from bulk solutions, with sodium chloride being highly soluble, while silver chloride is the least soluble metal(I) chloride in the literature.¹⁵ Similar minimum size values for HCl uptake by water clusters containing H⁺ and Na⁺ have recently been observed in flow reactor studies,¹⁶ which indicates that the minimum size of the cluster is an intrinsic property of the reaction system.

The first row transition metals V–Cu are known to occur in a variety of oxidation states, but with the possible exception of Cu, they do not form stable uncomplexed metal(I) ions in aqueous solutions. Despite that, however, we find that from the metals studied here, only V⁺ ions are readily oxidized upon reaction with HCl with evolution of hydrogen. If one considers the standard electrochemical series, and the potentials needed to oxidize the metals, one finds the order Mg < Al < V < Mn < Cr < Fe < Co < Ni < Cu < Ag. It therefore seems reasonable that the first three of these elements exhibit a redox chemistry in clusters, while the others do not, although the difference between the V and Mn oxidation potentials is quite small.

Unlike Mg⁺, Al⁺, and V⁺, which are, upon reaction with HCl, readily oxidized with the evolution of atomic or molecular hydrogen, the ions of Cr, Mn, Fe, Co, Ni, and Cu do not change their oxidation state even in the presence of the strongly corrosive hydrochloric acid; instead they react, similar to silver monochloride, without changing their oxidation state. The resulting cluster containing the chloride “precipitate” and a proton then gradually loses water ligands. When some specific number of water ligands n , which is characteristic of the particular metal, is reached, an HCl molecule is lost, and a hydrated monovalent metal cation M⁺(H₂O) _{n} remains. It is interesting to consider the charge transfer between H⁺ and a metal chloride occurring in the cluster:



This reaction is strongly exothermic in the gas phase ($n = 0$), but in view of the enormous lowering of the H atom ionization potential due to solvation, endothermic in bulk solution ($n = \infty$). Clearly, the thermochemistry of this reaction depends on the available solvent and has to reverse sign as n is reduced and solvent is lost. To predict the exact value of n where this will occur for a specific metal is difficult, since it will depend not only on its ionization potential, but also on the strength of the MCl bond, the preferred coordination of the metal cation, and on its hydration enthalpy.

Table 1 gives the number n_{\min} of solvent molecules remaining when the last HCl is eliminated for the precipitation reactions investigated in the present work and compares it with cations studied previously. The table also gives the ionization potentials of the metals, and where available, the solubility constant of the salt in

water. It is interesting to note that the solubilities correlate qualitatively with the values of n_{\min} . If this correlation has some broader validity, one could predict an extremely low solubility for MnCl which does not eliminate HCl even when $n = 3$ is reached, followed by FeCl, where the HCl loss at $n = 3$ is only observable after $t \approx 0.50$ s. Conversely, it would suggest for NiCl and CoCl solubilities higher than that of CuCl.

The low solubility of AgCl is usually explained by the strongly covalent character of the silver–chlorine interaction, and it is therefore perhaps quite reasonable that also other transition metals, with their partly filled d-shell should form relatively insoluble metal(I) chlorides. More surprising may appear our observation, that with the exception of vanadium, the singly ionized cations of the first-row transition metals are not readily oxidized into their more favored oxidation states, even in the presence of hydrochloric acid. Perhaps the rapid formation of a single-molecule chloride “precipitate” hinders the oxidation reaction kinetically, so that although thermodynamically favored, it does not occur on the ≈ 100 s time scale of our experiment.

Our study shows that one can generate transition metal(I) cations in water clusters and investigate their precipitation or other reactions on the single-ion level. This opens up the new experimental field of aqueous transition metal(I) chemistry and provides the key to a previously inaccessible realm of redox reactions and electrochemistry.

Acknowledgment. Financial support by the Deutsche Forschungsgemeinschaft, the Fonds der Chemischen Industrie, the EU through the RTN “Reactive Intermediates”, and the Leonhard Lorenz-Stiftung (M.K.B.) is gratefully acknowledged.

Supporting Information Available: Mass spectra of the reaction products (PDF). This material is available free of charge via the Internet at <http://pubs.acs.org>.

References

- Hollemann, A. F.; Wiberg, E.; Wiberg N. *Lehrbuch der Anorganischen Chemie*; Walter de Gruyter: Berlin, 1995.
- Stryer, L. *Biochemistry*; Freeman: New York, 1995.
- Achatz, U.; Joos, S.; Berg, C.; Schindler, T.; Beyer, M.; Albert, G.; Niedner-Schattburg, G.; Bondybey, V. E. *J. Am. Chem. Soc.* **1998**, *120*, 1876–1882.
- Fox, B. S.; Beyer, M. K.; Achatz, U.; Joos, S.; Niedner-Schattburg, G.; Bondybey, V. E. *J. Phys. Chem. A* **2000**, *104*, 1147–1151.
- Achatz, U.; Fox, B. S.; Beyer, M. K.; Bondybey, V. E. *J. Am. Chem. Soc.* **2001**, *123*, 6151–6156.
- Beyer, M.; Berg, C.; Görlitzer, H. W.; Schindler, T.; Achatz, U.; Albert, G.; Niedner-Schattburg, G.; Bondybey V. E. *J. Am. Chem. Soc.* **1996**, *118*, 7386–7389.
- Schindler, T.; Berg, C.; Niedner-Schattburg, G.; Bondybey, V. E. *Chem. Phys. Lett.* **1996**, *250*, 301–308.
- Fox, B. S.; Beyer, M. K.; Bondybey, V. E. *J. Phys. Chem. A* **2001**, *105*, 6386–6392.
- Dunbar, R. C.; McMahon, T. B. *Science* **1998**, *279*, 194–197.
- Schnier, P. D.; Price, W. D.; Jockusch, R. A.; Williams, E. R. *J. Am. Chem. Soc.* **1996**, *118*, 7178–7189.
- Sena, M.; Riveros, J. M. *Rapid Commun. Mass Spectrom.* **1994**, *8*, 1031–1034.
- Schindler, T.; Berg, C.; Niedner-Schattburg, G.; Bondybey, V. E. *Chem. Phys. Lett.* **1994**, *229*, 57–64.
- Berg, C.; Beyer, M.; Achatz, U.; Joos, S.; Niedner-Schattburg, G.; Bondybey, V. E. *Chem. Phys.* **1998**, *239*, 379–392.
- Beyer, M.; Achatz, U.; Berg, C.; Joos, S.; Niedner-Schattburg, G.; Bondybey, V. E. *J. Phys. Chem. A* **1999**, *103*, 671–678.
- Lide, D. R. *CRC Handbook of Chemistry and Physics*; CRC Press: Boca Raton, 1995.
- Gilligan, J. J.; Castleman, A. W., Jr. *J. Phys. Chem. A* **2001**, *105*, 5601–5605.
- du Maire, M. et al. *Gmelins Handbuch der Anorganischen Chemie*; Natrium, Verlag Chemie: Berlin, 1928.
- Fox, B. S. Diplomathesis, Technische Universität München, Garching, 1999.

JA017157R

Inclusion-Water-Cluster in a Three-Dimensional Superlattice of Gold Nanoparticles

Suhua Wang, Hiroshi Yao, Seiichi Sato, and Keisaku Kimura*

Department of Material Science, Himeji Institute of Technology, 3-2-1 Kohto, Kamigori-cho, Akou-gun, Hyogo 678-1297, Japan

Received December 19, 2003; E-mail: kimura@sci.himeji-tech.ac.jp

Assembling nanoparticles into ordered two-dimensional (2D) and 3D superstructures and investigating their collective properties have recently been receiving much attention.¹ Most of the reported nanoparticles are passivated with a long-chain alkane ligand, commonly hydrophobic in nature. An inherent van der Waals attraction and a hard-sphere repulsion are the driving forces for the particles to assemble orderly. Another candidate is hydrogen bonding by water that plays a crucial role in protein and molecular crystals. Water is included as an essential part of the structure in some cases, such as crystalline water, coordination water, or bound water. Utilization of hydrogen bonding in growing colloidal crystals became possible and practical when the preparation method for hydrophilic nanoparticles from hydrosol was established.² Gold nanoparticles are passivated with a short-chain dicarboxylic acid, mercaptosuccinic acid (MSA), which provides OH groups for the formation of hydrogen bonds. On the basis of the elemental analysis of well-dried particles, stoichiometric inclusion of water molecules was found.³ Well-grown faceted colloidal crystals made of Au–MSA are very stable upon exposure to most polar and nonpolar solvents.^{2,4} We have discovered self-correcting processes and inclusions of water molecules in the crystal during the equilibrium growth.^{4–6} Carboxylic acids tend to form dimers through hydrogen bonding. Therefore, hydrogen bonding among OH groups is presumed to be the force that connects the building gold nanoparticles in the gold-particle crystals.³ OH vibrational stretching modes have relatively high frequencies which are largely isolated from IR bands of other chemical bonds. Hence, the absorption band between 3000 and 3700 cm⁻¹ displays a characteristic window for intermolecular hydrogen bonding between OH groups. In this communication, therefore, IR spectroscopy was used to study the interactions among the developing gold nanoparticles within the crystals.

Three reference samples provide fundamental information on the configuration of MSA. The first two references are pure MSA (Figure 1A) and as-prepared gold nanoparticles (sample B). As demonstrated in previous works,^{3,5} MSA in the as-prepared gold nanoparticles without dialysis exist in the form of sodium carboxylate, but as the acid form in particle crystals. Figure 1B is depicted, based on the elemental analysis data for the as-prepared lyophilized powdered sample, showing that the ratio of MSA to H₂O is unity. Figure 1C was proposed on the grounds of the tendency of aggregates to form under humid conditions (The original was depicted for sodium salt).³ Therefore, the third reference, sample C, was protonated nanoparticles. The gold particle crystals (sample D) were produced following the literature method.^{2,5} These crystals reveal well-developed crystal facets (Figure 1D) and hexagonal close packing.⁵

In Figure 2 are shown the FT-IR spectra of samples (A), (B), (C), and (D), and all samples have obvious absorptions in the OH vibrational stretching region. However, the particle crystals have particular features in the band at the highest frequency and three

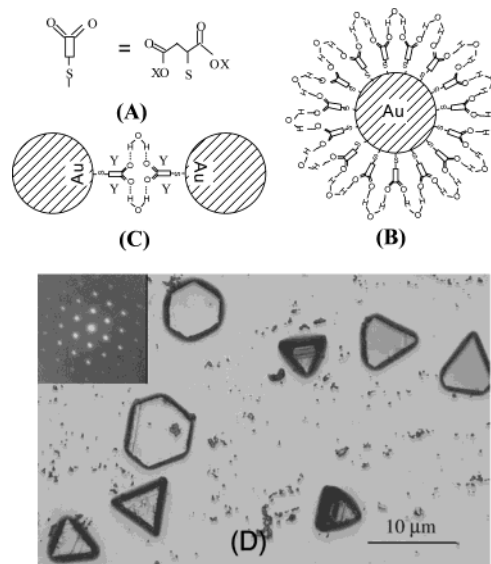


Figure 1. (A) Molecular structure of MSA, in which X denotes H or Na atom. (B) Configuration of MSA on the gold nanoparticle surface that allows one water molecule to connect with two carbonyl groups in the adjoining MSA to make a successive hydrogen-bonding network. (C) One water molecule connects with two carbonyl groups from different particles, which induces aggregation of two particles in a humid condition. Symbol Y stands for a possible spacing for water cluster. (D) Microscope images of gold particle crystals. Inset shows low-angle electron diffraction from one superlattice.

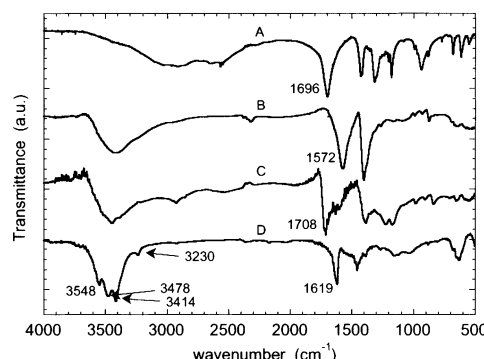


Figure 2. FT-IR spectra: (A) pure MSA molecules, (B) as-prepared gold nanoparticles (sodium salt), (C) protonated gold nanoparticles, and (D) gold colloidal crystals.

well-resolved absorption peaks. There are two sources of OH groups in the gold particle crystals. One is from the carboxylic groups of MSA molecules.³ The other is from water molecules, which are included in the superlattices during the equilibrium growth process. It is well-known that carboxylic acid molecules with no other polar groups usually exist predominantly as the hydrogen-bonded dimer,

which results in a very broad OH stretching band around 3000 cm^{-1} and an asymmetric C=O stretching band at $1740\text{--}1680\text{ cm}^{-1}$.⁷ This is clearly seen in Figure 2A. When MSA bonds to the surface of gold nanoparticles and forms carboxylate during nanoparticle preparation, a water molecule strongly binds to the MSA moiety even in well-dried powders as evidenced by an elemental analysis and by thermogravimetry.³ This bound water molecule can be released above 105°C . The shift of the C=O stretching peak to the low frequency of 1572 cm^{-1} (Figure 2B) is consistent with the formation of carboxylate ion (COO^-).⁸ It is also seen in Figure 2B that the carboxylic OH stretching band around 3000 cm^{-1} disappears and a new poorly resolved broad band appears, centering at 3400 cm^{-1} , which is attributed to water molecules bound to the as-prepared gold nanoparticles. When carboxylic acid molecules exist in the monomeric state, however, the OH stretching vibration absorbs at $3550\text{--}3500\text{ cm}^{-1}$, and the C=O stretching shifts simultaneously to a higher frequency around $1800\text{--}1740\text{ cm}^{-1}$.⁸ The observed C=O stretch peak in Figure 2C is 1708 cm^{-1} , slightly higher than that of pure MSA (1696 cm^{-1}) and lower than that of free carboxylic acid monomer. Observation of a band at around 3000 cm^{-1} and a broad band near 3400 cm^{-1} suggests the water-bound carboxylic acid in Sample C.

The OH symmetric (ν_1) and antisymmetric (ν_3) vibrational stretching fundamentals of the water monomer are at 3650 and 3755 cm^{-1} , respectively.⁷ For liquid water or bound water in many cases, however, the OH stretching band is red-shifted from ν_1 and ν_3 by several hundred wavenumbers due to hydrogen-bonding networks, and the features are completely masked by overwhelming background absorption from distant water molecules.⁷⁻⁹ That is, the hydrogen-bonded water molecules in a distributed-bound state result in an unresolved and broad OH band centered at 3400 cm^{-1} . However, for the gold particle crystals having the same chemical composition as in the protonated gold nanoparticle powders for MSA, three well-resolved peaks are detected as in Figure 2D at 3548 , 3478 , and 3414 cm^{-1} , respectively. All positions are about 300 cm^{-1} red-shifted from that of water monomer. The water molecules adsorbed in the as-prepared and protonated gold nanoparticles combine with the carbonyl groups of MSAs through hydrogen bonding.^{3,5} In this case, the OH stretching band of water showed nearly the same spectra as those in Figure 2B or C. Hence, we exclude hydrogen-bonding networks of bulk water or the existence of water monomers in sample D. The presence of 1619 cm^{-1} absorption in the crystals immediately rules out the MSA monomeric state. The low energy-shift of this band implies that the effective mass of C=O stretching is larger than that of the dimeric state of carboxylic acid, i.e. C=O is bound by several hydrogen bonds. Figure 2D shows no OH stretching band around 3000 cm^{-1} , implying that the OH groups of the MSA should not be free but probably bond with water.

We can also rule out the presence of water dimer in the superlattices, because the dimer exhibit OH vibrational peaks at ca. 3710 and ca. 3620 cm^{-1} which are slightly red-shifted to the water monomer bands.¹⁰ On the other hand, water clusters such as $(\text{H}_2\text{O})_n$ ($n = 8\text{--}10$) have been reported to exhibit well-resolved peaks in $3400\text{--}3600\text{ cm}^{-1}$, just falling in the region of the observed splitting IR band.¹¹ Therefore, it is reasonable to presume that the observed three peaks come from interstitial small water clusters, "inclusion-water-clusters" which combine with carboxylic groups through hydrogen-bonding interactions. The formation of hydrogen bonding between MSA molecules and water clusters lowers the

force constant of carboxylic OH bond. This will correspondingly result in a red-shift of the carboxylic OH stretching from $\sim 3520\text{ cm}^{-1}$ of the monomer.⁸ The obvious but relatively weak absorption peak at 3230 cm^{-1} is therefore attributed to the OH vibrational stretching of carboxylic groups in MSA. The approximately 300 cm^{-1} -shift is consistent with that of the OH stretching mode from water.

Although we could not determine the structures of interstitial water clusters from the IR spectra, the formation of water clusters is most probable in the superlattice. In a hexagonal close-packed alignment of surface-modified nanoparticles, a tetrahedral Td or octahedral Oh interstitial cavity is produced along with that between two adjacent nanoparticles. It is plausible that carboxylic groups in MSA combine with water cluster of definite size in the confined cavities through intermolecular hydrogen bonding. That is, water clusters intervene among MSA-modified gold nanoparticles, which stabilize the nanoparticle crystals. The size and structure of the clusters depend on their locations in the superlattice.¹²

In conclusion, we have found the "inclusion-water-cluster" for the first time. The results show that water clusters are trapped in the interstice of superlattices and connect the building gold nanoparticles through hydrogen bonding.

Acknowledgment. Financial support and granting the postdoctoral fellowship (P01261) from the Japan Society for Promotion of Science is gratefully acknowledged. We are indebted to support in part by Grants-in-Aid for Scientific Research (B:13440212) from MEXT and by Mitsubishi Research Institute, Japan Space Utilization Promotion Center and Hyogo Science and Technology Promotion Foundation.

Supporting Information Available: Experimental procedures and TEM and XRD data (PDF). This material is available free of charge via the Internet at <http://pubs.acs.org>.

References

- (a) Weller, H. *Curr. Opin. Colloid Interface Sci.* **1998**, *3*, 194. (b) Collier, C. P.; Vossmeye, T.; Heath, J. R. *Annu. Rev. Phys. Chem.* **1998**, *49*, 371. (c) Murray, C. B.; Kagan, C. R.; Bawendi, M. G. *Annu. Rev. Mater. Sci.* **2000**, *30*, 545. (d) Ohara, P. C.; Heath, J. R.; Gelbart, W. M. *Angew. Chem., Int. Ed. Engl.* **1997**, *36*, 1078. (e) Lin, X. M.; Jaeger, H. M.; Sorensen, C. M.; Klabunde, K. J. *J. Phys. Chem. B* **2001**, *105*, 3353. (f) Giersig, M.; Mulvaney, P. *Langmuir* **1993**, *9*, 3408. (g) Dabbousi, B. O.; Murray, C. B.; Rubner, M. F.; Bawendi, M. G. *Chem. Mater.* **1994**, *6*, 216. (h) Legrand, J.; Petit, C.; Pilani, M. P. *J. Phys. Chem. B* **2001**, *105*, 5643. (i) Harfenist, S. A.; Wang, Z. L.; Whetten, R. L.; Vezmar, I.; Alvarez, M. M. *Adv. Mater.* **1997**, *9*, 817. (j) Courty, A.; Araspin, O.; Fermon, C.; Pilani, M. P. *Langmuir* **2001**, *17*, 1372.
- (2) Kimura, K.; Sato, S.; Yao, H. *Chem. Lett.* **2001**, 372.
- (3) Chen, S.; Kimura, K. *Langmuir* **1999**, *15*, 1075.
- (4) Sato, S.; Yao, H.; Kimura, K. *Physica E* **2003**, *17*, 521.
- (5) (a) Wang, S.; Sato, S.; Kimura, K. *Chem. Mater.* **2003**, *15*, 1075. (b) Stoeva, S. I.; Prasad, B. L. V.; Uma, S.; Stoimenov, P. K.; Zaikovski, V.; Sorensen, C. M.; Klabunde, K. J. *J. Phys. Chem. B* **2003**, *107*, 7441.
- (6) (a) Sato, S.; Yamamoto, H.; Yao, Kimura, K. *Mater. Res. Soc. Symp. Proc.* **2002**, *703*, 375. (b) Wang, S. H.; Sato, S.; Kimura, K. *Chem. Lett.* **2003**, *32*, 520. (c) Yao, H.; Kojima, H.; Sato, S.; Kimura, K. *Chem. Lett.* **2003**, *32*, 698.
- (7) Braun, C. L.; Smirnov, S. N. *J. Chem. Edu.* **1993**, *70*, 612.
- (8) Colthup, N. B.; Daly, L. H.; Wiberley, S. E. *Introduction to Infrared and Raman Spectroscopy*, 3rd ed.; Academic Press: San Diego, CA, 1990; pp 256–260, pp 239–268, p 291.
- (9) Weber, J. M.; Kelley, J. A.; Nielsen, S. B.; Ayotte, P.; Johnson, M. A. *Science* **2000**, *287*, 2461.
- (10) Tursi, A. J.; Nixon, E. R. *J. Chem. Phys.* **1970**, *52*, 1521.
- (11) (a) Buck, U.; Ettischer, I.; Melzer, M.; Buch, V.; Sadlej, J. *Phys. Rev. Lett.* **1998**, *80*, 2578. (b) Jensen, J. O.; Krishnan, P. N.; Burke, L. A. *Chem. Phys. Lett.* **1995**, *246*, 13.
- (12) Relevant lattice parameters from TED are given and discussed in Supporting Information.

JA031822+

Characterization of Supramolecular (H_2O)₁₈ Water Morphology and Water-Methanol (H_2O)₁₅(CH₃OH)₃ Clusters in a Novel Phosphorus Functionalized Trimeric Amino Acid Host

Kannan Raghuraman,^{†,‡} Kavita K. Katti,[†] Leonard J. Barbour,[‡]
Nagavarakishore Pillarsetty,[‡] Charles L. Barnes,[‡] and Kattesh V. Katti*,^{†,‡,§}

Contribution from the Departments of Radiology, Physics, and Chemistry,
Rm #106 Alton Bldg Laboratories, 301 Business loop 70W, University of Missouri-Columbia,
Columbia, Missouri 65211

Received February 14, 2003; E-mail: kattik@health.missouri.edu

Abstract: Phosphorus functionalized trimeric alanine compounds (L)- and (D)-P(CH₂NHCH(CH₃)COOH)₃ **2** are prepared in 90% yields by the Mannich reaction of Tris(hydroxymethyl)phosphine **1** with (L)- or (D)-Alanine in aqueous media. The hydration properties of (L)-**2** and (D)-**2** in water and water-methanol mixtures are described. The crystal structure analysis of (L)-**2**·4H₂O, reveals that the alanine molecules pack to form two-dimensional bilayers running parallel to (001). The layered structural motif depicts two closely packed monolayers of **2** each oriented with its phosphorus atoms projected at the center of the bilayer and adjacent monolayers are held together by hydrogen bonds between amine and carboxylate groups. The water bilayers are juxtaposed with the H-bonded alanine trimers leading to 18-membered (H₂O)₁₈ water rings. Exposure of aqueous solution of (L)-**2** and (D)-**2** to methanol vapors resulted in closely packed (L)-**2** and (D)-**2** solvated with mixed water-methanol (H₂O)₁₅(CH₃OH)₃ clusters. The O-O distances in the mixed methanol-water clusters of (L)-**2**·3H₂O·CH₃OH and (D)-**2**·3H₂O·CH₃OH (O-O(average) = 2.857 Å) are nearly identical to the O-O distance observed in the supramolecular (H₂O)₁₈ water structure (O-O(average) = 2.859 Å) implying the retention of the hydrogen bonded structure in water despite the accommodation of hydrophobic methanol groups within the supramolecular (H₂O)₁₅(CH₃OH)₃ framework. The O-O distances in (L)-**2**·3H₂O·CH₃OH and (D)-**2**·3H₂O·CH₃OH and in (H₂O)₁₈ are very close to the O-O distance reported for liquid water (2.85 Å).

Introduction

The chemistry, physics, and biological aspects of hydrogen bonded liquids have attracted considerable theoretical and experimental interests.^{1–3} Water and methanol constitute important prototypes of hydrogen bonded liquids and investigations toward understanding hydrogen bonding patterns that exist within the individual liquids, and also more complex phenomenon that ensue upon mixing H₂O and MeOH, has been at the focus of attention for a number of decades.^{1–3} Because water plays an indispensable role in life-sustaining processes, investigations on its structure, properties and functions have received more scientific attention than any other substance.^{1–3} Several investigations to date, have provided evidence that the water trimer,⁴ tetramer,⁵ and pentamers⁶ have hydrogen bonded 2D cyclic minimum energy structures whereas pioneering efforts

by Saykally and others suggest 3D geometries for the larger water clusters with the hexameric forms representing the transition from 2D cyclic to the 3D geometries.^{7–11} Recent studies are focused on unraveling structural morphologies of water cocrystallized with various chemical entities because the lattice of a crystal host offers an attractive environment for stabilizing various topologies of water clusters and thereby provide quantitative characterization of the hydrogen bonded networks that exist in liquid water.^{3,12–15} Studies toward

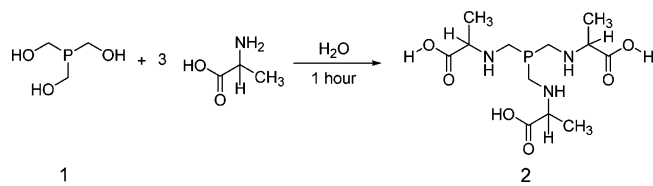
- (7) Liu, K.; Brown, M. G.; Carter, C.; Saykally, R. J.; Gregory, J. K.; Clary, D. C. *Nature* **1996**, *381*, 501–503.
- (8) Liu, K.; Cruzan, J. D.; Saykally, R. J. *Science*, **1996**, *271*, 929–933.
- (9) Gregory, J. K.; Clary, D. C.; Liu, K.; Brown, M. G.; Saykally, R. J. *Science* **1997**, *275*, 814–817.
- (10) Nauta, K.; Miller, R. E. *Science* **2002**, *287*, 293–295.
- (11) Gruenloh, C. J.; Carney, J. R.; Arrington, C. A.; Zwier, T. S.; Fredericks, S. Y.; Jordan, K. D. *Science* **1997**, *276*, 1678–1681.
- (12) (a) Barbour, L. J.; Orr, W. G.; Atwood, J. L. *Nature* **1998**, *393*, 671–673. (b) Atwood, J. L.; Barbour, L. J.; Ness, T. J.; Raston, C. L.; Raston, P. L. *J. Am. Chem. Soc.* **2001**, *123*, 7192–7193. (c) Blanton, W. B.; Gordon-Wylie, S. W.; Clark, G. R.; Jordan, K. D.; Wood, J. T.; Geiser, U.; Collins, T. J. *J. Am. Chem. Soc.* **1999**, *121*, 3551–3552. (d) Janiak, C.; Schramann, T. G.; Mason, S. A. *J. Am. Chem. Soc.* **2002**, *124*, 14 010–14 011. (e) Park, K.-M.; Kuroda, R.; Iwamoto, T. *Angew. Chem., Int. Ed. Engl.* **1993**, *32*, 884–886. (f) Doedens, R. J.; Yohannes, E.; Khan, M. I. *Chem. Commun.* **2002**, *62*–63. (g) Barbour, L. J.; Orr, G. W.; Atwood, J. L. *Chem. Commun.* **2000**, 859–860.
- (13) Moorthy, J. N.; Natarajan, R.; Venugopalan, P. *Angew. Chem., Int. Ed. Engl.* **2002**, *41*, 3417–3420.
- (14) Müller, A.; Krickemeyer, E.; Bögge, H.; Schmidtmann, M.; Roy, S.; Berkle, A. *Angew. Chem., Int. Ed.* **2002**, *41*, 3604–3608.

understanding the growth and properties of water clusters that are larger than hexamers are highly relevant in understanding solvation processes although the development of large size water clusters has been a challenging scientific endeavor.^{8,16–18}

Hydrogen bonding liquid methanol (MeOH) is the simplest amphiphile functionalized with hydrophobic ($-\text{CH}_3$) and hydrophilic ($-\text{OH}$) groups. Understanding of the solvation properties of MeOH as it relates to the disposition of hydrophobic/hydrophilic groups in polar or nonpolar solvents is of fundamental importance in biological and chemical sciences because amphiphiles are essential constituents making up cell membranes and are also extensively used in chemical industries as micelles (e.g., detergent action). In fact, the eccentric properties associated with water-alcohol mixtures have been the focus of numerous scientific investigations and significant technological applications.^{16,18–21} Frank and Evans interpreted the unusual entropic changes that ensue upon mixing methanol and water by proposing that the hydrogen bonds of water act like an “iceberg” and encapsulate the hydrophobic headgroups of methanol in a clathrate-like fashion,²² although this model has never been confirmed by concrete structural evidence. In contrary to this widely accepted model, Crain and co-workers have recently provided experimental evidence inferring that the hydrogen bonded network structure of water is not lost upon mixing methanol with water and that the polar hydroxyl group of methanol dictates the thermodynamic properties of methanol–water mixtures.^{23,24}

Indeed, structural elucidations and understanding hydrogen-bonding properties of supramolecular networks of water and water-methanol at nanometer scales have been a topic of significant challenge.³ Well characterized mixed water–methanol clusters are rare,^{25–28} although structural elucidation of such clusters is imperative to gaining insight into the anomalous properties and to understanding the hydrogen bonding and dynamics of water–methanol binary mixtures. We, herein, report (a) the experimental evidence for the existence of a 2D cyclic supramolecular (H_2O)₁₈ morphology within the layers of ($\text{HOOCCH}(\text{CH}_3)\text{NHCH}_2$)₃P, **2**, with structural features (average O–O bond distance in (H_2O)₁₈ = 2.858 Å) similar to those of liquid water (O–O bond distance in liquid water = 2.85 Å);¹⁷ (b) Our results on the application of single-crystal X-ray diffraction methods to probe the molecular scale hydrogen bonded structure of mixed supramolecular water-methanol (H_2O)₁₅(CH₃OH)₃ clusters and the evidence for the accom-

Scheme 1. Synthesis of P(CH₂NHCH(CH₃)COOH)₃ (**2**)



modation of methanol groups within the hydrogen bonded (H_2O)₁₈ framework.

Results and Discussion

Synthesis and Characterization of (L)-2 and (D)-2. As part of our continued efforts in the design and development of cancer diagnostic and therapeutic agents,^{29,30} we have recently developed new strategies for the preparation of peptide-mimetic dimeric and trimeric amino acid conjugates.³¹ Phosphorus functionalized trimeric amino acid (L)-(HOOCCH(CH₃)NHCH₂)₃P (**2**) and (D)-(HOOCCH(CH₃)NHCH₂)₃P (**2**) were prepared by the addition of tris(hydroxymethyl phosphine) **1** to 3-fold excess of (L)- or (D)-alanine, via a Mannich-reaction pathway, in water in 90% yields (Scheme 1). Compounds (L)-**2** and (D)-**2** are white, air-stable, crystalline compounds and are readily soluble in water. The ³¹P{¹H} NMR spectra of (L)-**2** and (D)-**2** in D₂O showed sharp singlets at δ –39.9 ppm. The ¹H and ¹³C NMR spectra of (L)-**2** and (D)-**2** in D₂O are consistent with the structure. The mass spectrum of (L)-**2** showed a molecular ion [M+H⁺] peak with *m/z* = 338.0 consistent with the formula weight (337.31).

Hydration Studies of (L)-2 and Characterization of (H₂O)₁₈. The high solubility and a balanced hydrophobic/hydrophilic functionalities in the trimeric alanine compound **2** prompted us to utilize this molecule as a host template with the hope of encapsulating water clusters within its crystal lattice. Indeed, this trimeric alanine molecule **2** crystallizes with four molecules of water as revealed by X-ray crystallography. The crystallographic data are summarized in Table 1.

The crystal structure analysis of (L)-**2**·4H₂O, reveals that the alanine molecules pack to form two-dimensional bilayers running parallel to (001). Figure 1 shows perspective view of the structurally rigid (H₂O)₁₈ supramolecular ice-like hydrogen bonding arrangement of water molecules. The layered structural motif depicts two closely packed monolayers of **2** each oriented with its phosphorus atoms projected at the center of the bilayer and adjacent monolayers are held together by hydrogen bonds between amine and carboxylate groups. Space filling model as shown in Figure 1 depicts the alanine amino acid clefts interfacing the supramolecular ice-like (H₂O)₁₈ bilayers. The ball-and-stick perspective view shows how the water bilayers are juxtaposed with the H-bonded alanine trimers leading to 18-membered water rings. This motif consists of two closely packed monolayers of (L)-**2**, each oriented with its phosphorus atoms projected toward the center of the bilayer. Although no direct intermolecular interactions are apparent between the molecules of each monolayer, adjacent monolayers are held together by hydrogen bonds formed between their amine and

- (15) Custelcean, R.; Aflorenoi, C.; Vlassa, M.; Polverejan, M. *Angew. Chem. Int. Ed. Engl.* **2000**, *39*, 3094–3096.
- (16) Buck, U.; Huisken, F. *Chem. Rev.* **2000**, *100*, 3863–3890.
- (17) Narten, A. H.; Thieszen, W. E.; Blum, L. *Science* **1982**, *217*, 1033–1034.
- (18) (a) Head-Gordon, T. *Proc. Natl. Acad. Sci.* **1995**, *92*, 8308–8312. (b) Head-Gordon, T.; Hura, G. *Chem. Rev.* **2002**, *102*, 2651–2670.
- (19) Frank, F.; Desnoyers, J. E. In *Water Science Reviews*; Franks, F., Ed.; Cambridge University Press: New York, 1985; Vol. 1, 171–232.
- (20) Murthy, S. N. *J. Phys. Chem. A* **1999**, *103*, 7927–7937.
- (21) Franks, F.; Ives, D. J. *G. Q. Rev.* **1966**, *20*, 1–45.
- (22) Frank, H. S.; Evans, M. W. *J. Chem. Phys.* **1945**, *13*, 507–532.
- (23) Dixit, S.; Crain, J.; Poon, W. C. K.; Finney, J. L.; Soper, A. K. *Nature* **2002**, *416*, 829–832.
- (24) Dixit, S.; Soper, A. K.; Finney, J. L.; Crain, J. *Europhys. Lett.* **2002**, *59*, 377–383.
- (25) Stockman, P. A.; Blake, G. A.; Lovas, F. J.; Suenram, R. D. *J. Chem. Phys.* **1997**, *107*, 3782–3790.
- (26) Laaksonen, A.; Kusalik, P. G.; Svishchev, I. M. *J. Phys. Chem. A* **1997**, *101*, 5910–5918.
- (27) Jorgenson, W. L.; Madura, J. D. *J. Am. Chem. Soc.* **1983**, *105*, 1407–1413.
- (28) Wilson, K. R.; Schaller, R. D.; Co, D. T.; Saykally, R. J.; Rude, B. S.; Catalano, T.; Bozek, J. D. *J. Chem. Phys.* **2002**, *117*, 7738–7744.

- (29) Raghuraman, K.; Pillarsetty, N.; Volkert, W. A.; Barnes, C.; Jurisson, S.; Katti, K. V. *J. Am. Chem. Soc.* **2002**, *124*, 7276–7277.
- (30) Pillarsetty, N.; Katti, K. K.; Hoffman, T. J.; Volkert, W. A.; Katti, K. V.; Kamei, H.; Koide, T. *J. Med. Chem.* **2003**, *46*, 1130–1132.
- (31) Berning, D. E.; Katti, K. V.; Barnes, C. L.; Volkert, W. A. *J. Am. Chem. Soc.* **1999**, *121*, 1658–1664.

Table 1. Crystallographic Data for L-2·4H₂O, L-2·3H₂O(CH₃OH) (193 K and 293 K), D-2·3H₂O(CH₃OH)

compd	L-2 containing (H ₂ O) ₁₈	L-2 containing (H ₂ O) ₁₅ (CH ₃ OH) ₃ (T = 193 K)	D-2 containing (H ₂ O) ₁₅ (CH ₃ OH) ₃ (T = 193 K)	L-2 containing (H ₂ O) ₁₅ (CH ₃ OH) ₃ (T = 293 K)
formula	C ₁₂ H ₃₂ N ₃ O ₁₀ P	C _{12.50} H ₃₃ N ₃ O ₁₀ P	C _{12.50} H ₃₃ N ₃ O ₁₀ P	C _{12.50} H ₃₃ N ₃ O ₁₀ P
formula weight	409.37	416.39	416.39	416.39
T	193(2) K	193(2) K	193(2) K	293(2) K
λ (Å)	0.71073	0.71073	0.71073	0.71073
crystal system, space group	hexagonal, P6 ₃	hexagonal, P6 ₃	hexagonal, P6 ₃	hexagonal, P6 ₃
a (Å)	12.2838(7)	12.2122(4)	12.2272(7)	12.3133(3)
c (Å)	15.7572(14)	15.8761(11)	15.8762(17)	16.0239(9)
volume	2059.1(2) Å ³	2050.51(17) Å ³	2055.6(3) Å ³	2104.01(14) Å ³
Z, ^a D _{Calc}	4, 1.321 Mg/m ³	4, 1.349 Mg/m ³	4, 1.345 Mg/m ³	4, 1.315 Mg/m ³
F(000)	880	896	896	896
crystal size (mm)	0.50 × 0.25 × 0.25	0.45 × 0.25 × 0.05	0.50 × 0.35 × 0.05	0.50 × 0.35 × 0.10
θ range (°)	1.91 to 27.12	1.93 to 27.15	1.92 to 27.09	1.91 to 27.11
reflections collected/unique	12424/2992	12976/2865	12936/3039	13419/3043
[R(int)]	0.0468	0.0616	0.0661	0.0385
GOF	1.066	1.080	1.041	1.089
R	0.0485	0.0519	0.0529	0.0415
R _w	0.1274	0.1138	0.1191	0.1007

^a Z = 4 can be rationalized as follows: There are 6-symmetry related positions in the unit cell, and the asymmetric unit consists of two separate fragment each consisting of a third of a molecules. For example, two independent trimeric alanine molecules are included in an asymmetric unit (2/3 × 6 = 4) and two water oxygens are located on the 3-fold axis 1/4 ((2 + 2/3) × 6) = 4.

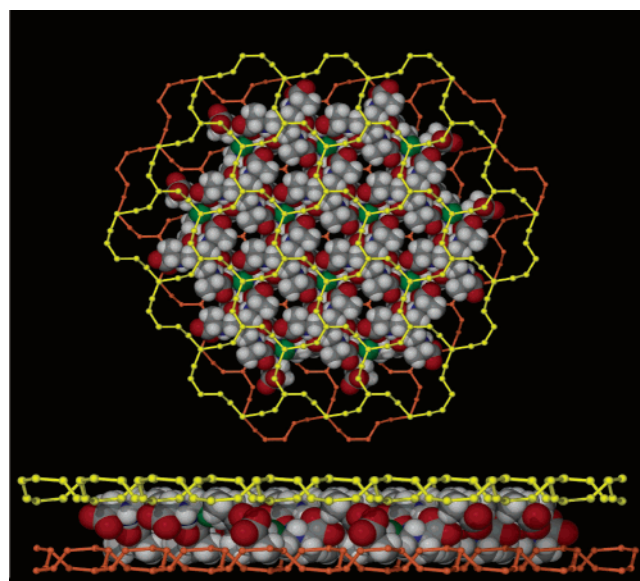


Figure 1. Perspective view of supramolecular (H₂O)₁₈ hydrogen bonding arrangement of water molecules. Colors are as follows: gray, carbon; dark blue, nitrogen; green, phosphorus; red, oxygen (carboxyl); yellow and orange, oxygen (water); white, hydrogen. Hydrogen atoms in water are omitted for clarity.

carboxylate groups. Thus, within the bilayer, each molecule of one monolayer interacts with three molecules of the adjacent monolayer. This intricate hydrogen bonded arrangement ensures that the bilayer is structurally rigid. Both surfaces of each bilayer are hydrophobic, being composed primarily of hydrogen atoms on aliphatic carbon atoms. Adjacent bilayers are in van der Waals contact with one another by virtue of these hydrogen atom surfaces. However, the packing arrangement of the molecules of each bilayer results in the formation of relatively large fissures in its surface. These fissures expose carboxylate oxygen atoms just below the plane of the surface, thus forming triangular hydrophilic clefs in the bilayer (Figure 2). Indeed, the clefts of adjacent bilayers overlap to form a two-dimensional network of hydrophilic channels running through the structure. These channels are occupied by water molecules which hydrogen bond to one another to form fused 18-membered water rings

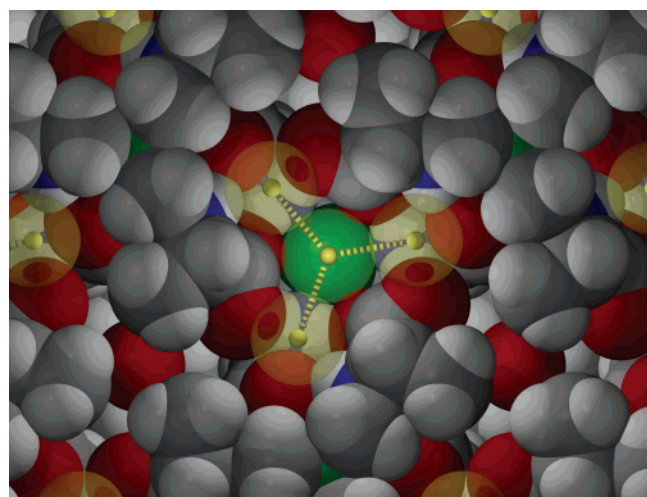


Figure 2. Perspective view showing triangular amino acid clefts accommodating four water molecules. Colors are as follows: gray, carbon; red, oxygen (carboxyl); green, phosphorus; yellow, oxygen (water); dark blue, nitrogen; white, hydrogen.

(Figure 1). The water molecules in the ice layer also hydrogen bond to the exposed oxygen atoms of the carboxylate groups of **2**. Each triangular cleft on the surface of the bilayer accommodates four water molecules (Figure 2). Three of these molecules are arranged as a regular equilateral triangle (side length = 4.951 Å). The fourth water molecule is situated 0.25 Å above the centroid of the triangle and hydrogen bonds to those at the vertexes (O···O = 2.869 Å). A slight overlap of the triangle vertexes of adjacent bilayers exists such that each triangle links to three triangles of the neighboring bilayer via an O···O hydrogen bond (2.848 Å) between the water molecules. The interplanar spacing between the best-fit planes defined by the triangles of adjacent bilayers is approximately 2 Å.

The nature of interaction of (H₂O)₁₈ with the host template (*L*)·**2** was probed by thermogravimetric analysis (TGA). The TGA data on (*L*)·2·4H₂O showed an 17.352% weight loss between room temperature and 150 °C which corresponds to 3.94 molecules of water (Figure 3). The facile removal of four

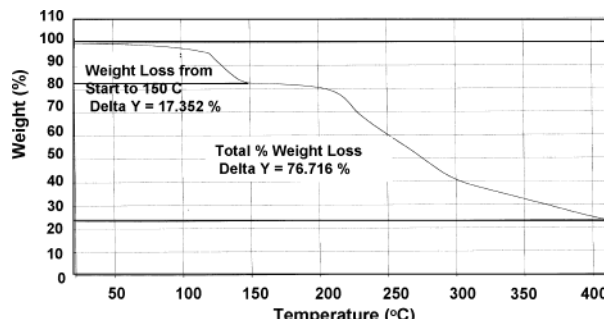


Figure 3. Thermogravimetric Curve of (L)-2·4H₂O at a heating rate of 10 °C.

molecules of water from (L)-2·4H₂O reconfirms that the (H₂O)₁₈ polygons have weak interactions with the host framework in **2** and that the supramolecular (H₂O)₁₈ cyclic water manifests liquid water properties. Indeed, such a large supramolecular 2D cyclic structure for water has not been observed before either in liquid water or in other low dimensional ice. Hitherto, pentagons/hexagons have been characterized to be the basic hydrogen bonding subunits in water clusters [(H₂O)_n, n = 8, 10, and 12] in supramolecular compounds.^{3,12–15} The unique structural morphology of water in (H₂O)₁₈ is in stark contrast to the ordered pentagonal and hexagonal water morphologies found in a majority of organic/inorganic supramolecular compounds.^{12–15} This supramolecular association of 2D water molecules in layers of (L)-2 is presumably enforced by the shape of trimeric alanine host channels, whose relatively narrow openings inhibit the formation of more stable three-dimensional water clusters. The average O–O distance of 2.858 Å in the supramolecular (H₂O)₁₈ morphology of (L)-2 is strikingly similar to the O–O distance of 2.85 Å found in liquid water suggesting close structural similarity of (H₂O)₁₈ in (L)-2 to liquid water structure.¹⁷

This experimentally observed (H₂O)₁₈ water cyclic morphology in **2** may be rationalized as follows: As the hydrophilicity of the solute molecules increase, water clusters tend to grow in size to the hexameric and higher membered water rings.^{8,17} Indeed, the high hydrophilicity of the trimeric alanine **2** may presumably result in a spatial arrangement of water such that it encloses hydrophobic sites within the polyhedral (H₂O)₁₈ water structure as a means of effecting minimal disruption from the preferred tetrahedral hydrogen bond arrangement. The O–O–O angle of 125.7° (average) observed in the supramolecular (H₂O)₁₈ is a significant deviation from the tetrahedral geometry and implies that this opening up of the O–O–O angle allows efficient perpetuation of hydrogen bonds.

Mixed Water–Methanol Clusters. Despite numerous investigations on water-alcohol binary mixtures, there is still considerable uncertainty about the nature of the hydration structure in aqueous alcohol.^{16,18–21,32–40} To gain insight into the reasons for the anomalous thermodynamic properties of alcohol–water mixtures, it is imperative to perform detailed structural analysis of hydrogen-bonded networks of water in the vicinity of alcohols. The structural integrity of hydrogen bonded (H₂O)₁₈ in (L)-2 and the interlayer spacing of ~2 Å as found within the layers of (L)-2 prompted us to investigate the feasibility of incorporation of other hydrogen bonding liquids within its layered lattice. In particular, we were interested in examining if the layers of (L)-2 serve as a fertile hydrogen

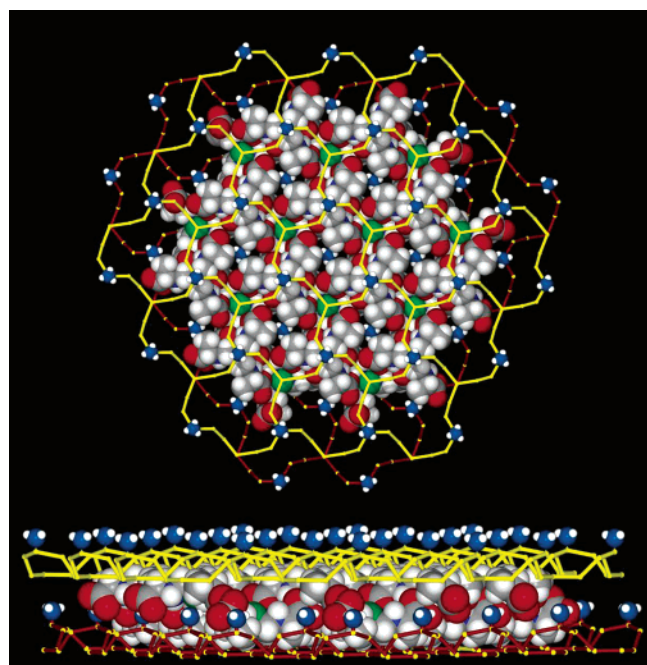


Figure 4. Perspective view of supramolecular hydrogen bonding network of water and methanol molecules in (H₂O)₁₅(CH₃OH)₃. Colors are as follows: gray, carbon; dark blue, carbon (methyl from methanol); green, phosphorus; red, oxygen (carboxyl); yellow and orange, oxygen (water); white, hydrogen.

bonding terrain to stabilize mixed water-methanol clusters. Our approach to the development of mixed methanol–water clusters involved exposure of methanol vapors to the aqueous solutions of (L)- or (D)-trimeric alanine compound **2**. Indeed, these studies resulted in the formation of mixed methanol–water clusters within the (L)- and (D)-trimeric amino acid **2** hosts. Single crystals suitable for X-ray diffraction studies were grown from exposing aqueous solution of (L)-**2** or (D)-**2** (0.05 g/mL of water) to the vapors of methanol (20 mL). The X-ray crystallographic data for (L)-**2**·3H₂O·CH₃OH and (D)-**2**·3H₂O·CH₃OH are shown in Table 1. The crystal structure of (D)-**2**·3H₂O·CH₃OH is isostructural to that of (L)-**2**·3H₂O·CH₃OH. We will, therefore, restrict our structural descriptions to (L)-**2**·3H₂O·CH₃OH. The crystal structure of (L)-**2**·3H₂O·CH₃OH constituted closely packed monolayers of the mixed methanol–water (H₂O)₁₅(CH₃OH)₃ cluster. Perspective view of supramolecular hydrogen bonding network of water and methanol molecules in (H₂O)₁₅(CH₃OH)₃ is given in Figure 4. Figure 4 shows space filling model of the alanine amino acid clefts interfacing the supramolecular mixed water–methanol (H₂O)₁₅(CH₃OH)₃ bilayers. The cross-sectional view (Figure 4) shows how the water-methanol bilayers are juxtaposed with the H-bonded alanine trimers leading to 18-membered water-methanol rings. The presence of the supramolecular hydrogen bonded mixed water-methanol (H₂O)₁₅(CH₃OH)₃ clusters encompass the amino acid layers in a two-dimensional network. Although no direct intermolecular interactions are apparent between the molecules of each monolayer, adjacent amino acid monolayers are held together by hydrogen bonds formed between their amine and carboxylate groups. Thus, within the bilayer, each molecule of one monolayer interacts with three molecules of the adjacent monolayer. This intricate hydrogen bonded arrangement ensures that the bilayer is structurally rigid. Both surfaces of each bilayer are hydrophobic, being composed primarily of hydrogen atoms on

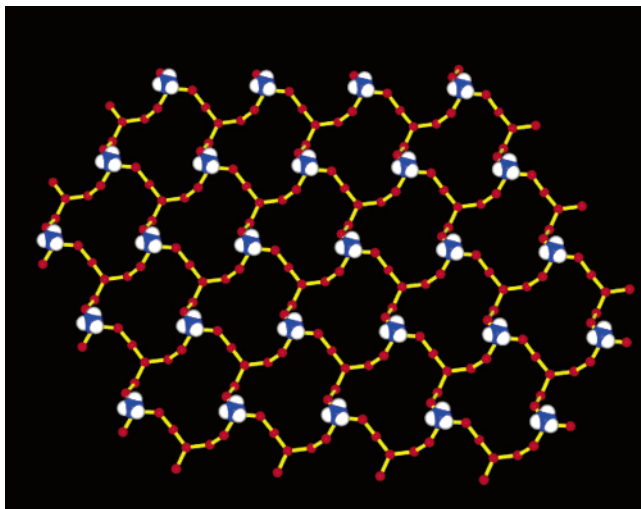


Figure 5. Perspective view showing the accommodation of hydrophobic headgroups of methanol within the water structure. Colors are as follows: dark blue, carbon (methyl from methanol); red, oxygen; white, hydrogen.

Table 2. O–O Distance (Å) in $(\text{H}_2\text{O})_{18}$ and $(\text{H}_2\text{O})_{15}(\text{CH}_3\text{OH})_3$

bond	$(\text{H}_2\text{O})_{18}^a$ (Å)	$(\text{H}_2\text{O})_{15}(\text{CH}_3\text{OH})_3^b$ (Å)	$(\text{H}_2\text{O})_{15}(\text{CH}_3\text{OH})_3^c$ (Å)	$(\text{H}_2\text{O})_{15}(\text{CH}_3\text{OH})_3^d$ (Å)
O1W–O2W	2.869	2.852	2.861	2.904
O2W–O3W	2.848	2.859	2.851	2.859
O3W–O1M	2.860	2.861	2.864	2.885

^a Crystallized with (L)-2 crystal structure determined at 193 K. ^b Crystallized with (L)-2 crystal structure determined at 193 K. ^c Crystallized with (D)-2 crystal structure determined at 193 K. ^d Crystallized with (L)-2 crystal structure determined at 293 K.

aliphatic carbon atoms. Adjacent bilayers are in van der Waals contact with one another by virtue of these hydrogen atom surfaces. However, the packing arrangement of the molecules of each bilayer results in the formation of relatively large fissures in its surface. These fissures expose carboxylate oxygen atoms just below the plane of the surface, thus forming triangular hydrophilic clefts in the bilayer. Indeed, the clefts of adjacent bilayers overlap to form a two-dimensional network of hydrophilic channels running through the structure. These channels are occupied by water and methanol molecules which hydrogen bond to one another “cooperatively” to form a supramolecular two-dimensional lattice composed of fused 18-membered rings in $(\text{H}_2\text{O})_{15}(\text{CH}_3\text{OH})_3$ (Figure 4). The extended structure is stabilized by an extensive array of intermolecular hydrogen bonds between layers of molecules with three molecules of the hydrophobic methanol encompassing the supramolecular $(\text{H}_2\text{O})_{15}(\text{CH}_3\text{OH})_3$ structure (Figure 5).

The X-ray structural details obtained for (L)-2·3H₂O·CH₃OH and (D)-2·3H₂O·CH₃OH (Figures 4 and 5) clearly suggests that the solute **2** in water upon exposure to the vapors of methanol, produces a mixed water-methanol cluster $(\text{H}_2\text{O})_{15}(\text{CH}_3\text{OH})_3$ constitution within **2**. The molecular constitution of the mixed water-methanol clusters in (L)-2·3H₂O·CH₃OH further confirms that the hydrophobic methanol molecules are readily accommodated within the hydrogen bonded water structure (Figure 5). The O–O distances (Table 2) in the mixed methanol–water clusters of (D)-2·3H₂O·CH₃OH and (L)-2·3H₂O·CH₃OH (O–O(average) = 2.857 Å) are nearly identical to the O–O distance observed in the supramolecular $(\text{H}_2\text{O})_{18}$ water structure (O–O(average) = 2.859 Å) implying the

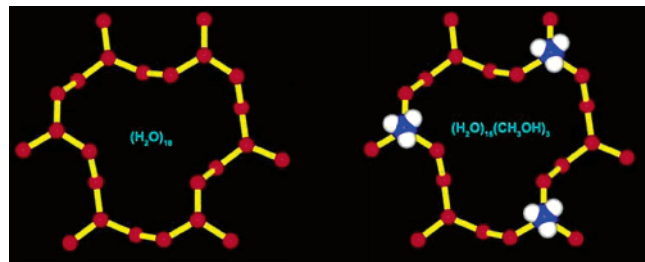


Figure 6. Perspective view for the comparison of structurally rigid supramolecular $(\text{H}_2\text{O})_{18}$ and mixed methanol–water $(\text{H}_2\text{O})_{15}(\text{CH}_3\text{OH})_3$ clusters. Hydrogen atoms are omitted for clarity. Colors are as follows: dark blue, carbon; red, oxygen; white, hydrogen.

retention of the hydrogen bonded structure in water despite the accommodation of the hydrophobic methanol groups within the supramolecular $(\text{H}_2\text{O})_{15}(\text{CH}_3\text{OH})_3$ framework. It is even more striking that the O–O distances in (D)-2·3H₂O·CH₃OH and (L)-2·3H₂O·CH₃OH and in $(\text{H}_2\text{O})_{18}$ (found in D-1) are very close to the O–O distance reported for liquid water (2.85 Å).¹⁷

Global Picture of H₂O–MeOH Interactions. Dielectric spectroscopy, thermodynamic measurements, neutron scattering and simulation studies on dilute aqueous methanol solution suggest that water molecules solvate the polar moiety in methanol before solvating the non polar moiety.^{23,24,33–41} However, structural evidence of such solvation models are still rare. Our results on the structures of $(\text{H}_2\text{O})_{15}(\text{CH}_3\text{OH})_3$ provide experimental evidence for the local structural environment of hydrophobic solutes. The three methyl groups within the $(\text{H}_2\text{O})_{15}(\text{CH}_3\text{OH})_3$ rings are situated within the hydrophobic pockets created by the methyl groups of the trialanine solute **2** (Figures 4 and 5). This spatial arrangement of hydrophobic groups not only maintains the structural integrity of the hydrogen-bonding network within the cyclic water structure but also aids in maximizing the cooperative hydrogen bonding with methanol molecules. The accommodation of hydrophobic headgroups of methanol within the water structure observed in $(\text{H}_2\text{O})_{15}(\text{CH}_3\text{OH})_3$ may be rationalized in terms of the cooperativity in hydrogen bonding networks of water and methanol with consequent structural arrangements leading to an optimized hydrogen bonded water structure embedded with methanol subunits (Figure 6). The cooperative phenomenon in hydrogen bonded chains in $(\text{H}_2\text{O})_{15}(\text{CH}_3\text{OH})_3$ is driven by the dual property of methanol to accept and donate protons. Each molecule of methanol in $(\text{H}_2\text{O})_{15}(\text{CH}_3\text{OH})_3$ interacts with three water molecules to form the 18-membered cyclic structure (Figure 6). Methanol molecules in $(\text{H}_2\text{O})_{15}(\text{CH}_3\text{OH})_3$ are hydrogen-bonded as a single proton donor and double acceptor to water molecules present in the water cluster (Figure 6).

- (32) Zhang, X.; Castleman, A. W., Jr. *J. Chem. Phys.* **1994**, *101*, 1157–1164.
- (33) (a) Dixit, S.; Poon, W. C. K.; Crain, J. *J. Phys.: Condens. Matter* **2000**, *12*, L323–L328. (b) González, L.; Mó, O.; Yáñez, M. *J. Chem. Phys.* **1998**, *109*, 139–150.
- (34) Soper, A. K.; Finney, J. L. *Phys. Rev. Lett.* **1993**, *71*, 4346–4349.
- (35) Sato, T.; Chiba, A.; Nozaki, R. *J. Chem. Phys.* **2000**, *112*, 2924–2932.
- (36) Kirschner, K. N.; Woods, R. J. *J. Phys. Chem. A* **2001**, *105*, 4150–4155.
- (37) Franks, F.; Reid, D. S. In *Water-A Comprehensive Treatise*; Franks, F., Ed.; Plenum: New York, 1973, Vol. 2, Chapter 5.
- (38) Fidler, J.; Rodger, P. M. *J. Phys. Chem. B* **1999**, *103*, 7695–7703.
- (39) Bolis, G.; Corongiu, G.; Clementi, E. *Chem. Phys. Lett.* **1982**, *82*, 299–306.
- (40) Okazaki, S.; Nakanishi, K.; Touhara, H. *J. Chem. Phys.* **1983**, *78*, 454–469.
- (41) (a) Tanaka, S. H.; Yoshihara, H. I.; Ho, A. W.-C.; Lau, F. W.; Westh, P.; Koga, Y. *Can. J. Chem.* **1996**, *74*, 713. (b) Tanaka, H.; Gubbins, K. E. *J. Chem. Phys.* **1992**, *97*, 2626–2634.

It is a well-accepted view that aqueous solution of alcohols at ambient temperatures must enhance water structure, as compared to the pure liquid water, if the observed heat of mixing and negative excess entropy are to be rationalized.^{16,18–24,34,37} It is also hypothesized that enhancement of water structure leads to a significant ordering of hydrogen bonds near the hydrophobic headgroups of alcohols. To put our own results in the perspective of currently held beliefs and much speculation on the nature of hydrophobic interaction with water at ambient temperatures, we have performed the X-ray crystallographic analysis of **L-2**·3H₂O·CH₃OH at ambient temperatures (see Table 1). Surprisingly, the H-bonded network in (H₂O)₁₅(CH₃OH)₃ cluster did not show any significant changes on going from 193 K to 293 K (Table 2). The uniformity in the ordered structure of water within (H₂O)₁₅(CH₃OH)₃ suggests that the hydrophilic group of methanol is capable of involving in hydrogen bonding interaction with water without causing orientation changes in the tetrahedral arrangement of bonding in water. This experimental finding provides a new mechanism for the loss of entropy via the generation of a highly ordered hydrogen bonded network incorporating hydrophobic entities within the water structure.

Several theoretical models have been used to examine the anomalous thermodynamic properties of H₂O/MeOH solutions and also to gain insight into the intrinsic static hydration structure of water around methanol in dilute solutions.^{16,18–21,38–40} Conventional models on hydrophobic hydration proposed by Frank and Evans attribute undue importance to the enhancement of water structure in the proximity of hydrophobic solutes.²² Water being unable to form hydrogen bonds with hydrophobic solutes, aggregation of the solute is considered a rationale to expel the structured water to the bulk solvent and thereby causing favorable entropy increase of the system. Although experimental demonstration for testing these models are scarce, the molecular structure studies of water–methanol solution, using neutron diffraction with H/D isotope substitution, recently reported by Crain and co-workers^{23,24} underscores the importance of experimental evidence in unraveling new information on the structure and dynamics of hydrogen bonds in mixed water-methanol systems. Molecular solids that can embed water or water–alcohol mixtures causing minimum or no alteration in the nature of hydrogen bonds are of paramount importance in gaining important information causing the hydrogen bonding patterns that exist in hydrogen bonding liquids. The results presented in this paper show how new chemical host templates, such as the trimeric alanine **2**, will allow the development and consequent structural elucidation resulting in an unprecedented understanding into the global picture of MeOH hydration.

Conclusions

Our results provide new insight and an improved understanding of the two-dimensional structural aspects of water with important implications in protein biology. Water molecules at the surfaces of proteins, which dictate their conformation, stability, function, and dynamics are implicated in important biological processes such as molecular recognition, catalysis and antigen–antibody association. Determination of the precise structure of water present at the protein surface is challenging because of the complex macromolecular domain of proteins. In this context, the results discussed in this paper are of particular significance because of the new supramolecular (H₂O)₁₈ morphology at the amino acid interface in **2** may serve as an

important model to understanding the nature of water packing at the protein water interface. The supramolecular ice-like (H₂O)₁₈ cyclic structure of water, complementary to that of bulk water, can be a favorable conformation for water at the amino acid interface. The packing diagram (Figure 1) show how the (H₂O)₁₈ structure provides high mobility and flexibility resulting in the hydrophilic amino acid water interface. Move across the interface, from one amino acid layer to the other, the (H₂O)₁₈ water cluster arrangement interlink amino acid surfaces via hydrogen bonds to polar groups on amino acids while making van der Waals contacts with non polar atoms. This arrangement of water facilitates a complementary relationship resulting in inter and intramolecular hydrogen bonds within and between the amino acid interfaces and provides a new macroscopic model for water–amino acid interactions in terms of packing efficiency and maximization of macromolecular interactions.

Our direct crystallographic measurements of mixed water-methanol clusters in (**L**)-**2**·3H₂O·CH₃OH and (**D**)-**2**·3H₂O·CH₃OH confirm the existence of a cooperative hydrogen bonding between polar groups in methanol and water. The disposition of the hydrophobic headgroups within the supramolecular domain of the mixed water-methanol (H₂O)₁₅(CH₃OH)₃ cluster, as shown in Figure 4, confirms that the hydrophobic methyl groups of methanol orient in such a fashion as to minimize disruption of hydrogen bonds in the water structure. The larger size of the water rings in (H₂O)₁₅(CH₃OH)₃ (and also in (H₂O)₁₈) clusters contrast the compact pentameric and hexameric water clusters found in a majority of structures discussed to date. The larger water rings presumably provide higher degrees of freedom and consequently favor larger distances between the hydrophobic headgroups within the (H₂O)₁₅(CH₃OH)₃ cluster. This spatial arrangement suggests that the cooperative hydrogen bonding of polar groups in methanol with the hydrogen bonds within the water structure is the dominant phenomenon within the larger water rings and that the well-known Frank and Evans hypothesis²² on the generation of clathrate-like cage water structure around hydrophobic headgroups may be limited to smaller pentameric or hexameric water structures.

Experimental Section

General Considerations. Synthesis of **2** was performed under dinitrogen atmosphere. The starting materials (**L**)-Alanine and Tris(hydroxymethyl)phosphine were commercially available and used without any purification. ¹H, ¹³C, and ³¹P NMR spectra were recorded at 300, 75 and 121 MHz, respectively, on a Bruker ARX300 spectrometer. Thermal gravimetry analysis (TGA) was performed on a Perkin-Elmer Pyris 1 TGA system using 17.135 mg and heating from 30 °C to 600 °C at a heating rate of 10 °C min⁻¹.

Conjugation of (L**)-Alanine/(**D**)-Alanine with Tris(hydroxymethyl)phosphine.** Tris(hydroxymethyl)phosphine (**1**) (0.500 g, 4.033 mmol) in 5 mL of distilled water was added dropwise to (**L**)-alanine/(**D**)-alanine (1.077 g, 12.00 mmol) in 10 mL of distilled water at 25 °C. The reaction mixture was stirred under dry nitrogen for 1 h. The solvent was removed in vacuo to obtain a white solid. The white solid was washed with methanol, and dried in vacuo to give the pure product (**L**)-**2** or (**D**)-**2** in 90% yield. ESI-MS calcd for C₁₂H₂₄N₃O₆P 337.3. Found 337.6. ¹H NMR (300 MHz, D₂O, δ): 1.38 (d, 9H, –NCH(CH₃)COOH, *J* = 6.0 Hz), 3.47 (d, 6H, PCH₂), 3.65 (m, 3H, –NCH(CH₃)COOH). ¹³C NMR (75 MHz, D₂O, δ): 14.84 (s, NCH(CH₃)COOH), 42.65 (d, PCH₂, *J*_{P-C} = 12.82 Hz), 59.35 (d, –NCH(CH₃)COOH, *J*_{P-C} = 5.77 Hz), 174.10 (s, NCH(CH₃)COOH). ³¹P NMR (121.5 MHz, D₂O, δ): –39.9 (s).

Single Crystals of (L)-2 in Water. Single crystals of X-ray quality of **2** were obtained by dissolving 0.05 g of **2** in 1 mL of water and left undisturbed for 3 d.

Single Crystals of (L)-2/(D)-2 in Water—Methanol. Single crystals of X-ray quality of **2** containing water-methanol cluster were obtained by exposing methanol (20 mL) vapors to solution of **2** (0.05 g) in water (1 mL). Single crystals were obtained after 12 h.

Crystallographic Data Collection and Refinement of Structure. A suitable crystal was chosen and mounted on a glass fiber with epoxy resin. The Crystal data and refinement results were given in Table 1. See the Supporting Information for CIF files. Data reduction and processing followed routine procedures. Structures were solved by direct

methods and refined on F_o^2 . Absorption correction were done by semiempirical equivalents.

Acknowledgment. This work was supported by the Departments of Radiology, Physics, and Chemistry and the University of Missouri Research Reactor.

Supporting Information Available: Crystallographic information files (CIF) for structures of **2** with $(H_2O)_{18}$ and $(H_2O)_{15}(CH_3OH)_3$. This material is available free of charge via the Internet at <http://pubs.acs.org>.

JA034682C

Thiolate Ligands for Synthesis of Water-Soluble Gold Clusters

Christopher J. Ackerson, Pablo D. Jadzinsky, and Roger D. Kornberg*

Department of Structural Biology, Stanford University, 299 Campus Drive West, Stanford, California 94305

Received June 30, 2004; E-mail: kornberg@stanford.edu

Organothiolate monolayer-protected gold clusters (MPCs) have been a focus of intensive research since they were first described, just over 10 years ago. Of three common synthetic methods for generating water-soluble, thiolate-protected gold nanoparticles,¹ the one- and two-phase syntheses of Brust et al.² have attracted the most attention,^{3,4} due to synthetic control over particle size, dispersity, and surface functionality, to size-dependent optical, catalytic, and capacitance properties, and to the extraordinary stability of the resultant thioalkane-protected products to air, long-term storage, solvents, temperature, and concentration extremes.

Other synthetic routes to water-soluble MPCs, notably, a two-phase method⁵ for replacing the triphenylphosphine ligands on clusters, such as undecagold and “Au₅₅”, have been reported. Insofar as these clusters have been analyzed, they have properties similar to those of clusters made by the method of Brust et al.

Early work employing the Brust MPC synthesis focused exclusively on MPCs soluble in nonaqueous solvents. This work showed that straight chain ligands at least as large as pentanethiol were needed to confer the remarkable stability of MPCs,⁶ unique among

aurous and nonaurous metal clusters. The stability was lower for clusters formed with C3 to C4 straight chain alkanethiolates and increased with increasing chain length.³ Alkanethiolate-protected MPCs with chain lengths shorter than C3 have not been described.

The first reports of water-soluble Brust MPCs came four years after the initial synthesis.^{7–9} Although the work has been extended,^{10–14} no systematic attempt has been made to demonstrate minimal ligand requirements for water-soluble MPCs, as was done for alkanethiolate MPCs. Here, we report on the results of Brust synthesis with many commercially available, water-soluble thiolate ligands. For some thiols, a thioether, and also a non-thiol chalcogenide that did not yield stable MPCs in the Brust synthesis, we tested the capacity to stabilize preformed “Au₅₅” cores through thiolate-for-phosphine exchange and phase transfer. The Brust MPC synthesis produces a cluster core whose size, shape, and atomic packing properties are determined in large part by the thiolate¹¹ and the thiolate-to-gold ratio used.⁶ Conversely, the generation of MPCs by thiolate replacement of triphenylphosphine begins with a preformed cluster core. This approach sometimes does⁵ and

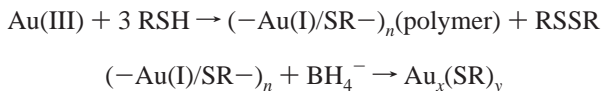
Table 1. Water-Soluble Thiolates and Their Ability to Passivate Gold Clusters

compound name	published synthesis	diameter (nm) ^k	soluble product	stability	synthetic method ^a	behavior in HD-PAGE gel
3-mercaptopropionic acid	ref 21	undetermined ^j	yes	days to weeks	Brust	did not enter matrix in HD or LD-PAGE ⁱ
4-mercaptopbutyric acid	no	4.0 ± 1.2	yes	weeks	Brust	not tested
3-mercaptop-1,2-propanediol	ref 14 ^b	4.7 ± 1.2	yes	days	Brust	single diffuse band in HD-PAGE
cysteine	ref 12 ^c	1.6 ± 0.3	yes	days	Brust ^f	entered gel matrix as single band; stalled; single band in LD-PAGE
methionine	no	2.4 ± 1.0	yes	weeks	Hutchison	did not enter matrix in HD or LD-PAGE
thiomalate	ref 13 ^d	2.1 ± 1.4	yes	weeks	Brust	single tight band surrounded by large halo
2-mercaptopbenzoic acid	no	2.1 ± 0.9	yes	minutes	Brust	did not enter matrix in HD or LD-PAGE
3-mercaptopbenzoic acid	no	1.6 ± 0.6	yes	days	Brust	did not enter matrix; single band in LD-PAGE
4-mercaptopbenzoic acid tiopronin	ref 7 ^e ref 9	1.8 ± 0.4 1.9 ± 0.7	yes yes	months months	Brust Brust ^f	2 tight bands single diffuse pink band in HD or LD-PAGE
selenomethionine	no	1.6 ± 0.4	yes	days	Hutchison	did not enter matrix in HD or LD-PAGE
1-thio-β-D-glucose	no	2.1 ± 0.5	yes ^g	months	Brust ^f	single band in LD-PAGE
glutathione	ref 8	1.4 ± 0.4	yes	months	Brust	5 bands
ITCAE pentapeptide ^h	no	1.4 ± 0.4	yes	days	Hutchison	not tested

^a Brust synthesis was in 1:1 water:methanol with a 3:1 thiolate:gold ratio. Typical concentrations were 10 mM gold and 30 mM thiolate. A 5-fold molar excess of NaBH₄ in a volume of water ~10% of the reaction volume was added to complete the cluster formation. Reactions denoted Hutchison were performed as described (ref 5). ^b A 1:1 ratio of thiolate:Au(III) and a 9-fold BH₄⁻ excess. ^c Cystine was used as the starting material to create cysteine MPCs. ^d Highest organothiolate:Au(III) ratio used was 5:2, with equimolar NaBH₄ to HAuCl₄, likely resulting in incomplete reduction. ^e A 1.8:1 thiolate:Au(III) ratio was used. ^f These compounds failed to form soluble products in 1:1 water:methanol, but did so under similar conditions in 6:1 methanol:acetic acid. ^g This compound formed product that remained in suspension following low-speed centrifugation, indicating cluster formation, but failed to redissolve after methanol precipitation; this product was not repeatably precipitable in methanol, but could be purified from starting materials by gel filtration and, otherwise, behaved as a stable water-soluble MPC. ^h The pentapeptide had the sequence Ile-Thr-Cys-Ala-Glu. ⁱ LD-PAGE was a standard 12% SDS-PAGE gel. ^j Particles form aggregates within which individual particle diameters cannot be measured. ^k See Supporting Information for images, histograms, and further analysis.

sometimes does not¹⁵ preserve the cluster core, which, in any case, never reaches the narrow dispersity that can be achieved following purification of products of a Brust MPC synthesis.¹¹ The phase transfer approach allows more promiscuous use of thiolate side chains than does the Brust MPC synthesis, while generating thiolate-protected gold particles that are typically more stable than the precursors.

The Brust synthesis proceeds in two steps:^{11,16}



The particle size of the product (value of x) depends on the thiolate-to-Au(III) ratio in the first step.⁶ Decreasing the thiolate load results in a larger value of x , but also in a more polydisperse product.¹⁶ Increasing the amount of borohydride reductant favors the formation of larger core sizes without great loss of the narrow dispersity characteristic of the Brust synthesis.¹¹ The synthesis usually yields a set of discrete products, each corresponding to a closed shell cluster.¹⁷ The distribution of products obtained, as well as many of the properties of an MPC, including the chemical and thermal stability, solubility, capacitance, and reactivity toward place exchange,¹⁸ depends on the nature of the thiolate used.

We performed Brust MPC synthesis with various water-soluble thiolates, using a 3:1 ratio of thiolate:gold throughout, and a 5-fold excess of NaBH₄ as reductant. Syntheses were done in a 1:1 water:methanol system, except where noted. Hutchison phase transfer syntheses were performed with 1.0 mg of "Au₅₅" dissolved in 5 mL of methylene chloride and a 10-fold or greater molar excess of replacement ligand over total ligand in the "Au₅₅" preparation. We used Schmid's original formula of Au₅₅PPh₁₂Cl₆, rather than the formulas arrived at by other analyses,^{5,19} for calculation of the number of ligands in an Au₅₅ preparation. Cluster formation was verified by UV-vis spectroscopy and high-resolution transmission electron microscopy (HR-TEM). Most clusters showed a featureless spectrum, rising smoothly from the visible into the UV, characteristic of sub-2 nm gold clusters.⁶ For HR-TEM analysis, samples were dried onto Formvar- or carbon-coated EM grids, which had been glow-discharged in either water or amyamine. Particle images and sizes may be found in the Supporting Information. Many gold cluster preparations were amenable to purification by high-density polyacrylamide gel electrophoresis,¹¹ and the number and quality of bands in the gel were noted. Examples may be found in the Supporting Information.

It can be assumed that virtually any ligand that succeeds in the Brust synthesis will also do so in phase transfer synthesis. We tested 22 water-soluble organothiols which failed to yield stable water-soluble products in the Brust single phase synthesis.²⁰

From the results for 36 ligands, we could draw the following conclusions: (1) Small positively charged ligands do not support the production of MPCs in the Brust synthesis. (2) The smallest negatively charged thiolate yielding a Brust MPC was mercapto-propionic acid. Larger acidic organic thiolates were also effective passivants. (3) The smallest uncharged organothiolate yielding a Brust MPC was 3-mercaptopropanediol, which formed clusters that remained in solution for days, but which did not exhibit long term stability. Thioglucose, also neutral, produced clusters with longer stability. Short polyglycol ligands recently reported,¹⁰ but not commercially available, may yield more stable MPCs with neutral monolayers. (4) Larger organothilates were generally better

stabilizers. (5) Penicillamine did not form soluble clusters, which was surprising in view of the success of cysteine. (6) Thus, the ligand size/cluster stability trend previously reported for alkanethiolate MPCs also applies to water-soluble MPCs, but with notable exceptions.

In summary, we have screened 36 water-soluble organothiols for their ability to form water-soluble MPCs. We report 13 such MPCs, 6 of which are novel, and 4 of which have been reported with nonstandard stoichiometries of ligand or borohydride in previous syntheses. While all clusters reported here were repeatably precipitable with methanol, most did not exhibit the extraordinary stability of alkanethiolate MPCs; a few exceptional ligands formed clusters that remained in solution indefinitely. We suggest that our survey of water-soluble MPCs affords a toolkit for future applications of such compounds. Further work is needed to characterize the gel-purified clusters with respect to core size, place exchange, capacitance, and other properties known to vary with monolayer composition.

Acknowledgment. This research was supported by NIH Grants GM63025 and AI21144 (R.D.K.), and by NIH Training Grant T32 GM08294 (C.J.A.).

Supporting Information Available: Additional figures. This material is available free of charge via the Internet at <http://pubs.acs.org>.

References

- (1) Daniel, M.-C.; Astruc, D. *Chem. Rev.* **2004**, *104*, 293–346.
- (2) Brust, M.; Fink, J.; Bethell, D.; Schiffrin, D. J.; Kiely, C. *J. Chem. Soc., Chem. Commun.* **1995**, 1655–1656.
- (3) Brust, M.; Kiely, C. *J. Colloids Surf., A* **2002**, *202*, 175–186.
- (4) Templeton, A. C.; Wuelfing, W. P.; Murray, R. W. *Acc. Chem. Res.* **2000**, *33*, 27–36.
- (5) Brown, L. O.; Hutchison, J. E. *J. Am. Chem. Soc.* **1997**, *119*, 12384–12385.
- (6) Hostetler, M. J.; Wingate, J. E.; Zhong, C.-J.; Harris, J. E.; Vachet, R. W.; Clark, M. R.; Londono, J. D.; Green, S. J.; Stokes, J. J.; Wignall, G. D.; Glish, G. L.; Porter, M. D.; Evans, N. D.; Murray, R. W. *Langmuir* **1998**, *14*, 17–30.
- (7) Johnson, S. R.; Evans, S. D.; Brydson, R. *Langmuir* **1998**, *14*, 6639–6647.
- (8) Schaaff, T. G.; Knight, G.; Shafiqullin, M. N.; Borkman, R. F.; Whetten, R. L. *J. Phys. Chem. B* **1998**, *102*, 10643–10646.
- (9) Templeton, A. C.; Chen, S.; Gross, S. M.; Murray, R. W. *Langmuir* **1999**, *15*, 66–76.
- (10) (a) Kanaras, A. G.; Kamounah, F. S.; Schaumburg, K.; Kiely, C. J.; Brust, M. *Chem. Commun. (Cambridge)* **2002**, 2294–2295. (b) Zheng, M.; Davidson, F.; Huang, X. J. *J. Am. Chem. Soc.* **2003**, *125*, 7790–7791. (c) Pengo, P.; Polizzi, S.; Battagliarin, M.; Pasquato, L.; Scrimin, P. *J. Mater. Chem.* **2003**, *13*, 2471–2478.
- (11) Schaaff, T. G.; Whetten, R. L. *J. Phys. Chem. B* **2000**, *104*, 2630–2641.
- (12) Naka, K.; Itoh, H.; Tampo, Y.; Chujo, Y. *Langmuir* **2003**, *19*, 5546–5549.
- (13) Li, D.; Li, J. *Chem. Phys. Lett.* **2003**, *372*, 667–673.
- (14) Sihai Chen, K. K. *Langmuir* **1999**, *15*, 1075–1082.
- (15) Woehrle, G. H.; Warner, M. G.; Hutchison, J. E. *J. Phys. Chem. B* **2002**, *106*, 9979–9981.
- (16) Alvarez, M. M.; Khouri, J. T.; Schaaff, T. G.; Shafiqullin, M.; Vezmar, I.; Whetten, R. L. *Chem. Phys. Lett.* **1997**, *266*, 91–98.
- (17) Donkers, R. L.; Lee, D.; Murray, R. W. *Langmuir* **2004**, *20*, 1945–1952.
- (18) Hostetler, M. J.; Green, S. J.; Stokes, J. J.; Murray, R. W. *J. Am. Chem. Soc.* **1996**, *118*, 4212–4213.
- (19) Rapoport, D. H.; Vogel, W.; Coelfen, H.; Schloegl, R. *J. Phys. Chem. B* **1997**, *101*, 4175–4183.
- (20) The following ligands produced water-insoluble material when used in the Brust synthesis: 2-mercaptoethanol, mercaptoethylamine, mercaptoacetic acid, 1*H*-1,2,4,5-tetraazole-3-thiol, 5-mercaptop-1-methyltetrazole, 2-mercaptop-1-methylimidazole, 2-mercaptopthiazoline, ethyl-2-mercaptopacetate, 2-thiouacil, 2-mercaptop-5-methyl-1,3,4-thiadiazole, D-(+)-penicillamine, mercaptobenzimidazole, mercaptobenzoxazoles, *N*-acetyl-L-cysteine, 2-mercaptop-6-nitrobenzothiazole, 2-amino-6-mercaptopurine-9-D-riboside hydrate, diisoamylthiomalate, 3-mercaptopropanol, 4-mercaptopbutanol, 2-(dimethylamino)ethanethiol, 2-mercaptop-5-methyl-1,3,4-thiadiazole, and 4,5-diamino-2,6-dimercaptopyrimidine.
- (21) Li, D.; Li, J.-H. *Chin. J. Chem.* **2003**, *21*, 392–395.

JA046114I

Geometrical H/D Isotope Effect on Hydrogen Bonds in Charged Water Clusters

Masanori Tachikawa^{*†} and Motoyuki Shiga[‡]

Quantum Chemical Physics Division, Graduate School of Science, Yokohama-City University, Seto 22-2, Kanazawa-ku, Yokohama 236-0027, and PRESTO, Japan Science and Technology Agency (JST), Tokyo, Japan, and Center for Promotion of Computational Science and Engineering, Japan Atomic Energy Research Institute (JAERI), Higashi-Ueno 6-9-3, Taito-ku, Tokyo 110-0015, Japan

Received May 13, 2005; E-mail: tachi@yokohama-cu.ac.jp

The isotope substitution of shared hydrogen has a subtle effect on the geometry, but it will sometimes have large influence on some properties of hydrogen-bonded systems. For example, it is believed that the large isotope effect in the phase transition temperature of hydrogen-bonded ferroelectric crystals such as potassium dihydrogen phosphate (KDP) is due to a small structural modification of the crystal by deuteration.¹ In the neutral liquid water, it is known that the geometrical isotope effect is small, but it is measurable by the synchrotron X-ray experiments² and a recent ab initio simulation.³

There have been a number of reports on the protonated and hydroxylated water clusters such as H_5O_2^+ and H_3O_2^- ions⁴ since they are representative species in proton- or hydroxy-transfer processes of aqueous solutions.⁵ In fact, the equilibrium structures⁶ and vibrational spectrum⁷ for these species are investigated from both experiment and theory. However, the isotope effect has not been reported in detail thus far, partly because these species have highly anharmonic motions that allow large-amplitude fluctuation in the geometries.⁸

The main subject of the present study is to address whether the geometrical isotope effect exists also for the hydrogen bonds in aqueous solutions or water clusters with acidity or basicity. We note that the interatomic forces are independent of the atomic masses and therefore the thermal distributions on the geometries of isotopomers are the same if the nuclei are treated classically. In this sense, the geometrical isotope effect is a purely quantum effect of nuclei.

Here, we study the isotope effect of H_5O_2^+ and H_3O_2^- ions at the room temperature 300 K by ab initio path integral molecular dynamics (PIMD) simulation.⁹ In this approach, the quantum nuclear distribution is obtained from the molecular dynamics for cyclic bead chains of atoms on the Born–Oppenheimer hypersurface, which is solved on the fly by ab initio quantum chemical calculation. In the present case, the ab initio calculation is performed based on the second-order Moller–Plesset perturbation theory (MP2) and 6-31+G** basis set by the Gaussian98¹⁰ program package, since it is quantitative within kcal/mol accuracy for these hydrogen-bonded systems. Previously, we have confirmed that the barrier height of the pyramidal H_3O^+ ion has an accuracy of more than 90% at this level.⁹ In this work, the ab initio PIMD run has been performed for 60 000 steps (6 ps) with the step size of 0.1 fs and $P = 24$.

In Figure 1, we show some representative snapshots from the PIMD simulation. We can see that these ionic species have a linear hydrogen bonding, sharing the hydrogen by two oxygens, O···H–(D)···O, where the protons/deuterons are broadly distributed as a result of thermal and quantum fluctuations. The quantum statistical

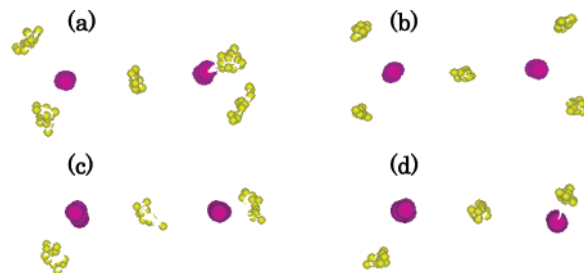


Figure 1. Representative snapshots in ab initio path integral molecular dynamics at 300 K for (a) H_5O_2^+ , (b) D_5O_2^+ , (c) H_3O_2^- , and (d) D_3O_2^- .

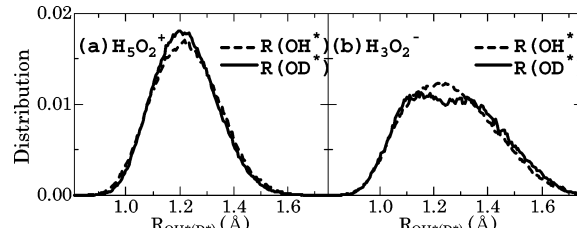


Figure 2. Distribution of $\text{OH}^*(\text{OD}^*)$ bond length $R_{\text{OH}(\text{D})^*}$ in (a) $\text{H}(\text{D})_5\text{O}_2^+$ and (b) $\text{H}(\text{D})_3\text{O}_2^-$. (a) The average $\text{OH}(\text{D})^*$ bond lengths of H_5O_2^+ and D_5O_2^+ are 1.224 and 1.220 Å, while the equilibrium one is 1.194 Å. (b) The average $\text{OH}(\text{D})^*$ bond lengths of H_3O_2^- and D_3O_2^- are 1.261 and 1.262 Å, while the R_{OD^*} distribution has two weak peaks at 1.15 and 1.35 Å. The equilibrium OH^* bond lengths are 1.398 and 1.095 Å.

averages of molecular configurations are taken respectively for H_5O_2^+ and H_3O_2^- , and their isotopomers by running the independent PIMD simulations. For clarity, we label the shared proton and deuteron as “H*” and “D*”. Figure 2 shows the distribution of the OH^*/OD^* bond lengths.

In the case of the cation, the average OH^* bond length of H_5O_2^+ (1.224 Å), is longer than the D_5O_2^+ counterpart (1.220 Å). This bond length shift is similar to the case of the H_2O molecule and the H_3O^+ ion,⁹ where the hydrogen is on a single-potential well. This can be explained from the difference of quantum zero-point fluctuation between the isotopomers on an anharmonic potential surface as to the OH^* bonds. In fact, the shared proton of H_5O_2^+ ion has a single potential minimum located at the center of two oxygens in the equilibrium structure.⁶ As shown in Figure 2a, the fluctuation of the R_{OH^*} bond in H_5O_2^+ (the root-mean-square displacement of the OH^* bond is $\Delta R_{\text{OH}^*} = 0.122$ Å) is slightly larger than that of R_{OD^*} in deuterated D_5O_2^+ ($\Delta R_{\text{OD}^*} = 0.114$ Å). Then, the quantum fluctuation induces the anharmonic motion making the $\text{OH}^*(\text{OD}^*)$ bonds stretch from the equilibrium position. The OO bonds stretch as the $\text{OH}^*(\text{OD}^*)$ bonds stretch. In fact, the average OO bond distance of H_5O_2^+ (2.422 Å) is longer than that of D_5O_2^+ (2.418 Å). In this way, the two oxygens are subject to the repulsive force by the nuclear quantum effect of the shared proton/deuteron, which acts stronger in H_5O_2^+ than in D_5O_2^+ .

[†] Yokohama-City University and PRESTO, Japan Science and Technology Agency (JST).

[‡] Japan Atomic Energy Research Institute (JAERI).

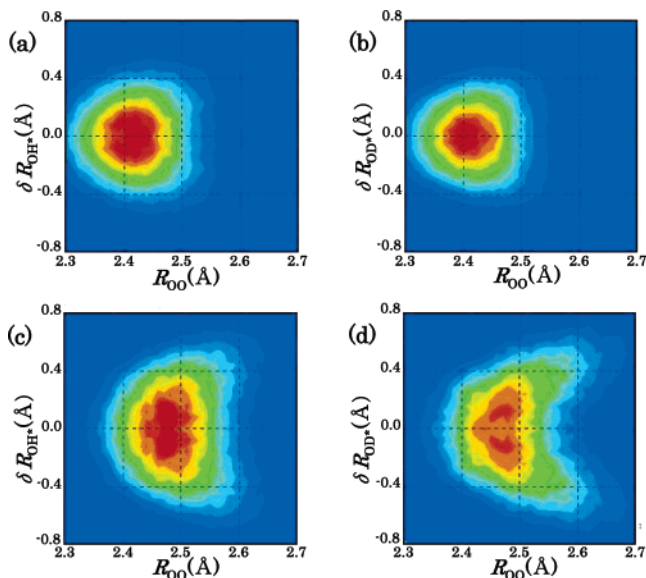


Figure 3. Two-dimensional distribution of $(R_{OO}, \delta R_{OH(D)^*})$ for (a) $H_5O_2^+$, (b) $D_5O_2^+$, (c) $H_3O_2^-$, and (d) $D_3O_2^-$. The peak positions ($R_{OO}, \delta R_{OH(D)^*}$) are around (2.42, 0.00) and (2.41, 0.00) for (a) $H_5O_2^+$ and (b) $D_5O_2^+$, while around (2.47, 0.00) and (2.48, ± 0.15) for (c) $H_3O_2^-$, and (d) $D_3O_2^-$, respectively.

On the other hand, the geometric isotope effect is found differently in the $H_3O_2^-$ anion. First, the average OH^*/OD^* bond lengths, 1.261 and 1.262 Å, are almost the same for $H_3O_2^-$ and $D_3O_2^-$ ions. The potential surface of $H_3O_2^-$ has a double minima in which the structure is asymmetric.⁶ The two different R_{OH^*} equilibrium bond lengths (1.398 and 1.095 Å) indicate that the shared hydrogen has two positions on either oxygen side. Thus, the average bond lengths of R_{OH^*} and R_{OD^*} are between these two positions. However, Figure 2b shows the clear difference between the radial distributions of R_{OH^*} and R_{OD^*} . While the R_{OD^*} distribution has two weak peaks at 1.15 and 1.35 Å, the R_{OH^*} distribution has only one peak at the central position 1.26 Å. Second, the average bond length $\langle R_{OO} \rangle$ of $D_3O_2^-$ (2.504 Å) becomes longer than that of $H_3O_2^-$ (2.498 Å). This implies that the nuclear quantum effect works as an attractive force between the oxygen atoms, in contrast to the $H_5O_2^+$ case.

In Figure 3, the geometrical distributions are shown in more detail as two-dimensional contours with respect to R_{OO} and anti-symmetric stretching coordinates δR_{OH^*} ($=R_{OaH^*} - R_{ObH^*}$). Contrary to the $H_5O_2^+$ case, two internal coordinates of R_{OO} and δR_{OH^*} in $H_3O_2^-$ are strongly correlated each other. The peak positions ($R_{OO}, \delta R_{OH^*}$) are found to be very close between $H_5O_2^+$ and $D_5O_2^+$ [around (2.42, 0.00) and (2.41, 0.00), respectively], while they differ substantially between $H_3O_2^-$ and $D_3O_2^-$ [around (2.47, 0.00) and (2.48, ± 0.15), respectively]. In the case of $H_3O_2^-$ and $D_3O_2^-$, there is a potential minimum at (2.49, 0.30). However, in $H_3O_2^-$, the proton is highly delocalized by quantum effect, and these minimum structures are washed out. This is because the potential barrier between these minima is very low. By contrast, the quantum effect in $D_3O_2^-$ is not strong enough to completely wash out the minimum structures, and the double peaks in the distributions show that the delocalization of the deuteron in $D_3O_2^-$ is limited. Here, a large contribution to proton delocalization in $H_3O_2^-$ comes from the quantum effect.⁴

At this point, we discuss an unusual isotope effect wherein the R_{OO} bond length is smaller in $H_3O_2^-$ and $D_3O_2^-$. This is hard to explain from the potential anharmonicity of the OH^* bond. Thus, we deal with this problem from a different point of view using the idea in the field of the hydrogen-bonded crystals. This is known as the “Ubbelohde effect”,¹¹ which represents the lattice expansion

of crystals as a result of the D substitution of O···H···O-type hydrogen bonds. The explanation of this effect is based on assumption that proton/deuteron mediates the attractive interaction of two oxygen. Chemically, the resonance of O···H···O and O–H···O is more likely to occur and the oxygens are more attractive by proton rather than by deuteron, because the proton can delocalize better than the deuteron. We consider that this idea can be used for the geometrical shift of $H_3O_2^-$ and $D_3O_2^-$ anions, since we have seen that proton is indeed more delocalized than deuteron in these systems. We note that the drastic difference in the delocalization can be realized under a relevant potential barrier at which the proton can exchange the hydrogen bonds easily while the deuteron cannot.

In summary, the results of ab initio path integral simulations have shown that the geometrical isotope effects for an $H_5O_2^+$ cation and an $H_3O_2^-$ anion are different from each other. By deuteration, the hydrogen bond is shortened in $H_5O_2^+$ while it is stretched in $H_3O_2^-$. We consider that there are two competing origins of the isotope shift. One comes from the difference of zero-point vibrations of the shared proton and deuteron which act as repulsive force between oxygens, and the other, which might be more interesting, comes from the difference of delocalization of the shared proton and deuteron which acts as an attractive force between oxygens. The former repulsion is dominant in the case of $H_5O_2^+$, where the shared hydrogen is in the single potential well between oxygens. However, the latter attraction becomes important in the case of $H_3O_2^-$ where the hydrogen is inclined to sit on either side of the double potential minima (nearer to one oxygen). In this case, the deuteration can localize on the shared deuteron, loosen the hydrogen bond, and as a result, lengthen the oxygen–oxygen distance.

Supporting Information Available: Complete ref 10. This material is available free of charge via the Internet at <http://pubs.acs.org>.

References

- (a) Blinc, R. *J. Phys. Chem. Solids* **1960**, *13*, 204. (b) McMahon, M. I.; Nelmes, R. J.; Kuhs, W. F.; Derwarth, R.; Piltz, R. O.; Tun, Z. *Nature* **1990**, *348*, 317.
- (a) Tomberli, B.; Benmore, C. J.; Egelstaff, P. A.; Neufeld, J.; Honkimaki, V. *J. Phys. Condens. Matter* **2000**, *12*, 2597. (b) Badyal, Y. S.; Price, D. L.; Saboungi, M. L.; Haefner, D. R.; Shastri, S. D. *J. Chem. Phys.* **2002**, *116*, 10833.
- Chen, B.; Ivanov, I.; Klein, M. L.; Parrinello, M. *Phys. Rev. Lett.* **2003**, *91*, 215503.
- (a) Tuckerman, M. E.; Marx, D.; Klein, M. L.; Parrinello, M. *Science* **1997**, *275*, 817. (b) Marx, D.; Tuckerman, M. E.; Hutter, J.; Parrinello, M. *Nature* **1999**, *397*, 601. (c) Tuckerman, M. E.; Marx, D.; Parrinello, M. *Nature* **2002**, *417*, 926.
- (a) Agmon, N. *Isr. J. Chem.* **1999**, *39*, 493. (b) Agmon, N. *Chem. Phys. Lett.* **2000**, *319*, 247.
- (a) Auer, A. A.; Helgaker, T.; Klopper, W. *Phys. Chem. Chem. Phys.* **2000**, *2*, 2235. (b) Samson, C. C. M.; Klopper, W. *J. Mol. Struct. (THEOCHEM)* **2002**, *586*, 201.
- (a) Asmis, K. R.; Pivonka, N. L.; Santambrogio, G.; Brummer, M.; Kaposta, C.; Neumark, D. M.; Woste, L. *Science* **2003**, *299*, 1375. (b) Robertson, W. H.; Diken, E. G.; Price, E. A.; Shin, J.-W.; Johnson, M. A. *Science* **2003**, *299*, 1367. (c) Diken, E. G.; Headrick, J. M.; Roscioli, J. R.; Bopp, J. C.; Johnson, M. A.; McCoy, A. B. *J. Phys. Chem. A* **2005**, *109*, 1487.
- (a) Dai, J.; Bacic, Z.; Huang, X.; Carter, S.; Bowman, J. M. *J. Chem. Phys.* **2003**, *119*, 6571. (b) Huang, X.; Braams, B. J.; Carter, S.; Bowman, J. M. *J. Am. Chem. Soc.* **2004**, *126*, 5042.
- (a) Shiga, M.; Tachikawa, M.; Miura, S. *J. Chem. Phys.* **2001**, *115*, 9149. (b) Tachikawa, M.; Shiga, M. *J. Chem. Phys.* **2004**, *121*, 5985.
- Frisch, M. J.; Trucks, G. W.; Schlegel, H. B.; Scuseria, G. E.; Robb, M. A.; Cheeseman, J. R.; Zakrzewski, V. G.; Montgomery, J. A., Jr.; Stratmann, R. E.; Burant, J. C.; Dapprich, S.; Millam, J. M.; Daniels, A. D.; Kudin, K. N.; Strain, M. C.; Farkas, O.; Tomasi, J.; Barone, V.; Cossi, M.; Cammi, R.; Mennucci, B.; Pomelli, C.; Adamo, C.; Clifford, S.; Ochterski, J.; Petersson, G. A.; Ayala, P. Y.; Cui, Q.; Morokuma, K.; Malick, D. K.; Rabuck, A. D.; Raghavachari, K.; Foresman, J. B.; Cioslowski, J.; Ortiz, J. V.; Stefanov, B. B.; Liu, G.; Liashenko, A.; Piskorz, P.; Komaromi, I.; Gomperts, R.; Martin, R. L.; Fox, D. J.; Keith, T.; Al-Laham, M. A.; Peng, C. Y.; Nanayakkara, A.; Gonzalez, C.; Challacombe, M.; Gill, P. M. W.; Johnson, B. G.; Chen, W.; Wong, M. W.; Andres, J. L.; Head-Gordon, M.; Replogle, E. S.; Pople, J. A. *Gaussian* 98, revision A.9; Gaussian, Inc.: Pittsburgh, PA, 1998.
- Ubbelohde, A. R.; Gallagher, K. J. *Acta Crystallogr.* **1955**, *8*, 71.

JA053135J

Formation of an Infinite 2D-Layered Water of $(\text{H}_2\text{O})_{45}$ Cluster in a Cryptand–Water Supramolecular Complex: A Template Effect

P. S. Lakshminarayanan, Eringathodi Suresh, and Pradyut Ghosh*

Analytical Science Discipline, Central Salt & Marine Chemicals Research Institute, Bhavnagar 364002, India

Received June 20, 2005; E-mail: pradyut@csmcri.org

Investigations on water have received considerable interest because of its fundamental importance.^{1–3} Structural studies on “discrete” water clusters within the lattice of a crystal host have significantly advanced our knowledge toward the first step of understanding the behavior of bulk water.^{4–6} Growth of larger water clusters and how the clusters link to form a large network, which is the bridge between clusters and bulk water, is still a challenging scientific endeavor.^{7–9} Some interesting polymeric water phases consisting of basic water tetramer, pentamer, and hexamer subunits have been reported.^{10,11} Very recently, two-dimensional (2D) water/ice layers containing large 12- or 18-membered water rings have been observed in the solid state which provide novel structural aspects of water.^{9,12} Herein, we describe the formation of an unprecedented, infinite 2D layer of $(\text{H}_2\text{O})_{45}$ clusters, each consisting of a basic cyclic eight-membered ring fused with a four-membered ring, further associated to water dimers and monomers. Hydrogen-bonding interactions between the 2D layers of water and cryptand moieties create a unique, infinite through-channel.

The homoditopic cryptand (**L**), containing eight amino nitrogen atoms, has been chosen in the present investigation.¹³ **L** crystallizes from water/acetonitrile binary solvents with 15 water molecules per cryptand (**1**) revealed by X-ray crystallography.¹⁴ **L**, having N_4 donor sets, facilitates the formation of a “crown shape” water structure at both ends via a hydrogen-bonding network as in biological systems (Figure 1b). Thus, the cryptand is acting as a template for the formation of channels of water layers.

The crystal structure reveals a high degree of symmetry, and the three-fold axis passes through the bridge-head nitrogen atoms of three independent cryptands, with 15 water molecules in the asymmetric unit. Out of the three independent cryptands, the phenyl rings in one show dynamic disorder. Although the data collection for the compound was carried out under liquid-nitrogen temperature conditions (100 K) most of the water hydrogens were never located; however, positions of the water molecules constituting the 2D-supramolecular architecture were determined unequivocally. The 2D layer of water is composed of a unique $(\text{H}_2\text{O})_{45}$ cluster (Figure 2a), which is constituted by the water molecules present in the asymmetric unit possessing C_3 -symmetry. The presence of **L**, generating the three-fold symmetry in the system, is obviously a template effect. The $(\text{H}_2\text{O})_{45}$ cluster unit is basically an assembly of three $(\text{H}_2\text{O})_{15}$ subunits (Figure 2b) which are interconnected via hydrogen bonding between ($\text{O}1\cdots\text{O}2$) and ($\text{O}11\cdots\text{O}12$).

The subunit $(\text{H}_2\text{O})_{15}$ has the shape of a puckered eight-membered ring ($\text{O}1, \text{O}2, \text{O}3, \text{O}4, \text{O}7, \text{O}8, \text{O}11, \text{O}12$) fused with a four-membered ring ($\text{O}6, \text{O}8, \text{O}11, \text{O}13$), and further hydrogen bonded to two water dimers ($\text{O}5, \text{O}15$) through $\text{O}1$ and ($\text{O}9, \text{O}14$) through $\text{O}4$, and one water monomer ($\text{O}10$) through $\text{O}13$ with an average $\text{O}\cdots\text{O}$ distance 2.746 Å which is very close to the corresponding value of 2.759 Å found in ice I_h at –90 °C.¹⁵ In the cyclic, puckered octamer the $\text{O}\cdots\text{O}$ distance ranges from 2.748 to 2.824 Å, resulting in an average $\text{O}\cdots\text{O}$ distance of 2.765 Å, whereas the $\text{O}-\text{O}-\text{O}$

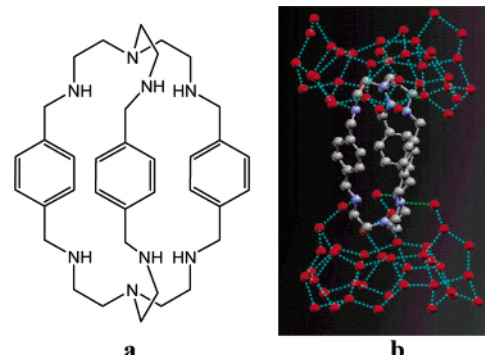


Figure 1. (a) Ligand structure **L**. (b) Depicting interaction of **L** with the water layers where N_4 units are covered by the “water crown” viewed down the *a*-axis; $\text{N}-\text{H}\cdots\text{O}$ interactions are shown in dotted green lines.

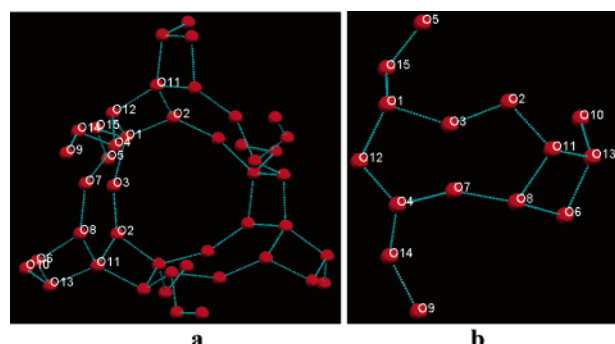


Figure 2. (a) Topology of supramolecular $(\text{H}_2\text{O})_{45}$ cluster having C_3 symmetry. (b) Topology of $(\text{H}_2\text{O})_{15}$ subunit in the asymmetric unit. Color code: red (water oxygen); blue (H-bonding interactions).

angle ranges from 98.23° to 140.48°.¹⁴ Blanton et al.^{5a} reported the first crystallographic characterization of an octameric water cluster having an approximately cube-cage-like conformation with C_i symmetry, whereas a cyclic, puckered arrangement with $-4m2$ symmetry of the $(\text{H}_2\text{O})_8$ cluster has been reported by Atwood et al.^{4c} with the $\text{O}\cdots\text{O}$ distance 2.745 Å. Our observation of the puckered geometry of an eight-membered ring in a 2D layer of water may be attributed to its different modes of connectivity with the surrounding water molecules and the interactions with the cryptand. In the asymmetric unit, the water octamer ring has hydrogen-bonding interactions with a water dimer ($\text{O}6, \text{O}13$), forming a fused cyclic tetramer with an average $\text{O}\cdots\text{O}$ distance 2.790 Å where the corresponding diagonal angles of $\angle\text{O}-\text{O}-\text{O}$ in the cyclic tetramer have similar values (85.88°, 85.33°) and (92.85°, 93.39°) and form a quasi-planar ring structure. $\text{O}1$ and $\text{O}12$ of the basic octamer water ring are further involved in hydrogen-bonding interactions with $\text{O}2$ and $\text{O}11$ water molecules from a neighboring octamer at a distance 2.764 and 2.801 Å, respectively, resulting in a quasi-planar four-membered ring with $\angle\text{O}-\text{O}-\text{O}$ ranging from 88.33° to 90.86°. However, water

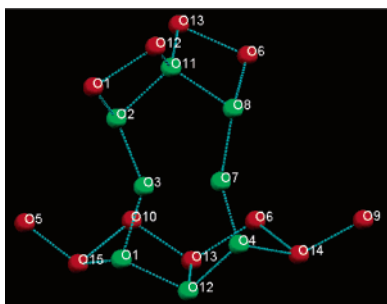


Figure 3. View depicting the puckered eight-membered ring (green balls) surrounded by other connectivity with lattice water molecules creating smaller rings.

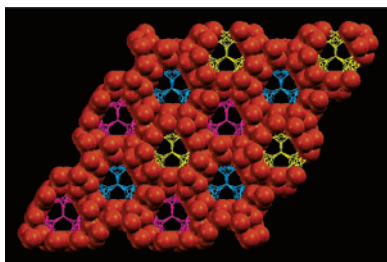


Figure 4. CPK diagram of the water structure making a through-channel down the *c*-axis.

molecules O1, O4, and O12 of the octameric ring along with O14 and O15 of the dimer, O10 of the monomer, and O6 and O13 of the fused tetramer from the asymmetric unit create two fused, cyclic, puckered five-membered rings (O1, O10, O12, O13, O15) and (O4, O6, O12, O13, O14).¹⁴ Apart from the interactions with the surrounding cyclic rings, the O4 water molecule of the octamer has hydrogen-bonding interaction with one of the secondary nitrogens of **L**, whereas monomer O10 and dimers (O5, O15 and O9, O14) are also forming N...O short contacts with the cryptand secondary amine at a distance which ranges from 2.673 to 2.867 Å.¹⁴ The cooperative effect of the surrounding fused four-membered and five-membered rings through O...O interactions along with NH...O interactions with **L** imposes the observed puckered geometry of the eight-membered basic ring (Figure 3).

Formation of the 2D-layer is generated by simple translation of the (H₂O)₄₅ cluster. The packing diagram viewed down the *c*-axis alternates arrangement of the cryptand and the 2D layer of water to generate a through-channel (Figure 4). The CPK diagram of the water structure clearly shows that the cryptand moieties are located inside the channel. The connectivity of “water crowns” from 2D layers with **L** forms an infinite channel along the *c*-axis.

Thermal analysis of **1** shows that onset of water loss starts at about 50 °C and complete loss of water takes place within 120 °C.¹⁴ Total weight loss in this temperature range is 29.53%, corresponding to 14.25 molecules of water. Fifteen water molecules per cryptand are also supported from the microanalysis results of **1**.¹⁴ Facile removal of water from **1** confirms that the 2D layer of water has weak interaction with **L**.

In FTIR spectroscopic studies of **1**, a relatively sharp band centered about 3459 cm⁻¹ is attributed to the O—H stretching frequency of the water cluster.¹⁴ The IR spectrum of the same crystals when heated for 2 h at about 100 °C under vacuum (0.1 mm) shows that disappearance of the cluster peak and spectra is

virtually superimposable with the standard sample of **L**. Powdered X-ray diffraction studies on **1** before and after expulsion showed major changes in the diffraction patterns and intensities which were attributed to the complete breakdown of the host lattice on exclusion of water.¹⁴ Deliberate immersion of dehydrated **1** in water overnight led to absorption of moisture into the lattice as indicated in the FTIR spectra. The X-ray diffraction pattern of the rehydrated sample showed a marginally different diffraction pattern and intensity compared to those of **1**, suggesting that the departure of the water layer from **1** may be a reversible process.¹⁴

In summary, we have characterized a novel 2D layer of the water structure composed of a unique (H₂O)₄₅ cluster under a confined condition. The present mode of the association of puckered cyclic eight-membered water ring, dimer, and monomer water has not been predicted theoretically nor previously reported experimentally. This new structural data definitely enhances understanding of the 2D structural aspects of water. Moreover, the observed templating effect of the cryptand on the formation of 2D-layered water that has an infinite channel is very important for correctly describing the association of water molecules in biological systems.¹⁶

Acknowledgment. P.G. gratefully acknowledges the Department of Science and Technology, New Delhi, India (Grant No. SR/S1/IC-21/2002) for financial support.

Supporting Information Available: Data on X-ray structure (CIF file, H-bonding distances and angles, packing diagram), NMR, elemental analysis, XRPD, FTIR, TGA for **1**. This material is available free of charge via the Internet at <http://pubs.acs.org>.

References

- (a) Jeffrey, G. A. *An Introduction to Hydrogen Bonding*; Oxford University Press: Oxford, 1997. (b) Ball, P. *H₂O: A Biography of Water*; Weidenfeld & Nicolson: London, 1999.
- (a) Ludwig, R. *Angew. Chem., Int. Ed.* **2001**, *40*, 1808–1827. (b) Henry, M. *ChemPhysChem* **2002**, *3*, 607–616.
- (a) Nauta, K.; Miller, R. E. *Science* **2000**, *287*, 293–295. (b) Keutsch, F. N.; Cruzan, J. D.; Saykally, R. J. *Chem. Rev.* **2003**, *103*, 2533–2578.
- (a) Barbour, L. J.; Orr, G. W.; Atwood, J. L. *J. Chem. Commun.* **2000**, 859–860. (b) Barbour, L. J.; Orr, G. W.; Atwood, J. L. *Nature* **1998**, *393*, 671–673. (c) Atwood, J. L.; Barbour, L. J.; Ness, T. J.; Ruston, C. L.; Ruston, P. L. *J. Am. Chem. Soc.* **2001**, *123*, 7192–7193.
- (a) Blanton, W. B.; Gordon-Wylie, S. W.; Clark, G. R.; Jordon, K. D.; Wood, J. T.; Geiser, U.; Collins, T. J. *J. Am. Chem. Soc.* **1999**, *121*, 3551–3552. (b) Müller, A.; Kricke, E.; Bögge, H.; Schmidtmann, M.; Botar, B.; Talismanova, M. O. *Angew. Chem., Int. Ed.* **2003**, *42*, 2085–2090.
- (c) Doedens, R. J.; Yohannes, E.; Khan, M. I. *Chem. Commun.* **2002**, 62–63. (d) Moorthy, J. N.; Natarajan, R.; Venugopalan, P. *Angew. Chem., Int. Ed.* **2002**, *41*, 3417–3420. (c) Ghosh, S. K.; Bharadwaj, P. K. *Angew. Chem., Int. Ed.* **2004**, *43*, 3577–3580. (d) Infantes, L.; Motherwell, S. *CrystEngComm* **2002**, *4*, 454–461.
- (e) Octoboy, N. S.; Blake, A. J.; Champness, N. R.; Wilson, C. *Chem. Eur. J.* **2005**, *11*, 1–13.
- (f) Liu, K.; Cruzan, J. D.; Saykally, R. J. *Science* **1996**, *271*, 929–933.
- (g) Buck, U.; Huisken, F. *Chem. Rev.* **2000**, *100*, 3863–3890. (h) Head-Gordon, T.; Hura, G. *Chem. Rev.* **2002**, *102*, 2651–2670.
- (i) Raghuraman, K.; Katti, K. K.; Barbour, L. J.; Pillarsetty, N.; Barnes, C. L.; Katti, K. V. *J. Am. Chem. Soc.* **2003**, *125*, 6955–6961.
- (j) Pal, S.; Sankaran, N. B.; Samanta, A. *Angew. Chem., Int. Ed.* **2003**, *42*, 1741–1743. (k) Ma, B.-Q.; Sun, H.-L.; Gao, S. *Chem. Commun.* **2004**, 2220–2221.
- (l) Custelcean, R.; Afloreaei, C.; Vlassa, M.; Polverejan, M. *Angew. Chem., Int. Ed.* **2000**, *39*, 3094–3096.
- (m) Janiak, C.; Scharman, T. G. *J. Am. Chem. Soc.* **2002**, *124*, 14010–14011. (n) Ma, B.-Q.; Sun, H.-L.; Gao, S. *Angew. Chem., Int. Ed.* **2004**, *43*, 1374–1376.
- (o) Chen, D.; Martell, A. E. *Tetrahedron* **1991**, *47*, 6895–6902.
- (p) See Supporting Information.
- (q) Eisenberg, D.; Kauzmann, W. *The Structure and Properties of Water*; Oxford University Press: Oxford, 1969.
- (r) Westhoff, E., Ed. *Water and Biological Macromolecules*; CRC Press: Boca Raton, FL, 1993.

JA054068W

Two-Dimensional Water and Ice Layers: Neutron Diffraction Studies at 278, 263, and 20 K

Christoph Janiak* and Tobias G. Scharmann

Institut für Anorganische und Analytische Chemie, Universität Freiburg, Albertstr. 21, D-79104 Freiburg, Germany

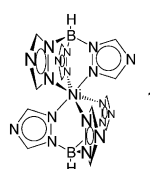
Sax A. Mason

Institut Laue-Langevin, BP 156, 38042 Grenoble Cedex 9, France

Received June 26, 2002

There is hardly a compound which has raised more interest than water because of its fundamental importance in many biological and chemical processes.¹ Recent investigations on water or ice include the properties of water clusters, such as $(\text{H}_2\text{O})_n$ ($n = 3-6$),² the structure of water oligomers, for example, $(\text{H}_2\text{O})_8$ or $(\text{H}_2\text{O})_{10}$ in supramolecular crystals,³ low-dimensional water polymers in supramolecular solids,⁴ different liquid water phases,⁵ molecular dynamics simulations of water freezing,⁶ of water/ice in hydrophobic nanopores,⁷ of hydrogen bonding and dynamics in bulk liquid water.⁸ Despite a myriad of studies water is still not a fully understood liquid. Here we report a neutron diffraction study of the molecular structure of water and ice confined in an organic slit-shaped nanospace. The two-dimensional (2D) ice layers show the existence of new ice phases with chain segments or eight-membered and condensed twelve-membered rings. Such phases have not been seen before in bulk or other low-dimensional ice. Hitherto experimental⁹ and theoretical¹⁰ studies on 2D ice suggested mostly a hexagonal honeycomb lattice. Experimental studies on 2D ice usually report a structure at a single temperature, whereas here the temperature range from 2D water at 278 K down to 20 K is covered, showing the liquid–solid and a solid–solid-phase transition.

A 2D layer of water molecules is stabilized between organic layers of the nickel(II) chelate complexes **1**. The supramolecular



layer clathrate structure has a slit-width for the water layer of about 3 Å (0.3 nm). Large blocky crystals with dimensions of $4 \times 3 \times 2$ mm³ were grown from the reaction mixture of NiCl_2 and potassium-tris(triazolyl)borate in D_2O or H_2O .¹¹ Single-crystal neutron structure investigations were carried out at 278, 263, and 20 K with a D_2O -containing crystal.^{12,13}

For each measuring temperature a different space group is found. The symmetry of the orthorhombic cell decreases from *c*-centered (*Cmca*) at 278 K¹⁴ via centrosymmetric primitive (*Pmn*_b) at 263 K¹⁵ to acentric primitive (*P2*₁*nb*) at 20 K.¹⁶ Some reflection intensities were recorded during the cooling and warming of the crystal (Figure 1). The abrupt change in intensity for the 3 0 1 reflection at 277 K is indicative of a phase transition. Going from *Cmca* to *Pmn*_b is a *klassengleich* (class-equal) transition of type 2

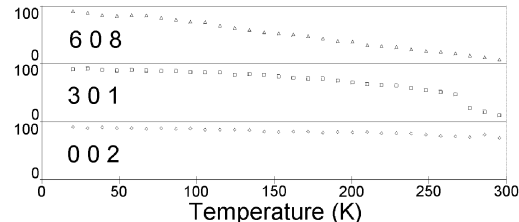


Figure 1. Relative changes in intensity of selected reflections upon warming of a crystal of **1**·6D₂O on the neutron diffractometer.

(k2); from *Pmn*_b to *P2*₁*nb* it is a *translationsgleich* (translation-equal) transition of type 2 (t2). The phase transition from *Pmn*_b to *P2*₁*nb* involves the loss of the inversion symmetry element and leads to merohedral twinning.¹⁷

The first phase transition upon cooling occurs close to the freezing point of H₂O (273.15 K, 0 °C) or D₂O (276.95 K, 3.8 °C) and was shown by differential scanning calorimetry to be at −0.3 °C for **1**·6H₂O and at +3.1 °C for **1**·6D₂O.¹⁸ The change in space group, that is, the loss of symmetry elements with decreasing temperature is solely due to an ordering phenomenon in the 2D water substructure as will be discussed in the following.

At 278 K (5 °C) and above, the water molecules in **1**·6D₂O exhibit pronounced disorder (Figure 2a) and interact only weakly with the surrounding layers of the complex molecules. Of the six molecules per formula unit four are disordered. The remaining two are H/D-bonded to the N atoms of the surrounding organic complex molecules. The disorder is indicative of the expected thermal mobility and dynamic nature of liquid water. The neutron diffraction experiment shows a time-averaged picture of the water structure. Each of four disordered D₂O molecules appears spread over three positions. At any given time only one of these positions will be occupied. Some of the O atom positions are within hydrogen-bonding distance of each other. Taking an O···O separation of 2.6–3.0 Å for hydrogen bonding, the 2D water layer can then be seen as being built-up from different, small D₂O clusters containing 2–6 molecules and free D₂O molecules.

Liquid 3D water can be modeled as a mixture of H₂O clusters of different sizes and single H₂O molecules between the clusters. In the center of the cluster the H₂O molecules are four-fold coordinated by H-bonds. At the cluster surface the H₂O molecules are involved in only one to three H-bonds. This leads to a dynamic increase or reduction of the cluster sizes.¹⁹ Thus, we see the water layer in **1**·6D₂O at 278 K as close to a 2D liquid phase. This is further supported by the observed loss of water from the crystal within minutes when the crystal is taken to an atmosphere not saturated with water vapor. When localized H-bonds exist to each water molecule such fast water loss is seldom observed, and there is also less disorder.

* To whom correspondence should be addressed. E-mail: janik@uni-freiburg.de.

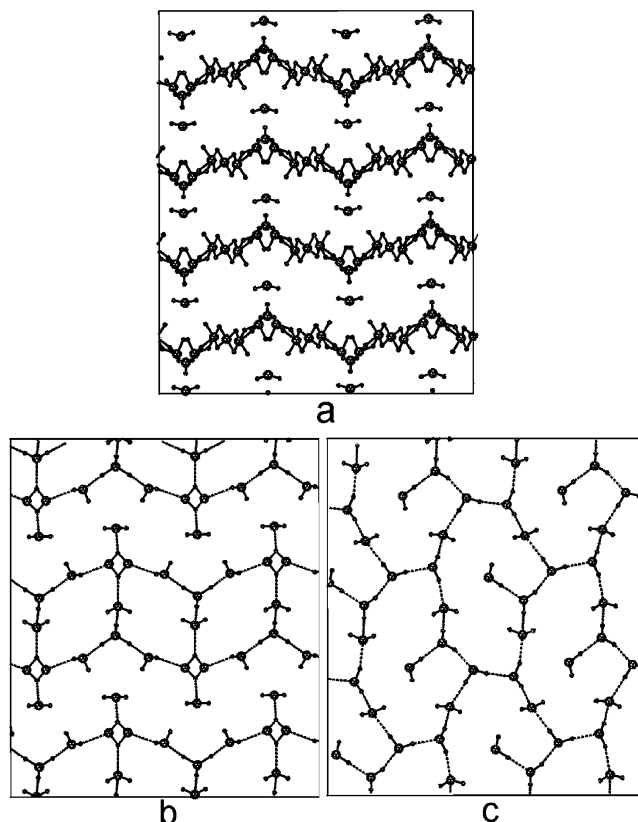


Figure 2. Two-dimensional infinite water/ice layers in $1 \cdot 6\text{D}_2\text{O}$ from a neutron diffraction study at (a) 278 K, (b) 263 K, and (c) 20 K.

Cooling of the crystal through the phase transition at 276 K leads to a strong increase in order, that is, freezing within the water layer. At 263 K observation of the individual hydrogen bonds becomes possible (Figure 2b). The water molecules are organized in kinked strands composed of rings of eight water molecules. But within the strands one O and a D atom are crystallographically disordered over two positions. Considering only one of these positions as fully occupied, the strands are disrupted, giving either individual rings of eight molecules or folded-chain segments. The interaction with the organic environment increases slightly with now two more D_2O molecules (per formula unit) entering into an, albeit very weak, hydrogen-bonded contact to a nitrogen atom.

At 20 K a fully localized water structure is found. There is no more disorder. All D atoms form typical hydrogen bonds to other water molecules or to nitrogen atoms of the complex molecules (Figure 2c). The water layer is an infinite 2D net of O_{12} rings with a dangling D_2O molecule. Both low-temperature structures feature water molecules which are surrounded by two or three other water molecules. One water molecule has only one D_2O neighbor.

Neutron diffraction studies have shown the stepwise freezing of a dynamic layer of pseudoliquid 2D water. The role of the complex molecules **1** is to provide the geometric constraints for the two-dimensionality of the water layer substructure; some H-bonding contacts to the surrounding organic complex molecules are unavoidable. The structure of 2D ice layers features novel rings of eight water molecules or folded-chain segments at temperatures below the freezing point. At very low temperature an unprecedented net of condensed irregular rings of 12 water molecules (plus a dangling D_2O) is observed. Both ice layers are different from hitherto known 2D ice phases which mostly consist of hexagonal honeycomb lattices.^{9,10} Our 2D ice layers do not satisfy the

conventional Bernal–Fowler “ice rules”,²⁰ hence, they cannot be stand-alone solid phases in a vacuum at low temperatures. Ice at and near the surface, however, has unique properties and reduced order parameters and is not in a Bernal–Fowler state due to the specific boundary conditions on the ice surface.²¹

Acknowledgment. Support by the DFG (Grant Ja466/11-1) and the FCI is appreciated. Dedicated to Professor Alfonso Castañeiras on the occasion of his 60th birthday.

Supporting Information Available: Crystallographic files for the structures of $1 \cdot 6\text{D}_2\text{O}$ at 278, 263 and 20 K (CIF). Figures with details of the water layer at 263 and 20 K, table with hydrogen bond distances and angles at 263 and 20 K (PDF). This material is available free of charge via the Internet at <http://pubs.acs.org>

References

- Ludwig, R. *Angew. Chem., Int. Ed.* **2001**, *40*, 1808. Ohmine, I.; Saito, S. *Acc. Chem. Res.* **1999**, *32*, 741.
- Nauta, K.; Miller, R. E. *Science* **2000**, *287*, 293. Gregory, J. K.; Clary, D. C.; Liu, K.; Brown, M. G.; Saykally, R. J. *Science* **1997**, *275*, 814. Liu, K.; Brown, M. G.; Carter, C.; Saykally, R. J.; Gregory, J. K.; Clary, D. C. *Nature* **1996**, *381*, 501. Liu, K.; Cruzan, J. D.; Saykally, R. J. *Science* **1996**, *271*, 929. Ugalde, J. M.; Alkorta, I.; Elguero, J. *Angew. Chem., Int. Ed.* **2000**, *39*, 717.
- Atwood, J. L.; Barbour, L. J.; Ness, T. J.; Raston, C. L.; Raston, P. L. *J. Am. Chem. Soc.* **2001**, *123*, 7192. Barbour, L. J.; Orr, G. W.; Atwood, J. L. *Chem. Commun.* **2000**, 859. Blanton, W. B.; Gordon-Wylie, S. W.; Clark, G. R.; Jordan, K. D.; Wood, J. T.; Geiser, U.; Collins, T. J. *J. Am. Chem. Soc.* **1999**, *121*, 3551. Gruenloh, C. J.; Carney, J. R.; Arrington, C. A.; Zwier, T. S.; Fredericks, S. Y.; Jordan, K. D. *Science* **1997**, *276*, 1678.
- Janeda, S.; Mootz, D. Z. *Naturforsch. B* **1999**, *54*, 103. Iiyama, T.; Nishikawa, K.; Otowa, T.; Kaneko, K. *J. Phys. Chem.* **1995**, *99*, 10075. Born, M.; Mootz, D.; Schaeffgen, S. Z. *Naturforsch. B* **1995**, *50*, 101.
- Johari, G. P.; Hallbrucker, A.; Mayer, E. *Science* **1996**, *273*, 90.
- Matsumoto, M.; Saito, S.; Ohmine, I. *Nature* **2002**, *416*, 409.
- Slovák, J.; Koga, K.; Tanaka, H.; Zeng, X. C. *Phys. Rev. E* **1999**, *60*, 5833. Koga, K.; Gao, G. T.; Tanaka, H.; Zeng, X. C. *Nature* **2001**, *412*, 802.
- Luzar, A.; Chandler, D. *Nature* **1996**, *379*, 55. Ohmine, I. *J. Phys. Chem.* **1995**, *99*, 6767. Vedamuthu, M.; Singh, S.; Robinson, G. W. J. *J. Phys. Chem.* **1994**, *98*, 2222.
- Albert, A.; Mootz, D. Z. *Naturforsch. B* **1997**, *52*, 615. Morgenstern, M.; Müller, J.; Michely, T.; Comsa, G. *Z. Phys. Chem.* **1997**, *198*, 43. Dahlems, T.; Mootz, D.; Schilling, M. Z. *Naturforsch. B* **1996**, *51*, 536. Park, K.-M.; Kuroda, R.; Iwamoto, T. *Angew. Chem., Int. Ed. Engl.* **1993**, *32*, 884.
- Silverstein, K. A. T.; Haymet, A. D. J.; Dill, K. A. *J. Am. Chem. Soc.* **1998**, *120*, 3166. Koga, K.; Tanaka, H.; Zeng, X. C. *Nature* **2000**, *408*, 564.
- Janiak, C. *Chem. Commun.* **1994**, 545. Janiak, C. *Chem. Ber.* **1994**, *127*, 1379.
- Thermal-neutron beam ($\lambda = 1.3143 \text{ \AA}$) instrument D19 at ILL equipped with a $4 \times 64^\circ$ position-sensitive detector. The crystal (dimensions $4.1 \times 3.8 \times 2.0 \text{ mm}^3$) together with some mother liquor was sealed in a glass capillary, mounted on an Al pin in a Displex cryorefrigerator. The reflections to a $2 - \theta$ value of at least 50° were then measured with ω scans in equatorial geometry and at higher angles with normal beam geometry. Intensities were corrected for absorption using the crystal dimensions. Formula of $1 \cdot 6\text{D}_2\text{O} \text{ C}_{12}\text{H}_{14}\text{BzD}_{12}\text{NiO}_6$, ($610.77 \text{ g} \cdot \text{mol}^{-1}$).
- Deuterium and hydrogen have very different neutron scattering length ($+0.68$ and $-0.36 \times 10^{-14} \text{ m}$, respectively) with that of D being surpassed by only a few other nuclei. Deuterium also greatly reduces the incoherent scattering. Bacon, G. E. *Neutron Diffraction*; Clarendon Press: Oxford, 1975. *Chemical Applications of Thermal Neutron Scattering*; Willis, B. T. M., Ed.; Oxford University Press: Oxford, 1973.
- Orthorhombic, *Cmca*, $a = 10.890(7) \text{ \AA}$, $b = 21.000(1) \text{ \AA}$, $c = 11.754(3) \text{ \AA}$, $V = 2688(3) \text{ \AA}^3$, $Z = 4$, $D_c = 1.509 \text{ g} \cdot \text{cm}^{-3}$, R , R_w 0.0666, 0.1534 for 1633 independent reflections with $I > 2\sigma(I)$.
- Orthorhombic, *Pmnb*, nonstandard setting of *Pnma*, $a = 10.852(2) \text{ \AA}$, $b = 20.919(3) \text{ \AA}$, $c = 11.696(1) \text{ \AA}$, $V = 2655.0(6) \text{ \AA}^3$, $Z = 4$, $D_c = 1.563 \text{ g} \cdot \text{cm}^{-3}$, R , R_w 0.0503, 0.1132 for 2048 independent reflections with $I > 2\sigma(I)$.
- Orthorhombic, *P2₁nb*, nonstandard setting of *Pna2₁*, $a = 10.755(1) \text{ \AA}$, $b = 20.736(2) \text{ \AA}$, $c = 11.587(2) \text{ \AA}$, $V = 2584.0(5) \text{ \AA}^3$, $Z = 4$, $D_c = 1.570 \text{ g} \cdot \text{cm}^{-3}$, R , R_w 0.0285, 0.0667 for 2881 independent reflections with $I > 2\sigma(I)$.
- Bärnighausen, H. *MATCH, Commun. Math. Chem.* **1980**, *9*, 139.
- Perkin-Elmer DSC 7 under nitrogen atmosphere. The crystal surfaces were carefully dried before the thermal analysis.
- Scheraga, H. A. *Acc. Chem. Res.* **1979**, *12*, 7.
- Bernal, J. D.; Fowler, R. H. *J. Chem. Phys.* **1933**, *1*, 515.
- Ryzhkin, I. A.; Petrenko, V. F. *Phys. Rev. B* **2002**, *65*, 012205.

JA0274608

Shape-Shifting Tetranuclear Oxo-Bridged Manganese Cluster: Relevance to Photosystem II Water Oxidase Active Site

Sumitra Mukhopadhyay,[†] Henry J. Mok,[†] Richard J. Staples,[‡] and William H. Armstrong^{*,†}

Department of Chemistry, Eugene F. Merkert Chemistry Center, Boston College, Chestnut Hill, Massachusetts 02467, and Department of Chemistry and Chemical Biology, Harvard University, Cambridge, Massachusetts 02138

Received April 27, 2004; E-mail: armstwi@bc.edu

Aggregates of transition metal ions bridged by either oxide/hydroxide (O^{2-}/OH^-) or sulfide (S^{2-}) ligands are plentiful and well characterized. Some of these compounds are of known biological relevance and many are redox-active. Examples of redox-active sulfide-bridged complexes include different types of iron–sulfur clusters. While subtle structural variations occur upon oxidation or reduction of these complexes, reflected by changes in bond distances and angles, the overall three-dimensional shape remains unchanged. In other words, the same structural isomer is observed for all oxidation states. The $[Fe_4S_4]^{n+}$ (where $n = 1, 2$, and 3) clusters exhibit a cubane-type geometry.¹ Heterometallic $[MFe_3S_4]$ clusters, where $M = V$,^{2a} Co, Ni, Zn, Cd,^{2b} or Mo,^{2c} also have been shown to undergo redox processes with no pronounced change in the cubane geometry.² Both $[Fe_6S_6]^{n+}$ (where $n = 3$ and 4)^{3a} and $[Fe_4Mo_2S_9]^{n+}$ (where $n = 0$ and 1)^{3b} complexes exhibit edged-bridged double cubane cores in both oxidized and reduced forms.

We reported redox behavior of the oxo-bridged tetramanganese complex $[Mn_4O_6(bpea)_4]^{4+}$ (where bpea = *N,N*-bis(2-pyridylmethyl)ethylamine), which retains its adamantane-type core structure upon reduction by one electron.⁴ The overall cubane topology of the $[Mn_4O_4(O_2PPh_2)_6]$ complex remains unaffected when oxidized by one electron.⁵ Examining these and a large body of additional data, it is natural to conclude that chalcogenide-bridged multinuclear clusters are structurally rigid upon oxidation state changes. We have recently discovered an important exception to this general observation.

As documented here, a complex we reported previously, $\{[Mn^{III,IV}_2(\mu-O)_2(tphpn)]_2\}^{4+}$ (**1**) (where Htphpn = *N,N,N',N'*-tetra(2-methylpyridyl)-2-hydroxypropanediamine),⁶ undergoes dramatic structural changes when oxidized or reduced by one electron. We also demonstrate that the structure determined for **1** in the solid state is not stable in solution and that a rearrangement occurs, albeit slowly, without redox “triggering”. As shown below, the observations described here have important implications regarding our understanding of Photosystem II.

The solid-state structure of **1** was previously established to be a stacked pair of $\{Mn_2(\mu-O)_2\}^{3+}$ units linked together by two heptadentate ligand anions, tphpn⁻.⁶ The first indication that **1** is not structurally rigid in solution arose from electronic absorption spectra, as shown in Figure 1. The data for **1** imply that a structural isomerization or “shape-shifting” occurs over time in solution, proceeding through isosbestic points at ~ 640 and ~ 728 nm. Confirmation comes from mass spectral data that show one parent-ion mass before and after the isomerization process is complete. Attempts to isolate the second isomer, compound **2**, were thwarted because the species isolated in high yield by crystallization was **1**. Thus, this isomerization process can be reversed by crystallization. This isomerization and its reversibility were also confirmed by ¹H

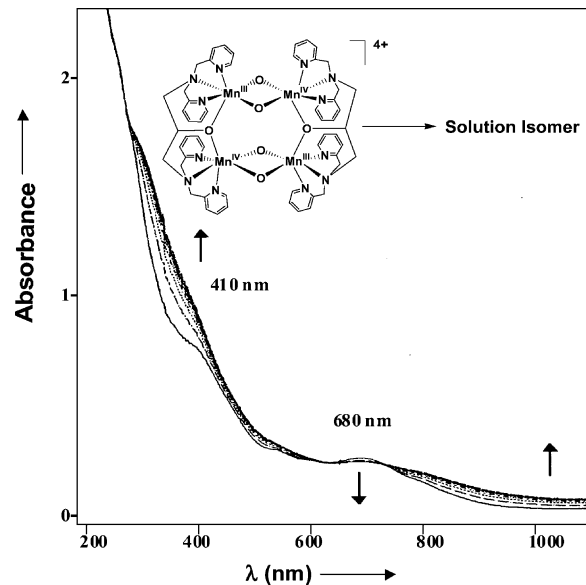


Figure 1. Conversion of **1** to **2** in acetonitrile over time as observed in electronic absorption spectra, taken at every 30 min over 12 h.

NMR and EPR measurements (see Figures S1 and S2, Supporting Information). We conclude that the “dimer-of-dimers” structure for **1** is the most stable isomer in the solid state, whereas **2**, whose structure is yet to be determined, is the isomer stable in solution.

Our early attempts to obtain reproducible electrochemical behavior of **1** were futile, as we were not aware of the isomerization mentioned above and because the solutions used must have had varying amounts of **1** and **2** present. Cyclic voltammograms of **1**(CF₃SO₃)₄ as freshly dissolved crystals and after being in solution for ~ 12 h are shown in Figure 2. Species **1** has a broad quasi-reversible one-electron oxidation at an $E_{1/2}$ value of 1.23 V ($\Delta E_p = 130$ mV) vs Ag/AgClO₄.⁷ A second well-defined reversible redox couple at $E_{1/2} = 0.92$ V ($\Delta E_p = 70$ mV) in the anodic scan begins to appear slowly in solution. This has been assigned as one-electron oxidation of **2**. It is interesting to note the relatively large shift (~ 300 mV) in the $[Mn^{IV}_3, Mn^{III}]/[Mn^{IV}_2, Mn^{III}_2]$ reduction potential upon isomerization. This shift is related to the energy “stored” in the dimer-of-dimers architecture.

Noting that a Mn^{IV}_3, Mn^{III} oxidation state of our tetranuclear species appeared to be accessible, we set out to isolate it in order to explore its structural and electronic properties. We were successful in oxidizing $[Mn_4(\mu-O)_4(tphpn)_2](OTf)_4$ in acetonitrile quantitatively by one electron employing a high-potential oxidant, $[Mn^{IV}(HB(3,5-Me_2pz)_3)_2](ClO_4)_2$ (where pz = pyrazolyl), developed in our laboratory.⁸ We were surprised to find that the crystal structure of $[Mn_4(\mu-O)_4(tphpn)_2](OTf)_2(ClO_4)_3$, **3**(OTf)₂(ClO₄)₃, shown in Figure 3, revealed that a large change in shape of the dimer-of-dimers aggregate accompanies oxidation, resulting in an

[†] Boston College.

[‡] Harvard University.

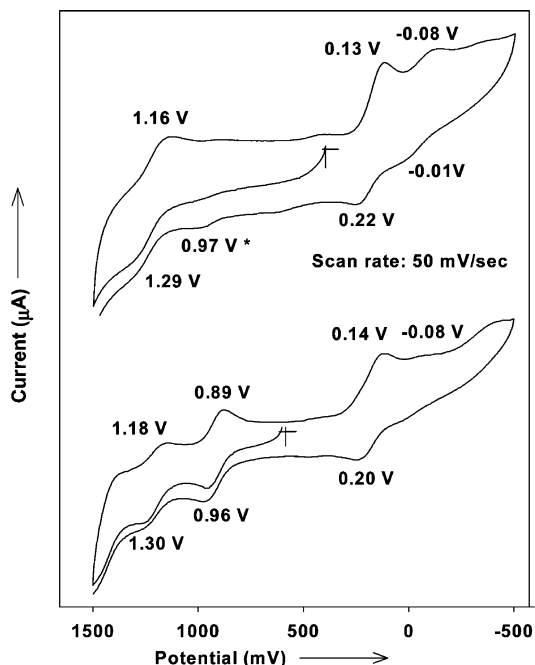


Figure 2. Cyclic voltammogram of **1**(OTf)₄ (top) and a mixture of **1**(OTf)₄ and **2**(OTf)₄ (bottom) in acetonitrile. Potentials are vs Ag/AgClO₄.

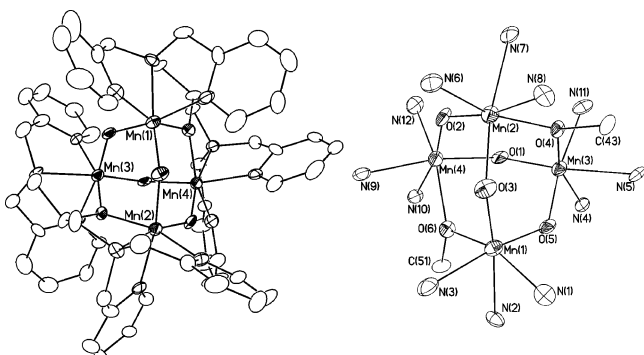
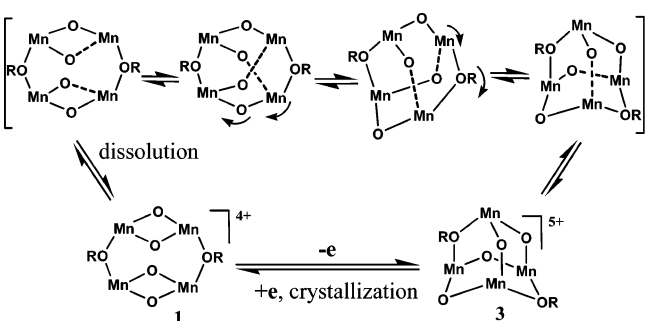


Figure 3. ORTEP views of the full cation (left) and the tetramanganese core (right) of **3**(OTf)₂(ClO₄)₃, showing 30% probability thermal ellipsoids (H atoms are omitted for clarity).

adamantane-like core complex.⁹ It is possible that compound **2** also has an adamantane core, yet this remains to be established owing to the difficulty of isolating **2** in crystalline form.

In terms of metrical parameters, the most dramatic change upon oxidation is that the average Mn—O_{oxo}—Mn angle increases from $\sim 94.2^\circ$ in **1** to ~ 132 – 135° in **3** (Figure S4). Consequently, the Mn···Mn separations are greatly increased. There are two discernible sets of distances between adjacent Mn atoms bridged by an oxide group. The average of distances Mn(2)···Mn(4) and Mn(1)···Mn(3) is 3.29 Å, whereas the same between Mn(1)···Mn(2) and Mn(3)···Mn(4) is 3.36 Å. The average bond distance between two adjacent Mn centers bridged by an alkoxo group (Mn(2)···Mn(3) and Mn(1)···Mn(4)) is 3.45 Å. The average Mn—O_{alkoxo}—Mn angle is 124°. The average Mn···Mn distance increase from **1** (2.65 Å)⁶ to **3** is of particular interest with regard to the tetranuclear manganese complex (Mn₄) found in the Photosystem II (PSII) water oxidase (WO) active site, which is responsible for catalytic conversion of water to dioxygen. The structure of WO Mn₄ is available in its “S₁” oxidation state.¹⁰ In the first two reports (3.7 and 3.8 Å),^{10a,b} no detailed structural assignment is ventured for the manganese region’s electron density. The most recent structure is at marginally higher resolution (3.5 Å),^{10c} yet the authors assign

Scheme 1



the active-site cluster as a Mn₃Ca cubane with an appended fourth Mn atom. In any event, none of the X-ray analyses to date shed light on the higher S states. EXAFS measurements reveal 2.7 Å and >3.3 Å Mn···Mn distances in the S₁ and S₂ states.^{11a,b} According to one group, advancement to the S₃ form is accompanied by marked Mn···Mn separation increases (from 2.7, 2.7, and 3.3 Å to 2.8, 3.0, and 3.3–3.5 Å),^{11c} although one might have expected shortened distances at a higher oxidation state due to shorter Mn—O_{oxo} bonds. However, this latter expectation is based on an assumption of relative structural rigidity for the PSII Mn₄. Our work demonstrates that a synthetic Mn₄ species readily rearranges at higher oxidation states, preferring a structure with more open Mn—O_{oxo}—Mn angles and thus larger Mn···Mn distances. On this basis, we put forward the hypothesis that the increase in metal–metal distance observed for the PSII Mn₄ when advancing from S₂ to S₃ states is consistent with a significant structure rearrangement or “shape-shift” rather than just lengthening of the Mn—O_{oxo} bonds.^{11b}

Analysis of the electrochemical properties (Figure S3) of **3** confirms that it is the one-electron oxidation product of **2**. The reduction of **3** by one electron was observed at $E_{1/2} = 0.90$ V ($\Delta E_p = 80$ mV), matching adequately with the one-electron oxidation of complex **2** ($E_{1/2} = 0.92$ V). Also, the second one-electron reduction of complex **3** is observed at $E_{1/2} = 0.17$ V ($\Delta E_p = 70$ mV), which is in agreement with the first one-electron reduction of complex **2** (Mn^{III}₂Mn^{IV}₂ → Mn^{III}₃Mn^{IV}). A reversible redox couple at $E_{1/2} = 1.42$ V ($\Delta E_p = 60$ mV) was observed in the oxidative scan of **3**, which corresponds to one-electron oxidation of **3** (Mn^{III}Mn^{IV}₃ → Mn^{IV}₄). The Mn^{IV}₄ species is yet to be isolated; however, adamantane structures containing only Mn^{IV} ions are known.^{4,12} The chemical reduction of complex **3** by one electron was performed with an equimolar amount of Fe(cp*)₂. The course of reduction was studied by ¹H NMR spectroscopy, demonstrating that the addition of 1 equiv of Fe(cp*)₂ to **3** generates complex **2** in solution (Figure S5), followed by crystallization to regenerate **1** in nearly quantitative yield. The conversion of **1** to **3** and vice versa likely involves several intermediates, as depicted in hypothetical Scheme 1, one of which may represent the structure of **2**.

The observation of quasi-reversible [Mn^{III}₂Mn^{IV}₂]/[Mn^{III}₃Mn^{IV}] reduction in the cathodic scans of **1** (or **2**) at $E_{1/2} = 0.17$ V ($\Delta E_p = 75$ mV), as shown in Figure 2, begged the question of whether a reduced form could be isolated as well. The one-electron reduced form of **1** is thought to have the same oxidation state as the PSII S₀ state (IV,III).^{11a} The latter species is known to have a hyperfine-rich EPR spectrum¹³ that can serve as a reference point for attempting to mimic the structural properties of the Mn₄ cluster at the S₀ state. In fact, complex **1** exhibits a parallel polarization EPR signal similar to that of the PSII S₁ state.⁶ Chemical reduction of **1** (and/or **2**) by one electron was carried out in acetonitrile solution using an equimolar amount of either Fe(cp*)₂ or sodium naphthalimide under inert atmosphere. Again, as for the oxidation reaction, an unexpected result was encountered; namely, we

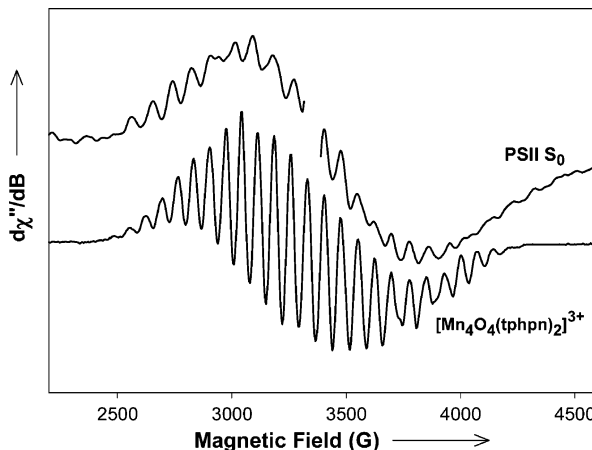


Figure 4. Comparison of the 4 K EPR spectra between the PSII S₀ state and complex **4** in acetonitrile.

observed two different species with the formulation [Mn^{III}₃Mn^{IV}(μ-O)₄(tphpn)₂]³⁺ (**4** and **5**), which have easily distinguishable EPR spectra. One of them (**5**) exhibits a 16-line EPR signal at $g \approx 2$ (Figure S8), consistent with a dimer-of-dimers geometry, because in the one-electron reduced form of the dimer-of-dimers structure, the antiferromagnetically coupled Mn^{III}Mn^{III} dinuclear unit would give rise to an $S = 0$ state, whereas the Mn^{III}Mn^{IV} dinuclear unit would result in an $S = 1/2$ ground state, giving rise to a 16-line EPR spectrum.¹⁴ An analogous 16-line spectrum was observed by Kawasaki et al. when their dimer-of-dimers-type complex, possessing a {[Mn^{III}^{IV}₂(μ-O)₂]₂}⁶⁺ core, supported by a similar heptadentate polypyridyl ligand, was oxidized by one electron to yield {[Mn^{III}^{IV}₂(μ-O)₂]}{Mn^{IV}₂(μ-O)₂}⁷⁺, which gives rise to an $S = 1/2$ ground spin state.¹⁵

The spectrum of species **4**, shown in Figure 4, contains a hyperfine-rich signal centered at $g \approx 2$ that bears a strong resemblance to the PSII S₀ state multiline signal.¹³ Mass spectrometry confirms a tetranuclear formulation [Mn^{III}₃Mn^{IV}(μ-O)₄(tphpn)₂]³⁺ for **4** (Figure S6) that must have arisen from an isomerization or “shape-shift” process. Cyclic voltammetric (Figure S7) and ¹H NMR studies of **4** indicate that this is most likely the one-electron reduced product of **2**. The close correspondence between EPR spectral properties of **4** and the PSII Mn₄ S₀ state suggests that they possess the same electronic spin topology, and perhaps the same 3D structure as well. To date, only two other tetranuclear model complexes, both generated by γ -irradiation reduction of a Mn_nO_n core complex ($n = 4$ or 6) at 77 K, displayed EPR “multiline” signals with overall spectral width comparable to the multiline signals observed for the Mn₄ cluster in PSII S₀ and S₂ states.¹⁶ However, these complexes are unstable, decaying at temperatures above 190 K. For the first time, our work provides a synthetic multiline cluster, which is stable at room temperature indefinitely in the solid state under inert atmosphere. Structural characterization of **4** has eluded us until now because it slowly transforms in solution to yet a third reduced isomer (**6**) possessing a broad EPR signal (see Figure S9) upon crystallization. The lifetime of **4** in solution is long enough that crystallographic characterization is promising, and this is one central aim of our continuing work.

Our work described here raises the possibility of “shape-shifting” for the PSII Mn₄ cluster. Complex **4** closely replicates the well-resolved hyperfine-structured multiline EPR signal with strikingly similar spectral width and intensity pattern compared to those of

the PSII S₀ state. We have also shown that the dimer-of-dimers structural framework in the Mn^{III}₂Mn^{IV}₂ oxidation state is not stable in solution, as indicated from the spectroscopic studies, and an intramolecular non-redox rearrangement occurs. Upon one-electron oxidation of **1**, an adamantane-shaped complex was isolated and structurally characterized. This transformation accompanies an overall increase in the Mn^{...}Mn bond distances, which also occurs during the oxidation of the S₂ state to the S₃ state. While we do not propose the adamantane complex as a structural model for the S₂ state, we do suggest that an intramolecular core conversion process may accompany S₂-to-S₃ state advancement.

Acknowledgment. We acknowledge the National Institutes of Health (GM-38275) for generous support of this research. We thank Prof. Jeff Peloquin at Boise State University for providing us the “PSII S₀ state” EPR spectrum and Bruker EPR facility at Billerica, MA, for assistance in recording EPR spectra of the Mn complexes.

Supporting Information Available: Crystallographic data of **3** and experimental preparation of the complexes; NMR of **1–3**, ESI-MS of **4**, and electrochemistry of **3** and **4**; EPR spectra of complexes **1**, **2**, **5**, and **6** (PDF, CIF). This material is available free of charge via the Internet at <http://pubs.acs.org>.

References

- (a) Goh, C.; Segal, B. M.; Huang, J.; Long, J. R.; Holm, R. H. *J. Am. Chem. Soc.* **1996**, *118*, 11844–11853. (b) Goh, C.; Holm, R. H. *Inorg. Chim. Acta* **1998**, *270*, 46–54. (c) Rao, P. V.; Holm, R. H. *Chem. Rev.* **2004**, *104*, 527–559.
- (a) Hauser, C.; Bill, E.; Holm, R. H. *Inorg. Chem.* **2002**, *41*, 1615–1624. (b) Zhou, J.; Scott, M. J.; Hu, Z.; Peng, G.; Müncck, E.; Holm, R. H. *J. Am. Chem. Soc.* **1992**, *114*, 10843–10854. (c) Fomitchev, D. V.; McLaughlan, C. C.; Holm, R. H. *Inorg. Chem.* **2002**, *41*, 958–966.
- (a) Kanatzidis, M. G.; Coucouvanis, D. *J. Am. Chem. Soc.* **1986**, *108*, 337–338. (b) Zhou, H.-C.; Su, W.; Achim, C.; Rao, P. V.; Holm, R. H. *Inorg. Chem.* **2002**, *41*, 3191–3201.
- Dubé, C. E.; Wright, D. W.; Bonitatebus, P. J., Jr.; Pal, S.; Armstrong, W. H. *J. Am. Chem. Soc.* **1998**, *120*, 3704–3716.
- Ruettinger, W. F.; Ho, D. M.; Dismukes, G. C. *Inorg. Chem.* **1999**, *38*, 1036–1037.
- (a) Chan, M. K.; Armstrong, W. H. *J. Am. Chem. Soc.* **1991**, *113*, 5055–5057. (b) Kirk, M. L.; Chan, M. K.; Armstrong, W. H.; Solomon, E. I. *J. Am. Chem. Soc.* **1992**, *114*, 10432–10440.
- Ferrocene was used as an external standard with an $E_{1/2}$ value of 0.45 V for the FeCp₂/FeCp₂ couple ($\Delta E_F \approx 65$ mV) vs Ag/AgClO₄.
- Chan, M. K.; Armstrong, W. H. *Inorg. Chem.* **1989**, *28*, 3777–3779.
- To our knowledge, the only other oxo-bridged metal clusters that rearrange are reported in the following: Klemperer, W. G.; Schwartz, C.; Wright, D. A. *J. Am. Chem. Soc.* **1985**, *107*, 6941–6950.
- (a) Zouni, A.; Witt, H.-T.; Kern, J.; Fromme, P.; Krauss, N.; Saenger, W.; Orth, P. *Nature (London)* **2001**, *409*, 739–743. (b) Kamiya, N.; Shen, J.-R. *Proc. Natl. Acad. Sci. U.S.A.* **2003**, *100*, 98–103. (c) Ferreira, K. N.; Iverson, T. M.; Maghlaoui, K.; Barber, J.; Iwata, S. *Science* **2004**, *303*, 1831–1838.
- (a) Robblee, J. H.; Cinco, R. M.; Yachandra, V. K. *Biochim. Biophys. Acta* **2001**, *1503*, 7–23. (b) Dau, H.; Iuzzolino, L.; Dittmer, J. *Biochim. Biophys. Acta* **2001**, *1503*, 24–39 (c) Liang, W.; Roelofs, T. A.; Cinco, R. M.; Rompel, A.; Latimer, M. J.; Yu, W. O.; Sauer, K.; Klein, M. P.; Yachandra, V. K. *J. Am. Chem. Soc.* **2000**, *122*, 3399–3412.
- Wieghardt, K.; Bossek, U.; Gebert, W. *Angew. Chem.* **1983**, *95*, 320.
- (a) Messinger, J.; Robblee, J.; Yu, W. O.; Sauer, K.; Yachandra, V. K.; Klein, M. P. *J. Am. Chem. Soc.* **1997**, *119*, 11349–11350. (b) Messinger, J.; Nugent, J. H. A.; Evans, M. C. W. *Biochemistry* **1997**, *36*, 11055–11060. (c) Ahrling, K. A.; Peterson, S.; Styring, S. *Biochemistry* **1997**, *36*, 13148–13152.
- (a) Zweygart, W.; Bittl, R.; Wieghardt, K.; Lubitz, W. *Chem. Phys. Lett.* **1996**, *261*, 272–276. (b) Mukhopadhyay, S.; Armstrong, W. H. *J. Am. Chem. Soc.* **2003**, *125*, 13010–13011.
- Kawasaki, H.; Kusunoki, M.; Hayashi, Y.; Suzuki, M.; Muneyawa, K.; Suenaga, M.; Senda, H.; Uehara, A. *Bull. Chem. Soc. Jpn.* **1994**, *67*, 1310–1319.
- (a) Blondin, G.; Davydov, R.; Philouze, C.; Charlot, M.-F.; Styring, T.; Åkermark, B.; Girerd, J.-J.; Boussac, A. *J. Chem. Soc., Dalton Trans.* **1997**, 4069–4074. (b) Dismukes, G. C.; Ruettinger, W.; Boelrijk, A. E. M.; Ho, D. *Photosynthesis: Proc. Int. Congress Photosynthesis* **1998**, *2*, 1259–1266.

JA0475508

Acid–Base Catalyzed Reactions in Ionic Water Clusters

Uwe Achatz, Stefan Joos, Christian Berg, Thomas Schindler, Martin Beyer,
Gerhard Albert, Gereon Niedner-Schatteburg, and Vladimir E. Bondybey*

Contribution from the Institut für Physikalische und Theoretische Chemie,
Technische Universität München, 85747 Garching, Germany

Received June 6, 1997

Abstract: Fourier Transform-Ion Cyclotron Resonance (FT-ICR) mass spectrometric studies of both cationic water clusters $\text{H}^+(\text{H}_2\text{O})_n$, $n = 1–70$, and anionic water clusters $\text{X}^-(\text{H}_2\text{O})_n$, $n = 1–30$, $\text{X} = \text{OH}, \text{O}$, with acetone and acetaldehyde are reported. For the cations a sequence of ligand exchange and fragmentation reactions results in “solvated proton” complex ion final products. In the anionic $\text{OH}^-(\text{H}_2\text{O})_n$ clusters, on the other hand, an OH^- catalyzed aldol addition of the carbonyl compounds with a true covalent bond formation is observed. The anionic and cationic water clusters thus behave similar to basic and acidic aqueous solutions.

I. Introduction

The rate or outcome of a condensed phase chemical reaction can be strongly affected by the solvent. Many important chemical reactions, including numerous industrially relevant processes, take place in solutions. The most important solvent for the processes in earth's troposphere is water, and the chemistry on which life itself is based takes place in aqueous solutions. Many organic and inorganic compounds are ionized in the polar water solvent, and the course of the reactions often can be altered by changing the composition of the solution and the ions present. Particularly important are the concentrations of the H^+ and OH^- ions, which are usually described by the pH value of the solution. Numerous “acid catalyzed” or “base catalyzed” reactions depend sensitively on their concentrations.^{1–4}

We have recently initiated studies of hydrated H^+ and OH^- ions in the gas phase and shown that they can be used as simple model systems for investigating charge-transfer processes and solution chemistry.^{5,6} We have constructed a supersonic expansion discharge source and interfaced it to our FT-ICR mass spectrometer, an arrangement that permits us to produce, store, and mass-select ions solvated with up to about 100 water molecules. We have also been able to show that such ion clusters, once prepared, gradually lose the solvent ligands one by one due to the absorption of the ambient temperature infrared background radiation.⁷ This provides us with a gentle way of removing the water ligands one at a time, and observing the effect of the removal of the stabilizing solvent upon the system properties and stability.

In the present paper we wish to address the question if and to what extent the solvated H^+ and OH^- ions can “catalyze”

chemical reactions. Specifically, we investigate reactions of simple carbonyl compounds, acetaldehyde and acetone, with water clusters. Several related previous studies of similar organic species are available in the literature.^{8–10} The dissociation energies of water molecules with organic compounds (e.g., CH_3CN , CH_3OH) have been investigated by high-pressure mass spectrometry by Meot-Ner,^{11–14} while the stability, structure, and unimolecular decomposition of protonated organic clusters were the subject of study by Castleman et al.^{15–17} Several interesting theoretical as well as experimental studies of reactions of proton bound organic clusters with small organic molecules originated in the group of Ch. Lifshitz.^{18–20} Adsorption of organic molecules on large water clusters was investigated by Ahmed et al.^{21,22} A prior investigation of chemical ionization of acetaldehyde revealed some evidence for acid-catalyzed aldol addition in the gas phase but remained somewhat inconclusive with respect to the mechanism.²³

- (8) Daly, G. M.; Gao, J.; El-Shall, M. S. *Chem. Phys. Lett.* **1993**, *206*, 500–508.
- (9) El-Shall, M. S.; Olafsdottir, S. R.; Meot-Ner (Mautner), M.; Sieck, L. W. *Chem. Phys. Lett.* **1991**, *185*, 193–198.
- (10) El-Shall, M. S.; Daly, G. M.; Gao, J.; Meot-Ner (Mautner), M.; Sieck, L. W. *J. Phys. Chem.* **1992**, *96*, 507–510.
- (11) Meot-Ner (Mautner), M. *J. Am. Chem. Soc.* **1988**, *110*, 3858–3862.
- (12) Meot-Ner (Mautner), M. *J. Am. Chem. Soc.* **1986**, *108*, 6189–6197.
- (13) Deakyne, C. A.; Meot-Ner (Mautner), M.; Campell, C. L.; Hughes, M. G.; Murphy, S. P. *J. Chem. Phys.* **1986**, *84* (9), 4958–4969.
- (14) El-Shall, M. S.; Marks, C.; Sieck, L. W.; Meot-Ner (Mautner), M. *J. Phys. Chem.* **1992**, *96*, 2045–2051.
- (15) Tzeng, W. B.; Wei, S.; Castleman, A. W., Jr. *Chem. Phys. Lett.* **1990**, *168*, 30–36.
- (16) Tzeng, W. B.; Wei, S.; Castleman, A. W., Jr. *Chem. Phys. Lett.* **1990**, *166*, 343–352.
- (17) Zhang, X.; Yang, X.; Castleman, A. W., Jr. *Chem. Phys. Lett.* **1991**, *185*, 298–302.
- (18) Feng, W. Y.; Goldenberg, M.; Lifshitz, C. *J. Am. Soc. Mass Spectrom.* **1994**, *5*, 695–703.
- (19) Martin, J. M. L.; Aviyente, V.; Lifshitz, C. *J. Phys. Chem. A* **1997**, *101*, 2597–2606.
- (20) Feng, W. Y.; Lifshitz, Ch. *Int. J. Mass Spectrom. Ion Proc.* **1995**, *149/150*, 13–25.
- (21) Ahmed, M.; Apps, C. J.; Hughes, C.; Watt, N. E.; Whitehead, J. C. *J. Phys. Chem. A* **1997**, *101*, 1250–1253.
- (22) Ahmed, M.; Apps, C. J.; Hughes, C.; Whitehead, J. C. *Chem. Phys. Lett.* **1995**, *240*, 216–223.
- (23) Wesedemiotis, C.; McLafferty, F. W. *Org. Mass. Spectrom.* **1981**, *16*, 381–382.

A first step of a base- or acid-catalyzed reaction is assumed to be addition of the H^+ or OH^- ion onto one of the reactants. It is easily seen that an $\text{H}^+(\text{H}_2\text{O})_n$ cluster with n around 55 will have the same relative H^+ "concentration" as a strongly acid solution with $\text{pH} \approx 0$, and a similarly sized $\text{OH}^-(\text{H}_2\text{O})_n$ ion can be compared with a $\text{pH} \approx 14$ basic medium. The specific purpose of the present study is to investigate to what extent one can view such solvated H^+ ions as "acid" and solvated OH^- ions as "basic" medium, and if and how the presence of in this case a single H^+ or OH^- ion will influence the chemistry taking place in the water cluster.

II. Experimental Section

All experiments were performed in a modified Fourier Transform Ion Cyclotron Resonance (FT-ICR) mass spectrometer Spectrospin CMS47X²⁴ equipped with a superconducting 4.7 T magnet, an ASPECT 3000 data station, and a cylindrical 60 × 60 mm "infinity" cell.²⁵ A fourth differential pumping stage was added to the original instrument to permit the use of external molecular beam cluster ion sources. In the source used in the present work, an argon-water mixture (200:1) was partially ionized by a low current corona discharge (1–3 kV, 1–4 mA).^{26,27} A subsequent adiabatic expansion through a 150 μm orifice leads to formation of both protonated water clusters $\text{H}^+(\text{H}_2\text{O})_n$, $n = 1$ –70,⁵ and hydrated anions $\text{X}(\text{H}_2\text{O})_n$, $n = 1$ –30, $\text{X} = \text{OH}^-$, O^- , O_2H^- , O_2^- .⁶ The initial distribution of the clusters depends somewhat on source conditions. Switching between anions and cations is accomplished by changing the polarity of the ion transfer optics. The temperature of the cluster ions is determined by a balance between evaporative cooling and radiative heating by the ambient temperature background and is estimated to be around $\lesssim 150$ K.⁷

Downstream of the source the molecular beam is skimmed (400 μm) and the cluster ions are transferred into the ICR cell by a system of electrostatic lenses. After accumulation of a sufficient number of ions (typically after ≈ 300 ms), the molecular beam is blocked by a mechanical shutter to prevent collisions of the stored ions with the background gas from the molecular beam. Typical pressures with the cluster source in operation are 5×10^{-3} mbar in the source chamber and 6×10^{-10} mbar in the cell region with a closed shutter.

The water cluster distribution $\text{Y}(\text{H}_2\text{O})_n$, $\text{Y} = \text{H}^+$ or OH^- and O^- , was allowed to react with acetone and acetaldehyde admitted through a leak valve at a pressure inside the cell of 7×10^{-8} mbar. The reaction and fragmentation processes occurring in the cell were followed by recording mass spectra after variable reaction delays.

III. Results and Discussion

(a) Reactions of Cationic Water Clusters with Acetone and Acetaldehyde. When cationic water clusters $\text{H}^+(\text{H}_2\text{O})_n$, $n = 2$ –80, are reacted with acetone at a pressure of about 7×10^{-8} mbar, which corresponds to about five collisions per second, basically two processes are observed, fragmentation and ligand exchange. The former process is not caused only by collisions, but as we have been able to demonstrate previously, it is in part due to absorption of infrared blackbody radiation.⁷ The ligand exchange efficiently replaces water molecules with acetone, and after some 300 ms, clusters containing one acetone already prevail over pure water clusters.

The reactions do not stop there, and solvated ions of the type $\text{H}^+(\text{H}_2\text{O})_n(\text{C}_3\text{H}_6\text{O})_k$ with two and eventually up to 8 acetone ligands form. The spectra at longer times get significantly simplified, due to the preferential stability of $\text{H}^+(\text{H}_2\text{O})_n(\text{C}_3\text{H}_6\text{O})_k$.

(24) Kruppa, G. H.; Caravatti, P.; Radloff, C.; Zuercher, S.; Laukien, F.; Watson, C.; Wronka, J. FT-ICR/MS: Analytical applications of Fourier Transform ion cyclotron resonance spectrometry; Asamoto, B., Ed.; VCH: Weinheim, 1991.

(25) Caravatti, P.; Allemann, M. *Org. Mass Spectrom.* **1991**, *26*, 514–518. Caravatti, P. U.S.-Patent Nr. 4 924 089, dated 8.5.1990.

(26) Searcy, J. Q.; Fenn, J. B. *J. Chem. Phys.* **1974**, *61*, 5282–5288.

(27) Engelking, P. C. *Rev. Sci. Instrum.* **1986**, *57*, 2274–2277.

ions with $k = n + 2$. The same stability pattern was previously observed in reactions of water clusters with ethers and other organic ligands.^{28–34} These stable structures correspond to a hydrophilic, hydrogen bonded $\text{H}^+(\text{H}_2\text{O})_n$ "core", completely terminated by a hydrophobic shell of the organic ligands, with an oxygen (or nitrogen) of the organic molecules bound to each of the $k = n + 2$ peripheral hydrogens. Even these particularly stable cluster ions fragment further, losing both acetone and water ligands. After a sufficiently long time (40 s), all water ligands are lost and a proton solvated with two acetone molecules, $\text{H}^+(\text{C}_3\text{H}_6\text{O})_2$, remains as an essentially unique "final" product ion.

The reactions of the cationic $\text{H}^+(\text{H}_2\text{O})_n$ clusters with acetaldehyde follow a very similar pattern as the reactions of acetone, but with a few important differences. While the protonated water clusters of all sizes studied (up to $n = 80$) efficiently ligand exchange with acetone (Figure 1a), in the case of acetaldehyde ligand exchange only for smaller clusters is observed. For $n > 25$ the rates decrease drastically, and essentially only fragmentation is noticeable for clusters with $n > 48$ (Figure 1b). The probable conclusion that one can draw from this observation is that acetone exchanges ligands with the "neutral" water surface, while acetaldehyde interacts efficiently only with smaller clusters, where the surface is activated by the proximity of the positively charged ionic core. This behavior may be the result of the higher polarity and a somewhat larger dipole moment of the acetone carbonyl group (2.88 D) compared with acetaldehyde (2.75 D). A consequence of this reluctance of larger clusters to ligand exchange with acetaldehyde is that the clusters $\text{H}^+(\text{H}_2\text{O})_n(\text{C}_2\text{H}_4\text{O})_k$ with $n > 2$ form to a much lesser extent than in acetone, and only trace quantities of $n > 4$ clusters are detected.

The differences in the carbonyl properties, and the higher proton affinities of acetone compared with acetaldehyde also result in some interesting differences in the stability of their clusters. This can be exemplified by the fragmentation of the size selected (n, k) = (1, 3) clusters of both species. The $\text{H}^+(\text{H}_2\text{O})(\text{C}_3\text{H}_6\text{O})_3$ loses a water molecule in the first step, resulting in a proton solvated by three acetones, with the final product then being formed by a loss of one of the acetone ligands. The order of fragmentation for the acetaldehyde species is reversed as shown by the first-order kinetics fit of the data (Figure 2), and the $(\text{H}_3\text{O})^+(\text{C}_2\text{H}_4\text{O})_3$ ion first loses an acetaldehyde ligand. The resulting (1, 2) cluster then loses water, forming proton solvated by two acetaldehydes, again an $n = 0$, $k = 2$ final product, with the $n = 0$, $k = 3$ cluster hardly appearing at all.

(b) Reactions of Water Anion Clusters with Acetone and Acetaldehyde. The anion reactions are somewhat complicated by the fact that the initial distribution contains not only "hydrated hydroxyl anion" species $\text{OH}^-(\text{H}_2\text{O})_n$, but also ions of the solvated O^- , O_2^- , O_2H^- types, and for larger values of n also "solvated electrons", $\text{e}^-(\text{H}_2\text{O})_n$, are present. Fortunately, the anions of the $\text{OH}^-(\text{H}_2\text{O})_n$ type are dominant, and only the $\text{O}^-(\text{H}_2\text{O})_n$ species represent a significant impurity. Although a

(28) Hiraoka, K.; Grimsrud, E. P.; Kebarle, P. *J. Am. Chem. Soc.* **1974**, *96*, 3359–3364.

(29) Veenstra, B. R.; Meijers, H. C.; de Lange, P. J.; Kommandeur, J. *Chem. Phys.* **1991**, *156*, 157–162.

(30) Schindler T.; Berg C.; Niedner-Schatteburg G.; Bondybey V. E. *Chem. Phys.* **1995**, *201*, 491–496.

(31) Meot-Ner (Mautner), M. *J. Am. Chem. Soc.* **1992**, *114*, 3312–3322.

(32) Stace, A. J.; Moore, C. *J. Am. Chem. Soc.* **1983**, *105*, 1814–1819.

(33) Stace, A. J.; Shukla, A. K. *J. Phys. Chem.* **1982**, *86*, 865–867.

(34) Stace, A. J.; Shukla, A. K. *J. Am. Chem. Soc.* **1982**, *104*, 5314–5318.

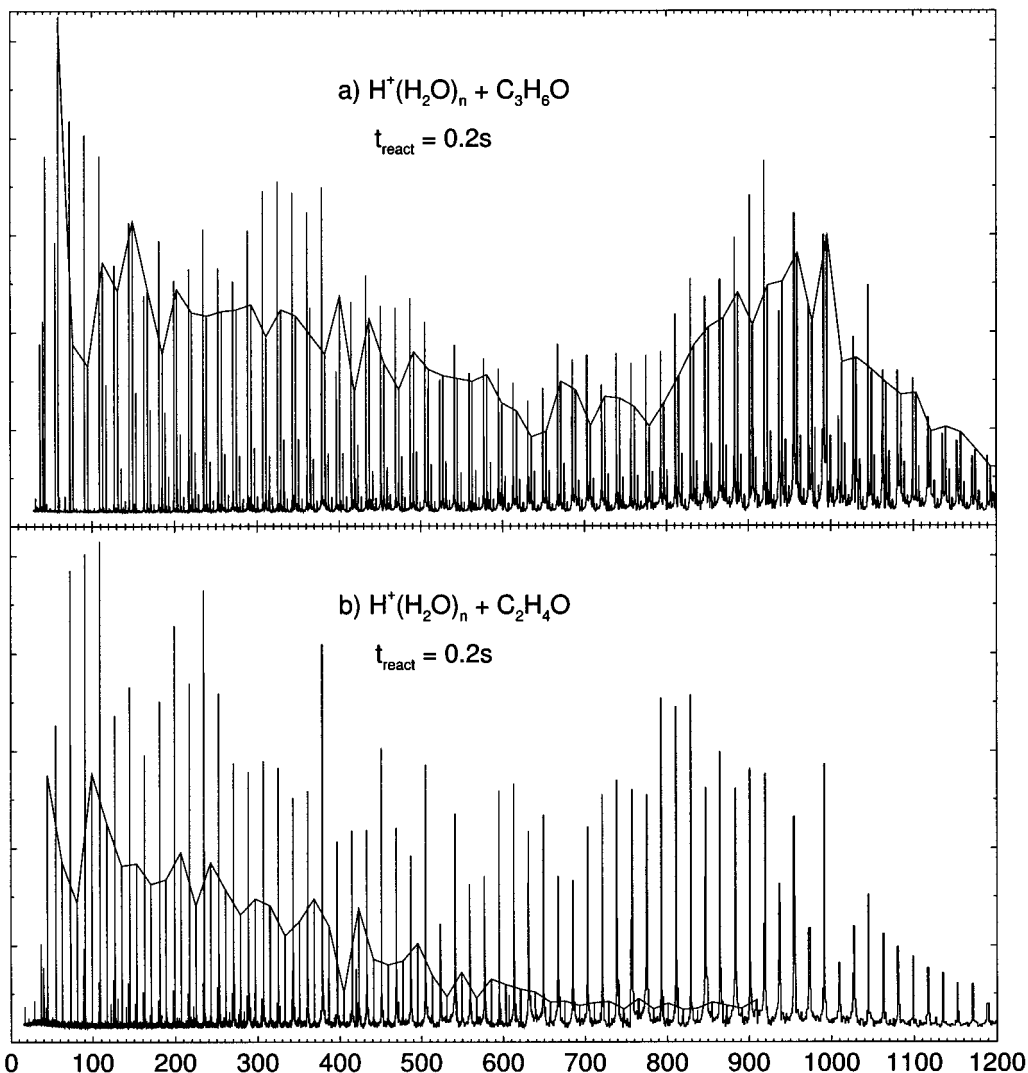


Figure 1. Reactions of protonated water clusters $\text{H}^+(\text{H}_2\text{O})_n$, $n = 2-80$, with acetone (a) and acetaldehyde (b) after a reaction delay of 0.2s ($p = 7 \times 10^{-8}\text{ mbar}$). The solid lines link clusters of the type $\text{H}^+(\text{H}_2\text{O})_m(\text{C}_3\text{H}_6\text{O})$ and $\text{H}^+(\text{H}_2\text{O})_n(\text{C}_2\text{H}_4\text{O})$. While the protonated water clusters ligand exchange over the entire mass range with acetone, only the smaller cluster sizes react with acetaldehyde.

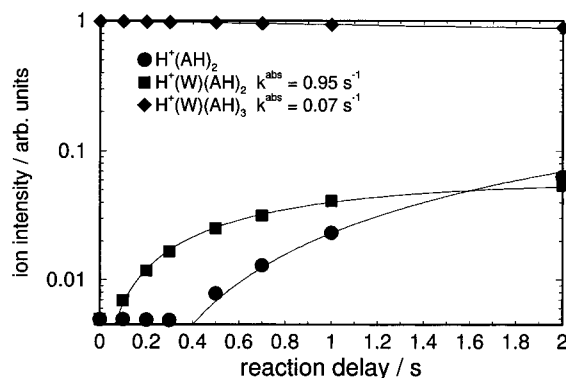


Figure 2. Time-resolved kinetics of the fragmentation of $\text{H}^+(\text{W})(\text{AH})_3$. The solid lines represent a first-order reaction kinetics fit to the data points. $\text{W}_n = (\text{H}_2\text{O})_n$ and $(\text{AH})_n = (\text{CH}_3\text{CHO})_n$.

full separation of the different groups of ions was not practicable, the solvated OH^- and O^- ions differed substantially in their reaction rates, so that their products could easily be distinguished from each other. The other types of ions which are present only in trace amounts simply exchange water for the organic ligands, and their overall contribution to the observed reaction products is very minor.

The hydrated O^- ions react nearly an order of magnitude faster than the other anionic clusters, so that already after about 3 s they are basically absent from the reaction mixture (Figure 3a, denoted by a downward pointing arrow). At the same time, product ions corresponding to the formula $(\text{CH}_3\text{COO})^-(\text{H}_2\text{O})_n$ grow rapidly in intensity. We conclude that the oxygen anion oxidizes the aldehyde to the acetate anion, as described in ref 35 for the naked O^- , with a concomitant loss of a hydrogen atom:



The rate of reaction 1 is surprisingly high for all cluster sizes over the whole mass range. One can argue that in contrast to $\text{OH}^-(\text{H}_2\text{O})_n$, where the hydroxide ion is positioned inside the cluster, the ion O^- may be located near the surface of the cluster, so it is able to react faster with the acetaldehyde molecules. This first step is followed by the uptake of a second acetaldehyde and further fragmentation and loss of the water ligands. Interestingly the last water molecule is not lost even at the longest time studied and remains in the cluster, resulting formally in a $(\text{CH}_3\text{COO})^-(\text{CH}_3\text{CHO})(\text{H}_2\text{O})$ final product (121 amu).

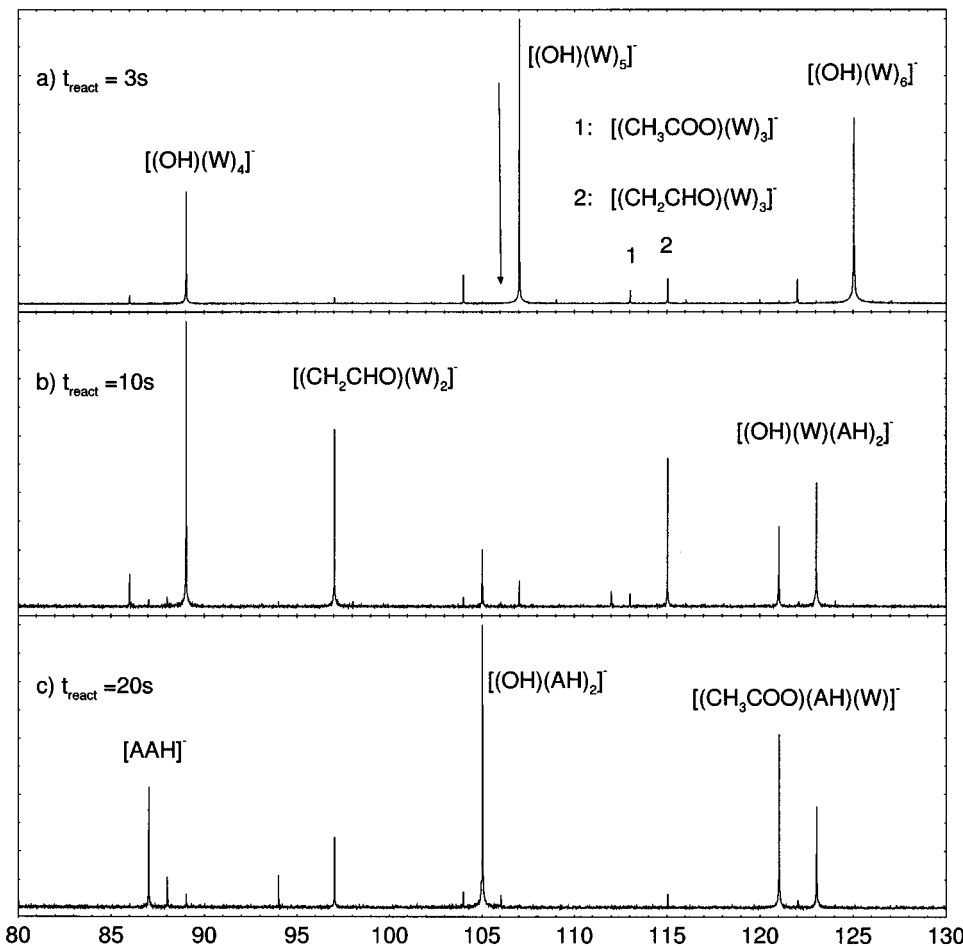


Figure 3. Reaction of anionic water clusters with acetaldehyde ($p = 7 \times 10^{-8}$ mbar) as a function of reaction delay. $\text{O}^-(\text{H}_2\text{O})_n$ clusters react with acetaldehyde an order of magnitude faster than the $\text{OH}^-(\text{H}_2\text{O})_n$ species yielding hydrated acetate ions. The $\text{OH}^-(\text{H}_2\text{O})_n$ react via ligand exchange and proton transfer (a, see text). In a secondary step condensation and aldol formation can take place (b, c). $\text{W}_n = (\text{H}_2\text{O})_n$, $(\text{AH})_n = (\text{CH}_3\text{CHO})_n$, $\text{AAH} = (\text{CH}_3\text{CHO}^-\text{CH}_2\text{CHO})$ — aldolate adduct.

Most interesting for the purpose of the present study are the most abundant cluster anions, of the type $\text{OH}^-(\text{H}_2\text{O})_n$. These react considerably more slowly, and as in the case of cations, the first reaction step formally appears to be a ligand exchange, and formation of ions containing one aldehyde ligand, $\text{OH}^-(\text{H}_2\text{O})_n(\text{C}_2\text{H}_4\text{O})$. In the second reaction step ions containing two ligands, that is corresponding to an overall formula $\text{OH}^-(\text{H}_2\text{O})_n(\text{C}_2\text{H}_4\text{O})_2$, are formed, but in contrast to the cation reactions, there is little evidence of formation of ions containing three or more organic ligands (Figure 3b). This may partially be due to the fact that the initial cluster anion distribution was narrower than that for the cations, with only species up to about $n = 30$ being efficiently produced.

In subsequent reactions, the clusters fragment and gradually lose their water ligands, forming smaller $\text{OH}^-(\text{H}_2\text{O})_n(\text{C}_2\text{H}_4\text{O})_2$, and the process is essentially complete after about 20 s (Figure 3c). Interestingly, the major product is not only an ion with 105 amu, corresponding to $n = 0$, but also a peak at 87 amu, 18 mass units lower, which would formally correspond to $n = -1$. This dominant product, a $(\text{C}_4\text{H}_7\text{O}_2)^-$ anion, indicates that the reactions occurring in this case are not simple exchange and loss of water ligands. Since at least one hydrogen atom from the acetaldehyde molecules is also lost, a more complex chemistry must be taking place, with covalent bonds being broken and perhaps also formed, and acetaldehyde losing its chemical identity. Furthermore, even though the mass 87 corresponds formally to a water molecule loss from the 105

amu species, the two ions are clearly not purely sequential fragmentation products. Their time evolution indicates that they grow in more or less in parallel, and even though already after about 10 s appreciable mass 87 ion signal is present, further fragmentation of the remaining mass 105 amu ions is quite inefficient. This can be seen in Figure 4a, where after 60 s the 105 amu peak remains quite prominent, comparable to the mass 87, and it persists with comparable intensity even after 150 s, the longest time investigated. It is rather clear that the two persistent peaks at 105 and 87 amu are two independent, structurally different products.

To gain more insight into the reactions occurring in the clusters, and to identify the source of the hydrogen atom being lost from the cluster, we have examined the reactions of isotopically substituted, deuterated acetaldehydes. The product spectrum resulting from reactions of acetaldehyde- d_1 , CH_3CDO , is shown in Figure 4b. All three major final products are shifted by two units to higher masses, indicating that both deuterium atoms are being retained, and that the hydrogen atom lost from the 87 amu product originates from the methyl, and not from the aldehydic group.

The conclusion that the mass peaks 105 and 87 are two chemically different species and not just sequential fragmentation products is confirmed by experiment with perdeuterated acetaldehyde- d_4 , exemplified by spectrum c in Figure 4. Here the mass peak at 105 amu in Figure 4a shifts to 113 amu confirming that all eight deuterium atoms are retained in this

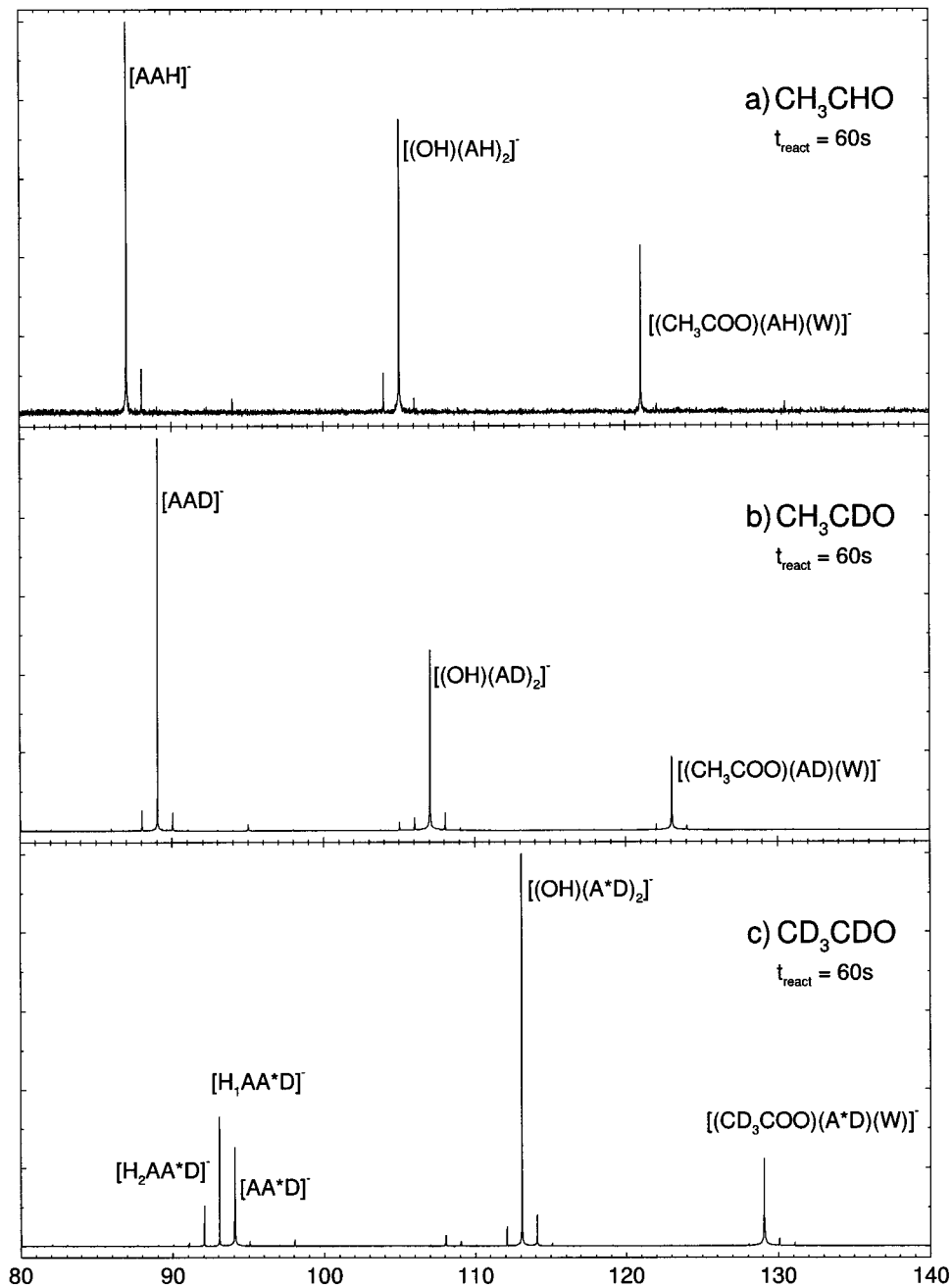
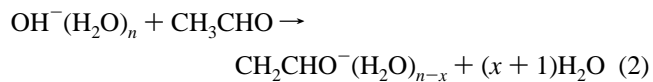


Figure 4. Reaction of $\text{OH}^-(\text{H}_2\text{O})_n$ and $\text{O}^-(\text{H}_2\text{O})_n$ with (a) acetaldehyde (CH_3CHO), (b) CH_3CDO , and (c) CD_3CDO (delay 60 s; $p = 7 \times 10^{-8}$ mbar); W = H_2O ; AH = CH_3CHO ; AD = CH_3CDO ; A*D = CD_3CDO ; AAH = $\text{CH}_3\text{CHO}^-\text{CH}_2\text{CHO}$ aldol; AAD = $\text{CH}_3\text{CDO}^-\text{CH}_2\text{CDO}$ (note that both D atoms remain in the product); AA*D = $\text{CD}_3\text{CDO}^-\text{CD}_2\text{CDO}$. Note peaks resulting from isotopic exchange 1, 2, and 3 amu below the fully deuterated product—see text.

product and no isotopic exchange with the water solvent has taken place. Similarly also the 121 amu signal shifts by eight mass units to 129 amu, indicating no deuterium loss. A quite different story is told by the third, 87 amu, product peak, which is replaced by strong signals at 94, 93, and 92 amu, with weak signals appearing also at mass 91 and 90. It is apparent that, in addition to the loss of one deuterium atom from the methyl group, in many of the product ions also one, two, or possibly even three or four additional deuterium atoms have been exchanged for hydrogens from the water “solvent”.

One can understand the results if one recalls the basic properties of carbonyl compounds, and reactions of aldehydes and ketones in basic solutions. In the first reaction step the acetaldehyde molecule apparently interacts with the “surface” of the hydrated hydroxide cluster, with a proton being trans-

ferred to the OH^- group, and a hydrated CH_2CHO^- anion being formed.

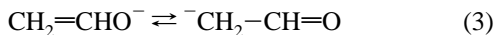


The above reaction is postulated to occur in basic aqueous solutions, and for the specific $n = 1$, $x = 1$ case, that is for OH^- bound to one molecule of water, it was in fact previously studied in the gas phase by Tanner et al.³⁶ They determined the absolute rate constant of the reaction of $\text{OH}^-(\text{H}_2\text{O})$ with

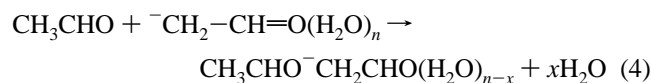
(35) Lee, J.; Grabowski, J. *J. Chem. Rev.* **1992**, 92, 1611–1645.

(36) Tanner, S. D.; Mackay, G. I.; Bohme, D. K. *Can. J. Chem.* **1981**, 59, 1615–1621.

acetaldehyde to be $(3 \pm 1) \times 10^{-9} \text{ cm}^3 \text{ molecules}^{-1} \text{ s}^{-1}$, nearly equal to the rate constant of the reaction of naked OH^- ($k^{\text{abs}} = (3.1 \pm 0.8) \times 10^{-9} \text{ cm}^3 \text{ molecules}^{-1} \text{ s}^{-1}$). With the help of deuterated measurements Stewart et al. and the group of Bohme^{37,38} were able to show that the proton transferred to the OH^- originates from the methyl group. The resulting CH_2CHO^- ion can be formally written as an equilibrium between two ionic forms, aldehydic and enolate:



In the presence of a second acetaldehyde (or another molecule containing a carbonyl bond), a nucleophilic addition of the anion to the carbonyl group of the nonionized molecule can take place, forming an anion of dimer containing both alcoholic and aldehydic groups, "aldol". This sequence of steps, that is reaction of the OH^- "catalyst" with a molecule of acetaldehyde (reaction 2), and the subsequent nucleophilic addition of the resulting enolate anion to a carbonyl group of a second molecule (reaction 4) is known in organic chemistry as the "aldol addition reaction":³⁹



In the finite size cluster, the reaction enthalpy will heat the cluster, and may result in evaporating one or more water molecules from the cluster ion. Due to the competition of blackbody heating and collisional fragmentation, we can make no definitive statement as to how many water molecules are lost in this process. In subsequent reaction steps further fragmentation and loss of complexed water molecules take place. A final, unique product of the reaction sequence at very long times is the aldolate dimer anion, $\text{C}_4\text{H}_7\text{O}_2^-$ at 87 amu. The presence of the hydroxyl anion in the cluster thus catalyzes dimerization of the acetaldehyde, the same way it does in strongly basic aqueous solutions.

Examination of reaction sequence 2 and 4 reveals that the aldehydic hydrogen is not involved. This is consistent with the results of experiments with CH_3CDO , that is acetaldehyde deuterated in the aldehydic group. The aldehydic hydrogens cannot exchange with the water solvent, and accordingly both deuterium atoms are retained with the final aldolate product, $\text{CH}_3\text{CDO}^- \text{CH}_2\text{CDO}$, which occurs at mass 89. In the perdeuteroacetaldehyde experiment, where the methyl group is also deuterated, the situation is different. In the course of the proton-transfer reaction 2, one of the deuterium atoms from the methyl group is lost to the water solvent. Since the proton transfer is reversible and can repeatedly proceed back and forth, more than one deuterium may be exchanged and lost from the final products. Accordingly, besides a fully deuterated aldolate at 94 amu, also products at masses 93, 92, and even 91 are detected, corresponding to an exchange of 1, 2, or even 3 deuterium atoms, in addition to the one lost in the condensation.

Interesting is the presence of the persistent product at mass 105 in Figure 4a. This signal after long reaction times is apparently not due to the condensed aldolate ion with one molecule of water, but is the result of "failed" aldol addition, which can perhaps be seen structurally as an OH^- anion "solvated" by two acetaldehyde molecules. Consistent with this

picture are the results of the isotopic experiments. Both deuterium atoms are retained in the CH_3CDO experiment with the product appearing at 107 amu, and the product shifts to mass 113 in the perdeutero study, again indicating all eight deuterium atoms are retained, and none have been exchanged and lost with the evaporating water solvent.

We have noted above that a cluster with one OH^- and 55 water molecules can be compared with a strongly basic solution with $\text{pH} = 14$. Extending this argument, one could predict that by further loss of water ligands the cluster will become increasingly "basic", further increasing the rate of base-catalyzed reactions. The presence of the mass 105 complex indicates that this is not the case. The aldol addition does not occur in the complete absence of water, and a minimum number of solvent molecules is apparently required for an efficient condensation to take place. If too many solvent molecules were lost before the condensation took place, only a complex ion, rather than the aldolate, will form as a final product. Unfortunately, competition of cluster fragmentation with their reactions makes it difficult to determine this minimum amount of solvent needed. Such an experiment could, however, easily be done in an instrument with cooled walls, where the blackbody fragmentation would be suppressed.

A further support for this interpretation and the presence of two independent, structurally different products can be found by observing the time evolution of the individual mass signals. It is clear that one cannot explain the 93, 92, or 91 amu signals in the perdeuteroacetaldehyde experiment (Figure 4c) as "dehydration" products of the prominent 113 amu ion. Loss of H_2O or HDO could only produce masses 95 and 94, respectively. The formation of the lighter, deuterium-depleted products must proceed via deuterium-depleted hydrated ions at mass 112 or 111. This can be verified by comparing the time evolution of the fully deuterated d_8 complex at mass 113 with, for instance, the 112 amu peak. While the 113 mass signal continuously grows during the experiment, as is appropriate for a final product, the 112 amu peak goes through a maximum at much earlier times, and is nearly absent in the final spectrum (Figure 4c). It disappears almost completely by losing ligand water, and contributes to the 93 and 92 amu aldolate anion final products.

As mentioned previously, the third rather strong peak appearing in the spectrum in Figure 4a, mass 121, is the final product of the $\text{O}^-(\text{H}_2\text{O})_n$ reactions, and corresponds at least formally to an acetate anion, CH_3COO^- , solvated with one water molecule and one additional acetaldehyde ligand, $(\text{CH}_3\text{COO})^-(\text{CH}_3\text{CHO})(\text{H}_2\text{O})$. Interesting and somewhat puzzling is the retention of all eight deuterium atoms in this product, which as noted above shifts from 121 to 123 amu in the acetaldehyde- d_1 and to 129 amu in the perdeutero experiment, indicating no deuterium exchange and loss. Perhaps the final product is an acetate ion bound over the water molecule and strong hydrogen bonds to the second aldehyde. The strong bonds to the bridging water molecule might perhaps explain the observed lack of deuterium loss and isotopic exchange.

The aldol addition is not a property of aldehydes alone, but can also take place in other compounds containing carbonyl groups, in particular ketones. In the present work, we have also examined, although in somewhat less detail, the reactions of anionic water clusters with acetone. As in the aldehyde case, we observe also for acetone an efficient aldol condensation. A similar OH^- catalyzed sequence of reactions, as described for the aldehydes, takes place in the hydrated hydroxyl anions, $\text{OH}^-(\text{H}_2\text{O})_n$. In the case of acetone it leads efficiently to a

(37) Stewart, J. H.; Shapiro, R. H.; DePuy, C. H.; Bierbaum, V. M. *J. Am. Chem. Soc.* **1977**, *99*, 7650–7653.

(38) Rakshit, A. B.; Bohme, D. K. *Can. J. Chem.* **1983**, *61*, 1683–1689.

(39) Streitwieser, A.; Heathcock, C. H. *Organische Chemie*; VCH: Weinheim, 1986.

$C_6H_{11}O_2$ -condensation product. This ion, the anion of 4-hydroxy-4-methyl-2-pentanone, is a well-known product of the aldol addition of acetone. The aldol condensation in solutions is an equilibrium process whose equilibrium constants are in the case of ketones often fairly unfavorable, leading to small yields. In the present case, the two acetone molecules are trapped in the same cluster. Evaporation of the water solvent prevents the reverse process from occurring once the addition has taken place, and the reaction proceeds almost completely to the addition product.

IV. Summary

In this paper we examine and compare the reactions of the simple organic compounds acetone and acetaldehyde with ionic water clusters. The results indicate that both acetone and

acetaldehyde react quite differently in hydrated proton, $H^+(H_2O)_n$, and hydrated hydroxyl, $OH^-(H_2O)_n$ clusters. While in the former, "acid" clusters only ligand exchange is observed, in the latter case OH^- catalyzed addition of two molecules of the carbonyl compound takes place, and a true covalent bond between them is formed. The reactions thus parallel the behavior of carbonyl compounds in strongly basic solutions, and in the hydrated hydroxyl anions an efficient OH^- catalyzed aldol addition takes place.

Acknowledgment. Financial support of the Deutsche Forschungsgemeinschaft through the Schwerpunktprogramm Molekulare Cluster and by the Fonds der Chemischen Industrie is gratefully acknowledged.

JA971869T

Interaction of Sugar and Anion in Water via Hydrogen Bonding: Chain-Length Dependent Agglutination of Oligosaccharide Clusters Induced by Multivalent Anion Binding

Osamu Hayashida, Masaki Kato, Kazuyuki Akagi, and Yasuhiro Aoyama*

Institute for Fundamental Research of Organic Chemistry
Kyushu University, Hakozaki, Higashi-ku
Fukuoka 812-8581, Japan
CREST
Japan Science and Technology Corporation (JST)

Received July 26, 1999

Oligosaccharides on the cell surfaces play important roles in various cellular recognition processes.¹ However, the chemical basis of information storage in oligosaccharides is still poorly understood. Simple saccharides (sugars), like simple salts, are too hydrophilic (extensively hydrated) to form hydrogen-bonded complexes in water. They can be strongly bound only under solvophobic conditions, i.e., in organic media.² The binding of such hydrophilic species in water is one of the most intriguing problems in molecular recognition. The present work is concerned with sugar–anion interaction, where sugar is a macrocyclic oligosaccharide cluster.³ We report here that the anions, especially the phosphates, are readily incorporated into clustering oligosaccharide pools via hydrogen bonding, thereby inducing chain-length dependent agglutination of the clusters.

Calix[4]resorcarene, with four alkyl (undecyl) tails in the present case, is a bowl-shaped resorcinol cyclic tetramer. As reported,^{3b} reaction of the aminoethoxy derivative with lactone of $\alpha(1\rightarrow 4)$ -linked diglucose (maltose) gives an amide-linked octakis(diglucose) compound (G2, Figure 1a). A similar reaction with that of pentaglucose (maltopentose) in methanol at 60 °C for 6 h affords (61% yield) the corresponding pentaglucose cluster G5 (molecular weight, 8065) having 40 glucose residues.⁴ Figures 1b (G2) and 1c (G5) show the schematic structures and space-filling CPK models. Cluster G5, like G2, is miscible with water (solubility, > 1 g/mL, i.e., ≥ 0.1 M) but is readily agglutinated by a phosphate salt such as Na₂HPO₄/NaH₂PO₄, Na₂RP (RP = D-ribose-5-phosphate), and nucleotides such as Na₂GMP (GMP = guanosine-5'-monophosphate) (Figure 1d) to give precipitates of a composition of G5:(HPO₄²⁻/H₂PO₄⁻) ≈ 1:50 or G5:RP²⁻ ≈ 1:10.

NMR studies reveal that complexation of the phosphate anions is taking place. (1) The ³¹P NMR signals for dianionic guests Na₂HPO₄ (line a) or Na₂RP (line b) 2 mM in D₂O-DMSO-*d*₆ (9:1)⁵ undergo upfield shifts in the presence of host G5 until

(1) (a) Hakomori, S. *Pure Appl. Chem.* 1991, 63, 473–482. (b) Kobata, A. *Acc. Chem. Res.* 1993, 26, 319–324.

(2) (a) Aoyama, Y.; Tanaka, Y.; Sugahara, S. *J. Am. Chem. Soc.* 1989, 111, 5397–5404. (b) Bonar-Law, R. P.; Davis, A. P.; Murray, B. A. *Angew. Chem., Int. Ed. Engl.* 1990, 29, 1407–1408. (c) Savage, P. B.; Gellman, S. H. *J. Am. Chem. Soc.* 1993, 115, 10448–10449. (d) Bonar-Law, R. P.; Sanders, J. K. M. *J. Am. Chem. Soc.* 1995, 117, 259–271. (e) Anderson, S.; Neidlein, U.; Gramlich, V.; Diederich, F. *Angew. Chem., Int. Ed. Engl.* 1995, 34, 1596–1599. (f) Mizutani, T.; Kurahashi, T.; Murakami, T.; Matsumi, N.; Ogoshi, H. *J. Am. Chem. Soc.* 1997, 119, 8991–9001. (g) Davis, A. P.; Wareham, R. *Angew. Chem., Int. Ed.* 1998, 37, 2270–2273.

(3) (a) Fujimoto, T.; Shimizu, C.; Hayashida, O.; Aoyama, Y. *J. Am. Chem. Soc.* 1997, 119, 6676–6677. (b) Fujimoto, T.; Shimizu, C.; Hayashida, O.; Aoyama, Y. *J. Am. Chem. Soc.* 1998, 120, 601–602.

(4) Anal. Calcd for C₃₂₈H₅₅₂N₈O₈·2H₂O: C, 48.60; H, 6.92; N, 1.38. Found: C, 48.40; H, 6.98; N, 1.55.

(5) Dynamic light scattering (DLS) shows that larger aggregates result from G5 (0.1 mM) and Na₂HPO₄ (10 mM) with higher contents of DMSO as an organic cosolvent; average diameter of aggregates in μ m (% DMSO content) = 3 (0) < 6 (10) < 11 (20). In the absence of Na₂HPO₄, there is no DLS-detectable aggregation of G5 in H₂O-DMSO (9:1).

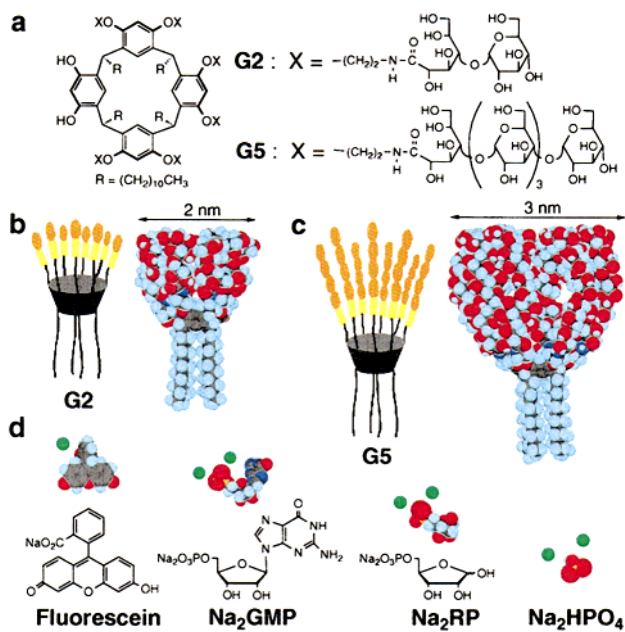


Figure 1. Structures of hosts (a–c) and guests (d). The saccharide moieties in schematic cluster structures in b and c are colored. The C, O, N, and P atoms and Na⁺ ions in space-filling models are shown in black, red, dark blue, light blue, orange, and green, respectively.

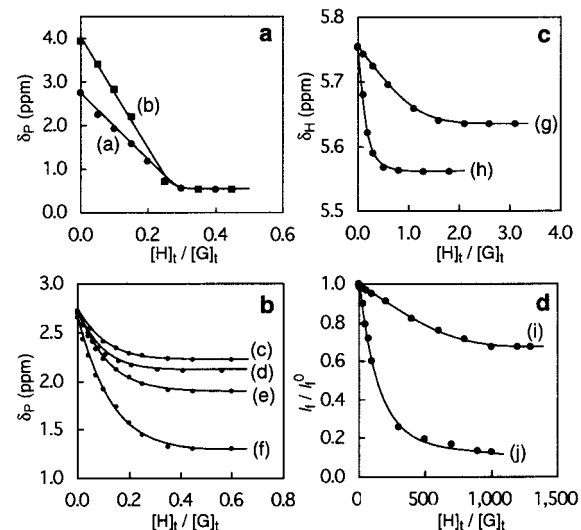


Figure 2. NMR and fluorescence titration of guests with host G2 or G5 at 25 °C: (a) ³¹P NMR (at 243 MHz) chemical shifts (δ_P , in reference to external H₃PO₄ in D₂O ($\delta_P = 0$)) for Na₂HPO₄ (a) and Na₂RP (b) (2 mM) with host G5 in D₂O-DMSO-*d*₆ (9:1). (b) ³¹P NMR chemical shifts (δ_P) for Na₂HPO₄ (2 mM) with host G2 in D₂O-DMSO-*d*₆ (10:0, c), (9:1, d), (7:3, e) or (5:5, f). (c) ¹H NMR (at 600 MHz) chemical shifts (δ_H) for 1'-H of the ribose ring of GMP (0.2 mM) with host G2 (g) or G5 (h) in D₂O-DMSO-*d*₆ (9:1). (d) Relative fluorescence intensities (I_r/I_r^0) for fluorescein (0.1 μ M) with host G2 (i) or G5 (j) in H₂O at pH 7.0 (HEPES) (I_r^0 refers to I_r in the absence of host). The change in pH, if any, resulting from addition of the host is too small to account for the host-induced change in chemical shifts.

saturation is reached at $[H]/[G] \approx 0.3$ (Figure 2a) (H = host, G = guest, and t = total). The complexation-induced shifts (CIS) of 2.2 ppm for HPO₄²⁻ and 3.4 ppm for RP²⁻ amount to 88 and 94%, respectively, of the chemical shift differences ($\Delta\delta_P$) between dianion and monoanion (2.5 ppm for HPO₄²⁻/H₂PO₄⁻ and 3.6 ppm for RP²⁻/HRP⁻). While concurrent turbidity precludes any

quantitative analysis, the data show that a large number ($\gg 1$) of dianions HPO_4^{2-} or ribose-5-OPO₃²⁻ are simultaneously bound to host G5 via strong host-to-guest hydrogen-bonding or even protonation to lead essentially (~90%) to the monoanionic state, H_2PO_4^- ($\delta_p = 0.15$) or ribose-5-O(H)PO₃⁻ ($\delta_p = 0.45$), as if the guests were in an environment of pH ≤ 6 ($pK_a = 7.0$ for $\text{HPO}_4^{2-}/\text{H}_2\text{PO}_4^-$). Fifty percent complexation occurs for both guests at $[\text{H}]/[\text{G}]_t \approx 0.15$ (Figure 2a), i.e., at host concentration of $[\text{H}]_{50} \approx 0.3 \text{ mM}$ ($[\text{G}]_t = 2 \text{ mM}$). The implication of $[\text{H}]_{50}$ is that $K_{\min} = 1/[\text{H}]_{50} \approx 3 \times 10^3 \text{ M}^{-1}$ represents the lower limit of the binding constant of H for a molecule of G, $\text{H} + \text{G} \rightleftharpoons \text{H}\cdot\text{G}$.⁶⁽²⁾ The short-chain host G2 also binds the guests, keeping apparently transparent solutions. Dianionic guests Na₂HPO₄ and Na₂RP in D₂O-DMSO-*d*₆ (9:1)⁵ exhibit a CIS of 0.6 ppm for Na₂HPO₄ (Figure 2b, line d) or 0.57 ppm for Na₂RP (not shown for clarity), corresponding to ~20% protonation. The saturation of Na₂HPO₄ occurs at $[\text{H}]/[\text{G}]_t \approx 0.4$, $K_{\min} \approx 7 \times 10^5 \text{ M}^{-1}$ being evaluated from $[\text{H}]_{50} \approx 0.15 \text{ mM}$ in a similar manner as above. As regards the solvent effects, % protonation (CIS/ $\Delta\delta_p \times 100$) increases with increasing contents of DMSO, in accord with the host-to-guest (G2-to-HPO₄²⁻) hydrogen-bonding; % protonation (CIS, $\Delta\delta_p$, % DMSO content) = 20 (0.49, 2.43, 0) < 24 (0.60, 2.53, 10) < 30 (0.83, 2.79, 30) < 45 (1.36, 3.06, 50) (Figure 2b). (3) The complexation of nucleotides at 0.2 mM can be followed also by ¹H NMR, i.e., by monitoring the diagnostic upfield shifts (0.1–0.2 ppm) for 1'-H on the ribose ring. The titration curves, as typically shown for GMP (Figure 2c, line g), fit with a 1:1 host:guest stoichiometry (also confirmed by Job plots) with $K = 4.0 \times 10^3$ (Na₂AMP), 1.6×10^4 (Na₂GMP), 2.9×10^4 (Na₂ADP), 3.7×10^4 (Na₂ATP), 1.3×10^4 (AMP), and $3.8 \times 10^4 \text{ M}^{-1}$ (GMP) from computer-aided least-squares curve-fitting (AMP and GMP are free acids in the zwitterionic form having a monoanionic phosphate group and AM(D)(T)P = adenosine-5'-mono(di)(tri)phosphate). The phosphate groups are responsible for the binding, since nucleoside adenosine lacking the phosphate group neither shows any detectable affinity to the host nor inhibits the complexation of nucleotides. (4) Long-chain host G5 binds GMP and AMP more efficiently with a saturation occurring at $[\text{H}]/[\text{G}]_t \approx 0.8$ for GMP (Figure 2c, line h); $K_{\min} \approx 3 \times 10^4 \text{ M}^{-1}$ for GMP and $2 \times 10^4 \text{ M}^{-1}$ for AMP. (5) Thus, the larger host G5 exhibits 1:*n* H:G stoichiometries (*n* > 1) even for the largest nucleotide guests, while that of the smaller host G2 is 1:1 except for the smallest Na₂HPO₄ guest. This may be easily understood on the basis of the sizes of hosts and guests (Figure 1). A Scatchard analysis⁷ of the titration data gives the values of *n* ≈ 10 for Na₂HPO₄ with G2 and *n* ≈ 4 for GMP and AMP with G5.

Other relevant points are as follows. (6) DLS (dynamic light scattering) and TEM (transmission electron microscopy) show that Na₂HPO₄ immediately induces aggregation of both G2 and G5 (0.1–1 mM in water) to give spheres/vesicles ($d = 100$ –400 nm), which further grow to μm -sized particles either very rapidly (in minutes) in case of G5⁵ or slowly (in days) in case of G2.⁸ (7) Host G5 is agglutinated/precipitated by various salts such as sulfate (Na₂SO₄), sulfonate (2,4,6-(O₂N)₃C₆H₄SO₃Na), borate (Na₃BO₃), perchlorate (NaClO₄), and dicarboxylate (sodium oxalate) in addition to phosphates but not by monocarboxylate

(6) If we assume that successive addition of G to H having *n* unit-binding sites (h) occurs independently ($\text{h} + \text{G} \rightleftharpoons \text{h}\cdot\text{G}$), the equilibrium constant can be expressed as $K_{\text{unit}} = k_{\text{a(hG)}}/k_{\text{d(hG)}} = [\text{h}\cdot\text{G}]/[\text{h}][\text{G}] = 1/(n[\text{H}]_{50} - 0.5[\text{G}]_t)$ at 50% complexation ($[\text{h}\cdot\text{G}] = [\text{G}]$) (k_a and k_d are association and dissociation rate constants). For the equilibrium $\text{H} + \text{G} \rightleftharpoons \text{H}\cdot\text{G}$, $k_{\text{a(hG)}} \approx nk_{\text{a(hG)}}$ for a statistical reason and $k_{\text{d(hG)}} \approx k_{\text{d(hG)}}$ and hence $K = k_{\text{a(hG)}}/k_{\text{d(hG)}} \approx nk_{\text{a(hG)}}/k_{\text{d(hG)}} = nK_{\text{unit}} = n/(n[\text{H}]_{50} - 0.5[\text{G}]_t) = 1/([\text{H}]_{50} - 0.5[\text{G}]_t/n) > 1/[\text{H}]_{50}$ (*n* < ∞).

(7) Scatchard, G. *Equilibrium in Solutions; Surface and Colloid Chemistry*; Harvard University Press: Cambridge, 1976.

(8) For aggregation behaviors of glycolipids and related amphiphiles, see: (a) Fuhrhop, J.-H.; Helfrich, W. *Chem. Rev.* **1993**, *93*, 1565–1582. (b) Takeoka, S.; Sou, K.; Boettcher, C.; Fuhrhop, J.-H.; Tsuchida, E. *J. Chem. Soc., Faraday Trans.* **1998**, *94*, 2151–2158.

(NaOAc) or halide (NaCl). (8) Simple saccharides such as maltose and maltpentaose and *N*-methylacetamide as single-chain or amide-linkage references of the present cluster hosts are inert to Na₂HPO₄, causing neither shifts in δ_p nor agglutination. (9) Fluorescein (Figure 1d) with $pK_a = 6.7$ forms a 1:1 complex with host G2 ($K = 1.1 \times 10^4 \text{ M}^{-1}$ from Benesi–Hildebrand analysis) or G5 ($K = 5.4 \times 10^4 \text{ M}^{-1}$) under conditions of host excess at pH = 7.0. The bound guest thereby loses 33% (with G2) or 87% (with G5) of the original fluorescence intensity (I_f^0) (Figure 2d) as if it were in an environment of pH = 6.6 (G2) or 5.4 (G5). This is in accord with the NMR results (items 1 and 2).

Combined evidence indicates that (a) anions are incorporated in the clustering oligosaccharide pools of hosts G2 and G5 via hydrogen bonding and (b) the hosts thereby undergo coaggregation with multivalent anions in a biphasic manner, i.e., rapid formation of submicrometer-sized particles followed by their oligosaccharide chain-length dependent agglutination.

Known examples of saccharide complexation in water are driven by hydrophobic (CH- π) forces.⁹ The phosphates form salts with cationic (mostly ammonium) hosts in both organic¹⁰ and aqueous¹¹ media. In this regard, the present interaction between the saccharide host (neutral) and an inorganic anion HPO₄²⁻ (by no means hydrophobic) in water (item a) must be free from any hydrophobic/CH- π or electrostatic assistance. Still, the binding affinity of $K \gg K_{\min} = 3 \times 10^3 \text{ M}^{-1}$ for G5 is comparable with those in the order of 10^{1-4} M^{-1} for the hydrogen-bonded saccharide-phosph(on)ate complexes in organic media.^{2e,12} In view of their amphiphilic nature, it is not surprising that the present hosts form aggregates, where the multiple hydrogen-bond forming anions may cross-link or glue the oligosaccharide chains in an intramolecular (intracluster), intermolecular (intercluster), or interaggregate fashion. The chain-length dependent agglutination (item b) may be taken in light of oligosaccharide-triggered cell adhesion.¹³

To summarize, the clustering oligosaccharide chains fixed on a rigid macrocycle act as a *macrosolvent* for anions. Simple salts which are otherwise soluble only in water can be readily extracted from water into the clusters. The present work may thus open an important yet unexplored area of molecular recognition of highly polar species in water and may also provide a clue to understand how oligosaccharides can be informative, e.g., adhesive, particularly in reference to the so-called saccharide cluster effects.¹⁴

Acknowledgment. This work was supported by Grants-in-Aid (Nos. 08CE2005 and 10134227) from the Japanese Government and also by CREST of Japan Science and Technology Corporation (JST).

JA992876F

(9) (a) Kobayashi, K.; Asakawa, Y.; Kato, Y.; Aoyama, Y. *J. Am. Chem. Soc.* **1992**, *114*, 10307–10313. (b) Poh, B.-L.; Tan, C. M. *Tetrahedron* **1993**, *49*, 9581–9592. (c) Jiménez-Barbero, J.; Junquera, E.; Martínpastor, M.; Sharma, S.; Vicent, C.; Penadés, S. *J. Am. Chem. Soc.* **1995**, *117*, 11198–11204. (d) Morales, J. C.; Penadés, S. *Angew. Chem., Int. Ed.* **1998**, *37*, 654–657.

(10) (a) Král, V.; Furuta, H.; Shreder, K.; Lynch, V.; Sessler, J. L. *J. Am. Chem. Soc.* **1996**, *118*, 1595–1607. (b) Schmidtchen, F. P.; Berger, M. *Chem. Rev.* **1997**, *97*, 1609–1646.

(11) (a) Lehn, J.-M. *Angew. Chem., Int. Ed. Engl.* **1990**, *29*, 1304–1319. (b) Hosseini, M. W.; Blacker, A. J.; Lehn, J.-M. *J. Am. Chem. Soc.* **1990**, *112*, 3896–3904. (c) Schneider, H.-J.; Mohammad-Ali, A. K. In *Comprehensive Supramolecular Chemistry*; Lehn, J.-M., Atwood, J. L., Davies, J. E. D., MacNicol, D. D., Vögtle, F., Eds.; Elsevier: Oxford, 1996; Vol. 2, Chapter 3.

(12) (a) Das, G.; Hamilton, A. D. *J. Am. Chem. Soc.* **1994**, *116*, 11139–11140. (b) Cotterón, J. M.; Hackett, F.; Schneider, H.-J. *J. Org. Chem.* **1996**, *61*, 1429–1435. (c) Das, G.; Hamilton, A. D. *Tetrahedron Lett.* **1997**, *38*, 3675–3678. (d) Dondoni, A.; Marra, A.; Scherrmann, M. C.; Casnati, A.; Sansone, F.; Ungaro, R. *Chem. Eur. J.* **1997**, *3*, 1774–1782.

(13) (a) Eggens, I.; Fenderson, B.; Toyokuni, T.; Dean, B.; Stroud, M.; Hakomori, S. *J. Biol. Chem.* **1989**, *264*, 9476–9484. (b) Kojima, N.; Hakomori, S. *J. Biol. Chem.* **1989**, *264*, 20159–20162.

(14) Lee, Y. C.; Lee, R. T. *Acc. Chem. Res.* **1995**, *28*, 321–327.

Microsolvation and Chemical Reactivity of Sodium and Water Clusters

Christopher J. Mundy, Jürg Hutter, and Michele Parrinello*

Max-Planck-Institut für Festkörperforschung
Heisenbergstrasse 1, 70569 Stuttgart, Germany

Received December 30, 1999

It has long been known that sodium and water react violently, yielding sodium hydroxide and hydrogen gas. Although this is a showcase reaction, the mechanism is still not fully understood. Motivated by recent experimental findings,^{1,2} we report a novel mechanism of the reaction of sodium and water in a molecular beam through a detailed first principles molecular dynamics investigation. While it is clear that the bulk-phase reactions proceed without difficulty, special conditions are necessary in order for the same reaction to occur in a beam.

Recent experimental observations have indicated that at least three sodium atoms must be present to initiate the chemistry.^{1,2} More specifically, it is the presence of a solvated sodium atom and its interaction with a sodium dimer that will give rise to the reactive species. To explain this unexpected observation, we used the Car–Parrinello molecular dynamics (CPMD) method.³ Using the experimental conditions as a guide, we started with initial conditions (reactants) of an equilibrated sodium water cluster ($\text{Na}(\text{H}_2\text{O})_6$) and a sodium dimer. We used plane waves as a basis within local spin density (LSD) functional theory with an energy cutoff of 70 Ry and a BLYP gradient-corrected functional.^{4,5} Norm-preserving pseudopotentials were used to describe the oxygen, hydrogen,⁶ and sodium cores. In the case of Na, the $2s^2$ – $2p^63s^1$ electrons were included explicitly.⁷ The CPMD dynamics were performed in an isolated cubic cell of length 15.87 Å using the Poisson solver of Martyna and Tuckerman.⁸

Our novel mechanism begins with the dissociation of the sodium dimer to yield a polarized Na^- and a solvated Na^+ . To explain this prediction we examine the electronic structure of $\text{Na}(\text{H}_2\text{O})_6$ cluster. To obtain a chemically intuitive description of the electronic structure we used the Boys localization⁹ criterion which obtains localized orbitals that minimize the fluctuations in the position operator for each electronic state.^{10,11} This methodology also affords us the centroid and spread of the orbital. It is known from a previous study of liquid water that the two lone-pair and bonding electrons have a spread of roughly 0.7 Å.¹² When we examine the electronic structure of the isolated $\text{Na}(\text{H}_2\text{O})_6$ we find something quite different, namely the presence of an extended state with a spread of nearly 3 Å. This corresponds to the delocalized 3s electron of the sodium atom as shown in Figure 1 and previously reported from independent studies.^{13,14} Figure 1 shows a snapshot of the density of the Boys localized 3s electron of the isolated $\text{Na}(\text{H}_2\text{O})_6$ undergoing CPMD. This computation was performed under conditions identical to those previously

- (1) Buck, U.; Steinbach, C. *J. Phys. Chem. A* **1998**, *102*, 7333.
- (2) Bewig, L.; Buck, U.; Rakowsky, M.; Reymann, M.; Steinbach, C. *J. Phys. Chem. A* **1998**, *102*, 1124.
- (3) Car, R.; Parrinello, M. *Phys. Rev. Lett.* **1985**, *55*, 2471.
- (4) Becke, A. D. *Phys. Rev. A* **1988**, *38*, 3098.
- (5) Lee, C.; Yang, W.; Parr, R. C. *Phys. Rev. B* **1988**, *37*, 785.
- (6) Sprik, M.; Hutter, J.; Parrinello, M. *J. Chem. Phys.* **1996**, *105*, 1142.
- (7) Hartwigsen, C.; Goedecker, S.; Hutter, J. *Phys. Rev. B* **1998**, *58*, 3641.
- (8) Martyna, G.; Tuckerman, M. *J. Chem. Phys.* **1999**, *110*, 2810.
- (9) Boys, S. F. *Rev. Mod. Phys.* **1960**, *32*, 296.
- (10) Silvestrelli, P. L.; Marzari, M.; Vanderbilt, D.; Parrinello, M. *Solid State Commun.* **1998**, *7*, 107.
- (11) Berghold, G.; Mundy, C. J.; Romero, A.; Hutter, J.; Parrinello, M. *Phys. Rev. B*, in press.
- (12) Silvestrelli, P. L.; Parrinello, M. *Phys. Rev. Lett.* **1998**, *82*, 3308.
- (13) Barnett, R. N.; Landman, U. *Phys. Rev. Lett.* **1993**, *70*, 1775.
- (14) Tsurusawa, T.; Iwata, S. *J. Phys. Chem. A* **1999**, *103*, 6134.

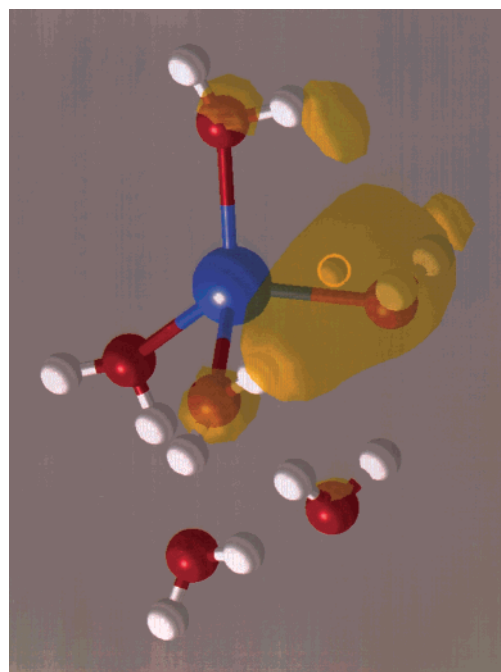


Figure 1. Snapshot of an isolated $\text{Na}(\text{H}_2\text{O})_6$ cluster undergoing CPMD dynamics. Blue denotes sodium, red water, and white the hydrogens. The yellow sphere is the centroid of the localized function. The extended 3s electron of the sodium is represented by the transparent yellow mesh with isosurface value of $0.165 \text{ e}^-/\text{Bohr}^3$. The structure here is similar to the 6(4 + 2) structure observed by Barnett and Landman.¹³

stated with a cubic cell of length 13.32 Å. Note the local tetrahedral coordination of the Na. Minimum energy structures of $\text{Na}(\text{H}_2\text{O})_6$ have been reported elsewhere¹³ and are in good agreement with the structure depicted in Figure 1. Attention should be brought to the Boys localized state that is distributed over some of the solvating water molecules in Figure 1. This leads to a very interesting and dynamic electronic state.¹⁵ During the finite temperature CPMD (roughly 100 K in accordance with experiment) this is a highly polarizable species. Through its interaction with this extended electronic state, the sodium dimer is aided in its dissociation. Thus, the reactive intermediate, Na^- , is formed (see Figure 2). From previous density functional theory calculations of the same accuracy we have inferred that indeed the charge-separated pair Na^- and Na^+ is stable under CPMD dynamics with six solvating molecules. It seems clear that the charge-separated dimer is a local minimum in the energy at finite temperature, but it is unlikely to occur spontaneously in the molecular beam without the aid of the solvated sodium acting as a catalyst.

Thus, after 3 ps of CPMD we can analyze the electronic structure of the full system (three sodiuns and six waters) in the same fashion. Here we find that instead of one state with a large spread, there are three electronic states with a spread of roughly 3 Å. One of the extended states is the 3s electron of the solvated sodium (as shown in Figure 1), and the two others are the spin-polarized 3s states of the Na_2 (see Figure 2). Figure 2 depicts a typical configuration after 3 ps of CPMD. The spontaneous cleavage of the Na_2 is evident. It is this polarized Na^- that is the reactive intermediate. Thus, the dipolar Na^- acts as a Lewis base and will attack a proton to form sodium hydride (NaH), completing the chemical process and yielding NaOH and H_2 .

(15) It should be noted that the extended state gives rise to a very active infrared mode. The spectroscopy of these clusters will be discussed in a future publication.

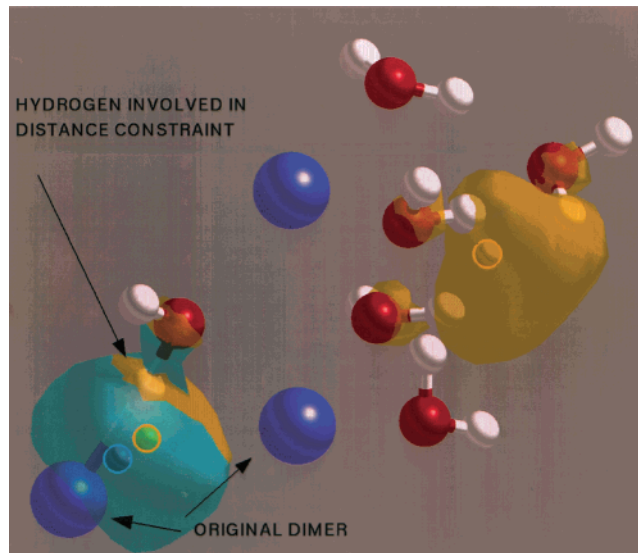


Figure 2. Snapshot of the full system, $\text{Na}_3(\text{H}_2\text{O})_6$, during the formation of NaH . The color coding is the same as in Figure 1 except for the addition of a light blue sphere and transparent mesh denoting the “spin-down” centroid and localized electron, respectively. All electron densities are represented by an isosurface value of $0.397 \text{ e}^-/\text{Bohr}^3$. It is clear from this figure that the Na_2 is severed and the electrons are spin polarized (blue and yellow centroids are not overlapping as would be in a spin paired state) located closer to one sodium, thus forming the reactive intermediate, Na^- .

However, it is the formation of NaH that is the rate-determining step and thus requires some care to gain understanding into its mechanism.

Because of the time scales involved in the experiment (e.g., microseconds^{1,2}), constraint algorithms must be employed to aid in sampling the reaction barrier. We would like to utilize a set of constraints that enable the reaction path to evolve in a natural way, rather than following the bias of the simulator. To this end, we use the coordination number constraint algorithm of Sprik.¹⁶ Recall that our assumption is that the rate-determining step is the formation of NaH . One can think of this as requiring the oxygen in a water molecule to go from coordination number two (H_2O) to coordination number one (OH^-). This then gives the water molecule the freedom to choose which proton to liberate, as well as allowing this proton to choose its own path to the Na^- . Following the work of Sprik, we choose the coordination number of the oxygen to be given by $n_o(\mathbf{r}) = \sum_{i>0} S(|\mathbf{r}_i - \mathbf{r}_o|)$. Here, $S(r) = 1/(\exp[\kappa(r - r_c)] + 1)$. In the work presented here, we choose $r_c = 1.32 \text{ \AA}$ and $\kappa = 1.58 \text{ \AA}$. The choice of our target oxygen can easily be deduced from Figure 2. It is clear from Figure 2 that the dipolar Na^- has a distinct directionality. It is this water, we believe, that is chosen in a natural way by the Na^- to be attacked. We believe that, by decreasing the coordination number by 3.5×10^{-5} every time step, the system is nearly equilibrated at every time step, and a reasonable upper bound to the reaction barrier to form NaH can be obtained either by integration of the

Lagrange multiplier or by taking energy differences. Utilizing the coordination number constraint, we find a barrier of 14 kcal/mol that translates into a reaction time of roughly $1 \mu\text{s}$ at the temperatures realized in the simulation which is in line with experiment. It is of interest to note that another candidate for the transition state of this reaction has been postulated, albeit in a different context.¹⁷ The structure of this transition state, based on studies of sodium chloride in water, leads to a concerted mechanism where the sodium hydroxide and hydrogen gas are formed in one step. This leads to a barrier roughly 3 times higher than what we report here, giving us confidence that our mechanism could be relevant. Furthermore, we have performed independent calculations using the more standard distance constraint (see Figure 2) where we assume that the reaction path is the $\text{O}-\text{H}$ distance getting bigger and the $\text{H}-\text{Na}$ distance becoming smaller simultaneously. This constraint was decreased at the same rate as the coordination number constraint and yielded almost quantitatively the same barrier.

After the formation of NaH , the reaction proceeds spontaneously to produce H_2 gas. The outline of the mechanism is as follows. First, a single sodium atom is solvated by six waters on the picosecond time scale: $\text{Na} + (\text{H}_2\text{O})_6 \rightarrow \text{Na}(\text{H}_2\text{O})_6$. Second, cleavage and solvation of a sodium dimer occur: $\text{Na}_2 + \text{Na}(\text{H}_2\text{O})_6 \rightarrow \text{Na}_3(\text{H}_2\text{O})_6$. Third, sodium hydride and sodium hydroxide are formed: $\text{Na}_3(\text{H}_2\text{O})_6 \rightarrow (\text{NaH})(\text{NaOH})\text{Na}(\text{H}_2\text{O})_5$. Fourth, a second sodium hydroxide and molecular hydrogen are formed: $(\text{NaH})(\text{H}_2\text{O})_5 \rightarrow (\text{NaOH})(\text{H}_2\text{O})_4 + \text{H}_2$. This reaction mechanism is able to explain experimental observations. Recall from refs 1 and 2 that in order to observe NaOH as a product the molecular beam interaction time must be on the order of a microsecond and molecular sodium (Na_2) must be present. The first criterion is corroborated by our upper bound on the reaction barrier. The second can be understood from the fact that the formation of Na^- is impossible from interactions of the cluster with neutral sodium atoms. It can be explained further by the novel observation that the role of the extended state of the $\text{Na}(\text{H}_2\text{O})_6$ could act as a catalyst in “cleaving” the Na_2 bond. The analogy of a catalyst could be further emphasized by the fact that it is consumed during the chemical process and is seemingly regenerated after the final products are formed; i.e., the remaining sodium atom will be again stabilized by solvating waters. This could lead to the additional formation of $(\text{NaOH})_2$ that is observed in experiments.^{1,2}

In conclusion, we have presented a novel mechanism for the reactions of sodium and water in a molecular beam. Not only does our mechanism explain experimental results, but our interpretation regarding the role of the outer solvated valence electron of Na leads to a picture that indicates that the solvation chemistry in clusters may differ from that in the bulk.

Acknowledgment. We acknowledge Professor B. P. Mundy for interesting discussions regarding Na^- , Daniel Katz for initiating some of the earlier simulations on this topic, and Professor U. Buck for useful discussions pertaining to his experiments.

JA994507P

(16) Sprik, M. *Faraday Discuss.* **1998**, *110*, 437.

(17) Barnett, R. N.; Landman, U. *J. Phys. Chem.* **1996**, *100*, 13950.

**Solution-to-Surface Molecular-Delivery System
Using a Macroyclic Sugar Cluster. Sugar-Directed
Adsorption of Guests in Water on Polar Solid
Surfaces**

Takako Fujimoto, Chikao Shimizu, Osamu Hayashida, and
Yasuhiro Aoyama*

Institute for Fundamental Research
of Organic Chemistry
Kyushu University, Hakozaki, Higashi-ku
Fukuoka 812-81, Japan

Received March 26, 1997

Cell-surface oligosaccharides occur as clusters. They play essential roles in various cell-recognition processes,¹ where saccharide–receptor interactions are often claimed to be multivalent.² The so-called cluster effect² has led many workers to investigate the receptor-binding properties of a variety of multiantennal synthetic saccharide derivatives (polymers and oligomers,³ dendrimers,⁴ surfactant aggregates,⁵ and metal complexes⁶). The present work is concerned with the interaction of a well-defined macrocyclic sugar cluster with a nonbiological polar solid surface as a simplified multivalent receptor site. We report here that the clustering sugar moieties in water can be irreversibly adsorbed or assembled on the silica surface. Coupled with the guest-binding ability of the macrocycle as a host, this leads to a novel sugar-directed solution-to-surface molecular delivery system.⁷

An octagalactose derivative of calix[4]resorcarene (**1f**; R = (CH₂)₁₀CH₃)⁸ was obtained by the reaction of lactonolactone (**2**) with octaamine **1e**, which was prepared in four steps from the parent macrocycle **1a**.⁹ Compound **1f** is highly soluble in water (>0.1 M). Nevertheless, it is readily adsorbed on the surface of quartz plate (silica glass) dipped in an aqueous solution of the former.¹⁰ Electronic absorption spectroscopy for the recovered plates¹⁰ indicates the following. (1) The

(1) *Carbohydrate-Protein Interactions*; Clarke, A. E., Wilson, I. A., Eds.; Springer-Verlag: Heidelberg, Germany, 1988.

(2) (a) Connolly, D. T.; Townsend, R. R.; Kawaguchi, K.; Bell, W. R.; Lee, Y. C. *J. Biol. Chem.* 1982, 257, 939–945. (b) Lee, R. T.; Lee, Y. C. *Biochem. Biophys. Res. Commun.* 1988, 155, 1444–1451.

(3) (a) Spaltenstein, A.; Whitesides, G. M. *J. Am. Chem. Soc.* 1991, 113, 686–687. (b) Glick, G. D.; Knowles, J. R. *Ibid.* 1991, 113, 4701–4703. (c) Salesan, S.; Duus, J. O.; Domaille, P.; Kelm, S.; Paulson, J. C. *Ibid.* 1991, 113, 5865–5866. (d) Callstrom, M. R. *Ibid.* 1992, 114, 378–380. (e) Roy, R.; Andersson, F. O.; Harms, G.; Kelm, S.; Schauer, R. *Angew. Chem., Int. Ed. Engl.* 1992, 31, 1478–1481. (f) Mortell, K. H.; Gingras, M.; Kiessling, L. L. *J. Am. Chem. Soc.* 1994, 116, 12053–12054.

(4) Aoi, K.; Itoh, K.; Okada, M. *Macromolecules* 1995, 28, 5391–5393. (5) Kingery-Wood, J. E.; Williams, K. W.; Sigal, G. B.; Whitesides, G. M. *J. Am. Chem. Soc.* 1992, 114, 7303–7305.

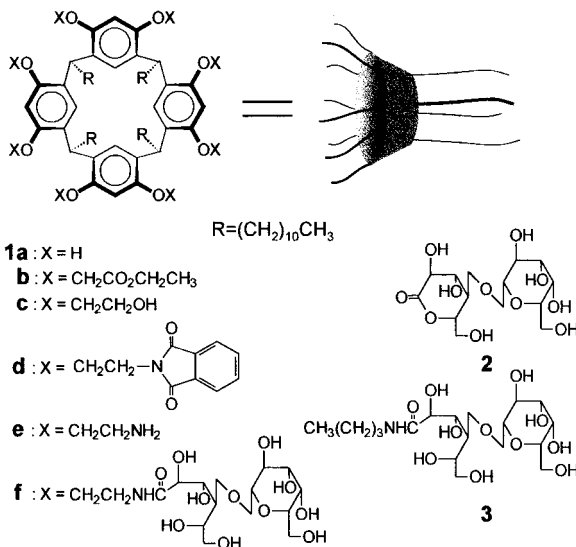
(6) Sakai, S.; Sasaki, T. *J. Am. Chem. Soc.* 1994, 116, 1587–1588.

(7) For an example of the saccharide-directed molecular delivery systems, see for example: Gordon, S.; Rabinowitz, S. *Adv. Drug. Delivery Rev.* 1989, 4, 27–47.

(8) For a calix[4]arene derivative having four side chains with a terminal sugar moiety, see: Marra, A.; Scherrmann, M.-C.; Dondoni, A.; Casnati, A.; Minari, P.; Ungaro, R. *Angew. Chem., Int. Ed. Engl.* 1994, 33, 2479–2481.

(9) **1a** → **1b** (BrCH₂CO₂CH₂CH₃ + K₂CO₃ in acetone at 80 °C for 3 h; 97%), **1b** → **1c** (LiAlH₄ in THF at 70 °C for 3 h; 90%), **1c** → **1d** (diethyl azodicarboxylate + PC₆H₅)₃ + phthalimide in THF at 70 °C for 30 h; 68%), **1d** → **1e** (N₂H₄ in ethanol at 60 °C for 4 h; 53%), **1e** → **1f** (**2** in methanol at 70 °C for 4 h; 79%). Compound **1f** was fully characterized by means of spectroscopy (IR, ¹H and ¹³C NMR, and TOF-MS) and elemental analysis. Dynamic light scattering indicates it is monomeric at 0.1 mM but forms aggregates ($\phi \approx 20$ nm) at 1 mM in water.

(10) Experimental procedure: 10 quartz plates (12 × 50 × 1 mm) were dipped for 10 min in an aqueous solution of compound **1f** ([**1f**]_{aq} ≥ 0.1 mM) at 25 °C, washed three times with 5 mL of pure water, and dried under nitrogen. The combined plates show an absorption band for adsorbed **1f** at $\lambda_{\text{max}} = 285$ nm ($\lambda_{\text{max}} = 283$ nm for **1f** in water). The maximal absorbance of $A = 0.0035$ per **1f**-coated plate, i.e., $A = 0.00175$ for each side of a plate is practically independent of [**1f**]_{aq} (0.1–10 mM).



adsorption is practically irreversible; **1f** adsorbed can not be rinsed out by repeated washing with water, although it is desorbed when washed with an aqueous solution of amine such as ethanolamine and pyridine. (2) There is a maximal or saturation amount of **1f** adsorbed, whose absorbance corresponds to a packing density of 0.28 molecules/nm² or an occupation area of 3.5 nm²/molecule.¹¹ (3) The saturation binding is achieved almost instantaneously (~10 s) when [1f]_{aq} ≥ 1 mM. The occupation area shown above is very similar to the cross-sectional area of the sugar-cluster part of compound **1f** ($\phi \approx 2$ nm at the most folded conformation; Figure 1). These results suggest that cluster **1f** forms a closely-packed monolayer on the quartz surface, as schematically shown in step a of Scheme 1.¹² In marked contrast to **1f**, a nonsugar analog (**1a**, R = (CH₂)₂SO₃Na) in water shows no sign of adsorption on quartz. Adsorption on silica gel also occurs readily. Thus, compound **1f** in water (0.1 mM, 10 mL) can be removed completely from the aqueous phase upon addition of a sufficiently excess amount (3 g) of chromatographic silica gel (Kaseigel 60–75). This is not the case for simple sugar derivatives such as galactose and phenyl β-galactopyranoside.

The lack of affinity to quartz of galactose (1 M) and lactonolactone–butylamine adduct **3** (1 M) as monovalent references and γ-cyclodextrin (0.1 M) as a 1,4-linked cyclic glucose octamer is evidenced by the competition experiments. Even in a large excess as indicated above, they neither inhibit the adsorption of cluster **1f** (0.1–1 mM) on the quartz surface nor promote desorption of **1f** adsorbed thereon. Thus, the octamer/monomer selectivity factor must be **1f**/**3** ≫ 10⁴. This reflects a remarkable efficiency of the multivalent interaction (step a in Scheme 1) between clustering sugar side chains of **1f** in water and the multivalent silica surface composed of silanol and silyl ether functionalities. There is little doubt that the interaction involves multiple **1f**–silica hydrogen-bonding, since it is disrupted by an amine base with decreasing efficiencies CH₃-NH₂ ($pK_a = 10.7$) > 4-(CH₃)₂NC₅H₄N (9.7) > HO(CH₂)₂NH₂ (9.5) > NH₃ (9.2) > C₅H₅N (5.2). Use of hydrogen-bonding in the formation of membranous aggregates in water has been noted.¹³

(11) The accurate amounts of host **1f** adsorbed and guest ANS coadsorbed on the quartz surface were determined after desorbing them into a 30% aqueous ethanolamine solution.

(12) Ichimura et al. have shown that derivatives **1a** (X = H, CH₂CO₂H, or CH₂CH₂OH) in apolar organic media can be adsorbed on a quartz plate to form closely-packed monolayers. For the adsorption on colloidal silica, see: Ueda, M.; Fukushima, N.; Kudo, K.; Ichimura, K. *J. Mater. Chem.* 1997, 7, 641–645. For the formation of monolayers of sulfide derivatives of macrocycle **1a** on the gold surface, see: Thoden van Velzen, E. N.; Engbersen, J. F. J.; de Lange, P. J.; Mahy, J. W. G.; Reinhoudt, D. N. *J. Am. Chem. Soc.* 1995, 117, 6853–6862.

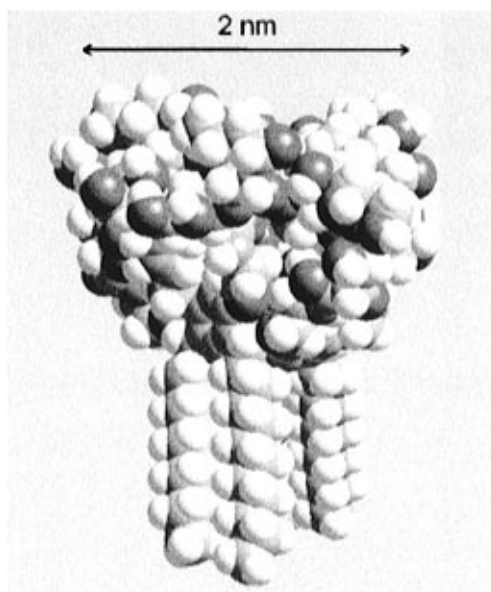


Figure 1. CPK model for compound **1f**. Dark, light dark, and white colors represent oxygen, carbon, and hydrogen atoms, respectively.

Another characteristic aspect of compound **1f** is that of a host.¹⁴ For example, it forms a stable 1:1 (from Job plot) complex with 8-anilinonaphthalene-1-sulfonate (ANS) in water (step b in Scheme 1). The large binding constant ($K = 2.2 \times 10^5 \text{ M}^{-1}$ at 25°C ,¹⁵ from fluorimetric titration at 479 nm ($[\text{ANS}] = 1.0 \times 10^{-6} \text{ M}$ and $[\mathbf{1f}] \leq 2.2 \times 10^{-5} \text{ M}$)) and the spectroscopic evidence¹⁶ strongly suggest that guest ANS is included, as for host **1a**,¹⁴ in the polyaromatic cavity of the host flexibly capped¹⁷ by the sugar side chains, as schematically shown by the structure for **1f**·guest in Scheme 1.

ANS alone in water is not adsorbed on a quartz plate (step c in Scheme 1) but is readily coadsorbed with host **1f** (step d). Spectroscopic analysis¹⁸ of the plates dipped in an aqueous solution of host and guest ($[\mathbf{1f}] = 1 \text{ mM}$ and $[\text{ANS}] \geq 1 \text{ mM}$) shows that (1) the host/guest molar ratio on the plate is $\sim 1:1$ (step d)¹¹ and (2) adsorbed guest ANS is gradually rinsed out upon repeated washing with water (step e), while (3) adsorbed host **1f** is not desorbed unless washed with an aqueous amine solution as above.¹¹ These results indicate that host **1f** not only as such but also as the complex **1f**·ANS is irreversibly adsorbed on the quartz surface (step d),¹⁹ where the included guest molecule is not completely encapsulated but exhibits at least

(13) Kimizuka, N.; Kawasaki, T.; Kunitake, T. *J. Am. Chem. Soc.* **1993**, *115*, 4387–4388.

(14) The guest-binding properties of lipophilic and hydrophilic derivatives of parent macrocycle **1a** ($R = (\text{CH}_2)_{10}\text{CH}_3$ or $(\text{CH}_2)_2\text{SO}_3\text{Na}$) have been extensively studied. For examples, see: (a) Aoyama, Y.; Tanaka, Y.; Sugahara, S. *J. Am. Chem. Soc.* **1989**, *111*, 5397–5404. (b) Kikuchi, Y.; Kato, Y.; Tanaka, Y.; Toi, H.; Aoyama, Y. *Ibid.* **1991**, *113*, 1349–1354. (c) Kobayashi, K.; Asakawa, Y.; Kato, Y.; Aoyama, Y. *J. Am. Chem. Soc.* **1992**, *114*, 10307–10313.

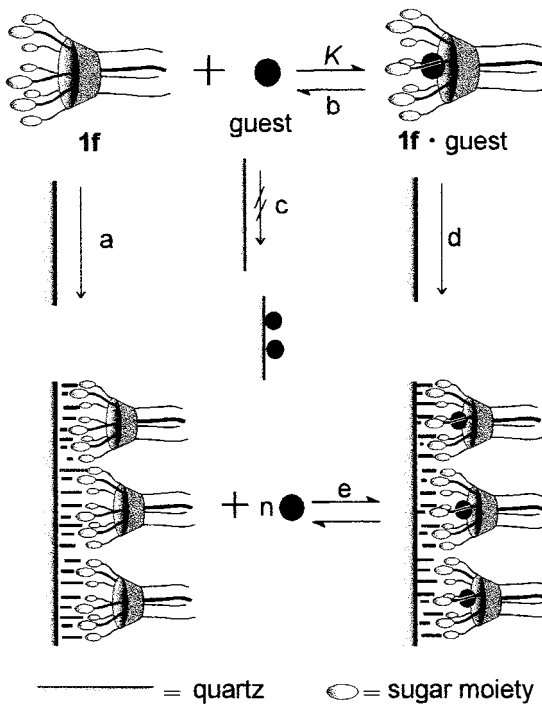
(15) The K values for ANS range from $\sim 10^2 \text{ M}^{-1}$ for β -cyclodextrin up to $\sim 10^6 \text{ M}^{-1}$ for octopus cyclophanes having eight alkyl chains (Murakami, Y.; Kikuchi, J.; Ohno, T.; Hayashida, O.; Kojima, M. *J. Am. Chem. Soc.* **1990**, *112*, 7672–7681).

(16) NMR spectra indicate significant complexation-induced upfield shifts for the protons of bound ANS. A remarkable enhancement in the fluorescence intensities (I) of ANS upon binding ($I = 103$ (arbitrary unit) at 479 nm for complex **1f**·ANS and $I \approx 0.3$ at 520 nm for free ANS) indicates that bound ANS is effectively insulated from bulk water.

(17) Emert, J.; Breslow, R. *J. Am. Chem. Soc.* **1975**, *97*, 670–672.

(18) Each plate was washed successively with a minimal amount (0.5 mL) of water. The absorbance at 285 nm (for **1f**) and 352 nm (for ANS) was monitored for the plate after each washing.

Scheme 1



some degree of reversibility (step e). In fact, complexation on the surface takes place when a **1f**-coated quartz plate is dipped in an aqueous solution of the guest (step e).

Silica gel experiments are consistent. Addition of the silica gel (Kaseigel, 3 g) to an aqueous solution of ANS (0.05 mM, 10 mL) results in preferential adsorption of water on the silica ($\sim 1.3 \text{ mL/g}$, as independently confirmed); the aqueous solution of ANS is concentrated by $\sim 50\%$ as a consequence. In the presence of host **1f** (0.1 mM), the fluorescent guest is completely transferred from the aqueous phase to the silica surface.

The significance of the present study is 3-fold. First, it demonstrates a remarkable sugar-cluster effect. Water effectively interferes with polar host–guest interactions. Sugar-binding via hydrogen-bonding has so far been effective only in apolar organic media.^{14a,20} The present work thus provides a new strategy for sugar-binding in water.^{14c,21} Second, the dual roles of compound **1f** as a host as well as an adsorbate leads to a novel solution-to-surface molecular transport or delivery system. Most carrier-mediated transport systems studied so far are concerned with membrane transport between two fluid phases (gas or liquid). Third, the present system thus suggests a potential utility in sugar-directed delivery or targeting of particular guest molecules as drugs or probes to the specific saccharide-receiving biological surfaces.

Acknowledgment. We are grateful to Professor K. Ichimura (Tokyo Institute of Technology) for valuable suggestions and discussion. This work was supported by grant-in-aid for COE Research “Design and Control of Advanced Molecular Assembly Systems” (no. 08CE2005) from the Ministry of Education, Science, and Culture of the Japanese Government.

JA9709536

(19) Methyl orange (MO) can also be coadsorbed with a 1:1 (**1f** to MO) stoichiometry; $K = 6.4 \times 10^5 \text{ M}^{-1}$ for complex **1f**·MO in water.

(20) For examples, see: (a) Huang, C.-Y.; Cabell, L. A.; Anslyn, E. V. *J. Am. Chem. Soc.* **1994**, *116*, 2778–2792. (b) Das, G.; Hamilton, A. D. *Ibid.* **1994**, *116*, 11139–11140.

(21) (a) Coterón, J. M.; Vicent, C.; Bosso, C.; Penadés, S. *J. Am. Chem. Soc.* **1993**, *115*, 10066–10076. (b) Shiomi, Y.; Saisho, M.; Harada, T.; Shinkai, S. *Tetrahedron* **1992**, *48*, 8239–8252.

Molecular Association in Binary Mixtures of *tert*-Butyl Alcohol–Water and Tetrahydrofuran–Heavy Water Studied by Mass Spectrometry of Clusters from Liquid Droplets

Toshiko Fukasawa,[†] Yasunori Tominaga,^{*,†} and Akihiro Wakisaka^{*,‡}

Department of Physics and Chemistry, Graduate School of Humanities and Sciences, Ochanomizu University, Otsuka, Bunkyo-ku, Tokyo 112-8610, Japan, and National Institute of Advanced Industrial Science and Technology, AIST, Tsukuba West, Onogawa 16-1, Tsukuba, Ibaraki 305-8569, Japan

Received: August 25, 2003

The cluster structures observed by means of mass spectrometry for binary mixtures—*tert*-butyl alcohol (TBA)–H₂O and tetrahydrofuran (THF)–D₂O—with varying mixing ratios exhibit striking contrast, even though both TBA and THF are miscible with water at any mixing ratio. In the TBA–H₂O mixtures at TBA mole fractions of (X_{TBA}) ≤ 0.01 –0.025, some of the H₂O molecules in the H₂O clusters are replaced by TBA molecules. For 0.01 –0.025 $\leq X_{\text{TBA}} \leq 0.2$ –0.3, the self-aggregation of TBA forms dominant cluster structures, and the hydrogen-bonded water clusters are disintegrated with increasing X_{TBA} . This TBA self-aggregation is reduced with further increasing TBA at $X_{\text{TBA}} \geq 0.3$. However, in the THF–D₂O mixtures, THF molecules have a weak additional interaction with D₂O clusters, and the self-aggregation of THF is not promoted in the THF–D₂O mixtures. The D₂O clusters still exist, even at a THF mole fraction of $X_{\text{THF}} = 0.3$. On the basis of the observed cluster structure, the mechanism for the mixing between water and the organic solvent and the controlling factors in the self-aggregation are proposed.

Introduction

Even though an organic solvent is miscible with water, the intermolecular interactions of water–water, water–organic molecule, and organic molecule–organic molecule are not the same. The interaction between water and the hydrophobic group of the organic solvent molecule should be especially weak in the mixtures. As a result of the balance of these intermolecular interactions in the water–organic solvent mixture, clusters will be formed easily in the mixture.

Because organic molecules have different kinds of intermolecular interactions in their aqueous solutions, we confine our focus to *tert*-butyl alcohol (TBA) and tetrahydrofuran (THF) because TBA has an OH group but THF does not. Although both of them are miscible with water at any mixing ratio, the balance of intermolecular interactions in a TBA–water mixture should be quite different from that in a THF–water mixture. This will lead to the difference in the cluster structure.

Many investigations have been performed on physical and chemical properties of the TBA–water^{1–4,7,8} and THF–water mixtures^{5–8} through various experimental and theoretical approaches. It has been concluded that the characteristic microscopic structure in these mixtures in a water-rich region is a cage structure of water molecules around TBA and THF molecules. However, the difference in the intermolecular interactions between TBA–water and THF–water was not exactly reflected in the reported results. Here we report how the difference in the intermolecular interactions is reflected in the cluster structure observed through the mass spectrometric

analysis of clusters isolated from liquid droplets. The resulting information on the cluster structures in these binary mixtures also shows the difference in the way of mixing at the molecular level.

Experimental Section

The mass spectra of clusters generated from liquid droplets were measured by a specially designed mass spectrometer. This original design was proposed by Nishi.^{9,10} The details have been provided elsewhere.^{9–12} The spectrometer consists of a heated nozzle, a quadrupole mass filter (Extrel C50-4000), and a four-stage differentially pumped vacuum system divided by the skimmers. A sample solution was injected into the first chamber (10^{-1} Torr) through the heated nozzle (160–155 °C) with a flow rate of 0.12 mL/min by using a liquid chromatograph pump (Shimazu, LC-10AD). The nozzle was heated electrically to form a flow of liquid droplets against the decrease in temperature due to the vaporization, and its temperature was monitored and controlled by two sets of thermocouples on the nozzle. When a part of the solution is vaporized in the nozzle, the resulting gas–liquid mixtures form a flow of liquid droplets. The temperature of the liquid droplets should be much lower than the nozzle temperature. This temperature difference was estimated to be 70–90 °C.^{9,10} Owing to the pressure gradient, the resulting liquid droplets are led to the second (10^{-3} Torr) and the third (10^{-5} Torr) chamber, which leads to the fragmentation of the liquid droplets into clusters via adiabatic expansion. The mass spectra of the clusters were measured by the quadrupole mass filter after an electron-impact ionization with 30.1 eV.

The pure water was prepared by Milli-Q SP. TOC (Millipore). The TBA (99.0%, Wako), THF (99.5%, no stabilizer, Wako), and D₂O (99.9%, Aldrich) were used without further purification. The concentrations of the sample solutions were expressed

* To whom correspondence should be sent. A.W. E-mail: akihiro-wakisaka@aist.go.jp. Y.T. E-mail: tominaga@phys.ocha.ac.jp.

[†] Ochanomizu University.

[‡] National Institute of Advanced Industrial Science and Technology.

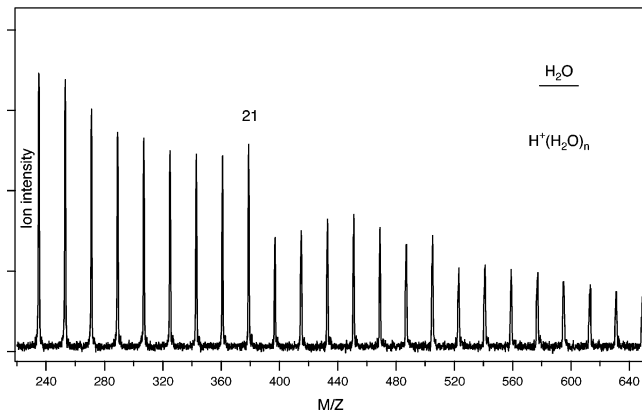


Figure 1. Mass spectrum for clusters generated from pure water (H_2O). The numbers written on the peaks represent n for $\text{H}^+(\text{H}_2\text{O})_n$.

by TBA mole fractions (X_{TBA}) and THF mole fractions (X_{THF}): $X_{\text{TBA}} = 0.0, 0.0024, 0.005, 0.0075, 0.01, 0.025, 0.05, 0.1, 0.2, 0.3, 0.4$; $X_{\text{THF}} = 0.0, 0.01, 0.05, 0.1, 0.2, 0.3, 0.6, 0.8$.

Results

1. TBA–Water Binary Mixtures. It was observed through mass spectrometry that the cluster structures in TBA–water mixtures varied remarkably depending on the TBA mole fraction (X_{TBA}). We could classify the TBA–water mixtures into three regions according to the observed cluster structures as follows: region A ($0 \leq X_{\text{TBA}} \leq 0.01\text{--}0.025$), region B ($0.01\text{--}0.025 \leq X_{\text{TBA}} \leq 0.2\text{--}0.3$), and region C ($0.3 \leq X_{\text{TBA}}$). The representative mass spectrum of each region is shown below.

Region A ($0 \leq X_{\text{TBA}} \leq 0.01\text{--}0.025$). The mass spectrum of clusters for pure water ($X_{\text{TBA}} = 0$) is shown in Figure 1. The hydrogen-bonded water clusters, $\text{H}^+(\text{H}_2\text{O})_n$, are observed as a series of clusters. This mass distribution is very reproducible and in good agreement with the reported results.^{11,12} Although $\text{H}^+(\text{H}_2\text{O})_n$ clusters from $n = 1\text{--}50$ were observed, the sensitivity and the resolution get worse in lower- and higher-mass regions, respectively. Furthermore, in lower-mass regions, fragmented clusters from larger clusters might be included. To avoid these influences, the region shown in each Figure was focused here. Some peaks are observed as the prominent peaks compared with their neighboring ones. The most representative one is the peak of $\text{H}^+(\text{H}_2\text{O})_{21}$, which is called “magic number species.” The magic number property indicates that more stable structure is included as one of the isomers. It should be noted here that the formation of magic number species reflects the stability after fragmentation of clusters via electron impact ionization. Therefore, the magic number anomaly does not reflect the mass distribution in the solution. However, when a sample solution such as a TBA–water mixture has the same hydrogen bonding network of water as that in the pure water, the mass distribution including the magic number species will be always observed. Here we use the magic number property as an index which reflects the clustering structure of the pure water.

At $0 \leq X_{\text{TBA}} \leq 0.01\text{--}0.025$, the hydrogen-bonded water clusters, $\text{H}^+(\text{H}_2\text{O})_n$, as observed in pure water (Figure 1), compose a main structure in the molecular clustering. Figure 2a shows a mass spectrum of clusters generated from a solution at $X_{\text{TBA}} = 0.0024$. In addition to the series of water clusters, TBA hydrate clusters, $\text{H}^+(\text{TBA})_m(\text{H}_2\text{O})_n$: $m = 1 \sim 5$, are observed as a series of clusters in this region A. The blue, red, yellow, and green lines in Figure 2a correspond to the cluster series of $\text{H}^+(\text{H}_2\text{O})_n$, $\text{H}^+(\text{TBA})_1(\text{H}_2\text{O})_n$, $\text{H}^+(\text{TBA})_2(\text{H}_2\text{O})_n$, and $\text{H}^+(\text{TBA})_3(\text{H}_2\text{O})_n$, respectively. When we focus on the series

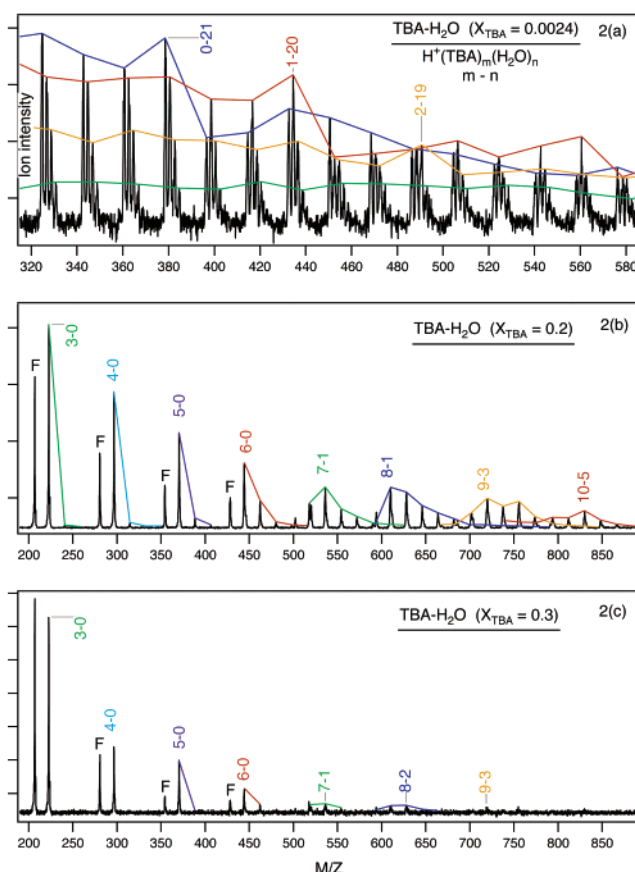


Figure 2. Mass spectra for clusters generated from *tert*-butyl alcohol (TBA)– H_2O mixtures. The paired numbers represent $m\text{--}n$ for $\text{H}^+(\text{TBA})_m(\text{H}_2\text{O})_n$. The peaks with the same number of TBA (m) are connected by the colored lines. The blue, red, yellow, and green lines correspond to the cluster series of $\text{H}^+(\text{H}_2\text{O})_n$, $\text{H}^+(\text{TBA})_1(\text{H}_2\text{O})_n$, $\text{H}^+(\text{TBA})_2(\text{H}_2\text{O})_n$, $\text{H}^+(\text{TBA})_3(\text{H}_2\text{O})_n$, respectively. The peaks labeled by F represent the clusters including a fragmented TBA molecule. (a) $X_{\text{TBA}} = 0.0024$, (b) $X_{\text{TBA}} = 0.2$, (c) $X_{\text{TBA}} = 0.3$.

of clusters composed of the same number of TBA molecules (m) and the varying number of water molecules (n), as shown by the connected lines in Figure 2a, each series of clusters is found to show mass distribution similar to that for the pure water. This indicates that the hydrogen-bonding network of water is not influenced by the mixing with TBA in this region A. Accordingly, the magic number species are also observed in each series of TBA hydrate clusters, but the number of water molecules varies to satisfy $m + n = 21$ for $\text{H}^+(\text{TBA})_m(\text{H}_2\text{O})_n$ clusters. In Figure 2a, the TBA hydrate clusters, $\text{H}^+(\text{TBA})_m(\text{H}_2\text{O})_n$ represented by $m\text{--}n$, show magic number property at 1–20 and 2–19. In addition to the magic number property, the mass distribution of each series of cluster is similar to that of the pure water. Therefore, the TBA molecule can have substitutional interaction with not only the magic number cluster but also with all the water clusters in the region A.

Region B ($0.01\text{--}0.025 \leq X_{\text{TBA}} \leq 0.2\text{--}0.3$). In region B, the TBA self-aggregation clusters form prominently instead of the water clusters. Figure 2b shows a mass spectrum of the solution of $X_{\text{TBA}} = 0.2$, as a typical one in the region B. In the clusters $\text{H}^+(\text{TBA})_m(\text{H}_2\text{O})_n$ represented by $m\text{--}n$, 3–0, 4–0, 5–0, and 6–0 are prominent in the relatively small clusters, while 7–1, 8–1, 9–3, and 10–5 are prominent in the relatively large clusters. The TBA self-aggregation clusters, $\text{H}^+(\text{TBA})_m$: $m \leq 6$, are stable, but those with $m \geq 7$ are stabilized by including water molecules. As for the large clusters $\text{H}^+(\text{TBA})_m(\text{H}_2\text{O})_n$:

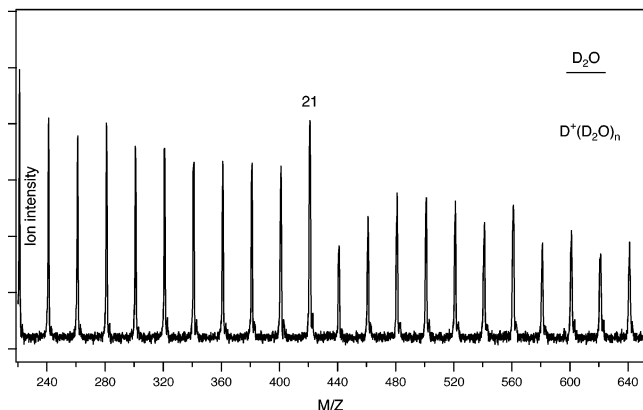


Figure 3. Mass spectrum for clusters generated from pure heavy water (D_2O). The numbers written on the peaks represent n for $D^+(D_2O)_n$.

$m = \sim 10$, we insist that the water molecules are incorporated into the hydrogen-bonding network of TBA. The TBA large clusters can exist stably only with existing water molecules, because water molecules adhere TBA molecules by hydrogen bonding.

Region C ($0.3 \leq X_{TBA}$). In region C, the self-aggregation of TBA promoted by the presence of water, as observed in region B, was obviously reduced with an increase of X_{TBA} . A typical mass spectrum, observed for $X_{TBA} = 0.3$, is shown in Figure 2c. The self-aggregation clusters $H^+(TBA)_m$ with $m \geq 4$ are difficult to form. The $H^+(TBA)_m(H_2O)_n$ clusters with $m \geq 7$ are also decreased markedly. At $X_{TBA} = 0.4$, the clusters larger than $H^+(TBA)_3$ were hardly formed. It is interesting that the large clusters, $H^+(TBA)_m$ with $m \geq 4$, are observed in the system with higher water contents.

2. THF–Heavy Water Binary Mixtures. In THF–heavy water mixtures, the observed cluster structures are in good contrast to those in the TBA–water mixtures. We used heavy water instead of normal water for the measurement of the THF–water binary mixtures, because the mass number of a THF molecule equals that of H_2O tetramer. We were able to distinguish hydrated THF from heavy water clusters clearly.

The mass spectrum of clusters generated from heavy water ($X_{THF} = 0$) is shown in Figure 3, and it is quite similar to that for normal water (Figure 1), except the difference in mass number between H_2O and D_2O .

When THF is added to heavy water up to the THF mole fraction, $X_{THF} = 0.3$, the water cluster structure is maintained with almost the same mass distribution as observed in pure heavy water. It is claimed that this may be related to the hydrogen bonding interaction among D_2O molecules being stronger than that among H_2O molecules. We have also confirmed that the water cluster structure is maintained in THF– H_2O ($X_{THF} = 0.3$), as observed in the pure water, even though the several peaks are overlapped. This indicates that the difference between D_2O and H_2O does not influence the observed cluster structures. The mass spectra representative of the THF– D_2O mixtures are shown in Figure 4. The blue, red, and yellow lines in Figure 4 correspond to the cluster series of $D^+(D_2O)_n$, $D^+(THF)_1(D_2O)_n$, and $D^+(THF)_2(D_2O)_n$, respectively. At $X_{THF} = 0.05$ (Figure 4a), water clusters, $D^+(D_2O)_n$, are observed dominantly, and THF monomer and its hydrate clusters, $D^+(THF)_1(D_2O)_n$, are also observed. The peak intensities of $D^+(THF)_1(D_2O)_n$ are quite weak compared with those of the water clusters and the THF monomer. With an increase of the THF concentration to $X_{THF} = 0.2$ and 0.3, the intensity of $D^+(THF)_1(D_2O)_n$ increases gradually, as observed in Figure

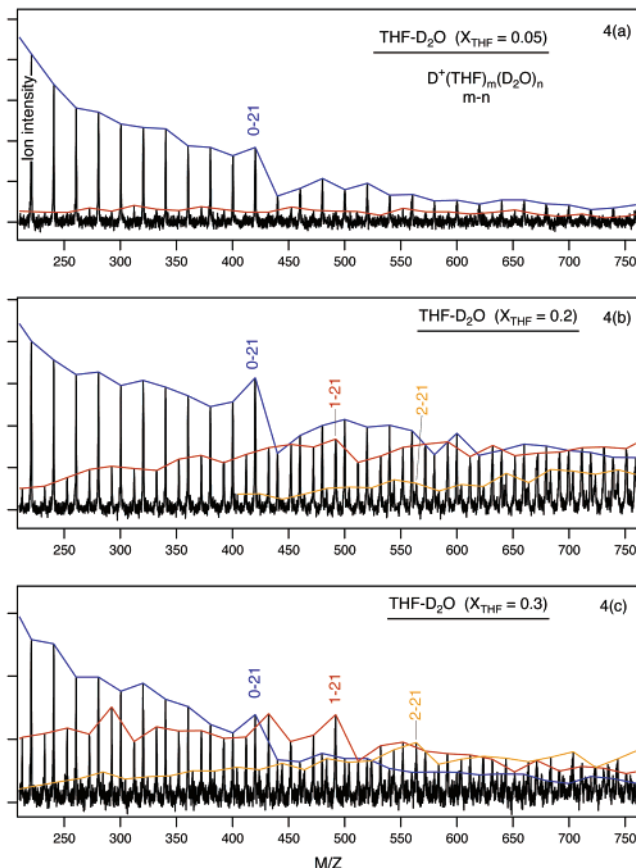


Figure 4. Mass spectra for clusters generated from tetrahydrofuran (THF)– D_2O mixtures. The paired numbers represent $m-n$ for $D^+(THF)_m(D_2O)_n$. The peaks with the same number of THF (m) are connected by the colored lines. The blue, red, and yellow lines correspond to the cluster series of $D^+(D_2O)_n$, $D^+(THF)_1(D_2O)_n$, and $D^+(THF)_2(D_2O)_n$, respectively. (a) $X_{THF} = 0.05$, (b) $X_{THF} = 0.2$, (c) $X_{THF} = 0.3$.

4b and c, respectively. The $D^+(THF)_2(D_2O)_n$ are also observed in Figure 4b and c. THF dimer without D_2O molecules cannot be observed, and the peak intensity of THF dimer hydrate clusters with a few water molecules are extremely weak. For the THF hydrate cluster series, $D^+(THF)_m(D_2O)_n$, $m = 1$ and 2, especially for $m = 2$, the intensities of relatively large clusters increase with increasing THF concentration. This suggests that THF molecules might exist in the space among the water clusters.

Furthermore, we have confirmed that the clusters, $D^+(THF)_m(D_2O)_n$: $m-n = 1-21$ and $2-21$, are observed as magic-number species in Figure 4b and c. The $D^+(THF)_m(D_2O)_n$ clusters with $n = 21$ show the magic number property, irrespective of the number of THF molecules in the cluster. This indicates that THF molecules have additional interaction with D_2O clusters. This is obviously different from the TBA–water substitutional interaction. Such an additional interaction between THF and water clusters will make the hydrogen-bonded D_2O clusters maintained even at $X_{THF} = 0.3$, as shown in Figure 4c. The self-aggregation of THF, as observed in the TBA– H_2O mixtures, is hardly promoted in the THF– D_2O binary mixtures.

At $X_{THF} \geq 0.6$, the peak intensities of D_2O clusters decreased and the size of D_2O clusters became small. Their mass distributions are different from that in pure D_2O . The hydrogen-bonding network of D_2O is disintegrated in this higher X_{THF} . The $D^+(THF)_m(D_2O)_n$ also decreases with increasing X_{THF} and was hardly observed at $X_{THF} = 0.8$.

Discussion

1. Difference in the Molecular Association. Both TBA and THF are miscible with water at any mixing ratio. However, the mass spectrometric analysis of clusters in these mixtures demonstrated that the molecular association found in the THF–D₂O system is very much different from the case in the TBA–H₂O system.

In TBA–H₂O mixtures (Figure 2), the water cluster structures are easily disintegrated by the addition of TBA, and the TBA self-aggregation clusters are formed instead of the water clusters. Such kind of microscopic change takes place even at the low TBA mole fraction ($X_{\text{TBA}} = 0.01 \sim 0.025$). On the other hand, in THF–D₂O mixtures (Figure 4), the water cluster structures are maintained even at $X_{\text{THF}} = 0.3$, as observed for D⁺(D₂O)_n and D⁺(THF)_{1, 2}(D₂O)_n, and the THF self-aggregation is not promoted by the addition of D₂O. In both mixtures, when one component forms self-aggregation clusters, the other component is broken up to the monomeric molecules to maintain single phase as stably as possible. The same kind of difference in the cluster structure has been also observed between methanol–water and acetonitrile–water binary mixtures.¹¹ Accordingly, it should be noted that the cluster structures observed herein TBA–water and THF–water show representative two types of mixing mechanism between water and organic solvents.

2. Controlling Factors in Cluster Formation. In TBA–H₂O mixtures, the stabilization for the hydrogen-bonding interactions H₂O–H₂O, H₂O–TBA, and TBA–TBA will be comparable, but the interaction of the large alkyl group of TBA with H₂O cannot provide stabilization. Therefore, the TBA self-aggregation is promoted by the increase of X_{TBA} , to complement the loss of stabilization caused by the contact of TBA with H₂O. In region B ($0.01 \sim 0.025 \leq X_{\text{TBA}} \leq 0.2 \sim 0.3$), each TBA molecule will have contact with the water molecules; therefore, the TBA–TBA interaction becomes relatively more stable than the TBA–H₂O interaction working at the same time. This will induce the TBA self-aggregation. However, in region C, since the TBA molecules that do not contact water molecules increase with increasing X_{TBA} , the relative stability for the TBA–TBA interaction against the TBA–H₂O interaction disappears with increasing X_{TBA} . It should be noted that the clustering of TBA is promoted in the presence of water, because it is controlled by the relative stability in the solution. In pure TBA, all TBA–TBA interaction is comparable, which cannot promote self-aggregation.

On the other hand, in THF–D₂O mixtures, the D₂O–D₂O interaction energy is much larger than the THF–THF interaction energy. Accordingly, D₂O clusters are maintained, and THF molecules should be surrounding the D₂O clusters.

Since there are several intermolecular interactions working at the same time in the binary mixtures, the difference in the clustering between TBA–water and THF–water mixture will be explained by the balance of interactions rather than the absolute interaction energy.

3. Correlation with Other Experimental and Theoretical Approaches. The resulting concentration effect on the TBA self-aggregation is in good correlation with the reported IR, X-ray scattering, computer simulation, and thermodynamic studies.

(i) **IR.** Infrared studies for TBA–water mixtures revealed the changes of the TBA C–H stretching band in the 3200–2800 cm⁻¹ frequency region as depending on the mixing ratio.¹³ It was observed that when the TBA concentration exceeds a critical concentration around $X_{\text{TBA}} \sim 0.025$, the C–H stretching band shifts to lower frequency with increase of X_{TBA} , while the C–H

stretching band keeps constant in $X_{\text{TBA}} \leq 0.025$. From this it was concluded that the shift of the C–H stretching band to the lower frequency region was due to the depletion of the aqueous environment around the TBA methyl group. This IR result can be connected to self-aggregation of TBA molecules observed through the mass spectrometry here. The mass spectra for the mixtures in the present study vary with increasing TBA concentration, but the changes are not linearly dependent on the TBA concentration. At $X_{\text{TBA}} = 0.01$, the peaks of the TBA self-aggregation clusters become obvious, but the TBA hydrated clusters and water clusters coexist. At $X_{\text{TBA}} = 0.025$, however, TBA self-aggregation clusters form prominently instead of the water clusters. The critical concentration between the region A and B, at $X_{\text{TBA}} = 0.01 \sim 0.025$, obtained through present mass spectrometric analysis for the cluster structures, is in good correlation with the critical concentration suggested by the IR studies.

(ii) **X-ray Scattering.** Small-angle X-ray scattering study showed that a large concentration fluctuation for TBA–water mixtures is enhanced strongly at $X_{\text{TBA}} = 0.14 \sim 0.17$.² It is suggested that heterogeneous mixing is most enhanced at this mixing ratio. This X_{TBA} value is in region B, proposed here by mass spectrometry. We have also observed that the self-aggregation of TBA is enhanced most markedly at X_{TBA} from 0.1 to 0.2. From this correlation, the concentration fluctuation is attributed to the self-aggregation of TBA molecules in the mixtures.

(iii) **Computer Simulation.** Computer simulation for TBA–water mixtures has been carried out on the site–site radial distribution function over the whole concentration range of TBA mole fraction.³ It was concluded that, in concentrated TBA, TBA molecules were associated into the zigzag-like hydrogen-bonding chains of TBA and that the hydrophobic attraction of the bulky *tert*-butyl groups in aqueous solutions was performed for approximately 3 to 6 TBA molecules. These findings agree well with the present result shown in Figure 2b, where the TBA self-aggregation clusters larger than H⁺(TBA)₇ incorporated with H₂O. Also, self-aggregation clusters of TBA can be formed up to H⁺(TBA)₆ without water molecules.

(iv) **Thermodynamic Properties.** Although the thermodynamic properties for TBA–H₂O and THF–H₂O binary mixtures look similar, the microscopic structures of TBA–H₂O mixtures are in good contrast with those of THF–D₂O mixtures. The excess molar enthalpies (H^E) of TBA–H₂O and THF–H₂O solutions are both negative in $X_{\text{TBA}} \leq 0.5$ and $X_{\text{THF}} \leq 0.6$, and they are both positive in $X_{\text{TBA}} \geq 0.5$ and $X_{\text{THF}} \geq 0.6$.^{4,6} In the region of negative H^E , the self-aggregation of one component molecules is promoted. TBA and D₂O formed self-aggregation clusters in TBA–H₂O and THF–D₂O mixtures, respectively. This was controlled by the relatively large interaction energy. On the other hand, in the regions of positive H^E , the self-aggregation clusters disintegrated to afford more random mixing with the other component.

Acknowledgment. This work is partly supported by a Grant-in-Aid for Scientific Research from the Japanese Ministry of Education, Science, Culture, and Sport.

References and Notes

- (1) Iwasaki, K.; Fujiyama, T. *J. Phys. Chem.* **1977**, *81*, 1908–1912.
- (2) Nishikawa, K.; Hayashi, H.; Iijima, T. *J. Phys. Chem.* **1989**, *93*, 6559–6565.
- (3) Yoshida, K.; Yamaguchi, T.; Kovalenko, A.; Hirata, F. *J. Phys. Chem. B* **2002**, *106*, 5042–5049.

- (4) Koga, Y. *Can. J. Chem.* **1988**, *66*, 3171–3175.
- (5) Takamuku, T.; Nakamizo, A.; Tabata, M.; Yoshida, K.; Yamaguchi, T.; Otomo, T. *J. Mol. Liq.* **2002**, *103–104*, 143–159.
- (6) Atkinson, G.; Rajagopalan, S.; Atkinson, B. L. *J. Phys. Chem.* **1981**, *85*, 733–739.
- (7) Matteoli, E.; Lepori, L. *J. Phys. Chem.* **1984**, *80*, 2856–2863.
- (8) Baumgartner, E. K.; Atkinson, G. *J. Phys. Chem.* **1971**, *75*, 2336–2341.
- (9) Nishi, N.; Yamamoto, K. *J. Am. Chem. Soc.* **1987**, *109*, 7353–7361.
- (10) Yamamoto, K.; Nishi, N. *J. Am. Chem. Soc.* **1990**, *112*, 549–558.
- (11) Wakisaka, A.; Abdoul-Carime, H.; Yamamoto, Y.; Kiyoizumi, Y. *J. Chem. Soc., Faraday Trans.* **1998**, *94*, 369–374.
- (12) Wakisaka, A.; Komatsu, S.; Usui, Y. *J. Mol. Liq.* **2001**, *90*, 175–184.
- (13) Freda, M.; Onori, G.; Santucci, A. *J. Phys. Chem. B* **2001**, *105*, 12714–12718.

Comparative FTIR Spectroscopy of HX Adsorbed on Solid Water: Ragout-Jet Water Clusters vs Ice Nanocrystal Arrays

J. P. Devlin*

Department of Chemistry, Oklahoma State University, Stillwater, Oklahoma 74078

M. Fárník† and M. A. Suhm

Institut fuer Physikalische Chemie, Universitaet Goettingen, Tammannstr. 6, D-37077 Goettingen, Germany

V. Buch

The Fritz Haber Institute for Molecular Dynamics, Hebrew University, Jerusalem 91904, Israel

Received: December 20, 2004; In Final Form: January 12, 2005

In addition to revealing the stretch-mode bands of the smallest mixed clusters of HCl and HBr (HX) with water, the ragout-jet FTIR spectra of dense mixed water–acid supersonic jets include bands that result from the interaction of HX with larger water clusters. It is argued here that low jet temperatures prevent the water-cluster-bound HX molecules from becoming sufficiently solvated to induce ionic dissociation. The molecular nature of the HX can be deduced directly from the observed influence of changing from HCl to HBr and from replacing H₂O with D₂O. Furthermore, the band positions of HX are roughly coincidental with bands assigned to molecular HCl and HBr adsorbed on ice nanocrystal surfaces at temperatures below 100 K. It is also interesting that the HX band positions and widths approximate those of HX bound to the surface of amorphous ice films at <60 K. Though computational results suggest the adsorbed HX molecules observed in the jet expansions are weakly distorted by single coordination with surface dangling-oxygen atoms, on-the-fly trajectories indicate that the cluster skeletons undergo large-amplitude low-frequency vibrations. Local HX solvation, the extent of proton sharing, and the HX vibrational spectra undergo serious modulation on a picosecond time scale.

Introduction

Because of the importance to atmospheric chemistry and the broad basic interest in solvation and ionic dissociation of common strong acids, there have been numerous studies of the interaction of HCl and HBr (HX) with ice surfaces and water clusters during the past dozen years. Such systems offer a level of control of the solvation process not available in aqueous solutions. A specific question that has provided a basis for several recent investigations is the level of solvation/ionization of HX when exposed to water confined to clusters, surfaces, or particles at temperatures below 100 K.

Early FTIR data were interpreted as evidence of kinetic stabilization of molecular HX below ~60 K on amorphous ice films¹ and ice nanocrystals.² However, results of a molecular mechanics calculation suggested that HCl should ionize spontaneously on an ice surface.³ Other computational results are in general agreement that a cluster of four water molecules will dissociate a single adsorbed HX^{4,5} (and other references in ref 6), but the system must first assume a favorable coordination geometry, requiring mobility that may be missing at surfaces

of clusters, ice particles, and ice films at low temperatures. Recently, detailed reports suggesting the retention of a high fraction of molecular HCl for dilute coverage of ice films (refs 7 and 8, reactive ion scattering) and ice nanocrystals (ref 6, FTIR spectra) up to 90 K seemed to establish rough limits to the kinetic stabilization of molecular HX at an ice surface. By contrast, FTIR studies of HCl molecular beams condensed on ultrathin ice films on a metal substrate gave no indication of the presence of molecular HCl, even at 10 K.⁹

Meanwhile, ragout-jet FTIR spectra have become available for dense supersonic jets containing both HX and water at ~20 K,^{10,11} with the temperature estimated from the HX–monomer rotational line intensities. The approach yielded novel spectra of the 1:1 and 2:1 small water–HX clusters. Further, the spectra of the denser jets, particularly those rich in HX, contain information about the interaction of HX and larger water clusters at these low temperatures. This letter considers the spectra of these larger clusters as they relate to the question of solvation/ionization of HX in water systems at low temperatures. Combined spectral evidence is presented, from ragout jets and nanocrystals,⁶ of the existence of adsorbed molecular HCl. The interpretation of both types of spectra is also advanced through pertinent computational results.

* devlin@okstate.edu.

† Present address: J. Heyrovsky Institute of Physical Chemistry, Dolejskova 3, 182 23 Prague 8, Czech Republic.

Experimental Section

The two experimental approaches, ragout-jet cluster FTIR^{10,11} and ice-nanocrystal 3D-array FTIR spectroscopy,^{6,12} have been described in detail. The cluster jets were characterized by a high density of comparable amounts of HX and water, with helium as the carrier gas. Because water nucleates at a much higher temperature than HX, it is presumed that water clusters form initially and adsorb HX. However, some incorporation of HX in growing water clusters is possible. The spectra show that much of the HX and water remain as monomers or in pure and mixed small clusters, while bands are also indicated for larger water and pure (HX)_n clusters. Data were collected for both HCl and HBr with H₂O, as well as for HCl with D₂O. Here, the focus is on sampling with the highest HX–water ratios.

The main challenge in the determination of spectra of HX on ice nanoparticle surfaces is to obtain a reasonable distribution of HX over the ice particles within an array. Vapor diffusion is not satisfactory, as the HX is soaked up by the particles near the front of the array, so that HX self-solvation promotes the release of protons. Even at 60 K, the resulting spectra are dominated by hydrated proton bands. This difficulty is overcome by mixing HX clusters among larger (~12 nm) ice crystals during array formation. The HX moves to the ice particles upon warming in the 50–60 K range. This gives a more nearly even distribution of HX on the ice surface so that, with average HX coverage of ~10% of a monolayer, the bands of the ionically dissociated acid (i.e., hydrated protons) are observed only very weakly. Despite the large surface-to-volume ratio provided by the nanocrystal arrays, adsorbed HX bands are generally not observed directly. Rather, subtraction of a spectrum of a comparable pure ice array is required.

Results and Discussion

Spectra of the ragout jets containing HX and water are presented as the bottom three curves of Figure 1. The sharper features from monomers, dimers, trimers, and so forth. have been analyzed in previous publications.^{10,11} Of greatest interest here are the broader bands labeled B2 and the response of the B2 bands to a change of acid or change of water isotopic composition. The broad B2 band, in the case of HCl with H₂O, is centered near 2570 cm⁻¹, which closely matches the position (but not the width; ~150 vs ~300 cm⁻¹) of the “hydrated proton” band of the amorphous HCl monohydrate (Figure 1 of ref 1). However, it also precisely matches, in both position and bandwidth, the absorption by HCl on an amorphous ice surface (Figure 5A of ref 1 and top curve of Figure 1) assigned to singly coordinated molecular HCl.⁶

Because it has been shown that the hydrated-proton band blue-shifts ~40 cm⁻¹ when HCl is replaced by HBr in the ionic monohydrate,¹ the position of the B2 band in the (top) HBr/H₂O spectrum of Figure 1 is particularly informative. The B2 band red-shifts ~300 cm⁻¹ when HBr replaces HCl in the HX–water jet. This is similar to the red-shift (220 cm⁻¹) reported for the substitution of HBr for HCl adsorbed on the surface of ice nanocrystals⁶ and matches the ~310 cm⁻¹ shift reported for amorphous ice films (Figures 5 and 6 of ref 1). Such large chloride–bromide red-shifts are expected for *molecular* HX, considering the 330 cm⁻¹ lower gas-phase frequency of HBr. Furthermore, MP2 calculations⁶ of a water cluster with a singly coordinated HCl molecule bound to a dangling O placed the HCl frequency within 50 cm⁻¹ of the observed band positions (2528 vs 2570 cm⁻¹ in Figure 1 and the nanocrystal value of 2480 cm⁻¹).

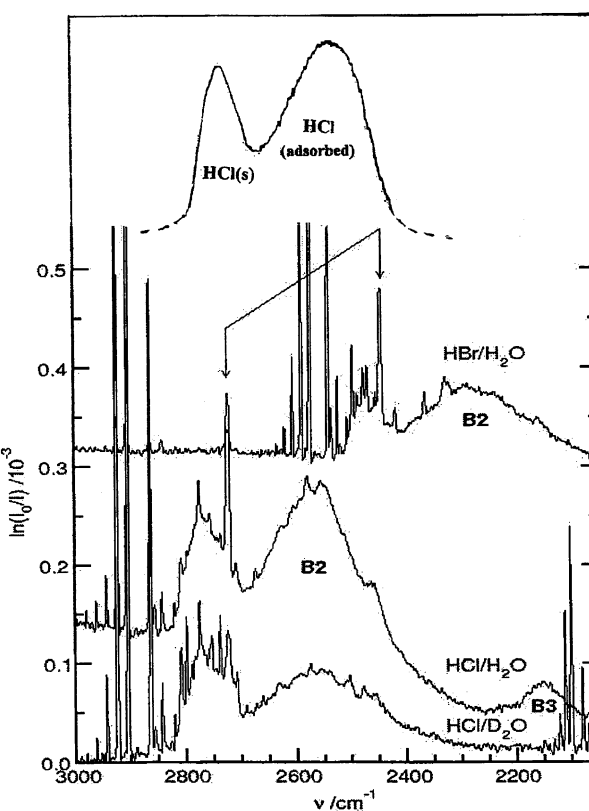


Figure 1. The bottom three curves are ragout-jet FTIR spectra of HX–water clusters adapted from ref 11. The molecular components within the supersonic jet are noted on each trace. The joined arrows indicate the corresponding mixed dimers. Other sharp bands are produced by monomers and small clusters. See the text for discussion of the broad bands labeled B2 and B3, and see refs 10 and 11 for details of the experimental conditions. The top spectrum is for HCl on amorphous ice at 60 K, as adapted from Figure 5 of ref 1.

This indication that the B2 bands of HX in Figure 1 have a molecular origin is confirmed by the lack of response of the HCl B2 band to the substitution of D₂O for H₂O in the ragout jet. The B2 band position and width are essentially unaffected by switching to D₂O water, inconsistent with B2 originating from hydrated (deuterated) protons. The expected influence on spectra from deuteration can be judged by comparing the spectra for amorphous protiated hydrates (Figure 1 of ref 1) with those of the deuterated hydrates (Figure 13 of ref 6). For all water–acid ratios, the major bands are red-shifted by hundreds of reciprocal centimeters. In particular, the 2550 band of the HCl monohydrate shifts to 2000 cm⁻¹. So, should B2 have a protonic origin, a strong deuteration shift from 2570 toward 2000 cm⁻¹ should be observed. A similar lack of band shift accompanied the replacement of H₂O with D₂O ice nanocrystals at 50 K (Figure 8 of ref 6). In that case, the intense D₂O ice band interfered with observation of the 2480 cm⁻¹ HCl band, but a second band, of dilute adsorbed HCl near 1740 cm⁻¹, was insensitive to deuteration of the ice. (This band, attributed to doubly coordinated, severely stretched molecular HCl, is outside the frequency range of the ragout-jet study.^{10,11})

One of the more convincing signs that a band is caused by molecular HX is its disappearance during warm-up of an ice array while bands attributed to the hydrated proton emerge. This can be seen in Figure 11 of ref 6. Figure 2 is included to show that, for our lowest HCl dosage of D₂O nanocrystals (~10% of a monolayer resulting in a minimum level of HCl self-solvation), the 1740 cm⁻¹ HCl band retains significant intensity up to 100 K. Meanwhile, a band assigned to molecular HCl attached to

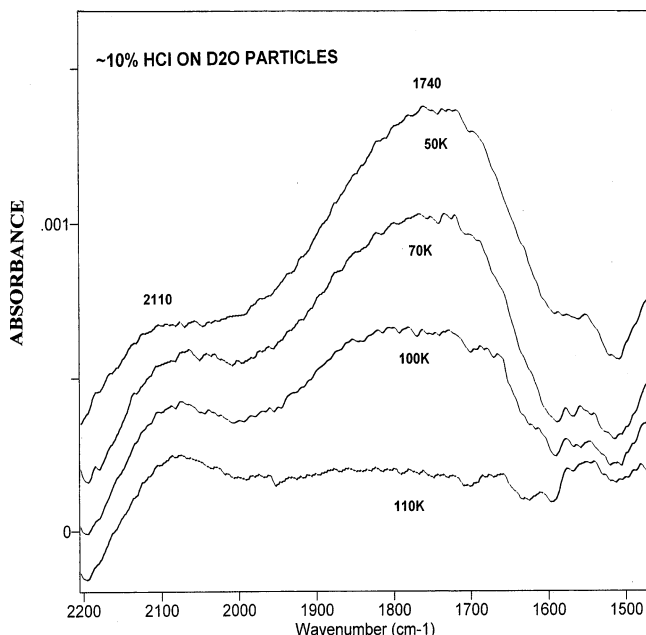


Figure 2. FTIR difference spectra for ~10% of a monolayer of adsorbed HCl on D₂O nanocrystals showing the temperature dependence of the 1740 cm⁻¹ HCl band.

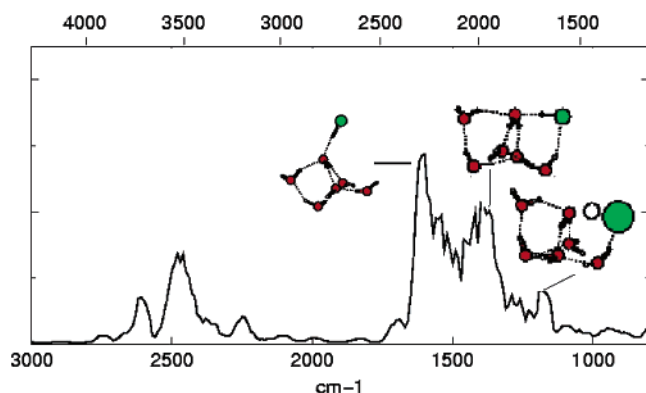


Figure 3. Infrared spectrum of a DCl(D₂O)₆ cluster from an on-the-fly 7 ps trajectory at 60 K. The different cluster structures (red—oxygen, black—hydrogen, and green—chloride), each identified with a DCl band component using sub-picosecond segments of the same trajectory, are described in the text. The larger chloride/hydrogen in the right structure signifies partial ionization. The frequency scale for protiated clusters (top) is also indicated. HCl frequencies are slightly underestimated at the present level of the calculation.

surface Cl⁻ from ionized HCl⁶ gradually intensifies near 2100 cm⁻¹. This emerging band resembles in position (2110 cm⁻¹) and bandwidth (~80 cm⁻¹) the B3 band of Figure 1, suggesting a low level of ionic dissociation of HX within the ragout jets. The B3 band does not appear in the HCl/D₂O spectrum, which was recorded for a lower HCl concentration.

Results in Figure 3, from an on-the-fly QUICKSTEP study of a mixed HCl–water cluster,¹³ help demonstrate qualitatively the type of vibrational dynamics that could lead to the observed HX spectra. A 60 K NVE (i.e., constant composition, volume, and energy) classical trajectory was calculated for a deuterated water hexamer with a single adsorbed DCl molecule (deuteration allows for larger time steps). The initial structure was adopted from Figure 60 of ref 6. The spectrum was determined from a 7 ps cluster trajectory, in the course of which the HCl intermittently probed an O-bonded singly coordinated molecular configuration, a doubly coordinated one, and occasionally, a proton-sharing configuration with a neighboring water molecule.

The lifetimes of the different configurations, in the ~0.1–1 ps range, included numerous HCl oscillations, and therefore, each produced a unique feature in the HCl spectrum, as marked in Figure 3. As expected, the highest-frequency feature originated from the singly coordinated configuration and the lowest from one with proton sharing. Many different but related HCl adsorbate configurations are sampled by experiment whether the HCl is adsorbed on a cluster or a particle surface, giving rise to an absorption continuum as in Figure 12 of ref 6, with maxima near 2570 cm⁻¹ (Figure 1) and 1750 cm⁻¹ (Figure 2). Ultimately, the solvation level and band positions are determined by factors such as the presence/absence of a second acceptor bond to the proton acceptor oxygen.^{6,17}

While the present computational example is not designed to sample all possible HCl–particle surface configurations, the results of Figure 3 exemplify several principles. A water–acid cluster, while including a sufficient number of solvent molecules for ionization, may be kinetically stabilized in a “particle–molecular adsorbate” configuration presumably because of an activation barrier.¹⁸ Rather, in the course of a trajectory, the cluster skeleton undergoes large-amplitude, low-frequency vibrations, which modulate the local solvation. The HX responds by transient adjustment of its vibrational frequency, resulting finally in a broad but structured infrared band. In this way, the same HCl molecule gives rise to three distinct spectroscopic features. Similar phenomena were observed in on-the-fly simulations of crystalline HX etherates.¹⁹ One can view this physical behavior as a “generalized Zundel effect” extended to the molecular acid.

Summary Conclusions

The presence of *molecular* acid adsorbate on icy particles at low temperatures is demonstrated in two independent experimental approaches. One pertains to water–acid clusters with tens of molecules at ~20 K. The other probes dilute acid adsorbates on water nanocrystals from 60 to 100 K. Because excess water is available for ionization in both cases, the molecular acid form appears to be kinetically stabilized. This interpretation of the experimental results is supported by an on-the-fly trajectory from QUICKSTEP¹³ for HCl bonded to (H₂O)₆.

However, the kinetic stabilization may have a quite different origin in the two cases. Only very dilute HX on ice nanocrystal surfaces resulted in dominant molecular bands at 60 K.⁶ The colder ragout jets leading to Figure 1 were comparably rich in acid and water on a molar basis. There are other condensed-phase examples in the literature where HX–water ratios near unity have resulted in the presence of a significant fraction of molecular HX. Giguere reported Raman spectra of supersaturated HX in water solutions with bands of HCl (2600 cm⁻¹) and HBr (2320 cm⁻¹) attributed to molecular HX complexes with water.²⁰ Though HX self-solvation can contribute significantly to proton transfer,^{6,19} it can be ineffective at high temperatures²⁰ and below ~50 K as indicated by the ragout-jet results and the spectra of films of excess HX deposited on amorphous ice surfaces (Figure 1 (top) and ref 1).

References and Notes

- (1) Delzeit, L.; Rowland, B.; Devlin, J. P. *J. Phys. Chem.* **1993**, *97*, 10312.
- (2) Delzeit, L.; Powell, K.; Uras, N.; Devlin, J. P. *J. Phys. Chem. B* **1997**, *101*, 2327.
- (3) Svanberg, M.; Pettersson, J. B. C.; Bolton, K. J. *J. Phys. Chem. A* **2000**, *104*, 5787.

- (4) Re, S.; Osamura, Y.; Suzuki, Y.; III, H. F. S. *J. Chem. Phys.* **1998**, *109*, 973.
- (5) Conley, C.; Tao, F. M. *Chem. Phys. Lett.* **1999**, *301*, 29.
- (6) Buch, V.; Sadlej, J.; Uras-Aytemiz, N.; Devlin, J. P. *J. Phys. Chem. A* **2002**, *106*, 41.
- (7) Kang, H.; Shin, T. H.; Park, S. C.; Kim, I. K.; Han, S. J. *J. Am. Chem. Soc.* **2000**, *122*, 9842.
- (8) Park, S. C.; Jung, K.-H.; Kang, H. *J. Chem. Phys.* **2004**, *121*, 2765.
- (9) Ayotte, P.; Hebert, M.; Marchand, P. Presented at the Symposium on Intermolecular interactions and reactions involving ions and open-shell systems; 227th ACS National Meeting, March 28–April 1, 2004; Anaheim, CA; PHYs 48.
- (10) Fárník, M.; Weimann, M.; Suhm, M. A. *J. Chem. Phys.* **2003**, *118*, 22.
- (11) Weimann, M.; Fárník, M.; Suhm, M. A. *Phys. Chem. Chem. Phys.* **2002**, *4*, 3933.
- (12) Devlin, J. P.; Buch, V. In *Water in Confining Geometries*; Buch, V., Devlin, J. P., Eds.; Springer: Berlin, 2003; Chapter 17, p 425.
- (13) Uras, N.; Buch, V.; Devlin, J. P. In progress. An on-the-fly molecular dynamics simulation was carried out with the help of the electronic structure code QUICKSTEP,¹⁴ which is part of the CP2K package.¹⁵ The method employs density functional theory; the Kohn–Sham orbitals are expanded using a linear combination of atom-centered Gaussian-type orbital functions, whereas an auxiliary basis set of plane waves is used to describe the electronic charge density.¹⁶ Calculations were at the BLYP/DZVP level. The Born–Oppenheimer energy and the forces were evaluated at each MD step. The code employs periodic boundaries with the simulated cluster in a box of 11 Å dimension. The spectrum was estimated as the squared Fourier transform of the cluster dipole, averaged over three perpendicular directions.
- (14) VandeVondele, J.; Krack, M.; Mohamed, F.; Parrinello, M.; Chassaing, T.; Hutter, J. *Comput. Phys. Comm.* Submitted 2004.
- (15) CP2K; <http://cp2k.berlios.de> (2000–2004).
- (16) Lippert, G.; Hutter, J.; Parrinello, M. *Mol. Phys.* **1997**, *92*, 477.
- (17) Gertner, B. J.; Hynes, J. T. *Science* **1996**, *271*, 1563.
- (18) Milet, A.; Struniewicz, C.; Moszynski, R.; Wormer, P. E. S. *J. Chem. Phys.* **2001**, *115*, 349.
- (19) Buch, V.; Mohamed, F.; Krack, M.; Sadlej, J.; Devlin, J. P.; Parrinello, M. *J. Chem. Phys.* **2004**, *121*, 12135.
- (20) Giguere, P. A.; Martel, C.; Turrell, S. *Chem. Phys. Lett.* **1978**, *56*, 231.

Infrared Spectroscopy of Water Cluster Anions, $(\text{H}_2\text{O})_{n=3-24}^-$ in the HOH Bending Region: Persistence of the Double H-Bond Acceptor (AA) Water Molecule in the Excess Electron Binding Site of the Class I Isomers

Joseph R. Roscioli, Nathan I. Hammer,[†] and M. A. Johnson*

Sterling Chemistry Laboratory, Yale University, P.O. Box 208107, New Haven, Connecticut 06520

Received: April 1, 2006; In Final Form: April 27, 2006

We report vibrational predissociation spectra of water cluster anions, $(\text{H}_2\text{O})_{n=3-24}^-$ in the HOH bending region to explore whether the characteristic red-shifted feature associated with electron binding onto a double H-bond acceptor (AA) water molecule survives into the intermediate cluster size regime. The spectra of the “tagged” $(\text{H}_2\text{O})_n^- \cdot \text{Ar}$ clusters indeed exhibit the signature AA band, but assignment of this motif to a particular isomer is complicated by the fact that argon attachment produces significant population of three isomeric forms (as evidenced by their photoelectron spectra). We therefore also investigated the bare clusters since they can be prepared exclusively in the high binding (isomer class I) form. Because the energy required to dissociate a water molecule from the bare complexes is much larger than the transition energies in the bending region, the resulting (linear) action spectroscopy selectively explores the properties of clusters with most internal energy content. The $(\text{H}_2\text{O})_{15}^-$ predissociation spectrum obtained under these conditions displays a more intense AA feature than was found in the spectra of the Ar tagged species. This observation implies that not only is the AA motif present in the class I isomer, but also that it persists when the clusters contain considerable internal energy.

Introduction

There has been a resurgence of interest in the water cluster anions, $(\text{H}_2\text{O})_n^-$, as model systems with which to explore how an excess electron is accommodated by well-defined water networks.^{1–12} This activity is, in turn, driven by a long-standing quest^{13–21} to understand the molecular-level mechanics underlying the curious properties of the bulk hydrated electron, a key intermediate in biological radiation damage.^{22,23} Recent studies have focused on the nature of three isomeric classes of the cluster anions that are differentiated according to their vertical electron detachment energies (VDE), with the three species denoted I, II, and III in decreasing order of their respective VDE values.^{3,4,11,24} In this paper, we report vibrational predissociation spectra of $(\text{H}_2\text{O})_n^-$ in the intramolecular HOH bending region to highlight the evolution of the cluster properties in the size range where the VDEs of types I and II rapidly diverge.^{4,11} This spectral region was chosen because it provides a distinct, well-isolated spectral signature when the excess electron binds primarily to a single water molecule that is attached to the network in a double H-bond acceptor (AA) motif. In this arrangement, both hydrogen atoms on the AA water molecule point directly into the electron cloud. The AA motif was established in the structures of the type I clusters in the small size ($n = 3–9$) range,^{11,12,25} and it is therefore of interest to determine whether this binding site is maintained in the larger type I clusters.

There are presently two scenarios in the literature that account for the differences between isomer classes I and II. Specifically, the Neumark group has considered the results of their recent ultrafast pump–probe studies of the electronically excited-state relaxation dynamics, as well as the size dependence of the cluster binding energies within each class, in the context of excess electron binding on either the cluster interior (type I) or the cluster surface (type II).^{4,26} Our group, on the other hand, has emphasized that, in addition to the overall solvation morphology, local binding may also play a crucial role in the determination of the cluster VDE. The latter suggestion was motivated by our spectroscopic observation that the I and II isomers of the hexamer anion both occur as surface states, but differ primarily in the molecular nature of the binding site.¹¹ In particular, the type II form of the hexamer does not display the spectral signature of the AA motif, exhibiting instead a band pattern consistent with the excess electron binding through the collective action of many water molecules. In this arrangement, several molecules stabilize the excess electron cloud by orienting one of their hydrogen atoms toward the electron while incorporating the other into the hydrogen bonding network.

Recent simulations by Rossky⁸ indicate that surface states can account for trends in the observed type I cluster properties, thus implicitly raising the issue of how different local binding motifs contribute to the distinction between the isomer classes. Moreover, Jordan and co-workers,²⁷ using a quantum Drude model coupled with Monte Carlo calculations, identified several AA-type motifs that survive at finite temperatures. These structures have vertical detachment energies similar to those found experimentally for isomer I. Interestingly, that study also

* To whom correspondence should be addressed: mark.johnson@yale.edu.

[†] Current address: Department of Chemistry, University of Massachusetts, Amherst, MA 01003.

recovered a new type of low-dipole-moment binding motif (“network-permeating”) in which correlation effects and polarizability are the primary forces at play in binding the electron.²⁷

The AA binding site identified in the smaller type I clusters yields a clear spectral signature in which the two stretching vibrations of the hydrogen atoms pointing into electron cloud account for a strong, red-shifted doublet in the OH stretching region, and its intramolecular bending fundamental appears uniquely red-shifted relative to the ν_2 band in the isolated water molecule. In an attempt to clarify the binding motifs at play in the larger members of the type I isomer class, we recently reported their OH stretch spectra through $n = 30$. Although aspects of the AA signature are retained in the larger clusters, the characteristic doublet evolved into a more red-shifted triplet around $n = 11$. Moreover, the AA stretching bands become increasingly embedded in the broad background arising from the H-bonded OH stretches of more remote water molecules, somewhat obscuring the features associated with the excess electron binding site. Therefore, in this study we extend the spectroscopic survey to cover the intramolecular bending region, where the red-shifted transition associated with the AA water molecule occurs well-separated from those arising from the supporting water network.²⁸

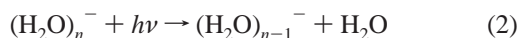
Because the photon energies necessary for excitation of the water bending transitions ($1500\text{--}1700\text{ cm}^{-1}$) are lower than the nominal water binding energy,²⁹ $D_0 \approx 3000\text{ cm}^{-1}$ (and the fact that the modest pulse energies available with tabletop laser sources in this energy range preclude multiphoton dissociation), acquisition of the bending region with action spectroscopy requires either the argon-tagged “messenger” technique³⁰ or working with warm bare clusters. Here, we use both approaches, and the resulting spectra establish that the AA motif not only survives throughout the $n = 11\text{--}24$ size range, but that it is actually most pronounced when the clusters contain the maximum internal energy possible within the evaporative ensemble ansatz.^{31,32}

Experimental Section

$(\text{H}_2\text{O})_n^-$ cluster ions were generated by secondary electron attachment to neutral water clusters, where the slow electrons were introduced by ionizing a pulsed nozzle (Parker-Hannefin general valve series #9, 0.5 mm orifice) expansion with a 1 keV counterpropagating electron beam. The expansion was formed by passing 4 atm Ar carrier gas over liquid water at room temperature. Coverage of the $600\text{--}1900\text{ cm}^{-1}$ energy range was carried out via nonlinear mixing in a AgGaSe₂ crystal, using the 1.5 and 3 μm outputs of a tunable solid-state IR laser source (8 ns Nd:YAG pumped Laser Vision OPO/OPA). Vibrational predissociation spectra were acquired by monitoring either argon loss



or water molecule evaporation



as a function of photon energy. The reported spectra resulted from the addition of 5–30 individual scans and were corrected for laser pulse energy variation over the scan range. Size-selective measurements were carried out using a double-focusing, tandem time-of-flight photofragmentation mass spectrometer described previously.^{33,34}

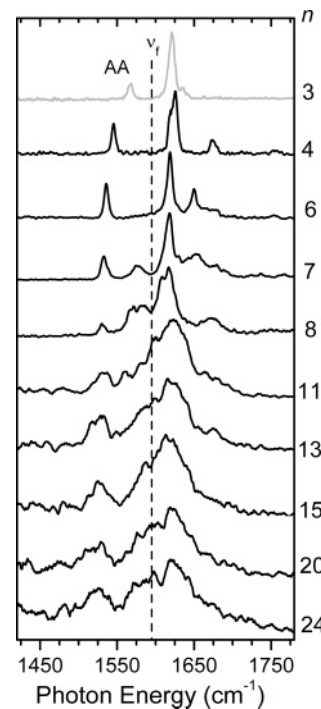


Figure 1. Predissociation spectra of $(\text{H}_2\text{O})_n^- \cdot \text{Ar}_m$ clusters in the HOH bending region. The dotted line (ν_f) indicates the position of the free water bend (1595 cm^{-1}). The upper trace shown in gray presents the spectrum of the $(\text{D}_2\text{O})_3^- \cdot \text{Ar}_6$ isotopologue, which is scaled by the ratio of bending frequencies in the isolated D_2O and H_2O molecules. Activity in the $1600\text{--}1700\text{ cm}^{-1}$ range is associated with water molecules that donate at least one hydrogen bond to the cluster network. The band near 1535 cm^{-1} is assigned to a water molecule in a double H-bond acceptor (AA) arrangement that interacts directly with the excess electron cloud. The persistence of this feature establishes that the AA motif plays an important role in this intermediate size range.

Results and Discussion

Intramolecular Bending Spectra of the $(\text{H}_2\text{O})_n^- \cdot \text{Ar}_m$ Species. The argon predissociation spectra of the $(\text{H}_2\text{O})_n^- \cdot \text{Ar}_m$ ($n = 4\text{--}24$) species in the HOH bending region are presented in Figure 1, along with the scaled spectrum of the $(\text{D}_2\text{O})_3^- \cdot \text{Ar}_6$ isotopologue¹² included in the top trace. Most importantly, all these species display the signature AA transition near 1535 cm^{-1} , which is red-shifted relative to the band in the isolated water molecule³⁵ (1595 cm^{-1} , dashed line labeled ν_f in Figure 1), establishing the persistence of an AA binding motif in the excess electron binding site over all sizes investigated. Interestingly, at $n = 7$ and 8 , although the AA transition is readily apparent, a second bending transition (labeled *) appears with about one third the red shift (relative to free water) as that displayed by the AA transition. The assignment of this new feature is not clear at present, and extended studies of these clusters are currently underway in our laboratory to clarify the motion responsible for this transition.

Isomer Distribution of the $(\text{H}_2\text{O})_{15}^- \cdot \text{Ar}_m$ Species. The use of argon-tagging to obtain predissociation spectra in the bending region introduces a complication because, as Verlet et al.⁴ have shown in their photoelectron study of the $(\text{D}_2\text{O})_n^-$ isotopologues, colder source conditions yield larger contributions from the more weakly bound (II and III) isomers. Since attachment of Ar likely results in even colder clusters, we must consider the possible role of isomers II and III in the $(\text{H}_2\text{O})_n^-$ system, even though only type I has been previously observed for the lighter isotope species in the larger ($n > 14$) size regime. To survey the possible role of isomers in the tagged $[(\text{H}_2\text{O})_n^- \cdot \text{Ar}]$ clusters, we recorded

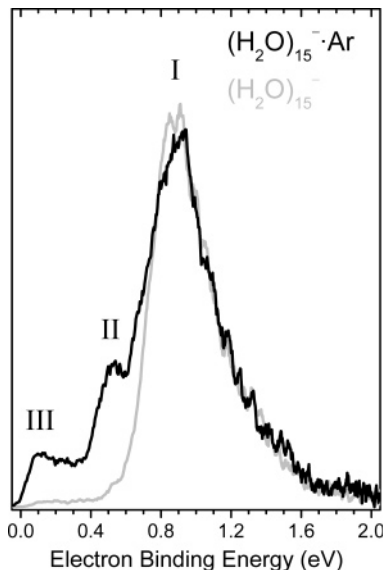


Figure 2. Photoelectron spectra of $(\text{H}_2\text{O})_{15}^-$ (gray) and $(\text{H}_2\text{O})_{15}^-\cdot\text{Ar}$ (black) clusters. Addition of argon atom to the cluster reduces the available internal energy and increases the fractional population of isomers II and III.

the (2.33 eV) photoelectron spectrum for $n = 15$ with the result compared with that of the bare cluster in Figure 2. Types II and III are indeed both present in the tagged cluster spectrum, and it should be noted that their relative contributions were highly dependent upon source conditions. In fact, it was often observed that isomer III was produced in greater abundance than isomer II. Because all three isomers contribute to the Ar-tagged ensemble, we are obliged to further investigate which of these is the carrier of the AA feature observed in the bending region (Figure 1), as discussed in the next section.

Isolating the Bending Spectrum of the Type I $(\text{H}_2\text{O})_{15}^-$ Isomer in Warm Clusters. Inspection of the photoelectron spectra in Figure 2 indicates that the bare $(\text{H}_2\text{O})_n^-$ clusters can be prepared exclusively in their type I form, thus presenting the possibility of isolating the spectrum of I in the bending region. Application of predissociation spectroscopy in the low-energy bending region is complicated, however, by the fact that the photon energy is significantly lower than the energy required to evaporate either a water molecule ($D_0 \approx 3000 \text{ cm}^{-1}$)²⁹ or the excess electron (at least in the large size regime).³⁶ This limitation is not straightforward to overcome with multiphoton absorption since the pulse output energy of our tabletop laser system is rather modest (~ 150 microjoules/pulse) in the bending region. We therefore must rely on selective excitation of clusters with sufficient internal energy that the photoexcited clusters decompose on the time scale of our experiment ($10 \mu\text{s}$).

The predissociation spectrum of the bare $(\text{H}_2\text{O})_{15}^-$ cluster is presented in Figure 3 along with that obtained from the Ar-tagged complex. The photofragment yield at 1525 cm^{-1} (the AA bend frequency) was indeed found to increase linearly as a function of pulse energy as expected for a one-photon process, and thus must reflect the character of parent clusters that contain considerable internal energy prior to photoexcitation. Interestingly, under these conditions, the AA feature is much more pronounced than that displayed in the Ar-tagged complex. This result, when combined with the photoelectron results (Figure 2), suggests that the more weakly binding isomers may not display the AA spectral signature, much like the situation observed earlier in the hexamer anion.¹¹

The persistence of the AA signature band in the bending region is significant because it indicates that the AA motif is

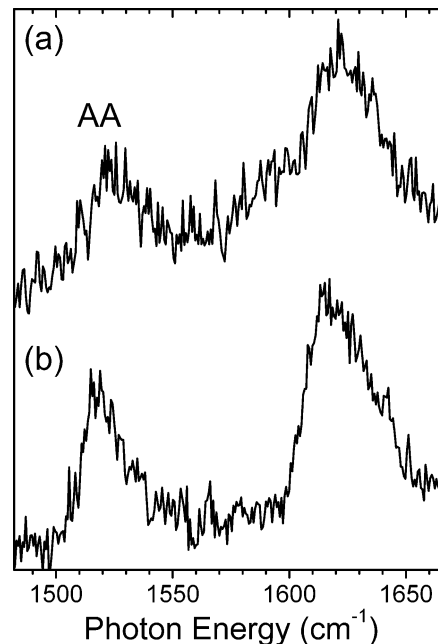
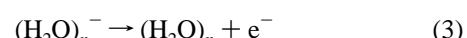


Figure 3. Comparison of the predissociation spectra arising from (a) $(\text{H}_2\text{O})_{15}^-\cdot\text{Ar}$, and (b) bare $(\text{H}_2\text{O})_{15}^-$. The enhancement of the strong transition at 1525 cm^{-1} establishes that the AA motif is present in the type I isomer at $n = 15$. The AA peak intensity in trace (b) was found to increase linearly with laser fluence, indicating that this action spectrum reflects a one-photon excitation process and thus results from clusters which contain significant internal energy prior to excitation.

retained as a feature of the type I isomers in the clusters above $n = 11$. This was not obvious in our earlier survey¹⁰ of the OH stretching bands, as the characteristic doublet in the $n = 4-9$ range evolved into a more red-shifted triplet that persists above $n = 11$ (at least up to $n = 30$). Also, having established that the AA motif is present in the larger clusters, it is now important to revisit the nature of the triplet found in the OH stretching bands in the vicinity of the features expected for the AA binding site. Note that the AA transition in the bending region does start to broaden at $n = 11$, suggesting that many structures likely contribute, perhaps arising from the plethora of H-bonding arrangements anticipated to be available for the supporting network at the larger sizes.^{37,38} Interestingly, the position of the AA feature of the bare complex appears somewhat red-shifted relative to the band in the colder, Ar-tagged clusters.

It is noteworthy that the signature band in the bending region is enhanced in the members of the ensemble that contain the most internal energy, indicating that it is a robust arrangement. This stability in the presence of high amplitude distortions of the neutral network was also observed theoretically by Herbert et al.,³⁹ where they found that the AA water molecule retains its relationship to the excess electron cloud even when the internal energy of the cluster is large enough to break hydrogen bonds elsewhere in the cluster scaffold. Although assignment of dependable temperatures to cluster ensembles formed in free jets is often problematic, the water clusters in this size range present a more favorable scenario, as Viggiano and co-workers have carried out high-pressure flow tube measurements to determine their reactivity and stability at well-defined temperatures.²⁹ The important observation for the present study is that the $(\text{H}_2\text{O})_n^-$ clusters were observed to spontaneously decompose by thermionic emission



above 130 K in the size range around $n = 15$. This sets a

reasonable upper limit on the (isokinetic) temperature characterizing the internal energy content of cluster ions in an evaporative ensemble.³¹ Thus, it would be most useful to engage theoretical analyses of the observed spectra with this starting point in mind.

Summary

Predisociation spectra of the $(\text{H}_2\text{O})_n^-\bullet\text{Ar}_m$ clusters in the HOH intramolecular bending region display the signature absorption arising from a double H-bond acceptor water molecule with both hydrogen atoms oriented into the excess electron cloud. A band is also recovered starting at $n = 7$, which occurs with about one third the red-shift as that of the AA molecule, whose assignment is presently unknown. Photoelectron spectra establish that many isomers contribute to the $n = 15$ Ar-tagged ensemble, but the bending predisociation spectrum of the type I form adopted by the bare cluster displays an intense transition in the location expected for the signature AA band. This indicates that the AA motif is retained for the high-binding class I isomers into the intermediate size regime, and that it survives as a persistent local binding site in clusters with considerable internal energy content.

References and Notes

- (1) Coe, J. V. *Int. Rev. Phys. Chem.* **2001**, *20*, 33.
- (2) Paik, D. H.; Lee, I.-R.; Yang, D.-S.; Baskin, J. S.; Zewail, A. H. *Science* **2004**, *306*, 672.
- (3) Bragg, A. E.; Verlet, J. R. R.; Kammrath, A.; Cheshnovsky, O.; Neumark, D. M. *Science* **2004**, *306*, 669.
- (4) Verlet, J. R. R.; Bragg, A. E.; Kammrath, A.; Cheshnovsky, O.; Neumark, D. M. *Science* **2005**, *307*, 93.
- (5) Herbert, J. M.; Head-Gordon, M. *J. Phys. Chem. A* **2005**, *109*, 5217.
- (6) Lee, H. M.; Lee, S.; Kim, K. S. *J. Chem. Phys.* **2003**, *119*, 187.
- (7) Lee, H. M.; Suh, S. B.; Tarakeshwar, P.; Kim, K. S. *J. Chem. Phys.* **2005**, *122*, 044309.
- (8) Turi, L.; Sheu, W.-S.; Rossky, P. J. *Science* **2005**, *309*, 914.
- (9) Shin, J.-W.; Hammer, N. I.; Headrick, J. M.; Johnson, M. A. *Chem. Phys. Lett.* **2004**, *399*, 349.
- (10) Hammer, N. I.; Roscioli, J. R.; Bopp, J. C.; Headrick, J. M.; Johnson, M. A. *J. Chem. Phys.* **2005**, *123*, 244311.
- (11) Hammer, N. I.; Roscioli, J. R.; Johnson, M. A. *J. Phys. Chem. A* **2005**, *109*, 7896.
- (12) Hammer, N. I.; Roscioli, J. R.; Johnson, M. A.; Myshakin, E. M.; Jordan, K. D. *J. Phys. Chem. A* **2005**, *109*, 11526.
- (13) Hart, E. J.; Boag, J. W. *J. Am. Chem. Soc.* **1962**, *84*, 4090.
- (14) Barnett, R. N.; Landman, U.; Cleveland, C. L.; Jortner, J. *J. Chem. Phys.* **1988**, *88*, 4421.
- (15) Long, F. H.; Lu, H.; Eisenthal, K. B. *Phys. Rev. Lett.* **1990**, *64*, 1469.
- (16) Schwartz, B. J.; Rossky, P. J. *J. Chem. Phys.* **1994**, *101*, 6917.
- (17) Silva, C.; Walhout, P. K.; Yokoyama, K.; Barbara, P. F. *Phys. Rev. Lett.* **1998**, *80*, 1086.
- (18) Kambhampati, P.; Son, D. H.; Kee, T. W.; Barbara, P. F. *J. Phys. Chem. A* **2002**, *106*, 2374.
- (19) Baltuška, A.; Emde, M. F.; Pshenichnikov, M. S.; Wiersma, D. A. *J. Phys. Chem. A* **1999**, *103*, 10065.
- (20) Pshenichnikov, M. S.; Baltuška, A.; Wiersma, D. A. *Chem. Phys. Lett.* **2004**, *389*, 171.
- (21) Beyer, M. K.; Fox, B. S.; Reinhard, B. M.; Bondybey, V. E. *J. Chem. Phys.* **2001**, *115*, 9288.
- (22) *Radiation Chemistry*; Farhataziz, Rodgers, M. A. J., Eds. VCH Publishers: New York, 1987.
- (23) Garrett, B. C.; Dixon, D. A.; Camaiioni, D. M.; Chipman, D. M.; Johnson, M. A.; Jonah, C. D.; Kimmel, G. A.; Miller, J. H.; Rescigno, T. N.; Rossky, P. J.; Xantheas, S. S.; Colson, S. D.; Laufer, A. H.; Ray, D.; Barbara, P. F.; Bartels, D. M.; Becker, K. H.; Bowen, H.; Bradforth, S. E.; Carmichael, I.; Coe, J. V.; Corrales, L. R.; Cowin, J. P.; Dupuis, M.; Eisenthal, K. B.; Franz, J. A.; Gutowski, M. S.; Jordan, K. D.; Kay, B. D.; LaVerne, J. A.; Lymar, S. V.; Madey, T. E.; McCurdy, C. W.; Meisel, D.; Mukamel, S.; Nilsson, A. R.; Orlando, T. M.; Petrik, N. G.; Pimblott, S. M.; Rustad, J. R.; Schenter, G. K.; Singer, S. J.; Tokmakoff, A.; Wang, L. S.; Wittig, C.; Zwier, T. S. *Chem. Rev.* **2005**, *105*, 355.
- (24) Coe, J. V.; Lee, G. H.; Eaton, J. G.; Arnold, S. T.; Sarkas, H. W.; Bowen, K. H.; Ludewigt, C.; Haberland, H.; Worsnop, D. R. *J. Chem. Phys.* **1990**, *92*, 3980.
- (25) Hammer, N. I.; Shin, J.-W.; Headrick, J. M.; Diken, E. G.; Roscioli, J. R.; Weddle, G. H.; Johnson, M. A. *Science* **2004**, *306*, 675.
- (26) Kammrath, A.; Verlet, J. R. R.; Bragg, A. E.; Griffin, G. B.; Neumark, D. M. *J. Phys. Chem. A* **2005**, *109*, 11475.
- (27) Sommerfeld, T.; Jordan, K. D. *J. Am. Chem. Soc.* In press.
- (28) Paul, J. B.; Provencal, R. A.; Chapo, C.; Roth, K.; Casae, R.; Saykally, R. J. *J. Phys. Chem. A* **1999**, *103*, 2972.
- (29) Arnold, S. T.; Morris, R. A.; Viggiano, A. A.; Johnson, M. A. *J. Phys. Chem.* **1996**, *100*, 2900.
- (30) Ayotte, P.; Weddle, G. H.; Kim, J.; Johnson, M. A. *Chem. Phys.* **1998**, *239*, 485.
- (31) Klots, C. E. *Z. Phys. D: At., Mol. Clusters* **1987**, *5*, 83.
- (32) Klots, C. E. *J. Chem. Phys.* **1985**, *83*, 5854.
- (33) Posey, L. A.; DeLuca, M. J.; Johnson, M. A. *Chem. Phys. Lett.* **1986**, *131*, 170.
- (34) Johnson, M. A.; Lineberger, W. C. In *Techniques for the Study of Ion-Molecule Reactions*; Farrar, J. M., Saunders, W. H. J., Eds.; Wiley: New York, 1988; Vol. XX, p 591.
- (35) *NIST Chemistry WebBook*; National Institute of Standards and Technology: Gaithersburg, MD, 2001.
- (36) Campagnola, P. J.; Cyr, D. M.; Johnson, M. A. *Chem. Phys. Lett.* **1991**, *181*, 206.
- (37) Tsai, C. J.; Jordan, K. D. *J. Phys. Chem.* **1993**, *97*, 11227.
- (38) Tharrington, A. N.; Jordan, K. D. *J. Phys. Chem.* **2003**, *107*, 7380.
- (39) Herbert, J. M. International Symposium on Molecular Spectroscopy, 2005, Columbus, OH.

Infrared Cavity Ringdown Spectroscopy of the Water Cluster Bending Vibrations

J. B. Paul, R. A. Provencal, C. Chapo, K. Roth, R. Casaeas, and R. J. Saykally*,†

Department of Chemistry, University of California, Berkeley, California 94720

Received: December 4, 1998

We report the first measurement of water monomer bending vibrations in gaseous $(\text{H}_2\text{O})_n$ clusters. Infrared cavity ringdown spectroscopy reveals discrete and sequentially blue-shifted bands near $6 \mu\text{m}$ for $n = 2-4$ and unresolved broad features for $n > 4$, supporting both theoretical predictions and solid-state spectroscopy results. These measurements provide a measure of the monomer distortion that accompanies sequential hydrogen bond formation, which will be valuable for the construction of potential energy surfaces for describing water.

Introduction

Recent experimental and theoretical advances in the study of water clusters are rapidly providing new insight into the nature of solid and liquid water. Most of this effort has involved the measurement and interpretation of terahertz vibration–rotation–tunneling (VRT) spectra, from which details of the intermolecular force fields and hydrogen bond rearrangement dynamics can be extracted. The coupling between inter- and intramolecular modes, as well as the distortion of monomers by polarization effects, is an important complementary feature that can be probed through measurements of the monomer covalent vibrations in the clusters. This was first accomplished in matrix isolation studies,^{1,2} but the associated strong environmental perturbations obfuscate the results of these experiments. Vernon and co-workers³ first measured the O–H stretching spectrum of gaseous water clusters by infrared predissociation measurements near $3 \mu\text{m}$. Subsequently, several other groups performed similar indirect measurements, all of which depend on consequences of photon absorption for detection of the spectrum.^{4–6} The dynamical processes convolved with the detection process obscure the vibrational transitions themselves, which are most directly probed in an absorption spectroscopy experiment. Such experiments, however, are difficult because of the relatively low sensitivity of direct absorption methods, particularly when used in conjunction with pulsed lasers. We recently reported the first direct absorption results for both the O–H and O–D stretching vibrations of water clusters using our recently developed infrared cavity ringdown technology.^{7,8} Here, we report the first measurement of the covalent bending vibrations in gaseous water clusters made by extending the CRLAS technique into the $6 \mu\text{m}$ region.

Experimental Section

The IR–CRLAS apparatus used to conduct these experiments has been discussed previously.^{7,9} Briefly, tunable infrared radiation is generated by Raman shifting a pulsed dye laser (Lambda Physik f13002e) into the third-Stokes band using a multipass cell containing 200 psi of H_2 gas. The bandwidth of the dye laser was switchable from 0.2 to 0.04 cm^{-1} by installing an intracavity Etalon. After spectral filtering, the laser light is aligned into a two mirror Ringdown cavity. The light leaving the cavity is focused by a 10 cm lens onto an LN_2 -cooled InSb

detector. The resultant signal is amplified, digitized, and transferred to a PC for real-time fitting to an exponential decay. The determined time-constant is divided into the cavity optical transit time to yield the per-pass fractional cavity intensity loss.

The water clusters were generated in a pulsed supersonic expansion. The helium carrier gas was bubbled through a reservoir of room-temperature water and directed through a 4 in. slit source¹⁰ contained within a Roots pumped vacuum chamber. Various methods were used to systematically adjust the expansion conditions, including altering the source stagnation pressure and limiting the amount of water in the expansion with a needle valve, as discussed below.

Results and Discussion

In contrast with the O–H stretching vibrations, the bending vibrations in water clusters are predicted to exhibit sequential *blue shifts* with increasing cluster size (for the lowest frequency vibrations) accompanied by a *decreasing* per-monomer absorption strength.¹¹ The hydrogen bonds constrain the motion in the bending coordinate, which accounts for these effects. This translates into a decreased sensitivity to larger clusters, as compared with measurements in the O–H stretch region, along with an increased band congestion, as the vibrational frequencies only spread out by ca. 50 cm^{-1} , rather than the several hundred wavenumber shifts observed for the stretching vibrations.

These theoretically predicted effects are clearly confirmed in the IR–CRLAS spectrum of water clusters in this spectral region, as shown in Figure 1. On the basis of the previous measurements of O–H stretch vibrations, only the absorption bands of the dimer and the trimer should be observable for the lowest concentrations employed here. Additionally, we know that under the present conditions the growth rates of features due to $(\text{H}_2\text{O})_2$ through $(\text{H}_2\text{O})_4$ with increasing water concentration become sequentially larger with increasing cluster size. Considering these factors, we assign the discrete absorption features appearing at 1600.6 , 1613.8 , 1614.7 , and 1628.6 cm^{-1} to $(\text{H}_2\text{O})_2$. The close proximity of the 1600.6 cm^{-1} band to the monomer bend band origin leads to the assignment of this band to the acceptor bend, while the band shape is consistent with that of a parallel transition ($\Delta K = 0$).

The remaining dimer features are assigned to a perpendicular transition ($\Delta K = \pm 1$) involving the donor bending vibration. These presumably correspond to the Q-branches of the A_2 acceptor tunneling component, which carries three times the

* Berkeley Miller Research Professor 1997-98.

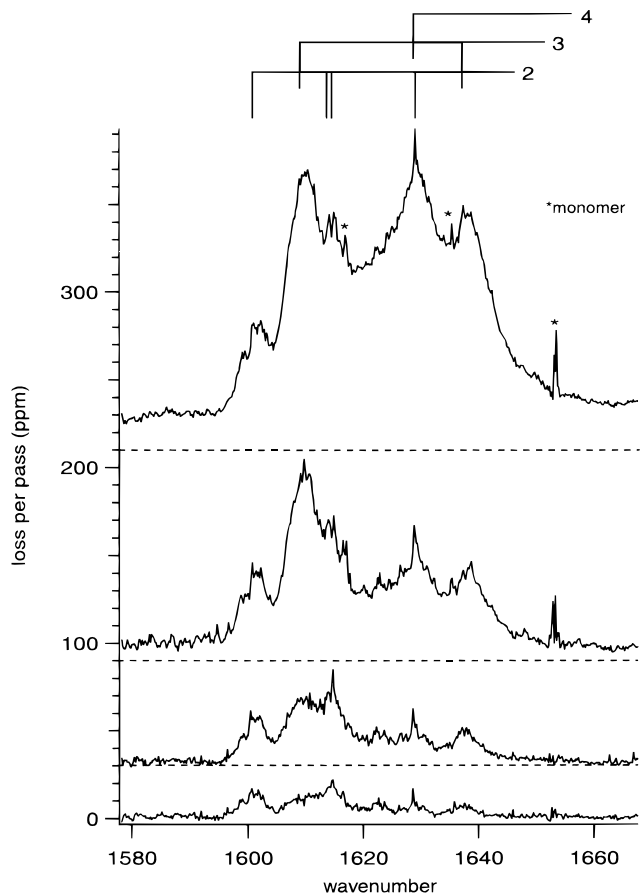


Figure 1. Water cluster spectra in the monomer bending region as a function of increasing water concentration in the expansion. The concentration is varied by seeding a H₂O/helium gas flow into a pure helium flow with a needle valve. The assignments of the discrete features to various sized clusters are given in the upper part of the figure.

nuclear spin-weight of the A₁ component. Additionally, the Q-branches offer sufficient line density to be observed in the present moderate (1 GHz) resolution study. In contrast, the P and R branches are extremely sparse, and are not easily observed with the present instrument resolution. Because the magnitude of acceptor switching splitting is similar to the (H₂O)₂ A rotational constant, the appearance of this band system is expected to be markedly different from that of a “normal” prolate-top perpendicular band, which displays subbands evenly spaced by ca. twice the A rotational constant. Furthermore, since this particular vibrational mode directly influences the hydrogen bond, the upper state tunneling splittings are likely to be significantly changed from those in the ground state. Without additional knowledge of these upper state splittings or of the actual P- and R-branch structure, therefore, the rotational assignment of these bands is not possible at the present time. Likewise, an accurate determination of the band origin is not possible from the present data.

Bands found at 1609 and 1638 cm⁻¹ grow dramatically with increasing concentration compared to the (H₂O)₂ bands, but they can still be observed at the lowest concentration employed in this study. Therefore, we assign these features to (H₂O)₃. At still higher concentration, a distinct band appears centered at 1629 cm⁻¹, which we assign to (H₂O)₄. Additionally, a broad, seemingly continuous absorption in the 1600–1650 cm⁻¹ region must be due to (H₂O)₄ and larger clusters. Finally, weak continuum absorption can be seen extending beyond 1650 cm⁻¹, which will be discussed below.

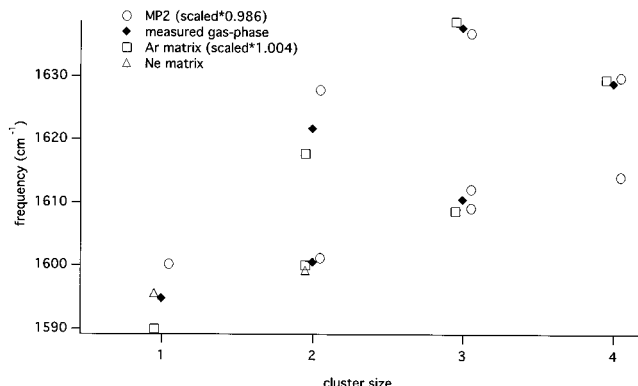


Figure 2. Comparison of the measured gas-phase, Ar matrix [ref 2], Ne matrix [ref 12], and ab initio [ref 11] bending frequencies of small water clusters. Note that the Ne matrix results are shown unscaled. (Monomer gas-phase data from ref 12.)

The above small cluster assignments are supported by comparison with results from both cryogenic matrix^{12,2} and ab initio studies.¹¹ The band positions from these studies are plotted along with the present measurements in Figure 2, as a function of cluster size. The previous results have been slightly scaled to provide the best match with the observed gas-phase band locations, with the matrix data requiring a scaling factor of 1.004, while the ab initio results require a factor of 0.986. Once these scaling factors are included, the agreement between the present results with both calculated and argon matrix band positions is excellent. In fact, every major feature observed in the matrix data is reproduced in the gas-phase results, and all of the previous solid-state carrier assignments agree with the present determinations.

While the ab initio (H₂O)₃ frequencies¹¹ compare favorably with the present results, the band intensities do not. Theory predicts that the low frequency feature is actually two bands with a combined intensity of 950 km/mol, whereas the higher frequency band strength is predicted to be only 11 km/mol. These values should be compared with the ca. 2:1 ratio measured in the present study. This discrepancy resembles the differences between the calculated and observed O–H stretch band intensities,¹³ and certainly warrants further investigation.

We attribute the broad absorption in the 1600–1650 cm⁻¹ region to water clusters in the 4 < n < 20 size range, based upon the range of source pressures for which absorption in this region continues to increase. Compared with the O–H stretch region, the band density is substantially higher due to the significantly narrower frequency distribution. This, combined with the lower absorption strength of larger clusters, explains why individual features are not readily discerned for clusters larger than n = 4 in the present spectra. Additionally, we do not observe a discrete feature for the (H₂O)₄ band predicted to lie near 1613 cm⁻¹ (Figure 2), presumably for these same reasons.

With conditions favoring the production large clusters (i.e. high water concentration, high source backing pressure) the O–H stretching spectrum is dominated by a broad red-shifted “ice-like” feature.⁷ The behavior in the bending region is dramatically different, as shown in Figure 3, which compares the weak blue-shifted continuum mentioned above with the absorptions of liquid¹⁴ and amorphous solid¹⁵ water. For reference, the absorption due to the smaller clusters (1600–1650 cm⁻¹) extends off the graph at this scale. As was found in the O–H region, the spectrum of clusters in this size range of hundreds or even thousands of water molecules per cluster is quite similar to that of the bulk forms of water. The magnitude

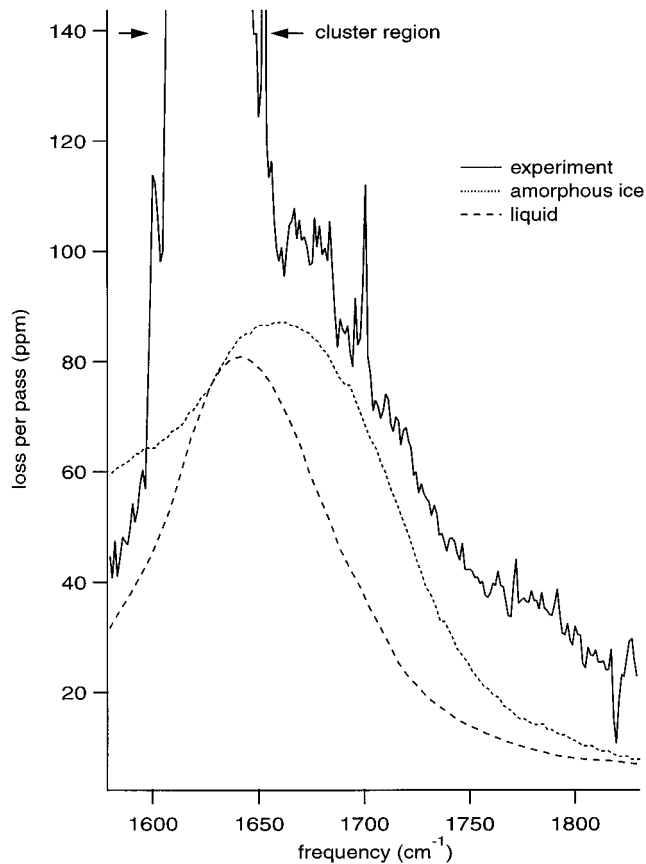


Figure 3. Comparison of the broad absorption feature presently observed with the absorptions of liquid [ref 14] and amorphous solid [ref 15] water.

of the blue shift of this broad feature is indicative of the strength of the hydrogen bonding network. The fact that the gas phase “ice” feature is most blue shifted suggests that the cooperative effects in the hydrogen bond network of clusters in this size range is stronger than those in amorphous ice.

In summary, this work reports a first characterization of the monomer bending vibrations of $(\text{H}_2\text{O})_n$ clusters. From these data, we are able to quantify the sequential blue shifts resulting from the cooperative effects in hydrogen bonding. This, in turn, provides a measure of the coupling between inter and intramolecular vibrations, which is essential to elucidate the effects of monomer distortion on the intermolecular potential energy surface.

Acknowledgment. This work was supported by the Chemical Physics Program of the Air Force Office of Scientific Research (AFOSR) and by the Experimental Physical Chemistry Program of the National Science Foundation (NSF).

References and Notes

- (1) Brentwood, R. M.; Barnes, A. J.; Orville-Thomas, W. J. *J. Mol. Spectrosc.* **1980**, *84*, 391.
- (2) Ayers, G. P.; Pullin, A. D. E. *Spectrochim. Acta* **1976**, *32A*, 1629.
- (3) Vernon, M. F.; Krajnovich, D. J.; Kwok, H. S.; Lisick, J. M.; Shen, Y. R.; Lee, Y. T. *J. Chem. Phys.* **1982**, *77*, 47–57.
- (4) Coker, D. F.; Miller, R. E.; Watts, R. O. *J. Chem. Phys.* **1985**, *82*, 3554–3562.
- (5) Huang, Z. S.; Miller, R. E. *J. Chem. Phys.* **1989**, *91*, 6613–6631.
- (6) Huisken, F.; Kaloudis, M.; Kulcke, A. *J. Chem. Phys.* **1996**, *104*, 17–25.
- (7) Paul, J. B.; Collier, C. P.; Scherer, J. J.; O’Keefe, A.; Saykally, R. J. *J. Phys. Chem.* **1997**, *101*, 5211–5214.
- (8) Paul, J. B.; Provencal, R. A.; Chapo, C.; Pettersson, A.; Saykally, R. J. *J. Chem. Phys.* **1998**. In press.
- (9) Paul, J. B.; Provencal, R. A.; Saykally, R. J. *J. Phys. Chem.* **1998**, *102*, 3279–3283.
- (10) Liu, K.; Fellers, R. S.; Viant, M. R.; McLaughlin, R. P.; Brown, M. G.; Saykally, R. J. *Rev. Sci. Instrum.* **1996**, *67*, 410–416.
- (11) Xantheas, S. S.; Dunning Jr., T. H. *J. Chem. Phys.* **1993**, *99*, 8774–8792.
- (12) Forney, D.; Jacox, M. E.; Thompson, W. E. *J. Mol. Spectrosc.* **1993**, *157*, 479–493.
- (13) Paul, J. B.; Provencal, R. A.; Chapo, C.; Pettersson, A.; Saykally, R. J. In preparation.
- (14) Downing, H. D.; Williams, D. *J. Geophys. Res.* **1975**, *80*, 1656.
- (15) Hagen, W.; Tielens, A. G. G. M.; Greenberg, J. M. *Chem. Phys.* **1981**, *56*, 367–379.

COMMENTS

Comment on ‘‘Dication–Water Interactions: $M^{2+}(H_2O)_n$ Clusters for Alkaline Earth Metals M = Mg, Ca, Sr, Ba, and Ra’’

Young-Kyu Han*

Department of Chemistry, Korea Advanced Institute of Science and Technology, Taejon, 305-701, Korea

Ho Young Jeong

Kumho Chemical Laboratories, P.O. Box 64, Yuseong, Taejon, 305-600, Korea

Received: May 20, 1996; In Final Form: September 12, 1996

The recent paper¹ by Glendening et al. is concerned with $M^{2+}(H_2O)_n$ clusters for alkaline earth metals M = Mg, Ca, Sr, Ba, and Ra. We wish to comment on the basis set quality of the metals by virtue of the calculations of alkaline earth metal dihydrates.

It is well-known that the alkaline earth metal dihydrates have equilibrium geometries of bent structures,^{1–3} which could be explained by core polarization or s–d hybridization.^{3–7} According to the reported results from the calculations of $M^{2+}(H_2O)_2$ for alkaline earth metals M = Mg, Ca, Sr, and Ba, the linearization energy ΔE and the bond lengthening upon linearization ΔR increase, and the O–M–O angle decreases as atomic number of the central metal grows. Since we regard it as a reasonable postulate that similar trends should be shown in the heaviest homologue $Ra^{2+}(H_2O)_2$ complex, we performed the calculations of $M^{2+}(H_2O)_2$, M = Ca, Sr, Ba, and Ra.

Geometry optimizations were performed at the RHF level of theory using the GAUSSIAN92⁸ and GAMESS⁹ programs. The

symmetry of bent structures is normally the C_s form. Electron correlation was treated at the MP2 level of theory using the RHF optimized geometries. We used the 10-valence-electron averaged relativistic effective core potential (AREP) for the Ca 5s4p, Sr 5s5p, and Ba and Ra 5s5p4d basis sets reported by Ermler et al.¹⁰ These sets were augmented by d polarization sets⁵ generated by Kaupp et al. and added to Ca and Sr. All basis sets of metals are uncontracted. For O, the 6-31+G* basis set is used. The ($n - 1$) outermost core electrons of Ca, Sr, Ba, and Ra were correlated in all calculations and correlation in the MP2 calculations. The calculation strategy is the same as Glendening’s work except for using more flexible basis sets for the metals.

Table 1 shows M–O and O–H distances, O–M–O angles, energies, ΔR ’s, and ΔE ’s for the $M^{2+}(H_2O)_2$ complexes. It is found that all the trends obtained from the calculations of Ca, Sr, and Ba complexes are extended to the heaviest homologue, the Ra case. The results of Glendening et al. are in good agreement with the results in Table 1 for $M^{2+}(H_2O)_2$ (M = Ca, Sr, Ba) complexes. However, their results for the complexes including Ra do not show the trend in any of ΔR , ΔE , and O–M–O angles. (See footnote in Table 1.) Usually, the linearization energies by the authors for $M^{2+}(H_2O)_2$ (M = Ca, Sr, Ba) are slightly larger than ones obtained from our calculations using a more flexible basis set. However, it is not the case in $Ra^{2+}(H_2O)_2$. The deviations from the trend of structural parameters and linearization energies in the $Ra^{2+}(H_2O)_2$ complex are mainly due to the inflexibility of the basis set originating from the insufficient basis or severe basis contraction of the Ra basis set in their calculations.

In order to confirm it, we calculated the ΔR ’s, ΔE ’s, and O–M–O angles for the $Ra^{2+}(H_2O)_2$ complex using various

TABLE 1: M–O and O–H Distances^a (Å), O–M–O Angles^a (deg), Energies (au), Linearization Energies ΔE (kcal), and Bond Lengthening upon Linearization ΔR (Å) for $M^{2+}(H_2O)_2$ Complexes

	sym	$r(M-O)^b$	$r(O-H)$	$\angle(OMO)$	HF	MP2
$Ca^{2+}(H_2O)_2$	D_{2d}^c	2.321	0.960	180.0	-187.883 782 3	-188.484 300 7
	C_s^c	2.312	0.960	130.4	-187.884 332 2	-188.484 549 2
	ΔR 0.009				ΔE 0.35	ΔE 0.16
$Sr^{2+}(H_2O)_2$	D_{2d}	2.507	0.959	180.0	-181.926 186 2	-182.471 397 2
	C_s	2.488	0.959	116.3	-181.927 397 4	-182.472 565 7
	ΔR 0.019				ΔE 0.76	ΔE 0.73
$Ba^{2+}(H_2O)_2$	D_{2d}	2.723	0.957	180.0	-176.752 350 8	-177.270 127 8
	C_s	2.696	0.957	110.7	-176.754 041 7	-177.271 944 8
	ΔR 0.027				ΔE 1.06	ΔE 1.14
$Ra^{2+}(H_2O)_2$	D_{2d}	2.816	0.957	180.0	-175.390 650 4	-175.893 401 2
	C_s	2.784	0.957	107.7	-175.392 526 1	-175.895 420 4
	ΔR 0.032				ΔE 1.18	ΔE 1.27

^a RHF/6-31+G* optimized geometries. ^b The $r(M-O)$ values for C_s forms are the average of two M–O distances. ^c D_{2d} is the linear form and C_s is the bent one. Glendening et al.’s results are as follows. Reference 1: $\Delta R(Ca) = 0.006$, $\angle(OCaO) = 132.6$, $\Delta E_{HF}(Ca) = 0.21$, $\Delta E_{MP2}(Ca) = 0.35$; $\Delta R(Sr) = 0.018$, $\angle(OSrO) = 116.3$, $\Delta E_{HF}(Sr) = 0.80$, $\Delta E_{MP2}(Sr) = 1.06$; $\Delta R(Ba) = 0.027$, $\angle(OBaO) = 110.9$, $\Delta E_{HF}(Ba) = 1.19$, $\Delta E_{MP2}(Ba) = 1.46$; $\Delta R(Ra) = 0.020$, $\angle(ORaO) = 112.5$, $\Delta E_{HF}(Ra) = 0.41$, $\Delta E_{MP2}(Ra) = -0.31$.¹¹

TABLE 2: Ra–O Distances^a (Å), O–Ra–O Angles^a (deg), Linearization Energies ΔE (kcal), and Bond Lengthening upon Linearization ΔR (Å) for $Ra^{2+}(H_2O)_2$ Complexes

contraction pattern	$r(Ra-O)^b$	$\angle(ORaO)$	$\Delta E(HF)$	$\Delta E(MP2)$
11111/11111/1111	2.784	107.7	1.18	1.28
11111/11111/211	2.788	107.6	1.10	1.23
11111/11111/31	2.788	107.6	1.08	1.41
11111/11111/4	2.801	107.3	0.42	-0.35
311/311/4 ^c	2.803	112.5	0.41	-0.31

^a RHF/6-31+G* optimized geometries. ^b The $r(M-O)$ values for C_s forms are the average of two Ra–O distances. ^c Reference 1.

forms of contracted d basis and summarized the results in Table 2. As shown in the table, the deviation of trends in the $\text{Ra}^{2+}\text{-}(\text{H}_2\text{O})_2$ complex originates from the severe contraction of the d basis set of Ra, except for the bond angle. It is found that at least two sets of d basis are necessary for obtaining monotonic trends for ΔR , O-M-O, and ΔE . In order to investigate the trends of change in various chemical phenomena down the periodic table, a balance of basis sets for each atom in the same family is necessary.

Acknowledgment. We thank Dr. Eric D. Glendening for valuable discussions.

References and Notes

- (1) Glendening, E. D.; Feller, D. *J. Phys. Chem.* **1996**, *100*, 4790.
- (2) Bauschlicher, C. W., Jr.; Sodipe, M.; Partridge, H. *J. Chem. Phys.* **1992**, *96*, 4453.
- (3) Kaupp, M.; Schleyer, P. v. R. *J. Phys. Chem.* **1992**, *96*, 7316.
- (4) Seijo, L.; Barandiaran, Z.; Huzinaga, S. *J. Chem. Phys.* **1991**, *94*, 3762.
- (5) Kaupp, M.; Schleyer, P. v. R.; Stoll, H.; Preuss, H. *J. Chem. Phys.* **1991**, *94*, 1360.
- (6) Kaupp, M.; Schleyer, P. v. R.; Stoll, H.; Preuss, H. *J. Am. Chem. Soc.* **1991**, *113*, 6012.
- (7) Kaupp, M.; Schleyer, P. v. R. *J. Am. Chem. Soc.* **1992**, *114*, 491.
- (8) Frisch, M. J.; Trucks, G. W.; Schlegel, H. B.; Gill, P. M. W.; Johnson, B. G.; Wong, M. W.; Foresman, J. B.; Robb, M. A.; Head-Gorden, M.; Replogle, E. S.; Gomperts, R.; Andres, J. L.; Ragavachari, K.; Binkley, J. S.; Gonzalas, C.; Martin, R. L.; Fox, D. J.; Defrees, D. J.; Baker, J.; Pople, J. A. *Gaussian 92/DFT, Revision F2*; Gaussian Inc.: Pittsburgh, PA, 1993.
- (9) Schmidt, M. W.; Baldridge, K. K.; Boatz, J. A.; Elbert, S. T.; Gordon, M. S.; Jensen, J. H.; Koseki, S.; Matsunaga, N.; Nguyen, K. A.; Su, S. J.; Windus, T. L.; Dupuis, M.; Montgomery, J. A. *J. Comput. Chem.* **1993**, *14*, 1347.
- (10) (a) Hurley, M. M.; Pacios, L. F.; Christiansen, P. A.; Ross, R. B.; Ermler, W. C. *J. Chem. Phys.* **1986**, *84*, 6840. (b) Lajohn, L. A.; Christiansen, P. A.; Ross, R. B.; Atashroo, T.; Ermler, W. C. *J. Chem. Phys.* **1987**, *87*, 2812. (c) Ross, R. B.; Powers, J. M.; Atashroo, T.; Lajohn, L. A.; Christiansen, P. A. *J. Chem. Phys.* **1990**, *93*, 6654. (d) Ermler, W. C.; Ross, R. B.; Christiansen, P. A. *Int. J. Quantum. Chem.* **1991**, *40*, 829.
- (11) According to Table 1 in ref 1 for the $\text{Ra}^{2+}\text{(H}_2\text{O})_2$ complex, the linear form is more stable than the bent form by 0.31 kcal. However, the bent form is more stable by the same amount in the text. From our calculations, we think the latter case should have opposite sign.

JP9614512

Considerable Stability and Visible Absorption of the Benzene–Water Hexamer Cluster Anion

Toshihiko Maeyama,* Takanobu Oikawa, Ko Seguchi, and Naohiko Mikami*

Department of Chemistry, Graduate School of Science, Tohoku University, Aoba-ku, Sendai 980-77, Japan

Received: July 3, 1997[®]

Time-of-flight mass spectrometry and photodestruction spectroscopy have been carried out for cluster anions of benzene–water, $Bz_m(H_2O)_n^-$. We have found that a distinct magic number $n = 6$ is associated with all the species of $m = 1–8$ and that an intense photoabsorption of $Bz(H_2O)_6^-$ occurs in the visible region. The results indicate that there is a strong interaction between the excess electron and valence orbitals of benzene, suggesting that these cluster anions can be a new model for the scavenging process of solvated electrons in condensed phases.

1. Introduction

In condensed phases, the disappearance of solvated electrons induced by impurity trapping is called the “scavenging” effect.^{1,2} It has been well-known that impurity molecules having not only positive but also negative electron affinity may act as electron scavengers. The electron-transfer mechanism has been considered to be feasible for such electron-scavenging processes. On the other hand, cluster anions of polar molecules, such as water or ammonia, are often considered to be a model of the solvated electrons in condensed phases. In this respect, therefore, it is interesting to investigate the electron-transfer process occurring in water cluster anions solvating an impurity molecule. The investigation will contribute to a microscopic view of the scavenging processes of hydrated electrons in condensed matter. In this Letter, we report the mass spectrometric and photodestruction spectroscopic investigation of cluster anions of water having benzene (Bz) molecule(s) as an impurity site; $Bz_m(H_2O)_n^-$, where the electron affinity of benzene^{3,4} is known to be -1.14 eV in the gas phase. We find that a remarkable magic number for the water cluster size occurs at $n = 6$ and that an intense absorption band appears in the visible region with a peak at 2.2 ± 0.1 eV, suggesting a novel interaction between the hydrated electron and the benzene site.

2. Experiment

The experimental setup and procedures are the same as those described elsewhere.⁵ Briefly, neutral clusters were formed in a supersonic jet of a gaseous mixture of benzene and water seeded in argon gas, and anions were generated by electron attachment to the neutrals. A zirconium metal surface was used as a electron source, from which photoejected electrons were prepared by the excitation with the fourth harmonic of a Nd:YAG laser. The cluster anions were mass-analyzed with a pulsed time-of-flight (TOF) mass spectrometer. To measure a photodestruction spectrum, we used an unfocused beam of either signal or idler outputs of an optical parametric oscillator (OPO; Spectra Physics MOPO 730) as a light source. Relative cross sections for photodestruction as a function of the photon energy were obtained by a logarithm plot of the depleted ion signal intensities. The fluence of the OPO pulse was kept around 10 mJ/cm² to avoid saturation effects and multiphoton processes.

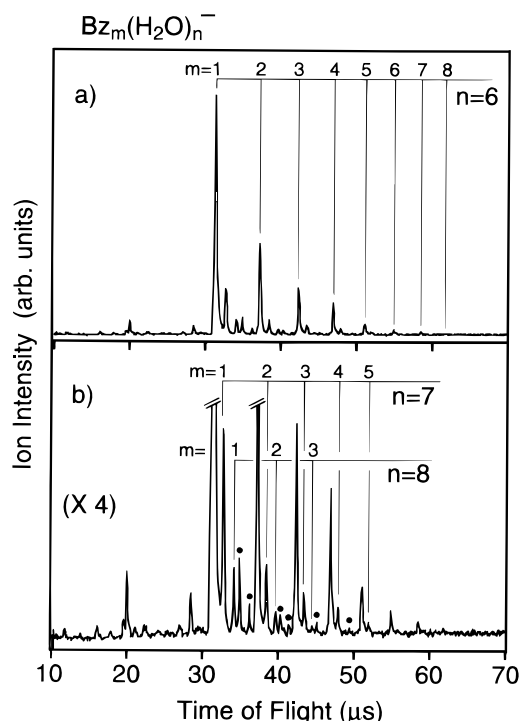


Figure 1. (a) Time-of-flight mass spectrum of cluster anions of the benzene–water mixture. The dominant progression is assigned to the $Bz_m(H_2O)_6^-$ clusters. (b) An expanded trace ($\times 4$) is given in the lower panel. Weak progressions of $Bz_m(H_2O)_n^-$, $n = 7$ and 8 , are seen. Peaks marked by dots are due to complexes of an impurity molecule ($M = 47 \pm 1$ amu) with $Bz_m(H_2O)_n^-$, $n = 6$ and 7 . Weak peaks in the range of flight-time less than $30 \mu s$ are attributed to impurities or product anions of dissociative electron attachment of benzene clusters.

3. Results and Discussion

It has been established by many investigators^{5–9} that exclusive magic numbers of neat water cluster anions, $(H_2O)_n^-$, are $n = 2, 6, 7$, and 11 for small cluster size and that ion signal intensities for $n = 6$ and 7 are comparable irrespective of different experimental conditions. Figure 1 shows a mass spectrum of cluster anions of the benzene–water mixture, $Bz_m(H_2O)_n^-$. The dominant progression corresponding to $Bz_m(H_2O)_6^-$ is seen in the spectrum, which is considerably more intense compared with those of $n = 7$ and 8 . The cluster anions of $n \leq 5$ and $n \geq 9$ were completely absent under several different conditions with respect to water vapor pressure. This result represents that the cluster anions involving a unit of water hexamer are substantially

[®] Abstract published in *Advance ACS Abstracts*, October 1, 1997.

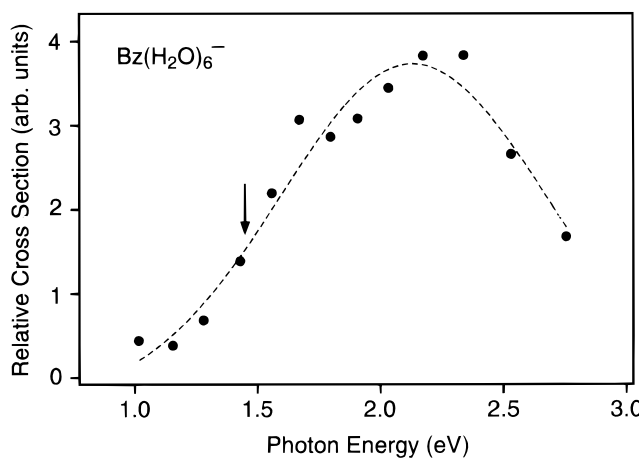


Figure 2. Photodestruction spectrum of $\text{Bz}(\text{H}_2\text{O})_6^-$. The broken line represents the least-squares fit of the Gaussian line-shape function. The arrow indicates the VDE value (1.45 eV) obtained by Negishi et al. (ref 10).

stabilized with respect to the other sizes. Among them, the considerable stability of $\text{Bz}(\text{H}_2\text{O})_6^-$ suggests a novel electronic interaction in the cluster anion of $n = 6$. Very recently, in fact, Nakajima and co-workers¹⁰ measured photoelectron spectra of $\text{Bz}(\text{H}_2\text{O})_n^-$. They found that vertical detachment energies (VDE's) for $n = 6, 7$, and 8 are 1.45 ± 0.1 , 0.4 ± 0.1 , and 0.75 ± 0.1 eV, respectively, indicating the characteristic stability for $n = 6$.

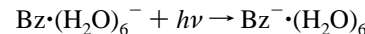
Despite many theoretical predictions,^{11,12} the question concerning the binding nature of the excess electron in $(\text{H}_2\text{O})_n^-$ is still a subject of debate.¹³ Recent ab initio calculations¹² for $(\text{H}_2\text{O})_6^-$ suggested that the stable structure with respect to intermolecular hydrogen bonds is an isomer with the prism-type form and the excess electron distribution is localized around dangling hydrogen atoms of the cluster anion. In the $\text{Bz}_m(\text{H}_2\text{O})_n^-$ system, however, the binding characteristics of the electron seem to be different from that of the neat water system, because the $n = 6$ anions are preferentially stabilized. Since benzene is a highly polarizable molecule and its aromatic ring is known to act as an effective acceptor for π -hydrogen bonding,^{14–16} it is feasible that the cluster form of the $(\text{H}_2\text{O})_6^-$ moiety in $\text{Bz}_m(\text{H}_2\text{O})_6^-$ is substantially modified by interaction with benzene molecule(s). In this respect, it is highly desirable that the cluster form is investigated by precise ab initio calculations including more extensive polarization functions as the basis sets.

To investigate the electronic structure, we measured a photodestruction spectrum of $\text{Bz}(\text{H}_2\text{O})_6^-$, which is reproduced in Figure 2. A broad absorption spectrum occurs in the visible region with a peak at 2.2 ± 0.1 eV. The spectrum is totally different from that of the neat water hexamer anion, $(\text{H}_2\text{O})_6^-$,^{5,6} for which the peak position lies in the infrared region. The spectrum is also quite different from that of the benzene anion, which was observed under matrix-isolated conditions by Shida and co-workers.¹⁷ The peak position of the absorption of $\text{Bz}(\text{H}_2\text{O})_6^-$ is considerably higher than its VDE value (1.45 \pm 0.1 eV).¹⁰ Moreover, the absorption intensity was found to be quite large; the absorption cross section at the peak position is estimated to be of the order of 10^{-17} cm 2 by comparing the signal intensity with those obtained for systems with known cross sections.⁵ This suggests that the absorption is not due to a direct electron detachment but to a bound-to-bound transition leading to an autodetachment process.

For the neat water cluster anions, $(\text{H}_2\text{O})_n^-$, it has been observed that the absorption tends to shift to the high-energy side with increasing n , as reported by Johnson's group⁶ as well

as by our group.⁵ The shifts are attributed to deepening of the electron binding potential with increasing cluster size, which leads to the electron localization.¹¹ In this sense, we first assumed for $\text{Bz}(\text{H}_2\text{O})_6^-$ that the electron localization is accelerated by solvation with a benzene molecule. Although it agrees with the considerable stability of $\text{Bz}(\text{H}_2\text{O})_6^-$, it cannot cause the bound-to-bound absorption with the energy being above the VDE, since an electron-bound excited state resulting from the electron localization should lie just below the detachment threshold. We therefore have to consider another assignment.

As such an intense transition, in the present case, one may easily expect an intracluster electron-transfer transition between the two moieties:



The transition of the excess electron bound in the $(\text{H}_2\text{O})_6^-$ site takes place to the lowest antibonding π^* orbitals of the benzene site. Since the electron affinity of benzene is not positive,^{3,4} the excess electron transferred from the $(\text{H}_2\text{O})_6^-$ site is unstable and is readily released from the benzene moiety. Energetically, it is expected that the π^* orbitals of the benzene are in the continuum and the bound electron in the $(\text{H}_2\text{O})_6^-$ site is slightly below it. The onset of the absorption represents the energy difference between the two, and the peak corresponds to the maximum of the Franck–Condon overlap for the electron-transfer transition. To confirm this, it would be necessary to observe more detailed photodestruction spectra covering the IR and UV region.

Finally, we note that the present work may provide a new insight onto the “scavenging” effect in condensed phases. Since solutions are considered as an ensemble of different size of clusters, the excess electron in the solution may be trapped not only by a solute molecule site but also by a cluster site of a suitable size, such as $\text{Bz}(\text{H}_2\text{O})_6$. This “cluster-trapping” mechanism seems to be in good agreement with the fact that an impurity molecule having a negative electron affinity even acts as an electron scavenger.

Acknowledgment. We are grateful to Dr. A. Nakajima and Professor K. Kaya of Keio University for providing us with unpublished results of photoelectron spectroscopy.

References and Notes

- Hunt, J. W. *Adv. Radiat. Chem.* **1976**, 5, 185.
- Razem, D.; Hamill, W. H. *J. Phys. Chem.* **1977**, 81, 1625.
- Boness, M. J.; Larkin, I. W.; Hasted, J. B.; Moore, L. *Chem. Phys. Lett.* **1967**, 1, 292.
- (a) Sanche L.; Schulz, G. J. *J. Chem. Phys.* **1973**, 58, 479. (b) Nenner I.; Schulz, G. J. *J. Chem. Phys.* **1975**, 62, 1747.
- Maeyama, T.; Tsumura, T.; Fujii, A.; Mikami, N. *Chem. Phys. Lett.* **1997**, 292, 264.
- (a) Campagnola, P. J.; Lavrich, D. J.; DeLuca, M. J.; Johnson, M. A. *J. Chem. Phys.* **1991**, 94, 5420. (b) Ayotte, P.; Johnson, M. A. *J. Chem. Phys.* **1997**, 106, 811.
- Harberland, H.; Ludewigt, C.; Schindler, H.-G.; Worsnop, D. R. *J. Chem. Phys.* **1984**, 81, 3742.
- Desfrancois, C.; Khelifa, N.; Lisfi, A.; Schermann, J. P.; Eaton, J. G.; Bowen, K. H. *J. Chem. Phys.* **1991**, 95, 7760.
- Coe, J. V.; Lee, G. H.; Eaton, J. G.; Arnold, S. T.; Sarkas, H. W.; Bowen, K. H.; Ludewigt, C.; Harberland, H.; Worsnop, D. R. *J. Chem. Phys.* **1990**, 92, 3980.
- Negishi, Y.; Hayakawa, F.; Nakajima, A.; Kaya, K. Unpublished results.
- For example: Barnett, R. N.; Landman, U.; Cleaveland, C. L.; Jortner, J. *J. Chem. Phys.* **1988**, 8, 4429.
- (a) Kim, K. S.; Park, I.; Lee, S.; Cho, K.; Lee, J. Y.; Kim, J.; Joannopoulos, J. D. *Phys. Rev. Lett.* **1996**, 76, 956. (b) Lee, S.; Lee, S. J.;

Lee, J. Y.; Kim, J.; Kim, K. S.; Park, I.; Cho, K.; Joannopoulos, J. D. *Chem. Phys. Lett.* **1996**, 254, 128.

(13) Ayotte, P.; Kim, J.; Bailey, C. G.; Johnson, M. A. Submitted to *J. Chem. Phys.* They proposed a cyclic form for $(\text{H}_2\text{O})_6^-$ according to results of vibrational predissociation spectroscopy of $(\text{H}_2\text{O})_6^-\cdot\text{Ar}_n$ clusters.

(14) Suzuki, S.; Green, P. G.; Bumgarner, R. E.; Dasgupta, S.; Goddard, W. A., III; Blake, G. A. *Science* **1992**, 257, 942.

(15) (a) Pribble, R. N.; Zwier, T. S. *Science* **1994**, 265, 75. (b) Pribble, R. N.; Zwier, T. S. *Faraday Discuss.* **1994**, 97, 229. (c) Fredericks, S. Y.; Jordan, K. D.; Zwier, T. S. *J. Phys. Chem.* **1996**, 100, 7810.

(16) Maxton, P. M.; Schaeffer, M. W.; Felker, P. M. *Chem. Phys. Lett.* **1995**, 241, 693.

(17) Shida, T. *Electronic Absorption Spectra of Radical Ions*; Elsevier: Amsterdam, 1988.

Effect of the Mobility of Ligands in Polyrotaxanes on Order Structure of Water Clusters

Hiroaki Hirose, Haruyuki Sano,* Goro Mizutani, Masaru Eguchi,
Tooru Ooya, and Nobuhiko Yui

School of Materials Science, Japan Advanced Institute of Science and Technology,
Tatsunokuchi, Ishikawa 923-1292, Japan

Received December 14, 2003. In Final Form: January 19, 2004

The effect of the mobility of ligands (maltose groups) in the polyrotaxanes (pRXs) on the structure of the surrounding water molecules was investigated. Raman spectra of collective OH stretching vibration of water molecules in aqueous solutions of maltose-pRX conjugates with different α -cyclodextrin (α -CD) threading on a poly(ethylene glycol) (PEG) chain was measured. The mobility of maltose groups was estimated by measuring the relaxation time T_2 of the C1 protons in maltose groups bound on α -CD by NMR experiment. A positive correlation between the Raman intensity of the collective band and the relaxation time T_2 was obtained. This result indicates that the degree of order of the water clusters is higher as the mobility of maltose groups increases in these conjugate solutions. It is suggested that rapid motion of maltose groups in the pRX conjugate can contribute to preserving ordered structure of the bulk water clusters.

Introduction

An inclusion complex consisting of cyclic molecules such as α -cyclodextrins (α -CDs) threaded onto a linear polymeric chain like poly(ethylene glycol) (PEG) capped with bulky end-groups is called as polyrotaxane (pRX). Since α -CDs in this complex can freely move along the PEG chain, the pRXs are expected to serve as molecular machines or molecular devices.^{1,2} In the mechanical property and reactivity of the pRX in aqueous solutions, molecular interaction between the pRX and the surrounding water molecules plays an important role. To clarify this type of interaction, the structure of water clusters around the pRX has been studied by observing the collective stretching vibration of OH bonds (collective band).³ In our study Raman intensity of the collective band was used as an indicator of the order of the structure of water molecules,^{3,4} and it was successfully found that the constituent molecules of the pRX, or linear polymeric chains and cyclic molecules, break the order in the hydration bonding in the surrounding water molecules, since they have the hydrophobic parts. On the other hand, this order is maintained when these molecules form inclusion complexes, because water molecules cannot approach to interact with their hydrophobic parts.

Recently, it has been found that ligand–polyrotaxane conjugates have a unique function for recognizing binding proteins due to the multivalent interaction.⁵ Of special interest is the fact that the mobility of ligands in the pRX conjugates contributes much to enhancing multivalent interaction with binding proteins. As the next step of this study, the investigation of the dynamic property of pRX has become important, since the dynamical property of the supramolecular assemblies is closely related to their function. Thus, in the present study, the effect of mobility

of ligands in the pRX conjugates on the structure of water clusters has been evaluated by Raman scattering. It has been found that the degree of order of the water clusters is closely related to the ligand mobility.

Experiment

Maltose-polyrotaxane conjugates consisting of PEG, α -CDs with maltose groups, and benzylloxycarbonyl-tyrosine as shown in Figure 1 were used in this study. The details of the sample preparation and the chemical structure of these conjugates were described in the previous paper.⁵ The introduction of maltose groups into α -CDs can have an effect on the order of water molecules because maltose has a strong interaction with water molecules. To control the mobility of maltose groups in the pRX, three pRX samples with 22%, 38%, and 53% CD threading on a PEG chain (the molecular weight = 20 000) were prepared, as shown in Table 1. The concentration of these samples was 3.33×10^{-5} M. For eliminating the influence of the difference in maltose concentration, the number of maltose groups per pRX in these samples was set at a similar value (about 240). Consequently, the maltose concentration in three sample solutions was approximately the same ($\sim 8 \times 10^{-3}$ M).

As reference samples, maltose- α -CD conjugate solutions including two, three, and four maltose groups were prepared, as shown in Table 1. α -CD and maltose concentrations of 2Mal-CD, 3Mal-CD, and 4Mal-CD solutions were almost the same as those of 53%CD-pRX, 38%CD-pRX, and 22%CD-pRX solutions, respectively. As another reference sample, maltose–poly(acrylic acid) conjugate solution with the concentration of 3.33×10^{-5} M was prepared (sample name Mal-PAA in Table 1). The Mal-PAA is suitable as a control of maltose-pRX conjugates, because the Mal-PAA exhibits the similar number of maltose and carboxyl groups without any supramolecular structure. By comparing these samples, the effect of the dynamic motion of maltose in relation to the mobility of α -CDs along with PEG chain on the water clusters can be assessed under the same conditions of ligand and ionic groups. The number of maltose groups per molecule and the maltose concentration in this solution were almost the same as those of maltose-pRX conjugate solutions. All the samples were dissolved in a 0.1 M phosphate-buffered saline (PBS) solvent (pH 7.4) containing 0.1 mM CaCl_2 and 0.1 mM MnCl_2 .

The details of the Raman measurement have been described in our previous paper.³ Briefly, Raman spectra of the samples in glass cells were measured in 90° scattering geometry. The incident light was the 632.8 nm line of a He–Ne laser, and the

* To whom correspondence should be addressed. Phone: +81-761-51-1522. Fax: +81-761-51-1149. E-mail: h-sano@jaist.ac.jp.

(1) Harada, A. *Acc. Chem. Res.* 2001, 34, 456.

(2) Fujita, H.; Ooya, T.; Yui, N. *Macromolecules* 1999, 32, 2534.

(3) Sano, H.; Ichi, T.; Kumashiro, Y.; Kontani, K.; Kuze, T.; Mizutani, G.; Ooya, T.; Yui, N. *Spectrochim. Acta A* 2003, 59, 285.

(4) Maeda, Y.; Kitano, H. *Spectrochim. Acta A* 1995, 51, 2433.

(5) Ooya, T.; Eguchi, M.; Yui, N. *J. Am. Chem. Soc.* 2003, 125, 13016.

Table 1. Samples for Raman Measurement

sample name	no. of a-CD	a-CD threading, ^b %	no. of maltose per a-CD	no. of maltose	concen of a-CD, 10^{-3} M	concen of maltose, 10^{-3} M
22%CD-pRX ^a	50	22	4.6	230	1.66	7.65
38%CD-pRX ^a	85	38	2.9	244	2.83	8.12
53%CD-pRX ^a	120	53	2.0	240	3.99	7.98
2Mal-CD	1		2.0	2	3.99	7.98
3Mal-CD	1		3.0	3	2.66	7.98
4Mal-CD	1		4.0	4	2.00	7.98
Mal-PAA ^a				240		7.98

^a Concentration is 3.33×10^{-5} M. ^b a-CD threading (%) = (no. of a-CD)/(stoichiometric no. of a-CD) $\times 100$ (see ref 5).

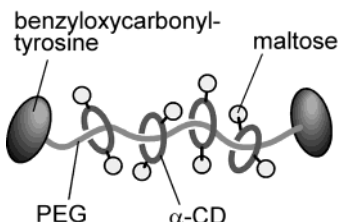


Figure 1. Molecular structure of maltose–polyrotaxane conjugate.

power was 7 mW. The measured spectral range was from 2500 to 4000 cm^{-1} , covering the OH stretching mode frequencies. The polarization combinations were such that the exciting and the scattered polarizations are parallel or perpendicular to each other. All the measurements were performed at room temperature.

The intensity of the collective band (I_C), attributable to the synchronous stretching vibration of OH bonds in H_2O clusters, can be obtained from a difference between the integrated Raman scattering intensities in the parallel and perpendicular polarization configurations ($I_{||}$ and I_{\perp}):^{3,4}

$$I_C(\omega) = I_{||}(\omega) - I_{\perp}(\omega)/\rho_{\text{OH}} \quad (1)$$

where ρ_{OH} is the depolarization ratio of the noncollective band. Before this subtraction process, the following treatments to minimize the analysis error were performed: (i) the background caused by dark noise, stray light, and luminescence from the samples was removed from the measured spectra and (ii) the smooth spectra were obtained by fitting with four Gaussian curves. Furthermore, I_C is normalized as

$$C_X = \int I_C(\omega) \text{ d}\omega / \int I_{||}(\omega) \text{ d}\omega \quad (2)$$

The mobility of a-CDs in the pRX was estimated by measuring the relaxation time T_2 of C1(H) of maltose groups in the NMR experiment.⁵

Results and Discussion

Figure 2a shows the measured intensities of collective band of three maltose-a-CD conjugate solutions. The horizontal axis represents the concentration of a-CD in the sample solutions, and the vertical axis represents the collective band intensity normalized by that of the PBS solution. The result of Figure 2a indicates that the collective band intensity linearly decreased, or the degree of the order of the water clusters became lower, with increasing the a-CD concentration. Since the concentration of maltose in these solutions is the same, this result cannot be explained from the effect of maltose groups. In our previous study,³ it was suggested that large hydrophobic parts of inner cavity of CD break the order of bulk water clusters because the clathrate hydration around the hydrophobic part invokes a different structure of water molecules from that of bulk water clusters. Based on this consideration, the result of Figure 2a can be interpreted that the increase in the number of the exposed inner cavity of a-CD leads to the disorder of bulk water clusters.

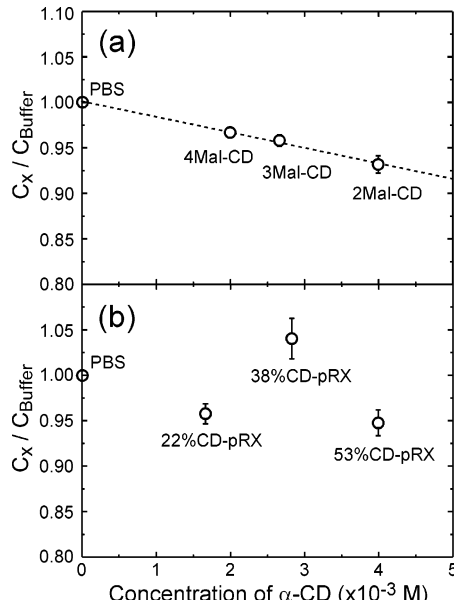


Figure 2. Normalized Raman intensity of collective band of OH stretching vibration for (a) solutions of maltose-a-CD conjugates and (b) solutions of maltose polyrotaxane conjugates as a function of the concentration of a-CD.

Figure 2b shows the measured intensities of the collective bands of three maltose-pRX conjugate solutions. The collective band intensity of 38%CD-pRX solution was remarkably larger than those of any other conjugates, and the magnitude was slightly larger than unity. This result indicates that the order of the water clusters was preserved in 38%CD-pRX solution much more than in 22%CD-pRX and 53%CD-pRX solutions, and the degree was greater than in PBS solution. The latter result is not an unusual phenomenon, because water molecules in buffer solution are not completely ordered, and this order can be further increased by the effect of certain solute molecule.⁶ It should be noted that there is no great difference in the concentration of linear chain molecule (PEG), bulky blocking group (benzyloxycarboxyl-tyrosine), and ligand (maltose) among three pRX solutions. It is obvious to see a significant difference in the dependence of the collective band intensity on the concentration of a-CD between the maltose-a-CD conjugate solution and the maltose-pRX conjugate solution. Because a-CDs in the pRX are threaded onto a PEG molecule, the hydrophobic parts of the inner cavity of a-CDs are shielded from surrounding water molecules. Therefore, the effect of the inner cavity must be canceled in the case of Figure 2b.

Figure 3 shows the normalized Raman intensity of the collective band of maltose-pRX conjugate solutions as a function of the relaxation time T_2 of C1(H) of maltose

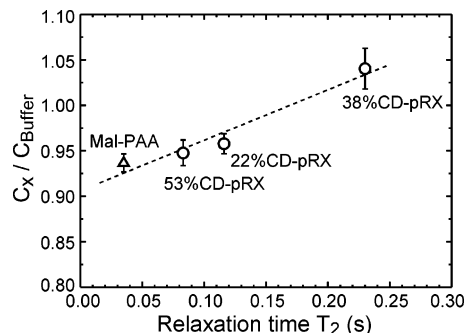


Figure 3. Normalized Raman intensity of the collective band for solutions of maltose–polyrotaxane conjugates (circles) and maltose poly(acrylic acid) (triangle) as a function of T_2 relaxation time of C(1)H of maltose groups.

groups bound on α -CDs. The relaxation time T_2 in the Mal-PAA, one of the reference samples, was very small. This is considered due to the covalent binding of maltose groups onto the PAA backbone. A clear positive correlation between the collective band intensity and the relaxation time T_2 was observed in Figure 3. It is well-known in the NMR measurement that higher mobility of molecules causes longer relaxation time T_2 due to the motional narrowing effect.⁷ Thus, the result of Figure 3 indicates that the degree of order of the water clusters is higher as the mobility of maltose groups is higher in these solutions.

At present, the reason for the correlation observed in Figure 3 has not been clarified yet. However, we suggest the following mechanism. If maltose- α -CDs stand still, or their motion is very slow as observed in the case of maltose-PAA, a stable and rigid network of water molecules is probably formed around maltose groups and exposed PEG chains, and their structure may be different from the structure of bulk water clusters. In this case, it is likely

(7) Bloembergen, N.; Purcell, E. M.; Pound, R. V. *Phys. Rev.* **1948**, *73*, 679.

that the particular hydration structure around maltose-pRX conjugates breaks the order of the bulk water clusters. On the other hand, if maltose- α -CDs rapidly move, water molecules around maltose-pRX conjugates may not form the above-mentioned particular structure, but the water molecule structure may be preserved, similar to bulk water clusters. Consequently, rapid motion of maltose groups in the pRX conjugate can contribute to preserving the bulk water clusters. In the case of 38%CD-pRX sample, this mechanism probably works well so that the degree of the order of water molecules is higher than that of PBS solution. Further studies are now in progress.

Conclusion

Raman spectra of the OH stretching mode of water molecules in aqueous solutions of maltose-pRX conjugates with different α -CD threading were measured, and the degree of order of water clusters was evaluated from the Raman intensity of the collective bands of OH oscillators. It was found that the degree of order of water clusters was higher in the pRX conjugate solution exhibiting higher mobility of maltose groups. Since the preservation of the water cluster is considered to be one of factors for exhibiting good biocompatibility,⁸ the maltose-pRX conjugates are applicable for biomaterials such as specific protein detection⁵ and blood-compatible polymers.⁹

Acknowledgment. This study was financially supported by JAIST Research Grant (grant for in-house research projects) and a Grant-in-Aid for Scientific Research (B) (No. 14380397), from the Ministry of Education, Science, Sports and Culture, Japan.

LA036354W

(8) Kitano, H.; Sudo, K.; Ichikawa, K.; Ide, M.; Ishihara, K. *J. Phys. Chem. B* **2000**, *104*, 11425.

(9) Park, H. D.; Lee, W. K.; Ooya, T.; Park, K. D.; Kim, Y. H.; Yui, N. *J. Biomed. Mater. Res.*, **2002**, *60*, 186.

Supramolecular Aggregation of Hexameric Water Clusters into a 2D Water Polymer Containing $(H_2O)_{18}$ Holes

Rosa Carballo,* Berta Covelo, Nuria Fernández-Hermida, Emilia García-Martínez, Ana B. Lago, Miguel Vázquez, and Ezequiel M. Vázquez-López

Departamento de Química Inorgánica, Facultade de Química, Universidade de Vigo, 36310 Vigo, Spain

Received November 8, 2005; Revised Manuscript Received January 18, 2006

ABSTRACT: We report herein a novel infinite two-dimensional water morphology, found in a metallo-organic host, made up of discrete cyclic water hexamers and which contains large circular holes defined by 18 molecules of water.

In recent years, the theoretical and experimental study of small water clusters became relevant since they are the first step toward understanding the behavior of bulk water.^{1–5} Several water clusters found in organic or metallo-organic crystal hosts have been structurally characterized.³ However, very little is known about how these clusters link themselves to form larger networks of water molecules, which structurally lie between small water clusters and bulk water.⁶ Very recently, significant progress has been made with respect to the structural characterization of one-dimensional (1D) aggregates such as water chains and tapes.⁷ In contrast, there are very few examples of two- or three-dimensional (2D or 3D) water polymers.^{8,9} The structural elucidation of these novel water morphologies is important to gain insight into some of the unexplained properties of water,^{2,4,10} into the processes that occur at the ice–liquid, ice–air, and liquid–air interfaces,^{11,12} and into the nature of water–water and water–solute interactions.¹²

To our knowledge, all the 2D water polymers reported previously are associations of small cyclic water clusters fused by “edge-sharing” and without discontinuities in their structures.⁸ We describe herein a novel water morphology, a 2D holed polymer, observed in the crystalline solid $\omega^2[Cu(Hmal)(4pds)] \cdot 6H_2O$ (**1**) (4pds: 4,4'-dipyridyl disulfide; Hmal²⁻: dianion of malic acid).

Compound **1** was prepared at room temperature by slow diffusion of an ethanol solution of 4pds into an aqueous solution containing copper(II) malate in a 1:1 molar ratio.¹³ Single-crystal diffraction analysis revealed that **1** contains one 4pds ligand, one Cu²⁺, one Hmal²⁻ anion, and six water molecules in the asymmetric unit (Figure 1).¹⁴ Each copper(II) ion is six-coordinated by two pyridine nitrogen atoms from two 4pds ligand units, and by four oxygen atoms from two Hmal²⁻ anions, in an axially elongated [4+1+1] octahedral geometry. The elongations of these Cu–O bonds [Cu–O5 2.287(6) and Cu–O4 2.683(6) Å] may be ascribed to the Jahn Teller effect. The Cu²⁺ ions are linked by 4pds moieties along the *a*-axis, forming zigzag chains [$d(Cu^{2+}-4pds-Cu^{2+})$ = 10.676(3) Å, symmetry code 1: $1 + x, y, z$]. These chains are transversally joined by the Hmal²⁻ anions [$d(Cu^{2+}-Hmal^{2-}-Cu^{2+})$ = 5.861(2) Å, symmetry code 1: $1/2 - x, -1/2 + y, 5/2 - z$]. The α -hydroxycarboxylate moiety of the Hmal²⁻ ligand chelates one copper(II) ion, while the remaining carboxylate group acts as bridge between two neighboring metal centers. Therefore, the global structure should be described as a 2D coordination polymer that grows along the *ab*-plane (Figure 1).

There are two classes of 2D coordination polymers in **1**. One of them is constituted by M enantiomers of the 4pds ligand and D-enantiomers of the Hmal²⁻ anion (“MD” sheets). The other one is formed by P-4pds and L-Hmal²⁻ ligands (“PL” sheets). These “PL” and “MD” chiral sheets are disposed in an alternate sequence in the crystal cell of **1** that, consequently, has an achiral nature.

The hydrogen-bonding association of lattice water molecules in **1** leads to the formation of cyclic hexamers with a “puckered-boat”

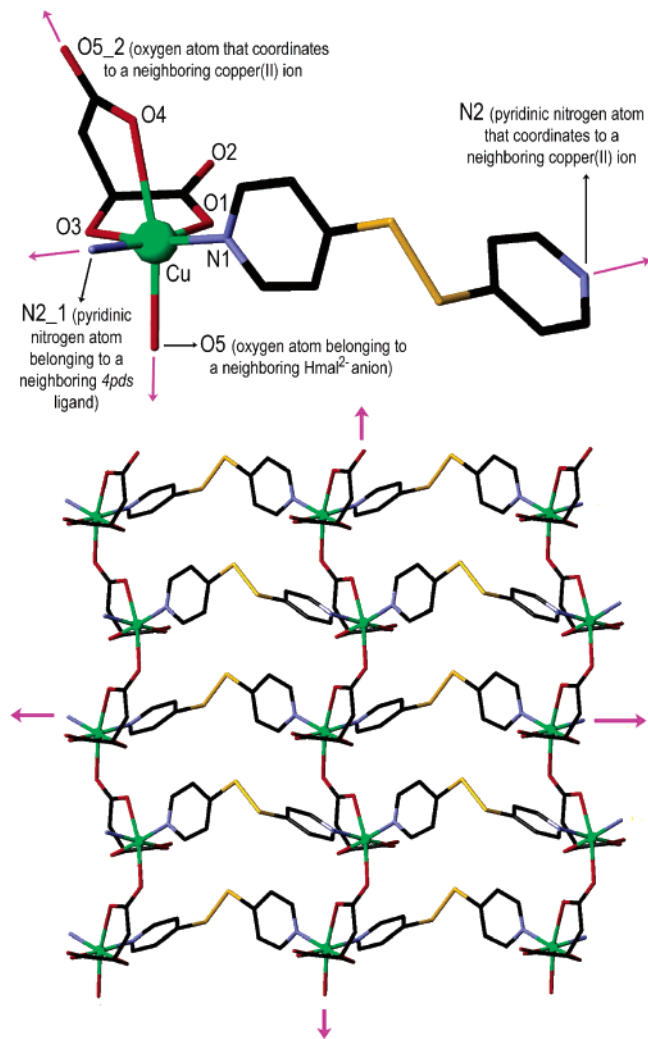


Figure 1. Ball-and-stick representations of the asymmetric unit (top) and of a “PL” sheet of the 2D coordination polymer (bottom) found in the crystal cell of **1**. Water molecules and hydrogen atoms have been omitted for clarity. Symmetry codes, 1: $x - 1, y, z$ and 2: $-x + 1/5, y - 1/2, -z + 5/2$.

conformation (Figure 2).^{2,7d,8a,15} The average O···O distance in the hexamer is 2.78 Å. This distance is shorter than those observed in liquid water (2.85 Å)¹⁶ and comparable to the corresponding value in hexagonal ice (I_h) (2.76 Å).^{5a,17} Moreover, the average O···O···O angle is 107.3°, slightly shorter than the corresponding value of 109.3° in I_h .

Each water cluster is connected to other three identical hexamers by hydrogen bonding (Figure 2). The interhexamer water–water connections have an average O···O distance of 2.998 Å. The water clusters do not share any water molecules with their neighbors:

* To whom correspondence should be addressed. E-mail: rcrial@uvigo.es.

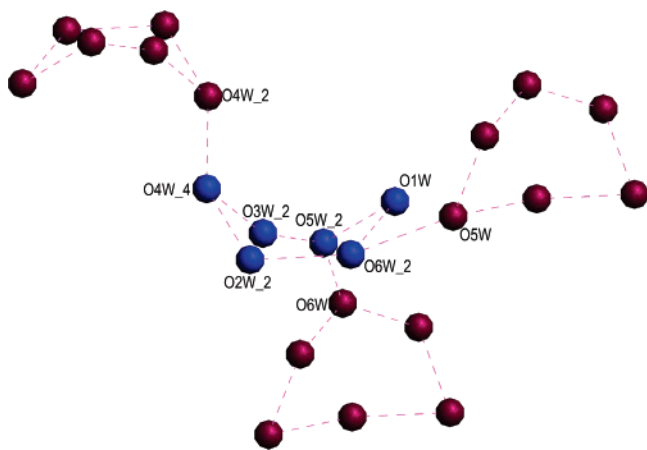


Figure 2. Ball representation of the “puckered-boat” hexameric water clusters (in blue) found in the crystal cell of **1**. The red balls are water molecules belonging to neighboring water hexamers. Symmetry codes 2: $3/2 - x, 1/2 + y, 1/2 - z$ and 4: $1/2 + x, 3/2 + y, 1/2 + z$.

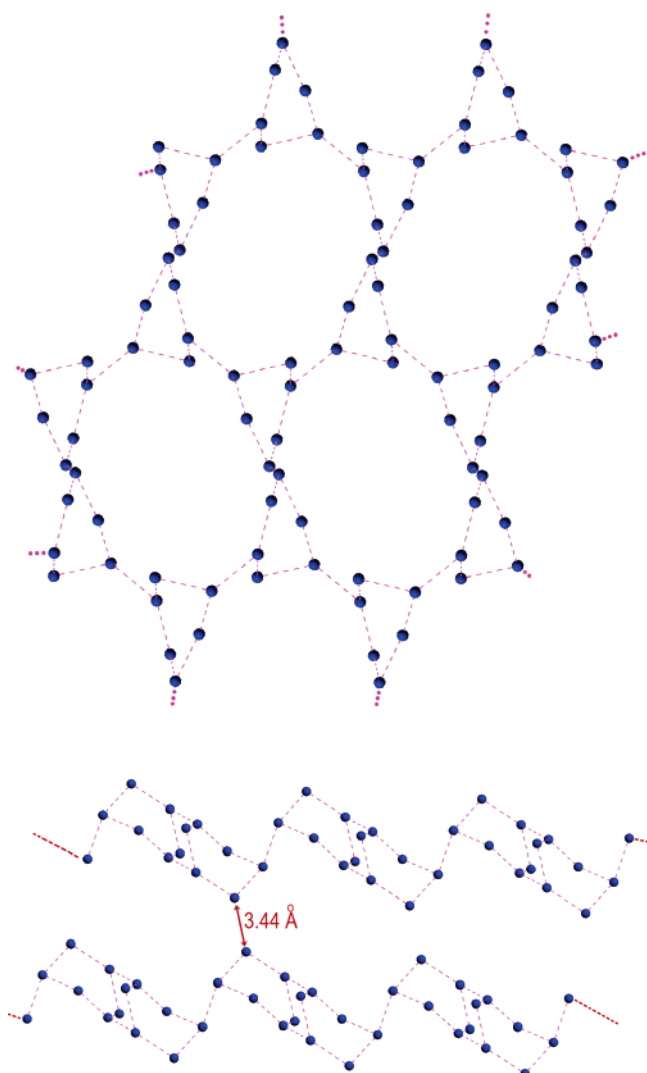


Figure 3. Top, ball representation of the 2D holed water polymer found in **1**. The diameter of the 18-membered water holes has an average value of 11.76 \AA . The corrugated water sheets are piled along the a -axis of the crystal cell (bottom).

they are discrete moieties. The aggregation of the hexamers is controlled by an unprecedented “vertex-connected” association mode, in contrast with previously reported water associations where clusters are always fused by “edge-sharing”.⁸ This novel cluster

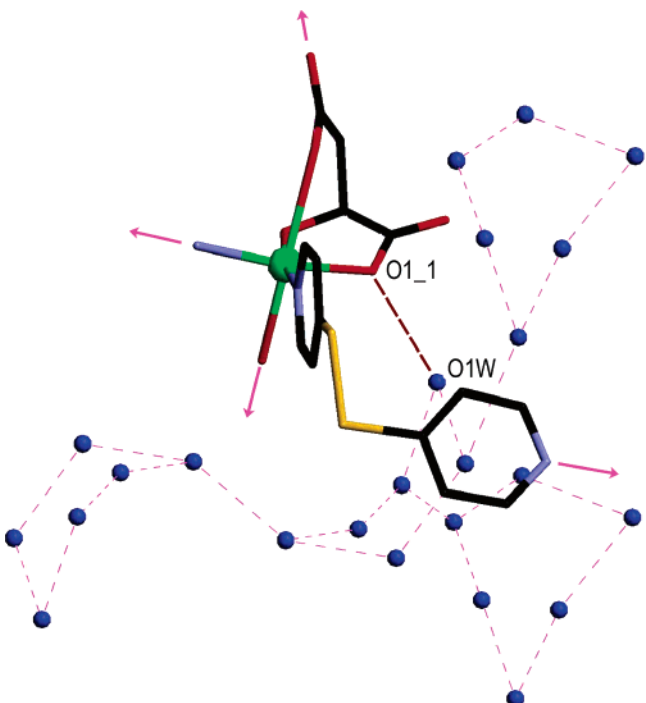


Figure 4. Part of the unit cell of **1**, exhibiting the unique class of hydrogen-bonding interactions between the water net and the coordination polymer.

aggregation mode leads to formation of a corrugated 2D framework of water molecules along the bc -plane (Figure 3). Interestingly, the water sheets are not continuous and contain large circular holes defined by 18 molecules of water. The average diameter of these gaps is 11.76 \AA . It must be noted that the cavity dimensions described here are crystallographic scalar quantities only and do not take into account the van der Waals radii of the atoms defining the cavity. The water sheets are piled along the a -axis of the crystal cell, forming cylindrical water channels. The minimum $\text{O}\cdots\text{O}$ distance between two water sheets is 3.44 \AA . To our knowledge, this is the first example of a 2D water polymer containing holes in its structure, that is, a 2D holed water polymer.

The 2D holed water network is interpenetrated with the metallo-organic host. The 4pds ligands of the coordination polymer pass through the holes of the water network, whereas the $[\text{Cu}(\text{Hmal})_n]$ chains are disposed in the space between two water sheets (Figure 4). There are two 4pds ligand units, belonging to two different sheets of the 2D coordination polymer, in each water hole. The planes of the water polymer and of the metallo-organic network are inclined one with respect to the other (Figure 4), forming an angle of 85° . There is an unique class of connection between both polymers. The O1 atom of the Hmal^{2-} ligand is hydrogen bonded [$\text{O1w}\cdots\text{O1}_1 = 2.84(2) \text{ \AA}$, symmetry code **1**: $3/2 - x, -1/2 + y, 3/2 - z$] to one water molecule of a cyclic hexamer (Figure 4). Consequently, the overall structure could be considered as a 3D metalloc-supramolecular network (Figure 5).

In conclusion, a novel infinite 2D water framework made up of discrete cyclic water hexamers has been structurally characterized. To our knowledge, this is the first example of a 2D holed water polymer. We believe this water assembly brings to light a novel mode of the cooperative association of water molecules and enhances the understanding of the 2D structural aspects of bulk water.

Acknowledgment. This research was supported by the European Rural Development Fund and the Directorate General of Research of the Spanish Ministry of Education and Science through the research project BQU200203543. B.C. also thanks Fundación CaixaNova for a postdoc grant. M.V. also thanks Xunta de Galicia for a postdoc contract under the “Isidro Parga Pondal” Program.

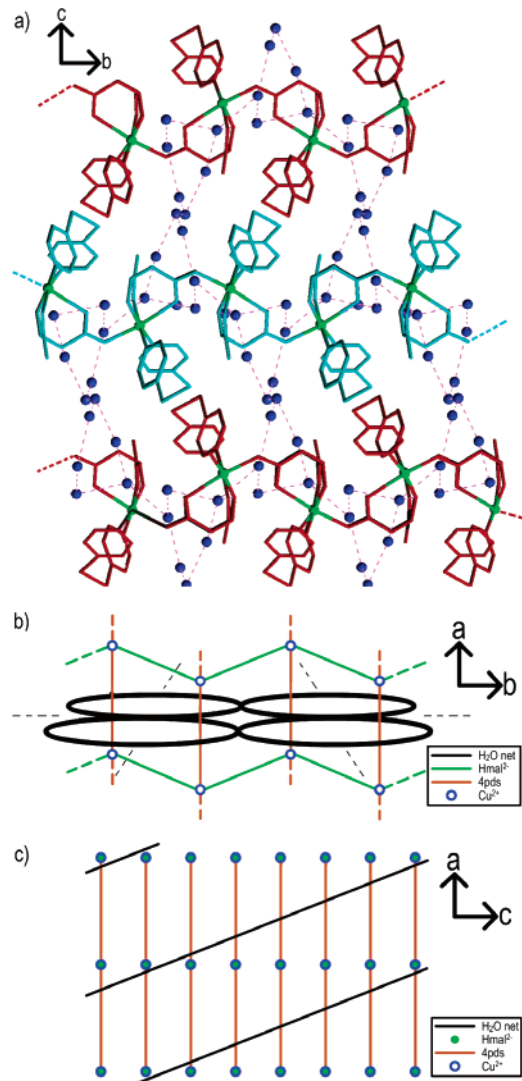


Figure 5. (a) Part of the unit cell of **1**, exhibiting the interpenetration between the metallo-organic and the water 2D polymers. Red and cyan colors represent “MD” and “PL” metallo-organic sheets, respectively. There are two $[\text{Cu}(4\text{pds})\text{Cu}]$ units, belonging to two different metallo-organic sheets, in each water hole. (b) Illustration of the interpenetration mode from the *ab*-plane of the crystal cell of **1**. (c) Schematic view of the interpenetration mode between both polymers from the *ac*-plane.

Supporting Information Available: X-ray crystallographic file in CIF format of compound **1**. This material is available free of charge via the Internet at <http://pubs.acs.org>.

References

- (a) Liu, K.; Brown, M. G.; Carter, C.; Saykally, R. J.; Gregory, J. K.; Clary, D. C. *Nature* **1996**, *381*, 501. (b) Liu, K.; Cruzan J. D.; Saykally, R. J. *Science* **1996**, *271*, 929. (c) Weinhold, F. J. *Chem. Phys.* **1998**, *109*, 367. (d) Kim, J.; Majumdar, D.; Lee H. M.; Kim, K. S. *J. Chem. Phys.* **1999**, *110*, 9128. (e) Nauta K.; Miller, R. E. *Science* **2000**, *287*, 293. (f) Ugalde, J. M.; Alkorta, I.; Elguero, J. *Angew. Chem., Int. Ed.* **2000**, *39*, 717.
- (2) Ludwig, R. *Angew. Chem., Int. Ed.* **2001**, *40*, 1808.
- (3) (a) Barbour, L. J.; William Orr, G.; Atwood, J. L. *Nature* **1998**, *393*, 671. (b) Blanton, W. B.; Gordon-Wylie, S. W.; Clark, G. R.; Jordan, K. D.; Wood, J. T.; Geiser, U.; Collins, T. J. *J. Am. Chem. Soc.* **1999**, *121*, 3551. (c) Barbour, L.; William G.; Atwood, J. L. *Chem. Commun.* **2000**, 859. (d) Atwood, J. L.; Barbour, L. J.; Ness, T. J.; Raston, C. L.; Raston, P. L. *J. Am. Chem. Soc.* **2001**, *123*, 7192. (e)
- Narasimha Moorthy, J.; Natarajan, R.; Venugopalan, P. *Angew. Chem., Int. Ed.* **2002**, *41*, 3417. (f) Ghost S. K.; Bharadwaj, P. K. *Inorg. Chem.* **2003**, *42*, 8250. (g) Ghost, S. K.; Bharadwaj, P. K. *Angew. Chem., Int. Ed.* **2004**, *43*, 4390. (f) Ma, B.-Q.; Sun, H.-L.; Gao, S. *Chem. Commun.* **2005**, 2336.
- (4) Silverstein, K. A. T.; Haymet, A. D. J.; Dill, K. A. *J. Am. Chem. Soc.* **1998**, *120*, 3166.
- (5) (a) Kuhs, W. F.; Lehman, M. S. *J. Phys. Chem.* **1983**, *87*, 4312. (b) Koga, K.; Tanaka, H.; Zeng, X. C. *Nature* **2000**, *408*, 564.
- (6) (a) Ludwig, R. *ChemPhysChem* **2002**, *1*, 53. (b) Henry, M. *ChemPhysChem* **2002**, *3*, 607.
- (7) (a) Custelcean, R.; Afshoraei, C.; Vlassa, M.; Polverejan, M. *Angew. Chem., Int. Ed.* **2000**, *39*, 3094. (b) Rather, B.; Zaworotko, M. J. *Chem. Commun.* **2003**, *830*. (c) Pal, S.; Sankaran, N. B.; Samanta, A. *Angew. Chem. Int. Ed.* **2003**, *42*, 1741. (d) Ren, Y.-P.; Long, L.-S.; Mao, B.-W.; Y-Z. Yuan, Y.-Z.; Huang, R.-B.; Zheng, L.-S. *Angew. Chem., Int. Ed.* **2003**, *42*, 532. (e) Ma, B.-Q.; Sun, H.-L.; Gao, S. *Chem. Commun.* **2004**, 2220. (f) Zhao, B.; Cheng, P.; Cheng, C.; Shi, W.; Liao, D.; Yan, S.; Jiang, Z. *J. Am. Chem. Soc.* **2004**, *126*, 3012. (g) Mukherjee, A.; Saha, M. K.; Nethaji, M.; Chakravarty, A. *Chem. Commun.* **2004**, *716*. (h) Liu, Q.-Y.; Xu, L. *CrystEngComm.* **2005**, *7*, 87. (i) Naskar, J. P.; Drew, M. G. B.; Hulme, A.; Tocher, D. A.; Datta, D. *CrystEngComm* **2005**, *7*, 67. (j) Zhang, X.-L.; Chen, X.-M. *Cryst. Growth. Des.* **2005**, *5*, 617.
- (8) (a) Park, K.-M.; Kuroda, R.; Iwamoto, T. *Angew. Chem., Int. Ed. Engl.* **1993**, *32*, 884. (b) Janiak, C.; Schramm, T. G. *J. Am. Chem. Soc.* **2002**, *124*, 14010. (c) Raghuraman, K.; Katti, K. K.; Barbour, L. J.; Pillarssetty, N.; Barnes, C. L.; Katti, K. V. *J. Am. Chem. Soc.* **2003**, *125*, 6955. (d) Rodríguez-Cuamatz, P.; Vargas-Díaz, G.; Höpfl, H. *Angew. Chem., Int. Ed.* **2004**, *43*, 3041. (e) Ma, B.-Q.; Sun, H.-L.; Gao, S. *Angew. Chem., Int. Ed.* **2004**, *43*, 1374.
- (9) Carballo, R.; Covelo, B.; Lodeiro, C.; Vázquez-López, E. M. *CrystEngComm* **2005**, *7*, 294.
- (10) Eisenberg, D.; Kauzmann, W. *The Structure and Properties of Water*; Oxford University Press: Oxford, 1969.
- (11) (a) Scatena, L. F.; Brown, M. G.; Richmond, G. L. *Science* **2001**, *292*, 908. (b) Rossky, P. J. *Nature* **2002**, *419*, 889.
- (12) Baldelli, S.; Schnitzer, C.; Campbell, D. J.; Shultz, M. J. *J. Phys. Chem. B.* **1999**, *103*, 2789.
- (13) Selected data for $[\text{Cu}(\text{Hmal})(4\text{pds})] \cdot 6\text{H}_2\text{O}$ **1**: Elemental analysis found: C, 32.7; H, 4.8; N, 5.9; S, 12.9. $\text{C}_{14}\text{H}_{24}\text{CuN}_2\text{O}_{11}\text{S}_2$ requires: C, 32.0; H, 4.6; N, 5.3; S, 12.2%. IR (KBr, cm^{-1}) 3449 s; 1592 vs; 1479 m; 1218 w; 817 m; 718 m; 1631 s; 1397 m. $\mu = 1.75 \mu\text{B}$.
- (14) X-ray crystallography: Data were collected with a CCD area detector diffractometer, using monochromatized Mo K α radiation. Data were processed using the WinGX package (Farrugia, L. *J. Appl. Crystallogr.* **1999**, *32*, 837). Solution and refinement used the programs SHELXS97 (Sheldrick, G. M. *Acta Crystallogr., Sect. A* **1990**, *46*, 467) and SHELXL97 (Sheldrick, G. M. *SHELXL-97. Program for the Solution and Refinement of Crystal Structures*; University of Göttingen; Germany, 1997). Crystal data for $[\text{Cu}(\text{L-Hmal})(4\text{pds})] \cdot 6\text{H}_2\text{O}$ **1**: $\text{C}_{14}\text{H}_{24}\text{CuN}_2\text{O}_{11}\text{S}_2$, $M = 524.01$, monoclinic, space group $P2(1)/n$, $a = 10.676(3)$, $b = 10.220(3)$, $c = 21.095(5)$ Å, $V = 2261.6$ – (11) Å 3 , $D_c = 1.539 \text{ g cm}^{-3}$, $Z = 4$, $\mu(\text{Mo K}\alpha) = 1.206 \text{ mm}^{-1}$, 4992 unique reflections of which 1505 assumed as observed ($I > 2\sigma(I)$). Final R indexes ($I > 2\sigma(I)$) $R_1 = 0.0704$, $wR_2 = 0.1492$; R index (all data) $R_1 = 0.2622$. Because of the high degree of hydration and thermal motion, hydrogen atoms could not be located for the crystallization water molecules. Hydrogen bonding was inferred by considering the O···O close contacts of water molecules involved (O···O distance less than the sum of van der Waals radii 3.04 Å).¹⁸
- (15) Ghost, S. K.; Bharadwaj, P. K. *Inorg. Chem.* **2004**, *43*, 5180.
- (16) (a) Narten, A. H.; Thiessen, W. E.; Blum, L. *Science* **1982**, *217*, 1033. (b) Jeffrey, G. A. *An Introduction to Hydrogen Bonding*; Oxford University Press: Oxford, 1997. (c) Gregory, J. K.; Clary, D. C.; Liu, K.; Brown, M. G.; Saykally, R. J. *Science* **1997**, *275*, 814.
- (17) (a) Fletcher, N. H. *The Chemical Physics of Ice*; Cambridge University Press: Cambridge, 1970. (b) Matsumoto, M.; Saito, S.; Ohmine, I. *Nature* **2002**, *416*, 409.
- (18) Infante, L.; Motherwell, S. *CrystEngComm* **2002**, *4*, 454.